THE ROLE OF VISUAL PIGMENT IN PRIMARY EVENTS LEADING TO RETINAL DYSFUNCTION AND DEVELOPMENT OF AGE-RELATED MACULAR DEGENERATION

KINGA ELŻBIETA HANDZEL

Ph.D. 2010

ProQuest LLC
789 East Eisenhower Parkway
P.O. Box 1346
Ann Arbor, MI 48106-1346

DECLARATION

This work has not previously been accepted in substance for any degree and is not concurrently submitted in candidature for any degree.

Signed ...Kinga Handzel... (candidate) Date 11/10/2010

STATEMENT 1

This thesis is being submitted in partial fulfillment of the requirements for the degree of .....(insert MCh, MD, MPhil, PhD etc, as appropriate)

Signed ..Kinga Handzel.....(candidate) Date 11/10/2010

STATEMENT 2

This thesis is the result of my own independent work/investigation, except where otherwise stated.
Other sources are acknowledged by explicit references.

Signed ...Kinga Handzel..... (candidate) Date 11/10/2010

STATEMENT 3

I hereby give consent for my thesis, if accepted, to be available for photocopying and for inter-library loan, and for the title and summary to be made available to outside organisations.

Signed ...Kinga Handzel..... (candidate) Date 11/10/2010

Acknowledgements

Firstly, I would like to thank my supervisor Dr Małgorzata Różanowska for her unique role in supervising my project, her support and constant enthusiasm about the research. Without her advice I have received I would not have reached this points. I would also like to thank my other supervisor, Prof. Mike Boulton, for his advice and support throughout.

I would like to thank Dr Anthony Hann from Biosciences whose help and assistance with TEM was invaluable and Dr William Ford from the School of Pharmacy for his help with statistical analysis. I cannot forget to thank the support staff in the optometry department – Steve, Rob, Phil and Sue for their help and support in many aspects.

Special mention goes out to other postgrads who made the experience of PhD special. I would particularly like to thank: Magda, who shared good and bad times with me, Gosia, Paulina, Tatiana, Miguel, Basia, Patrycja for their intellectual and moral support and their wonderful diversity. Special big thanks is due to the members of my "monthly meeting" group – Linda for providing me technical help and sharing her experience and Matt for his support and specific sense of humour. Also Yadan – her help and support was invaluable especially in the final stage of my PhD.

I would also like to thank my parents and siblings for encouraging me throughout and having faith in me that provided the motivation to go further every day. Special thanks to my "Polish friends" who showed me that there is something more than "scientific world".

Above all, I want to thank Cris for being my reassurance, giving me support and just being there whenever needed.

Abstract

The aim of this study was to gain a deeper understanding of the role of the visual pigment in retinal damage and its contribution to initial pathways in the pathogenesis of age-related macular-degeneration (AMD).

Initially, the kinetics of all-*trans*-retinal (ATR) hydrolysis from opsin and its reduction to retinol formation were determined. Based on the results, singlet oxygen generation was investigated as a function of ATR position and the availability of cofactors required for retinol formation. The yield of singlet oxygen generated by ATR increased upon hydrolysis of ATR from opsin and further, upon its release to the disc membrane. The presence of ATP and NADPH did not influence the signals significantly.

(Photo)cytotoxicity studies revealed that both ATR and its degradation products (dATR) are toxic to cells, with dATR having a more deleterious effect. Toxic effects of dATR were prevented by α-tocopherol, retinol and phosphatidylethanolamine, whereas none of hydrophilic antioxidants tested exerted a substantial effect.

Both ATR and dATR exhibited a similar ability to generate singlet oxygen when excited with visible light, whereas products of ATR degradation were characterised by greater photosensitising properties than ATR for shorter wavelengths. The yield of singlet oxygen for retinol was lower than for ATR in acetone. Although, retinyl ascorbate has a great potential to be a strong singlet oxygen quencher, the difference in the quenching rate was not found to be statistically significant when compared with all-*trans*-retinol or ascorbyl palmitate.

Accumulation of products of rhodopsin bleaching increased the formation of lipofuscin-like inclusion bodies. Exposure of cells to light was associated with higher levels of fluorescence characteristic for oxidised cellular components.

In summary, the results suggest that products of visual pigment bleaching may contribute to the toxic effects of light on the retina. In conjunction with published findings, it supports the theory that ATR can play an important role in causing RPE dysfunction as occuring in retinal aging and AMD.

Contents

Abbreviations

11-*cis*-RAL	11-*cis*-retinal
11-*cis*-RDH	11-*cis* retinol dehydrogenase
11-*cis*-RE	11-*cis*-retinyl esters
11-*cis*-REH	11-*cis*-retinyl ester hydrolase
A2E	N-retinylidene-N-retinylethanolamine
A2E	2-[2,6-dimethyl-8-(2,6,6-trimethyl-1-cyclohexen-1-yl)-1*E*,3*E*,5*E*,7*E*-octotetraenyl]-1-(2-hydroxylethyl)-4-[4-methyl-6-(2,6,6-trimethyl-1-cyclohexen-1-yl)-1*E*,3*E*,5*E*-hexatrienyl]-pyridinium
A2-PE	phosphatidyl-pyridinium
ABCR (ABCA4)	ATP-binding cassette transporter
AGE	advanced glycation end products
all-*trans*-RE	all-*trans*-retinyl esters
all-*trans*-ROL	all-*trans*-retinol
AMD	age-related macular degeneration
ANOVA	analysis of variance
ApoE	Apolipoprotein E
AREDS	Age-Related Eye Disease Study
ARMS2	age-related maculopathy susceptibility 2
AsA-Pal	ascorbyl palmitate
ATCC	American Type Culture Collection
ATP	adenosine 5'-triphosphate
ATR	all-*trans*-retinal
BF	complement factor B
BSA	bovine serum albumin
BSA	bovine serum albumine
C2	complement component 2
C3	complement component 3
CAREDS	Carotenoids in Age-Related Eye Disease Study
CD36	Cluster of Differentiation 36
CFB	complement factor B

CFH	complement factor H
cGMP	cyclic guanosine monophosphate
CRALBP	cellular retinaldehyde binding protein
CRP	C-reactive protein
D	dark
dATR	degraded all-*trans*-retinal
DHA	docosahexaenoic acid
DMEM:F12	Dulbecco's modified Eagle's medium and Ham's F12 medium
DMPC	1,2-dimyristoyl-*sn*-glycero-3-phosphocholine
DMPE	1,2-dimyristoyl-*sn*-glycero-3-phosphoethanolamine
DMSO	dimethyl sulfoxide
DNA	Deoxyribonucleic acid
D-PBS	Dulbecco's phosphate buffered saline
EDTA	ethylenediaminetetraacetic acid
EL2	second intradiscal loop
ER	*endoplasmic reticulum*
FCS	fetal calf serum
FITC	fluorescein isothiocyanate
GDP	guanosine diphosphate
GMP	guanosine monophosphate
GPCR	G protein-coupled receptors
GPX	glutathione peroxide
GSH	glutathione
GST	glutathione S-transferase
GTP	guanosine triphosphate
HHE	hydroxy-2(*E*)-hexenal
HNE	hydroxynonenal
HTRA1	HTRA serine protease 1
IPM	interphotoreceptor matrix
IRBP	interphotoreceptor retinoid-binding protein
iso-A2E	*iso*-N-retinylidene-N-retinylethanolamine
*iso*Rh	*iso*rhodopsin

L	light
LH	unsaturated lipid
$LO^{\cdot}$	lipid alcoxyl radical
$LOO^{\cdot}$	lipid peroxyl radical
LC-PUFA	long-chain polyunsaturated fatty acid
LRAT	lecithin:retinol acyltransferase
MAC	Membrane Attack Complex
MerTK	c-mer proto-oncogene tyrosine kinase
Meta I	metarhodopsin I
Meta II, MII	metarhodopsin II
Meta III, MIII	metarhodopsin III
MTT	3-(4,5-dimethylthiazol-2-yl)-2,5-diphenyl tetrazolium bromide
NAC	*N*-acetylcysteine
NAD	nicotinamide adenine dinucleotide
NADH	nicotinamide adenine dinucleotide reduced form
$NADP^{+}$	nicotinamide adenine dinucleotide phosphate oxidised form
NADPH	nicotinamide adenine dinucleotide phosphate reduced form
Nd:YAG	neodymium-doped yttrium-aluminium-garnet
NRPE	N-retinylidene-phosphatidylethanolamine
OPO	optical parametric oscillator
OS	outer segments
PBS	phosphate buffer saline
PC	phosphatidylcholine
PC	phosphatidylcholine
PDE	phosphodiesterase
PE	phosphatidylethanolamine
PEDF	pigment epithelium-derived growth factor
PI	propidium iodide
POS	photoreceptor outer segments
prRDH	photoreceptor retinol dehydrogenase
PUFA	polyunsaturated fatty acid
PXAL	pyridoxal

PXAM	pyridoxamine
RA-AsA	retinyl ascorbate
RB	rose Bengal
RDH	retinol dehydrogenase
RGR	retinal G protein-coupled receptor
Rh	rhodopsin
Rh	rhodopsin
RK	rhodopsin kinase
RLBP1	cellular retinaldehyde-binding protein gene
RNA	ribonucleic acid
ROL	all-*trans*-retinol
ROS	reactive oxygen species
RPE	retinal pigment epithelium
RPE65	RPE-specific 65 kDa protein
SD	standard deviation
SEM	standard error of the mean
SOD	superoxide dismutase
TEM	transmission electron microscopy
TGF	transforming growth factor
TM	transmembrane
Trp	tryptophan
UV	ultraviolet
VEGF	vascular endothelial growth factor
$VitB_6$	Vitamin B_6
VitC	vitamin C
VitE	vitamin E

Chapter 1

Introduction

1.1 General introduction

Age-related macular degeneration (AMD) is the predominant cause of vision loss in the elderly in developed countries. The disease mainly affects the outer part of the retina: photoreceptors and the retinal pigment epithelium (RPE) (Pulido, 2002). The RPE is believed to be the primary site of dysfunction. As photoreceptors rely on the RPE for their survival and performing their function in vision, RPE dysfunction leads to dysfunction and loss of photoreceptors. Photoreceptor outer segments are in close proximity to the RPE and are extremely susceptible to oxidative damage imposing a risk that damage spreads to the RPE. However, the mechanism responsible for initiating that damage is not clear.

The regenerable visual pigment rhodopsin has been shown to be an essential factor for retinal damage, and many studies have revealed a positive correlation between the rhodopsin content in the retina and the degree of retinal damage (Noell et al., 1966; Organisciak et al., 1991; Organisciak and Winkler; 1994; Grimm et al., 2000; Grimm et al., 2001). It is hypothesised that the correlation between the retinal damage and rhodopsin is caused by all-*trans*-retinal (ATR) formed after rhodopsin bleaching. ATR is a potent photosensitiser and its contribution to the photodamage of the retina has been suspected for over two decades. It has been shown to contribute to lipid and protein damage followed by enzyme dysfunction and formation of products not susceptible to lysosomal degradation (Sun and Nathans, 2001). Availability of ATR in the retina and exposure to light have been shown to be the main factors responsible for accumulation of lipofuscin granules - a product of incomplete lysosomal digestion of shed and phagocytosed apical tips of POS, within the RPE (Katz et al., 1999; Katz and Redmond, 2001). This thesis aims to provide further understanding of the role of the visual pigment in retinal damage contributing to the onset of photoreceptor damage, RPE dysfunction and AMD.

This introduction will provide a background to the normal structure and functions of photoreceptors and the RPE and discuss a role of the visual pigment and light in retinal damage.

1.2 The retina

1.2.1 Structure

The retina is composed of the neural part and the RPE (Oyster, 1999). The neural retina is a thin layer of tissue with purple/red colouring due to the presence of visual pigments. This part contains the following layers: outer segments of photoreceptors, inner segments of photoreceptors, external limiting membrane, outer nuclear layer, outer plexiform layer, inner nuclear layer, inner plexiform layer, ganglion cell layer, optic fiber layer and inner limiting membrane (according to Cohen, 1992).

1.2.2 Blood flow in the retina

The retina is characterised by high metabolic activity that is correlated with its blood supply. Most of the blood to the inner retina is supplied by the central retinal arteries, whereas the outer part of the retina, including RPE and photoreceptors are supplied by the choriocapillaris, which lies beneath Bruch's membrane (Pulido, 2002). The choriocapillaris produces a high blood flow rate, therefore, this part of the retina is very well oxygenated. It has significant consequences in relation to photo-oxidative damage. Blood flow in the neural retina is autoregulated – the changes depend on the nutritional demands of the tissue. The blood-retina barrier is provided by the tight junctions of endothelial cells of retinal blood vessels and of the RPE (Forrester et al., 2002).

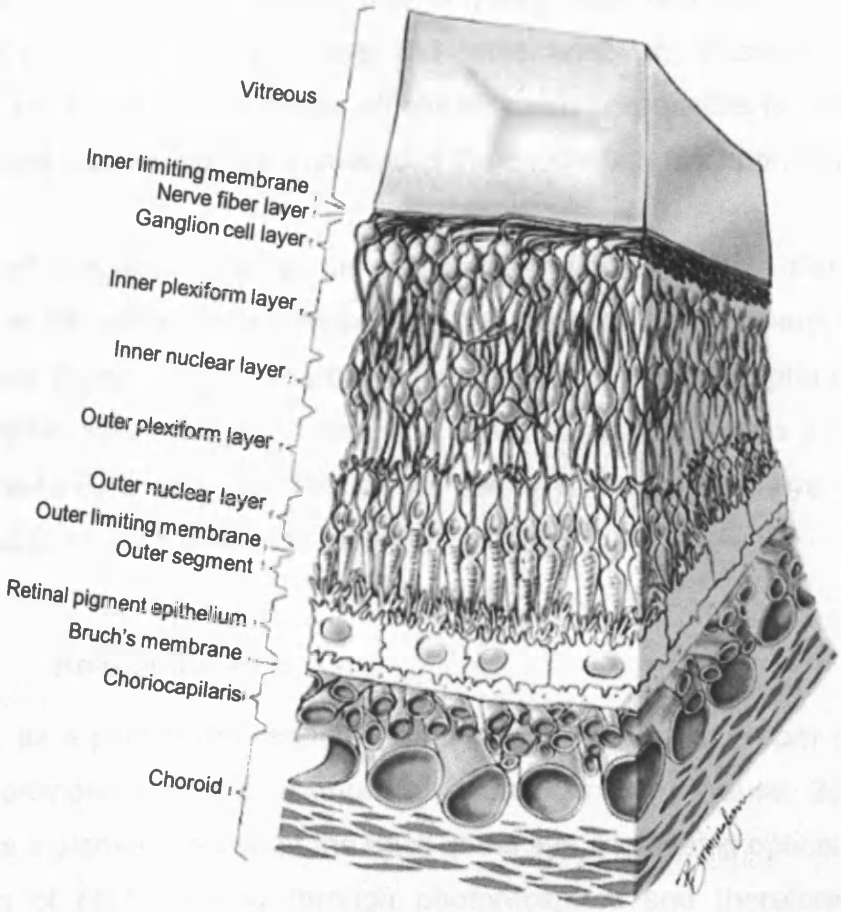

Figure 1.1 Layers of retina (from Pulido, 2002).

1.2.3 **Retinal pigment epithelium – RPE**

1.2.3.1 **Structure of the RPE**

The RPE is a monolayer of hexanocuboidal epithelial cells, which block the free passage of ions and water between the neural retina and the choroidal blood supply (Marmor, 1998).

The apical part of the RPE extends towards the photoreceptors while its basal part faces Bruch's membrane. The apical surface is equipped with a great number of long microvilli that reach and partially envelop outer segments of photoreceptors. The cytoplasm in the apical part contains microtubules,

microfilaments and the greatest concentration of melanin granules. Polarised distribution of melanin is present only in young RPE and with age, melanin granules become distributed more and more uniformly throughout the cell (Weiter et al., 1986). The nucleus, all cell elements responsible for reactions of synthesis and lysosomes, are localised in the middle part (Marmor, 1998).

The size of epithelial cells in the region of the macula is in the range of 10-14 µm in diameter. They increase their size toward the periphery, becoming broader and flatter. In the periphery, the number of photoreceptors overlying each epithelial cell is roughly constant – about 45 photoreceptors per cell. The mean cone-to-RPE ratio for the foveal center in the human eye has been determined to be 23:1 (Gao and Hollyfield, 1992).

1.2.3.2 Role of the RPE

The RPE, as a part of the retina, plays a critical role in the proper process of vision. It provides a crucial support for photoreceptors (Strauss, 2005). The RPE forms a pigmented wall at the back of the eye, increasing optical quality by absorption of light passing through photoreceptors and therefore reducing scattered light. Pigments such as melanin can absorb light energy that could otherwise lead to pro-oxidative processes.

The RPE also contains a range of enzymes, which are engaged in membrane transport, changes of waste products, metabolism of visual pigment, regulation of the environment of photoreceptors and the RPE by humoral and growth factors (Marmor, 1998). Two growth factors are important in particular: vascular endothelial growth factor (VEGF) and pigment epithelium derived growth factor (PEDF). They play an important role in controlling angiogenesis, and it appears that the ratio between pro-angiogenic VEGF and anti-angiogenic PEDF is critical to maintain proper functions of the eye (Bhutto *et al.*, 2006). Upregulated VEGF with decreased levels of PEDF has been shown to be characteristic of the neovascular form of AMD (Lopez et al., 1996; Bhutto et al., 2006).

The plasma membrane of RPE contains various receptors and channels for metabolites and ions, which determine their transport (Fox et al., 1988; Kindzelskii et al., 2004). The RPE also regulates the transport of nutrients and metabolites such as amino acids and glucose (Ostwald and Steinberg, 1981; Takagi et al., 1994). The RPE can transport water and ions from the apical side or the subretinal space to the blood via its basolateral side (Strauss, 2007). It is also responsible for delivery of docosahexaenoic acid (DHA) to photoreceptors – a phospholipid necessary to build tissue of neurons, which is particularly abundant in photoreceptor membranes, accounting there for 80% of long chain polyunsaturated fatty acids (Fliesler and Anderson, 1983). The RPE is able to preferentially take up DHA in a concentration-dependent manner.

Due to RPE involvement, a disposal of large quantities of photoreceptor membranes is possible. These epithelial cells are able to phagocytose photoreceptor outer segments and digest waste products allowing them to be renewed (Anderson et al., 1978). Enzymes of the RPE are also involved in the visual cycle. Metabolism of retinoids involves the presence of a specific isomerising system to form the 11-*cis*-retinoid conformation, allowing the visual pigment chromophore 11-*cis*-retinal from all-*trans*-retinoids to be synthesised (Lamb and Pugh, 2004).

It has been shown that the RPE is one of the structures responsible for formation and maintenance of the interphotoreceptor matrix (IPM), which is localised in the extracellular space between the photoreceptors of the retina and the apical surface of the RPE. The bonding properties and viscosity of the IPM are controlled by the RPE and they are critical for retinal adhesion and proper functioning of photoreceptors (Jablonski et al., 2000). All the functions of the RPE are summarised in the Fig. 1.2.

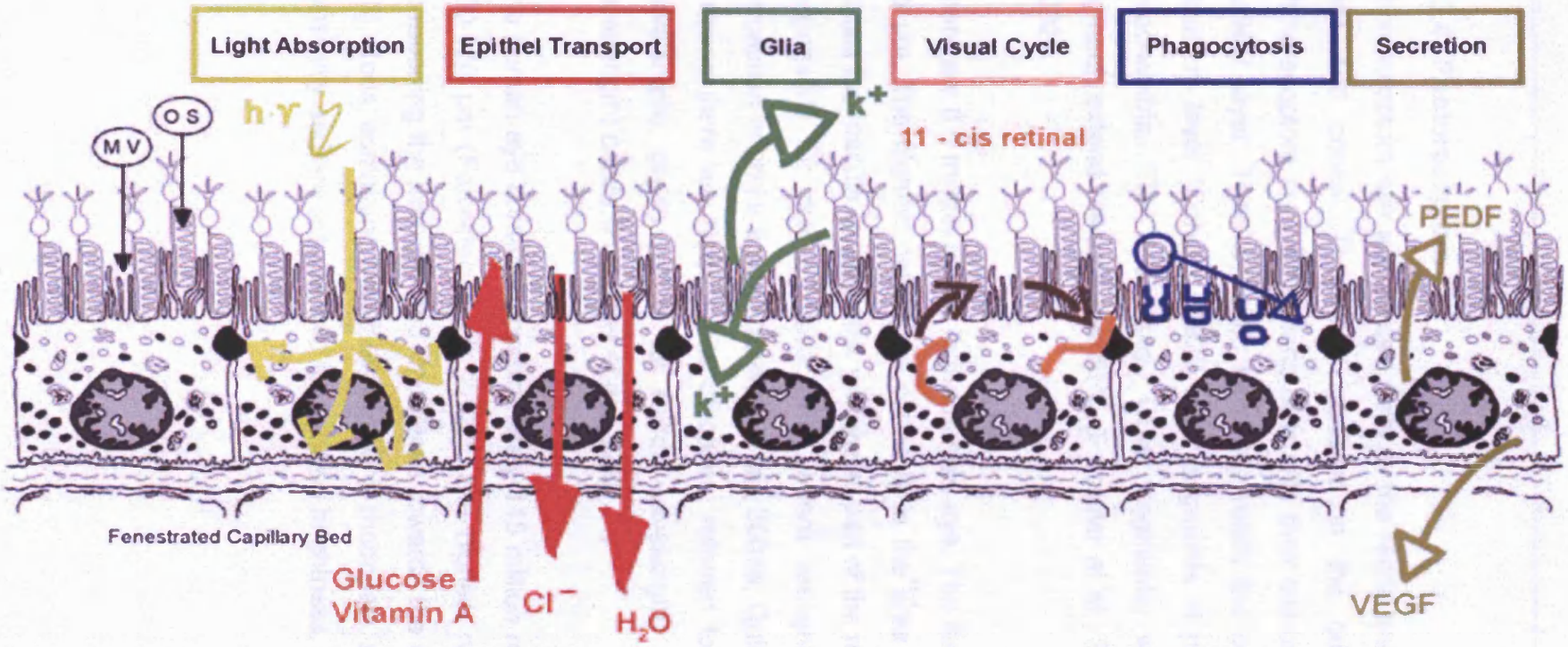

Figure 1.2 Summary of retinal pigment epithelium (RPE) functions. PEDF= pigment epithelium-derived growth factor; VEGF = vascular epithelium growth factor; Epithel = epithelium (from Strauss, 2007).

1.2.4 **Photoreceptors**

Photoreceptors are specialised cells in the retina and there are of two types: rods and cones. They are localised in the outer part of the retina. Photoreceptors are narrow long cells with their cell bodies located in the outer nuclear layer. Their synaptic terminals reach the outer aspect of the outer plexiform layer (Cohen, 1992). Inner segments of photoreceptors are rich in mitochondria, ER- and Golgi. Outer segments, which contain the visual pigment, extend towards the RPE (Forrester et al., 2002; Quillen and Barber, 2002).

There are 6.5 million cones in the human eye. The length of cones is about 60-75 µm. The highest density of cones is in the area of the fovea, decreasing across the macula towards the peripheral part of the retina (Fig. 1.3). Cones are responsible for colour vision and pattern recognition and provide visual perception in bright light (Forrester et al., 2002a; Quillen and Barber, 2002). In humans there are three types of cones, referred to as blue (or S for short-wavelength), green (or M for middle-wavelength) and red (or L for long-wavelength) cones (Forrester et al., 2002).

The human eye contains approximately 115 million rods. The length of rods is 100-120 µm (Forrester et al., 2002). The highest rod density is in the area surrounding the macula, and decreases towards the centre of the macula (Fig. 1.3). Rods, containing the visual pigment, rhodopsin, are characterised by great sensitivity and are responsible for sensing brightness, contrast and motion.

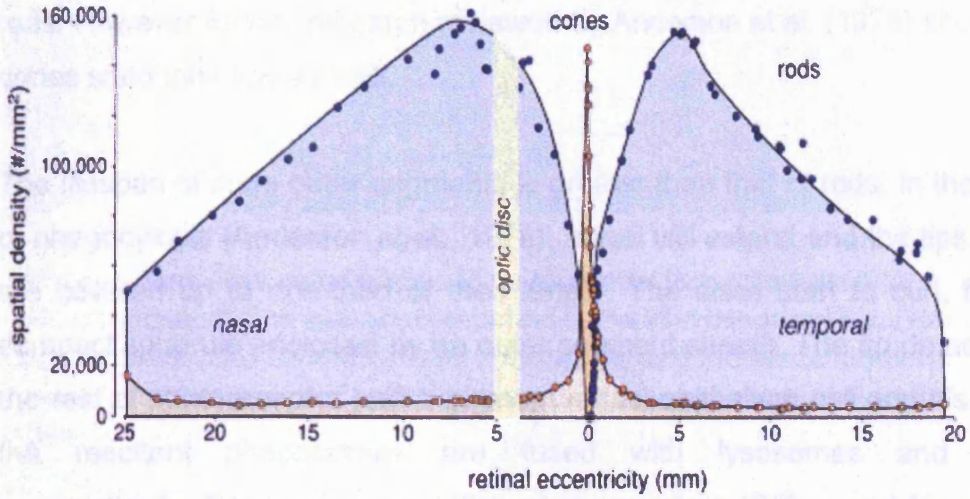

Figure 1.3 Distribution of rods and cones (from Rodieck, 1988).

1.2.4.1 Outer segment discs renewal and removal

Photoreceptors, as cells of the nervous system, do not undergo further cell division and replacement of damaged or senescent cells following cell differentiation (Oyster, 1999). Thus, a mechanism of constant renewal of these elements is critical for proper functioning of the eye. Research on rats, mice and frogs carried out by Young and Droz (Young, 1967; Young and Droz, 1968) with use of radiolabelled proteins showed that the photoreceptor outer segments are continually renewed. Renewal of outer segments occurs by production of newly formed discs, which are continually replaced by newer discs added at the base of the outer segments. According to Young (1967) the renewal of outer segments is light- and temperature-dependent, exhibiting an increase in renewal with increase of temperature and retinal illumination.

Some differences between rods and cones have been observed (Young and Droz, 1968). In cones, the disc membranes in the POS are continuous with one another, allowing for diffusion of the visual pigment across the whole length of the outer segments, whereas the rod discs are separated from the plasma membrane so once incorporated into a particular disc, the protein is trapped there. It was speculated that cones do not undergo renewal in the same way as

rods. However further research reviewed by Anderson et al. (1978) showed that cones shed their tips as well.

The lifespan of cone outer segments is greater than that of rods. In the process of phagocytosis (Anderson et al., 1978), apical villi extend and the tips of cones are covered up to one-third of their length. The discs start to curl, forming a compact spherule enclosed by an outer segment sheath. The tip detaches from the rest of photoreceptor and a pigment retinal epithelium cell engulfs it so that the resultant phagosomes are fused with lysosomes and digested enzymatically. Research on goldfish photoreceptors (O'Day and Young, 1978) showed that shedding of cone membranes occurs early in the night.

Rod outer segments undergo a process of phagocytosis and renewal, similarly to cones. The production of disks takes place at the base of outer segments. However, in rods the tips contain the oldest cellular components (lipids and proteins) due to formation of separate discs and constant formation of new discs. Since fusion of discs does not occur in cones, new cellular components can be mixed with older molecules. It takes about 10 days for an outer segment disc to get from the base of the outer segment to the tip engulfed by RPE apical microvilli and undergo phagocytosis, carried out by the RPE (Fig. 1.4).

To maintain proper size and function of photoreceptors, removal of shed outer segments becomes a necessity (Oyster, 1999). The RPE is involved in this process, which was confirmed by the presence of phagosomes containing OS discs.

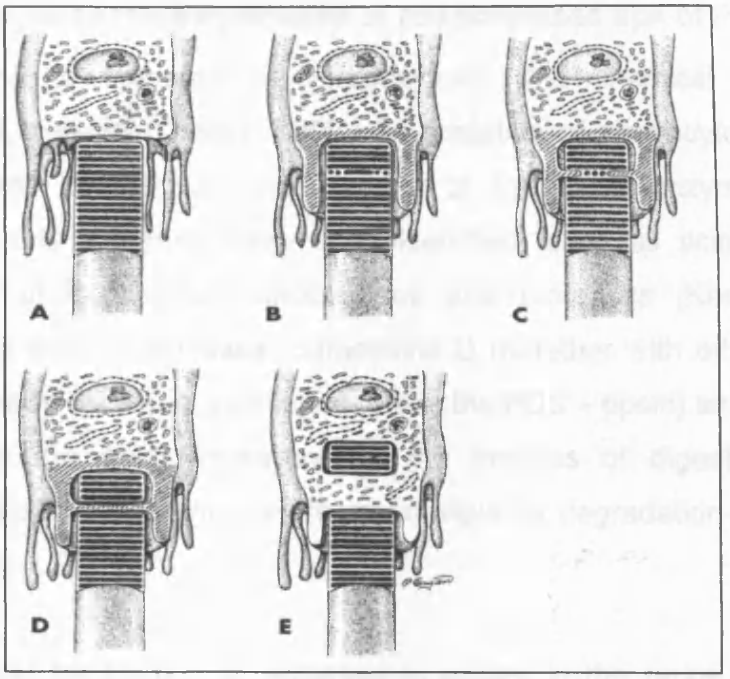

Figure 1.4 Diagram showing the contribution of photoreceptors and the RPE to rod outer segment disc shedding and phagocytosis. **A**, The distal part of the outer segment is only surrounded by apical microvilli from the RPE. **B**, Alterations take place within some distal discs, and pseudopodia protrude from The RPE. **C** and **D**, Pseudopodia protrude into the outer segment, separating the distal discs from the remainder of the outer part of segment. **E**, The pseudopodia withdraw, transporting the obtained structure deeper into the epithelium cytoplasm (from Bernstein, 1999).

The process of shedding demands active processes in the RPE and the distal outer segments (Bok, 1985; Matsumoto et al., 1987). The component responsible for phagocytic activity of the RPE and communication between the RPE and photoreceptors has been found. The rod outer segment distal tip seems to be ensheathed by pseudopodial processes of the RPE (as shown in Fig. 1.4). Initially, POS specifically bind to the apical membranes of The RPE. Recognition of POS binding is then transferred to the intracellular space by activation of a second messenger cascade. This in turn can activate the ingestion of bound POS (Strauss, 2007). CD36 (the macrophage scavenger receptor), MerTK (the receptor tyrosine kinase c-*mer*), and integrin receptors have been found to regulate POS phagocytosis.

1.2.4.2 Lysosomal degradation of phagocytosed tips of POS

Disc shedding is followed by phagocytosis and chemical changes of phagocytosed material (Oyster, 1999). Degradation of phagocytosed parts of outer segments occurs with participation of lysosomal enzymes. In RPE lysosomes, many enzymes have been identified, such as acid lipase, acid phosphatase, phospholipase, glicosidases and proteases (Kennedy et al., 1994). Among RPE proteinases, cathepsins D (together with other lysosomal enzymes degrade the main protein present in the POS – opsin) and cathepsin S appear to be the most important for the process of digestion of POS. Phospholipases and acid lipases are responsible for degradation of POS lipids (Eldred, 1998).

The optimal pH for lysosomal enzymes is acidic, in the range of about 4-6 (Berman, 1971; Lentrichia et al., 1978). The release of these enzymes from lysosomes seems to be sensitive to pH and temperature, with differential effects for enzymes (Shiono et al., 1983).

1.2.5 Protective enzymes and antioxidants

The RPE and its functions are determined by the environment of the outer retina they are a part of. The outer retina is not only exposed to the light energy focused by the cornea and lens, but also to high concentration of oxygen thanks to high blood perfusion of the choriocapillaris. The combination creates favourable conditions for photo-oxidation and subsequent oxidative damage in the presence of photosensitisers. This photo-oxidative activity is worsened by the number of reactive oxygen species produced by phagocytosis of photoreceptor outer segments. The high metabolic activity of photoreceptors is related to the generation of reactive oxygen species, such as superoxide, as a by-product of mitochondrial respiration. These specific conditions the outer retina is exposed to demand special protective mechanisms and features that the RPE is equipped with.

The RPE is equipped with both enzymatic (great concentration of superoxide dismutase and catalase) and nonenzymatic antioxidants (lipoate, glutathione, ascorbate, α-tocopherol, carotenoids such as zeaxanthin and lutein, and β-carotene).

One of the ways in which the RPE provides protection is through the presence of melanin, a protective pigment present within cytoplasmic granules (melanosomes) (Schmidt and Peisch, 1986). The antioxidant properties of RPE melanosomes and melanin have been studied in many model systems (reviewed by Boulton et al., 2001). Melanin has been shown to exhibit the ability to scavenge free radicals and quench the excited states of photosensitisers and singlet oxygen. It was demonstrated that melanin can protect choroidal blood vessels against light toxicity (Peters et al., 2006). Różanowski and colleagues (Różanowski et al., 2008) showed that human RPE melanosomes can act as effective antioxidants by preventing iron ion-induced oxidation. However, photodegradation of melanosomes leads to the loss of these antioxidant properties, although their ability to deactivate cationic photosensitisers is preserved.

Seagle and colleagues (2006) showed that supplementation of cultured cells with melanin may protect cells from light damage. However, other studies have shown no protection in cultured cells fed with melanosomes (Zareba et al., 2006) or even phototoxic effects (Różanowski et al. 2008). Additionally it has been shown that light-activation of melanosomes may lead to production of reactive oxygen species and lipid peroxidation, with increased photoreactivity with age (Różanowska et al., 2005; Dontsov et al., 1999; Różanowska et al., 2002).

The third mechanism of RPE cell defence is connected with the physiological ability to repair damaged DNA and various cellular components such as proteins and lipids, and to remove deleterious products of oxidation (Strauss, 2007).

1.2.6 **Phototransduction**

The RPE is essential for proper functions of photoreceptors, which are involved in the main process in the retina responsible for visual perception - phototransduction – the transformation of light energy into an electrical signal. This process includes activation of visual pigments (rhodopsin in rods and cone visual pigments in cones), cGMP hydrolysis and hyperpolarisation of photoreceptor plasma membranes (Forrester et al., 2002b; Quillen and Barber, 2002). Conformational changes in rhodopsin induced by light, lead to a change in the protein structure and density in the plasma membrane surrounding the protein. This process allows binding and activation of transducin (G-protein). Activated transducin causes an increase in activity of cGMP phosphodiesterase. This leads to a dramatic decrease in the concentration of cGMP and results in the closure of cGMP-gated Na^+ channels. The final result of these processes is the hyperpolarisation of photoreceptor plasma membranes, precluding the release of neurotransmitter from its synaptic terminal, what normally takes place in the dark.

1.2.7 **Rhodopsin - structure and properties**

Rhodopsin is a member of Family A of G protein-coupled receptors (GPCRs) – a class of cell surface signal transducing receptors (Ridge and Palczewski, 2007). It is an intrinsic membrane protein with a molecular weight of about 40,000 Da. It is present in the discs of both types of photoreceptors and in the plasma membranes of the rod outer segments, but in smaller concentrations (Whikehart, 2003). It occupies about 50% of the disc surface area, being the predominant membrane protein (Ridge and Palczewski, 2007).

Half of the rhodopsin molecule containing 7 α-helices is embedded in the hydrophobic part of the membrane. The remaining rhodopsin is situated equally on each surface of the membrane. This orientation is necessary for maintaining the proper, functional role of rhodopsin.

C-terminus of rhodopsin is exposed on the cytoplasmic part of the disc and contains several hydroxyl amino acids. These amino acids can be phosphorylated, and this process is responsible for turning off the ability to bind and therefore activate transducin. The N-terminal sequence of rhodopsin, containing two short-chain oligosaccharides, appears to be exposed on the intraluminal space. The role of these sugars is to orient or anchor the protein and possibly stabilize the disc structure (Shichi, 1999; Whikehart, 2003).

11-*cis*-retinal is a nonprotein component of rhodopsin. This molecule is situated in the part of the protein which is associated with membrane lipids. It is bound to the 296Lysine on the protein *via* a protonated Schiff base (Whikehart, 2003). Analysis of crystal structure of rhodopsin shows compact intradiscal (extracellular) arrangement, with a part of it being folded inward to enclose its chromophore 11-*cis*-retinal together with the second extracellular loop (Ridge and Palczewski, 2007). The cytoplasmic domain, on the other hand, is not as compact and highly organised as the extracellular domain. The plasticity of the region is likely to be required for the function of rhodopsin.

A broad absorption spectrum of rhodopsin peaks in humans at 498 nm (Różanowska and Sarna, 2005). Absorption of light by the visual pigment results in structural changes of 11-*cis*-retinal, isomerisation to the all-*trans* form followed by conformational changes in protein and hydrolysis of all-*trans*-retinal. In order for photoreceptors to sustain sensitivity to light stimuli, the chromophore needs to be replaced so all-*trans*-retinal undergoes structural and chemical changes to allow 11-*cis*-retinal and therefore rhodopsin to be regenerated. This involves the concerted action of retinoid-binding proteins and various enzymes to metabolize and traffic different forms of retinoids between photoreceptors and the RPE. This process is known as the visual cycle and is described in the section below.

1.2.8 **Regeneration of rhodopsin – visual cycle**

Absorption of light by the visual pigment is the primary event in the retina induced by light. This process leads to rapid photoisomerisation around the $C_{11} = C_{12}$ double bond of 11-*cis*-retinal to all-*trans*-retinal completed within 200 fs (Ritter et al., 2008). This event results in a chain of conformational changes in the molecule of rhodopsin. The first intermediates formed after isomerisation are bathorhodopsin (Batho) and lumirhodopsin (Lumi) with maxima of absorption at 540 nm and 496 nm, respectively (Fig. 1.5). Relaxation of an early form of photoactivated rhodopsin goes through metarhodopsin I (Meta I) state and finally, an active form of rhodopsin is formed – metarhodopsin II (Meta II). The transition from Meta I to Meta II_a (absorption maximum at 380 nm) involves a crucial step – the breakage of the salt bridge by proton transfer from the Schiff base to its counterion Glu113. It has been suggested that proton uptake from the bulk phase is required to form Meta II_b, which finally binds and activates the G-protein. There is equilibrium between Meta I and Meta II, but it can be shifted from metarhodopsin I to II by increasing temperature or decreasing pH (Matthews et al., 1963). This equilibrium also depends on other factors such as lipid environment and pressure.

The decay of Meta I/Meta II by direct dissociation into opsin and free all-*trans*-retinal is the predominant decay pathway at acidic to neutral pH, whereas Meta I/Meta II decays to metarhodopsin III (Meta III) mainly at alkaline pH (Bartl and Vogel, 2007). It has also been shown that illumination of active Meta II can lead to the formation of Meta III with a maximum of absorption at 475 nm (Ritter et al., 2007) (Fig. 1.6). Meta III can account for up to 80% of total photoactivated rhodopsin depending on the conditions. It excludes the chromophore from the regeneration pathway in a very efficient way because of its long lifetime - it may decay into opsin and all-*trans*-retinal, albeit on a timescale of hours (Ritter et al., 2008). Meta III can be also converted back to Meta II. It is reached by illumination with 470 nm light (Heck et al., 2003; Różanowska and Sarna, 2005; Bartl and Vogel, 2007). It has been shown that addition of transducin to Meta III (1:5 stoichiometric concentration) at pH 7.5 and 20°C induces a rapid decay of

metarhodopsin III to opsin and ATR by hydrolysis of the retinal Schiff base with a half time of 11 minutes, whereas in the absence of transducin, the decay of Meta III is much slower (7.5 hours) (Bartl and Vogel, 2007).

Meta II can catalyse activation of transducin, the heterotrimeric G-protein, by allowing for the exchange of GDP for GTP in its subunit α (Tα), and the dissociation of Tα with bound GTP from the βγ subunits (Tβγ) (Bartl and Vogel, 2007). The released activated subunit Tα interacts with phosphodiesterase (PDE). Activated PDE can catalyse the hydrolysis of cGMP to 5'GMP. The decrease in the level of intracellular cGMP results in the closure of the plasma membrane cGMP-gated channels and therefore an inhibited influx of Na^+ and Ca^{2+} cations. Na^+K^+ pumps in the inner segment remove Na^+ from the cytoplasm and the levels of intracellular Ca^{2+} decrease, leading to hyperpolarisation of the photoreceptor cell plasma membrane.

Activation of transducin can be catalysed by Meta II until it is phosphorylated by rhodopsin kinase (RK) and binds arrestin, which completely blocks activation of transducin (Surya et al., 1995). The decay of Meta II form results in hydrolysis of the Schiff base linkage of opsin with ATR, which leads to the release of ATR from the hydrophobic binding pocket. ATR is moved to the "exit site" of the protein, with non-covalent binding until the protein is regenerated by binding of another 11-*cis*-retinal to the active site of rhodopsin (Travis et al., 2007). Using intrinsic fluorescence of tryptophan it is possible to monitor the path of all-*trans*-retinal through a native receptor protein (Schadel et al., 2003). ATR, being in the active site of rhodopsin, quenches fluorescence of the protein and once it is hydrolysed an increase of Trp fluorescence occurs (Schadel et al., 2003). There are five tryptophan residues in total (positions 35, 126, 161, 175, and 265) in the primary structure of bovine rhodopsin and they are located on different helices (Lin and Sakmar, 1996). Trp265 is conserved in all pigments and is located on helice 6 in the closest position to the retinal chromophore.

Hydrolysed ATR is then reduced to retinol (ROL) (Liu et al., 2000). The process is carried out in an NADPH-dependent process by photoreceptor retinol dehydrogenase (prRDH), identified as RDH8 and RDH12 (Maeda et al., 2009). There are two pathways leading to the reduction of all-*trans*-retinal (as shown on Fig. 1.7): ATR can be reduced by prRDH, while still bound to the "exit site" of opsin, or after it is released to the inner leaflet of the disc membrane upon binding 11-*cis*-retinal to opsin and regeneration of rhodopsin (Heck et al., 2003; Fig. 1.7). However, ATR in the inner leaflet of POS discs needs to be transported to the outer leaflet to become available as a substrate of prRDH. ATR, being in the inner leaflet of the disc membrane, can form complexes with an abundant phospholipid – phosphatidylethanolamine (PE), leading to the formation of N-retinylidine-phosphatidylethanolamine (NRPE). The complex is transported to the cytoplasmic disc surface by the retina-specific ATP-binding cassette transporter rim protein (ABCR, also known as ABCA4), and released on the cytoplasmic site of the disc membrane as all-*trans*-retinal, where it becomes available for prRDH so it can be reduced to ROL (Liu et al., 2000).

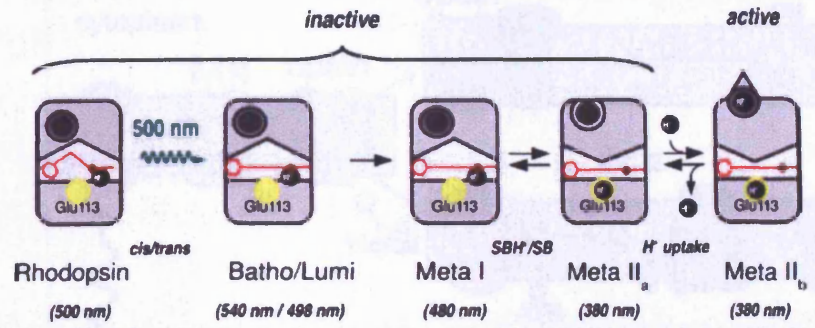

Figure 1.5 Scheme of light-induced reactions of rhodopsin (from Ritter et al., 2008). The dark state of rhodopsin is characterised by 11-*cis*-retinal (red) bound to the apoprotein by a protonated Schiff base that is stabilised by its counterion Glu113 (yellow). Absorption of green light leads to isomerisation (wave arrow) of 11-cis conformation to *all*-trans. The early intermediate Batho is formed, which relaxes through the intermediates Lumi and Meta I into the active state Meta II$_b$ (solid arrows).

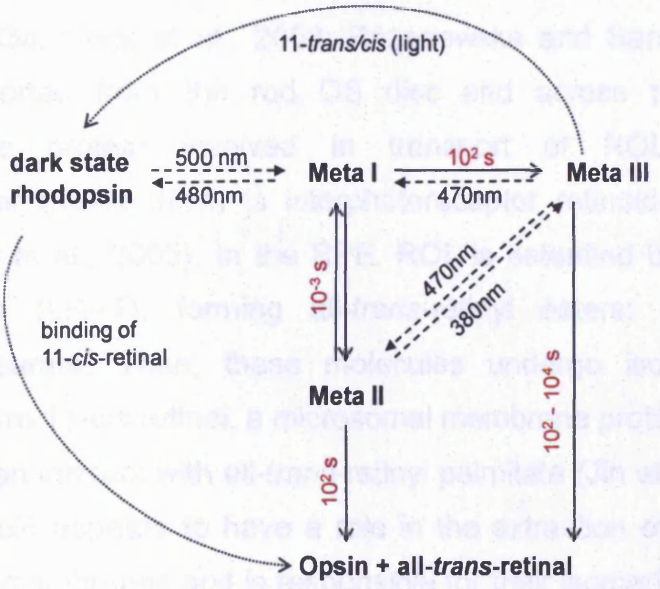

Figure 1.6 A summary of light-induced (dashed arrows) and thermal (smooth arrows) reactions of rhodopsin. Excitation wavelengths of light-induced states are given as well as approximate time constants for the thermal reactions (adapted from Bartl and Vogel, 2007).

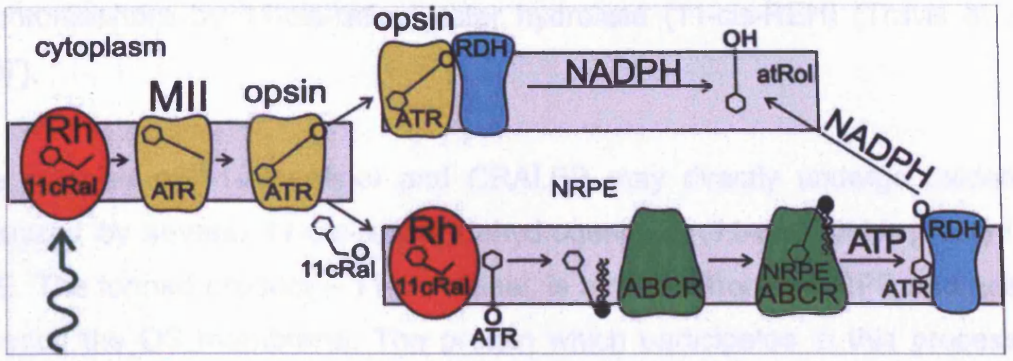

Figure 1.7 Bleaching of rhodopsin and ways of ATR reduction to ROL. Rh – rhodopsin, 11cRal – 11-*cis*-retinal, MII – metarhodopsin II, ATR – all-*trans*-retinal, RDH – retinol dehydrogenase, NRPE - N-retinylidine-phosphatidylethanolamine (adapted from Różanowska and Różanowski, 2008).

ROL is then moved to the RPE, which contain enzymes responsible for its conversion back to 11-*cis*-retinal (Chader et al., 1998; Forrester et al., 2002; Heck et al., 2003a; Heck et al., 2003; Różanowska and Sarna, 2005). ROL must be transported from the rod OS disc and across the OS plasma membrane. The protein involved in transport of ROL through the interphotoreceptor matrix (IPM) is interphotoreceptor retinoid-binding protein (IRBP) (Qtaishat et al., 2005). In the RPE, ROL is esterified by lecithin:retinol acyl transferase (LRAT), forming all-*trans*-retinyl esters: all-*trans* retinyl palmitate or stearate. Then, these molecules undergo isomerisation and hydrolysis. To form 11-*cis*-retinol, a microsomal membrane protein is essential – RPE65, which can interact with all-*trans*-retinyl palmitate (Jin et al., 2005; Wolf, 2005). This protein appears to have a role in the extraction of all-*trans*-retinyl esters from lipid membranes and is responsible for their isomerisation to 11-*cis*-retinol and a free fatty acid (Wolf, 2005; Maeda et al., 2006). The regulation of RPE65 isomerase activity has been suggested to depend on the non-photoreceptor opsin, the RPE-retinal G protein-coupled receptor (RGR) (Travis et al., 2007).

11-*cis*-retinol binds to cellular retinal-binding protein (CRALBP). It may be esterified by LRAT to form 11-*cis*-retinyl esters, which are a stable-storage form of retinoid. These esters can be hydrolyzed back to 11-*cis*-retinol for synthesis

of chromophore by 11-cis-retinyl ester hydrolase (11-cis-REH) (Travis et al., 2007).

The complex of 11-*cis*-retinol and CRALBP may directly undergo oxidation catalyzed by several 11-*cis*-retinol dehydrogenases (11-cis-RDHs) present in RPE. The formed product – 11-*cis*-retinal, is removed from the RPE and needs to reach the OS membrane. The protein which participates in this process is IRBP (Różanowska and Sarna, 2005).

In the OS discs, 11-*cis*-retinal can be bound to opsin. Firstly binding proceeds through a non-covalent bond at its "entry site" (Travis et al., 2007). Rhodopsin is then regenerated by formation of a covalent Schiff-base linkage between 11-*cis*-retinal and Lys296.

A summary of the visual cycle is presented below (Fig. 1.8).

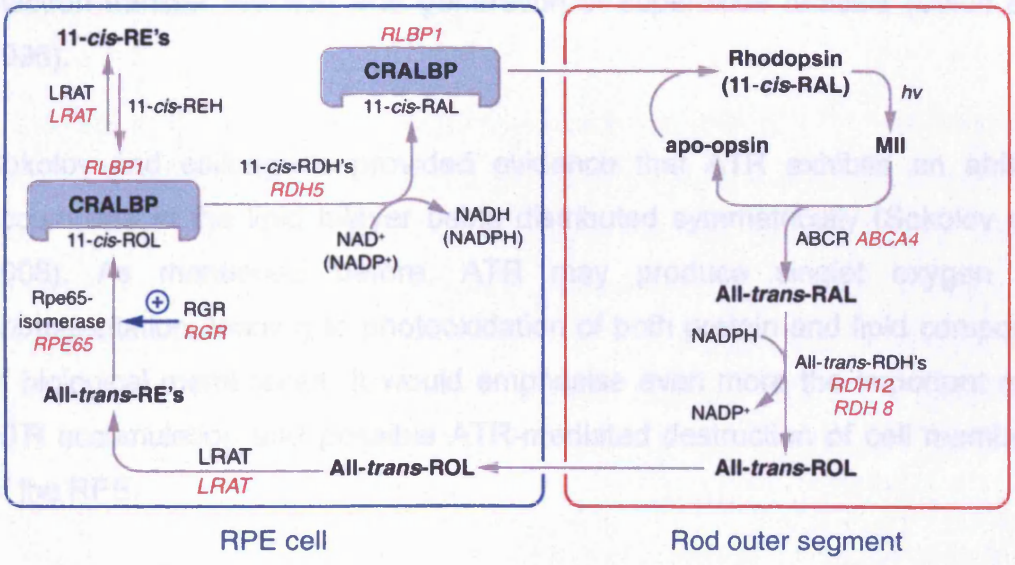

Figure 1.8 A summary of the visual cycle. Description in text. hv – a photon of light, MII – metarhodopsin II, ABCR - ATP-binding cassette transporter rim protein, RDH – retinol dehydrogenase, LRAT – lecithin:retinol acyl transferase, all-trans-RE's – all-trans-retinyl esters, RPE65 – RPE-specific 65 kDa protein, RGR – the RPE-retinal G protein-coupled receptor, CRALBP - cellular retinaldehyde-binding protein, RLBP1 - gene for CRALBP, 11-*cis*-RE's – 11-*cis*-retinyl esters (adapted from Travis et al., 2007).

1.3 All-*trans* retinal (ATR)

ATR is a major intermediate of the visual cycle described above. It is a product of photoisomerisation of rhodopsin chromophore – 11-*cis*-retinal, whose regeneration is essential for continuous renewal of the light-sensitive visual pigment.

A possible role of ATR in retinal damage has been an important subject of various studies since it has been shown that ATR is a potent photosensitiser (Delmelle, 1978a; Harper and Gaillard, 2001; Fu et al., 2003; Loginova et al., 2008). Its absorption spectrum includes the visible part of the electromagnetic spectrum. After photoexcitation with UV or blue light to its excited singlet state, ATR undergoes intersystem crossing, forming an excited triplet state. The energy of the excited triplet state can be transferred to molecular oxygen, resulting in the formation of singlet oxygen (Delmelle 1978a, Boulton et al., 2001; Pawlak et al., 2003). Moreover, the photoexcitation of ATR may lead to electron transfer reaction and generation of superoxide radicals (Dillon et al., 1996).

Sokolov and colleagues provided evidence that ATR exhibits an ability to accumulate in the lipid bilayer being distributed symmetrically (Sokolov et al., 2008). As mentioned before, ATR may produce singlet oxygen upon photoexcitation, leading to photooxidation of both protein and lipid components of biological membranes. It would emphasise even more the important role of ATR accumulation and possible ATR-mediated destruction of cell membranes of the RPE.

It needs to be stressed that ATR is susceptible to photodegradation, forming products absorbing shorter wavelengths. For example, photooxidation of retinal gives 5,8-endoperoxide in low yield as reported by Fu and colleagues (Fu et al., 2003). Products of irradiation of all-*trans*-retinal with white or gold fluorescent light depends on the solvents used – in chloroform, retinal isomerises to the 7-, 9-, 11- and 13-*cis* isomers, whereas irradiation in hexane results in the

formation of only the 13- and 9-*cis* isomers in significant quantities (Fu et al., 2003). Baron and colleagues (1989) identified photoproducts of photooxygenation of ATR in acetonitrile with laser irradiations (λ = 333.6 or 350.7 nm). In deoxygenated solutions, 13-*cis* and 9-*cis* retinal seem to be the major product, whereas all-*trans* and 13-*cis* 5,8-peroxyretinal are obtained in large amounts in oxygenated solutions. It has not been determined if photooxidation products of ATR retain photosensitising properties of ATR.

1.3.1 **Free ATR in the retina and its accumulation**

There is some debate on whether or not free ATR exists in the retina (reviewed by Różanowska and Sarna, 2005). However, recent studies seem to support the view on possible accumulation of free ATR (Maeda et al., 2009). Clearance of ATR after rhodopsin bleaching involves two steps: 1 - the translocation of ATR across the photoreceptor disc membranes by ABCR protein, 2 – reduction of ATR to ROL by RDH8 (expressed in outer segments) and RDH12 (located in inner segments of photoreceptors).

If the rate of rhodopsin regeneration exceeds the rate of ATR reduction at the opsin exit site, ATR is released to the lipid membrane and is not reduced to ROL. ATR can form condensation products with PE, forming NRPE, which is characterised by completely different photochemical properties (Różanowska and Sarna, 2005). As described before, NRPE is a substrate for ABCR protein, which flips it over to the cytoplasmic site and releases ATR upon hydrolysis of ATP. This makes ATR accessible for prRDH-mediated reduction.

It has been shown that ATR can induce photodamage to ABCR protein (Sun and Nathans, 2001), resulting in loss of its ATP-ase activity (Sun and Nathans, 2001). It is also suggested that the photodamage of ABCR *in vivo* may be needed to lock NRPE within the protein, thus further catalytic removal of ATR to the cytoplasmic site is disabled (Sun and Nathans, 2001). This results in the accumulation of ATR within the disc membrane. As a result, not only may NRPE be formed, but also conjugates of NRPE with other ATR molecules, such

as all-*trans*-retinal dimer-PE conjugate and predominantly A2PE (a precursor of a component of the age pigment, lipofuscin, described in sections below), as a product of condensation of another molecule of ATR and NRPE (Różanowska and Różanowski, 2008). Research on ABCR-/- mice and Stargardt's disease patients showed the presence of an increased concentration of PE in outer segments of photoreceptors in comparison with wild type mice and age-matched cadavers with no retinal disease, respectively (Weng et al., 1999). Thus, it is speculated that the higher concentration of PE may play a protective role, facilitating formation of NRPE when removal of ATR is delayed. Indeed, Mata and colleagues reported delayed clearance of ATR and elevated NRPE levels in the retina following light exposure in mice with knockout mutation on the *ABCR* gene (Mata et al., 2000). It needs to be stated that the formation of NRPE is not instantaneous. Thus, substantial concentrations of ATR may build up in the retina upon exposure to high levels of light together with efficient rhodopsin regeneration and induce (photo)oxidative damage to POS and neighbouring RPE (Różanowska and Różanowski, 2008). In addition, morphological examination of the RPE shows numerous intracellular lipofuscin-like inclusion bodies in ABCR-/- retinas (Weng et al., 1999). Also, various products of ATR and PE condensation are present such as A2PE, ATR dimer-PE conjugate, A2E (2-[2,6-dimethyl-8-(2,6,6-trimethyl-1-cyclohexen-1-yl)-1*E*,3*E*,5*E*,7*E*-octotetraenyl]-1-(2-hydroxylethyl)-4-[4-methyl-6-(2,6,6-trimethyl-1-cyclohexen-1-yl)-1*E*,3*E*,5*E*-hexatrienyl]-pyridinium) and various degradation products of A2E. In humans, *ABCR* mutations result in severe retinal degenerations, such as Stargardt's disease, recessive retinitis pigmentosa and cone-rod dystrophy. They are manifested by rapid accumulation of lipofuscin (described in detail below) early in life and are followed by degeneration of the outer retina, and finally, vision loss. Heterozygous mutations of *ABCR* have been correlated with increased risk of developing AMD (Allikmets, 2000).

Another enzyme involved in ATR clearance is photoreceptor dehydrogenase, prRDH. Research on the *prRDH* knockout mouse showed a 4-fold decreased of RDH activity in POS resulting in increased levels of ATR in POS after rhodopsin

bleaching (Maeda et al., 2005). Dark adaptation was found to be substantially slower in the knockout mice than in the wild type animals. Knockout animals were characterised by inhibited synthesis of ROL and all-*trans*-retinyl esters. Additionally, when animals were reared in 12h light/ 12h dark cycle for 7 to 9 months, they accumulated 4-fold greater amounts of A2E than wild type animals.

A loss of function mutations in the *RDH12* gene causes insignificant inhibition of NADPH-dependent RDH activity when compared with wild type animals (Maeda et al., 2006). As a result, levels of ATR were significantly increased after 3 minute bleaching of about 35% of rhodopsin followed by 30 minutes of dark adaptation in comparison with the wild type animals. Interestingly, levels of 11-cis-retinal were also increased in the mutant animals compared with the wild type animals. Although, the mechanism of the RDH12 influence on the 11-*cis*-retinal synthesis is not known yet, it can be suggested that the resulting faster rate of rhodopsin regeneration leads to a faster rate of ATR removal from the opsin "exit site" and thus, greater ATR accumulation in disc membranes resulting from constant irradiation. It may be the main explanation of a 2-fold increase of A2E levels in *RDH12* mice in comparison with wild type animals.

Maeda and colleagues provided direct evidence for the toxic effect of ATR accumulation (Maeda et al., 2008; Maeda et al., 2009). They reported that in mice lacking both RDH8 and ABCR, severe RPE/photoreceptor dystrophy at an early age is observed. The phenotype was characterised by the presence of drusen, basal laminar deposit, lipofuscin, choroidal neovascularization and Bruch's membrane thickening. Importantly, the condition was exacerbated by light. Retinylamine (a visual cycle inhibitor), on the other hand, was found to attenuate the changes. Moreover, it has been suggested that the mechanism of the toxicity may involve plasma membrane permeability and poisoning of mitochondria that results in caspase activation and cell death associated with mitochondria.

1.4 A2E and lipofuscin in the retina - formation and role

1.4.1 Composition of lipofuscin

As mentioned above, ATR can form complexes with PE in the POS membrane leading to formation of NPRE. Products of further chemical transformation of NRPE and ATR have been found to be one of the components of the age-pigment present in the RPE – lipofuscin. Lipofuscin is a heterogenous material consisting of different lipids and proteins. It constitutes residual bodies, accumulated within the RPE and is a common morphological symptom of the aging process. Bodies contain the residues of incomplete digestion of photoreceptor outer segments, which provide a unique group of proteins and more importantly, retinoids and their metabolites (Katz and Redmond, 2001). These products undergo certain modification such as glycosylation and oxidation, before they form a final product (Kennedy et al., 1995; Boulton et al., 2004). It was also shown that the increase in accumulation of lipofuscin occurs during vitamin E deficiency. The great reduction in the accumulation of lipofuscin, on the other hand, occurs during vitamin A deficiency (Boulton et al., 2004).

Lipids and proteins account for at least 93% of the dry mass of lipofuscin. Free fatty acids (~40%), PE (~13%) and phosphatidylcholine (~30%) have been the main lipids found in lipofuscin granules (Bazan et al., 1990). Proteomic analysis of lipofuscin revealed up to 160 proteins, including proteins of photoreceptor outer segments, mitochondrial and endoplasmic origin, several lysosomal enzymes, retinoid chaperones as well as proteins originating from erythrocytes and blood plasma (reviewed by Różanowska and Różanowski, 2008). Proteins found in the granules exhibit various oxidative modifications, shown by the presence of components such as adducts with products of lipid peroxidation: carboxyethylpyrrole, malondialdehyde, 4-hydroxynonenal or with advanced glycation end products (reviewed by Glenn and Stitt, 2009).

Recent studies show that after treatment of lipofuscin granules with SDS and proteases, only minimal levels of proteins are retained in the granules but confirm the presence of oxidised lipid-protein adducts and A2E (Gu et al., 2003; Ng et al., 2008).

Several fluorophores of lipofuscin have been identified and A2E is one of them (Lamb and Simon, 2004; Różanowska and Sarna, 2005; Sparrow and Boulton, 2005). It is a product of condensation of ATR with PE, that is followed by binding of another molecule of ATR to the Schiff base and oxidation to form a pyridinium bis-retinoid. The phosphate ester is finally hydrolysed to A2E (Ben-Shabat et al., 2002; Boulton et al., 2004; Różanowska and Sarna, 2005; Sparrow and Boulton, 2005). There are two forms of this molecule: A2E and *iso*-A2E. Both are generated from the precursor phosphatidyl-pyridinium - A2-PE, by phosphate hydrolysis (Sparrow et al., 2003). A2E is found as a factor with amphiphilic properties, which can cause membrane permeabilization, inducing leakage of lysosomal membranes (Schutt et al., 2002). Leakage of toxic compounds and hydrolytic enzymes may result in the damage of cellular structures. It was suggested that *via* this mechanism, A2E may be a pronecrotic molecule in the RPE (Schutt et al., 2002). Accumulated A2E may interfere with normal function of lysosomes. The addition of A2E to the RPE led to some disturbance of the acidic intralysosomal milieu. The result of this process was a decrease in hydrolase activity and accumulation of undegraded substances (Holz et al., 1999). It was shown that A2E may inhibit degradation of low-density lipoproteins and POS lipids, whereas the influence on the rate of degradation of POS proteins was not observed (Finnemann et al., 2002; Fishkin et al., 2003).

Another conjugate of two molecules of ATR with PE has been detected and is called ATR-dimer-PE (Fishkin et al., 2005). Both A2E and ATR dimer-PE conjugate are susceptible to oxidation and photodegradation (reviewed by Różanowska and Różanowski, 2008). The presence of several derivatives of those compounds has been revealed in the human RPE, including mono- and

poly- peroxy-A2E, and furan-A2E derivatives as well as many carbonyl derivatives of A2E.

1.4.2 **Distribution of lipofuscin in the retina**

Accumulation of lipofuscin is not uniform across the retina. The greatest number of lipofuscin granules is in the parafoveal area corresponding to the greatest rod density (Różanowska and Różanowski, 2008).

1.4.3 **Formation of lipofuscin**

Phagocytosed POS seem to be the main substrate for lipofuscin formation in the RPE (Feeney, 1978; Katz, 1989; Boulton et al., 1989). Studies on animals show substantially diminished accumulation of RPE lipofuscin in rats, with a mutation in the gene encoding a tyrosine kinase, which is essential for phagocytosis of shed POS (*MERTK)* (D'Cruz et al., 2000). Lack of this enzyme has been shown to eventually lead to photoreceptor death (Gal et al., 2000). However, an up to 2 year long-term culture of the RPE without POS revealed the presence of accumulated fluorescent material (Burke and Skumatz, 1998). This suggests that autophagy may also play a role in lipofuscin accumulation in the RPE.

Acceleration of lipofuscin accumulation can occur due to lysosomal dysfunction (Katz, 1989; Rakoczy et al., 2002). Rapid accumulation of intracellular material with autofluoresent properties was observed in rats and dogs upon inhibition of lysosomal proteases (Katz, 1989). Moreover, it has been demonstrated that expression of an inactive cathepsin D – a RPE lysosomal enzyme involved in degradation processes of POS rhodopsin, in transgenic mice was correlated with the accumulation of a substantially greater number of fluorescent residual bodies in the RPE when compared with wild type mice (Rakoczy et al., 2002).

Since early studies, oxidative conditions have been suggested to play a significant role in lipofuscin formation (reviewed in Różanowska and

Różanowski, 2008). Experiments on the RPE *in vitro* and animals *in vivo* show that lipofuscin formation is stimulated by oxidative stress, while the presence of antioxidants counteracting the oxidants formed in the retina, has been correlated with a reduction of lipofuscin formation. Injection of iron ions (a potent mediator of oxidative stress due to the involvement in decomposition of lipid hydroperoxides and hydrogen peroxide, leading to the formation of hydroxyl radicals and free radical-mediated chains of lipid peroxidation) results in the accumulation of autofluoresent granules within the RPE of rat retinas within a week following the injection (Katz et al., 1994). Another study showed that oxidized protein-lipid complexes may have an effect on activation and lysosomal maturity, indirectly inhibiting different signalling molecules or forming products which are resistant to lysosomal digestion (Hoppe et al., 2004a,b).

The critical factor for lipofuscin accumulation involves hydrolysis and clearance of isomerised rhodopsin chromophore, ATR, from opsin. Inadequate clearance of ATR may lead to formation of NRPE and other products of ATR condensation as discussed before. The presence of the regeneratable visual pigment has been shown to be required for accumulation of RPE lipofuscin (Katz et al., 1999; Katz and Redmond, 2001), and there is a strong association between exposure to light and lipofuscin accumulation (Boulton et al., 2004; Różanowska and Różanowski, 2008).

Impairment of the regeneration of 11-*cis*-retinal within the RPE, caused either by defective or absent RPE65 protein, was shown to result in inhibition in the accumulation of A2E (Katz and Redmond, 2001; Kim et al., 2004). 13-*cis*-retinoic acid (Isotretinoin; Accutane) has been shown to slow down 11-*cis*-retinal synthesis due to competitive binding to RPE65 and 11-*cis*-RDH, and also blocks the slower, age-dependent accumulation of A2E/lipofuscin in wild-type mice (Law and Rando, 1989; Radu et al., 2003; Gollapalli and Rando, 2004). It would suggest that the accumulation of lipofuscin and its chromophores depends also on the supply of 11-*cis*-retinal to the OS.

1.4.4 Spectral and fluorescent properties of lipofuscin

Morphologic features of lipofuscin granules are similar in each of the age groups but age-related changes in their spectral properties are observed (Boulton et al., 2004). Results of the optical absorption measurements indicate that lipofuscin has a broad-band absorption including the UV and visible spectrum. This complex is characterised by yellow-orange autofluorescence after excitation with UV and blue light (Boulton et al., 2004). Excitation of lipofuscin granules with 364 nm is characterised by emission with a broad maximum at 600 nm with multi-exponential decay (Boulton et al., 1990). Its absorption and fluorescent properties undergo age-related changes. Thus, it could be concluded that the chromophores and/or the environment of fluorophores of lipofuscin granules change with age.

1.4.5 Toxicity of retinal lipofuscin

Dorey and colleagues revealed a correlation between age-dependent lipofuscin accumulation and loss of photoreceptor cells (Dorey et al., 1989). It has been suggested that it may be related to a certain threshold level of lipofuscin, and exceeding of this threshold can cause dysfunction of the RPE leading to photoreceptor death. This scenario may underlie the formation of atrophic areas in the outer retina similar to the ones observed in age-related macular degeneration (AMD, described in details below), as suggested by others (Schmitz-Valckenberg et al., 2006). Racial distribution, age-relationship and spatial topography seem to be remarkably similar to degeneration patterns seen in AMD. However, it has been arguable whether lipofuscin is just a marker of progression of the atrophy or a causative factor (Różanowska and Różanowski, 2008).

In vitro studies of lipofuscin properties showed that it exhibits photosensitising properties. Irradiation of purified lipofuscin granules under aerobic conditions lead to the formation of reactive oxygen species including superoxide radical, singlet oxygen, hydrogen peroxide, lipid-derived aldehydes and lipid

hydroperoxides (Różanowska and Różanowski, 2008). It has been proven to mediate photo-induced oxidation of extragranular proteins and lipids. It has been also shown that lipofuscin is (photo)toxic to the RPE *in vitro* and is responsible for an age-related increase in susceptibility of human RPE to photooxidation (Boulton et al., 2004).

Lipofuscin is also capable of inactivating enzymes (such as catalase and acid phosphatase) and reduces the efficacy of antioxidant and lysosomal systems (Shamsi and Boulton, 2001). It was shown that lipofuscin is also able to compromise DNA integrity and cause RPE atrophy (Boulton et al., 2004). Oxidative stress imposed to the RPE by lipofuscin may induce pro-inflammatory and pro-angiogenic signalling (Różanowska and Różanowski, 2008). It has been demonstrated that A2E, as a component of lipofuscin, induces up-regulation of cyclooxygenase-2 – a potent pro-inflammatory factor, in ARPE-19 cells (Lukiw et al., 2006). Moreover, monitoring of the cleavage products of complement component C3, known to trigger inflammatory responses, in cultures, ARPE-19 cells have revealed that implementation of oxidative stress by blue light irradiation leads to activation of complement cascade in human serum in contact with the RPE (Zhou et al., 2006). The presence of A2E during exposure to light causes increased activation of complement. In addition, identified products of A2E oxidation – peroxy- and furano-A2E, are correlated with a significantly higher level of C3 cleavage product – iC3b.

Since the RPE is considered to be a major source of antiangiogenic and angiogenic factors, any dysregulation of the balance between them may potentially lead to the development of choroidal neovascularisation. Some lipofuscin components such as 4-hydroxy-2-nonenal and A2E+light have been shown to up-regulate VEGF expression, which can promote choroidal neovascularisation (reviewed by Różanowska and Różanowski, 2008).

Studies involving lipofuscin have shown that it is a photoreactive molecule with the capacity to generate reactive oxygen species and impose an oxidative

stress within the cell, while certain components of lipofuscin exhibit pro-inflammatory and pro-angiogenic properties. Thus, lipofuscin is likely to contribute to diseases of the retina such as age-related macular degeneration (AMD).

1.5 Age-related macular degeneration – AMD

1.5.1 Age-related changes in the outer retina

As mentioned before, the retina, the outer part in particular, undergoes many age-related changes due the nature of its environment. Damage of the retina through free radical generation can be manifested at the level of photoreceptors, Bruch's membrane-RPE complex and dysfunction of the RPE leading to atrophy of the outer retina (reviewed by Glenn and Stitt, 2009). Thickening of Bruch's membrane can lead to re-modelling of this extracellular matrix, having serious implications for the RPE, which relies on the proper functioning of Bruch's membrane (Starita et al., 1996). The main changes observed in aging is a reduction in RPE density and a decrease in melanin content, altered lysosomal degradative capacity and proteasome in surviving cells (reviewed by Glenn and Stitt, 2009). As mentioned above, lipofuscin accumulation occurs throughout life, which can be visualised in the fundus due to its cytoplasmic autofluorescence. It is accompanied by the formation of extracellular deposits referred to as drusen or basal laminar deposits (BLD) between the RPE and inner layer of Bruch's membrane (reviewed by Glenn and Stitt, 2009).

1.5.2 Characteristics of AMD

Age-related macular degeneration (AMD) is a leading cause of severe visual impairment in the elderly (Berger et al., 1999). It is a retinal degenerative disease, affecting primarily people over 65 years of age (Zurdel and Richard, 2001; Constable, 2004). The sick may suffer due to the loss of substantial

numbers of photoreceptor cells, which is observed particularly in the central part of the retina (Curcio et al., 1996). Early stages of AMD are manifested by funduscopically-visible focal drusen and/or pigmentary changes, while late stages are implicated by choroidal neovascularisation and/or RPE atrophy that lead to severe visual loss (Schutt and Holz, 2001).

AMD is divided into the wet (exudative) type and the dry (non-exudative) type, which is the most prevalent (Thompson, 2006). In the case of dry AMD there is deposition of basal laminar deposits (BLD) and drusen, including debris at the level of Bruch's membrane. It is thought that the origin of debris is incomplete metabolism of degenerating RPE, leading to the accumulation of undegraded products (Thompson, 2006). The debris is believed to impair transport of oxygen, nutrients and waste products between the RPE and choriocapillaris, leading to RPE dysfunction and death, followed by death of neighbouring photoreceptors. Only a minority of patients with dry AMD may progress to geographic atrophy, which is gradually progressive and may lead to central visual loss (Cook et al., 2008).

Wet AMD is characterised by the separation of the integrity of the Bruch's membrane/RPE complex, forming a pigment epithelial detachment. The second feature of this type of AMD is neovascularisation manifested by the ingrowth of new vessels, which originate from the choroid (Zurdel and Richard, 2001). In the end-stage of the disease, changes referred to as the wet form of AMD result in an atrophic or fibrovascular macular scar and permanent damage to central vision (Cook et al., 2008).

1.5.3 **Risk factors of AMD**

1.5.3.1 Genetic factors

There have been several genes identified and associated with a significantly greater risk of AMD development: heat shock serine protease (HTRA1), age-related maculopathy susceptibility 2 (ARMS2; known also as *LOC387715*),

complement factor H (CFH), complement component 3 (C3), complement factor B (BF), complement component 2-complement factor B (C2-CFB) and Apolipoprotein E (ApoE) (reviewed by Ting et al., 2009 and Katta et al., 2009).

Htra1 serine peptidase is a heat shock serine protease, suggested to play a dual role in the degradation of extracellular matrix proteins (ECM) and in cellular survival or growth (Oka et al., 2004; Ding et al., 2009). Extracellular protease activities of Htra1 may favour neovascularisation in chronic inflammatory conditions. It may involve enhanced degradation of ECM through increased expression of matrix metalloproteinases (Grau et al., 2006) or binding to one of the angiogenic factors - transforming growth factor (TGF)-ß (Oka et al., 2004). Since Htra1 is a member of the inhibitor of TGF-ß family, blockage of its proteolytic activity may lead to a restoration of TGF-ß signalling and subsequent neuronal death (Launay et al., 2008). In addition, TGFß may potentially play a role in the inhibition of the immune response (Launay et al., 2008).

The function of the *ARMS2* gene is still poorly understood (Rivera et al., 2005; Scholl et al., 2007). However, the *ARMS2* polymorphism shows a strong association with AMD.

Complement factor H (CFH) is responsible for the inhibition of multiple steps of the alternative pathway of inflammation (Janeway et al., 2001). It has been demonstrated that CFH binds C-reactive protein (CRP) and inhibits the response to tissue damage mediated by CRP. CFH dysfunction may lead to impairment of the complement-mediated removal of cellular debris, resulting in enhanced inflammation between the RPE and the choroid.

The BF and C2 are involved in the controlling of the complement pathways, being activators of alternate and classical pathways, respectively (Katta et al., 2009). C3 is an important plasma protein and its activity is critical for the formation of the terminal membrane attack complex (MAC), leading to cell lysis (Katta et al., 2009).

ApoE is a lipophilic glycoprotein playing an integral role in cholesterol and lipid transport (Mahley, 1988). Klaver and colleagues (Klaver et al., 1998) suggested that an active biosynthesis of the glycoprotein is required to efficiently support the high rate of renewal of photoreceptors in the region of the macula.

Some studies suggested that mutation of the *ABCA4* gene may be correlated with a higher risk of AMD since they are present in older patients with AMD (Allikmets et al., 1997; Allikmets, 2000). However, other studies are in opposition to the hypothesis, suggesting a lack in significance of the mutations in patients with AMD (Kuroiwa et al., 1999; Guymer et al., 2001; Webster et al., 2001; Schmidt et al., 2003).

There was a great variety in the prevalence of AMD among different ethnic groups observed (Katta et al., 2009). The prevalence of all forms of AMD was relatively greater in the white populations (1.91 – 3.5 %) compared to the non-whites (0.19 – 1.4 %) (Friedman et al., 1999; Bressler et al., 2008).

1.5.3.2 Environmental factors

There are several environmental risk factors for AMD, such as age, ethnicity, cigarette smoking, hypertension and chronic exposure to light (reviewed by Katta et al., 2009). There are some additional putative risk factors including increased C-reactive protein in serum, increased white blood cell count, diets rich in baked goods, female gender, hyperopia and blue iris colour (Spaide, 2006). Some studies showed a correlation between the prevalence of AMD and systemic hypertension (Hyman et al., 2002; Clemons et al., 2005), greater BMI (Klein et al., 1994; van Leeuwen et al., 2003; Johnson, 2005) and cataract surgery (Wang et al., 2003; Nirmalan et al., 2004).

It has been demonstrated that age is a consistent risk factor of AMD (Katta et al., 2009). Subjects in the age group of 60-80 years exhibited a three-fold

greater risk of developing an advanced stage of AMD when compared with subjects <60 years.

It has been shown that prior and current smokers are prone to show signs of AMD at least 5-10 years before non-smokers (Delcourt et al., 1998; Age-Related Eye Disease Study Research Group, 2000; Berendschot et al., 2002), and a two or greater risk ratio was observed for neovascular AMD. It was speculated that the mechanism behind the harmful effect of smoking may involve oxidative stress to the outer retina that may affect the antioxidant metabolism and lowering the levels of circulating antioxidants (Berendschot et al., 2002).

The role of light in the development of AMD will be discussed in detail in the section below.

1.5.4 **The role of light in retinal damage**

The interior structures of the eye determine the spectral characteristic and irradiance of the retina (Boettner and Wolter, 1962). A progressive build-up of UV-absorbing chromophores in time leads to a reduction in the spectrum of light that reaches the retina, and by the age of 22, only visible light above 390 nm is effectively transmitted through the lens. A gradual decrease in transmission to the retina of short-wavelength visible light is a characteristic feature for aging (Dillon et al., 2004).

There have been many cases of retinal photodamage reported in various studies. Gazing at the sun while watching a solar eclipse has been shown to lead to damage to the retina (Young, 1988; Schatz et al., 2004). Exposure to mid-day sun (1.5 - 12 W/cm^2 depending on the diameter of the pupil; Friedman and Kuwabara, 1968; Ham et al., 1978) lasting several minutes to tens of minutes were associated with ophthalmoscopically visible damage to the retina. Studies of Friedman and Kuwabara (1968) showed that in monkeys, 5-450X smaller retinal irradiance levels of retinas with similar duration of exposure

caused retinal damage that could be detected upon histological examination. Several studies provide evidence for the view that even ocular surgery in humans may impose a risk of light-induced damage to the retina (McDonald and Irvine, 1983; McDonald and Harris, 1988; Poliner and Tornambe, 1992). The retinal irradiance from an operating microscope during surgery can reach up to 0.97 W/cm^2 and the procedure may take up to 2 hours (Kirkness, 1986).

Although the behavioural aversion response to bright light and ocular geometry provides protection against exposure to excessive fluxes of visible light reaching the retina, estimated to be in a range of 0.01 - 0.1 mW/cm^2 (Sliney, 1983), the mechanisms are insufficient to completely prevent retinal photodamage (Sliney, 2002). It has been shown that chronic exposure to bright sunlight may result in reduced visual acuity and impairment of dark adaptation and night vision (Marlor et al., 1973). The susceptibility to retinal photodamage may also be associated with genetic background (Dowling and Sidman, 1962; Heckenlively et al., 1991). Heckenlively and colleagues (1991) showed that the severity of retinitis pigmentosa in patients with the proline-23-histidine (P23H) mutation in rhodopsin (it results in a poor ability to fold properly after synthesis) is associated with a history of strong exposure to the sun or other light sources. Transgenic mice carrying the same mutation were shown to be more susceptible to photodamage than wild-type animals (Wang et al., 1997; LaVail et al., 1999; Organisciak et al., 2003; Vaughan et al., 2003).

Analysis of the wavelength dependence of light-induced retinal damage revealed differences between diurnal primates and nocturnal animals such as rats, which are more susceptible to light damage than diurnal primates. The action spectrum of retinal damage with its peak at 500 nm was observed only in rats that were adapted to circadian dim light/dark cycles for at least 2 weeks (Noell et al., 1966; Williams and Howell, 1983). The most damaging wavelength corresponds to the absorption maximum of rhodopsin. In rhesus monkeys, the damage can be induced selectively by green, red or blue light (Harwerth and Sperling, 1975; Sperling et al., 1980). Repeated exposure to blue

light led to an irreversible loss of sensitivity to blue light and degeneration of blue cones, whereas the function of red and green cones was recovered after induced damage. Exposure of the retina to relatively high irradiance levels leads to similar action spectra observed in both rodents and primates, indicating that there is a rapid increase in efficiency of retinal damage induction below 500 nm, and a further increase with decreasing irradiation wavelength up to the shortest monitored wavelength of 320 nm (Ham et al., 1982; Gorgels and van Norren, 1995). The threshold doses of UV and short-wavelength blue light in the range of 320-440 nm are associated with damage of only photoreceptors (Gorgels and Vannorren, 1995), whereas damage induced by longer wavelength blue light (>440 nm) also affects the RPE (Ham et al., 1978; Gorgels and van Norren, 1995).

1.5.5 **The role of light in the development of AMD**

The role of light in the development of AMD has been questionable and there have been conflicting reports on the association of visible or ultraviolet light with the disease. The results of West and colleagues, based on a survey conducted on 838 Maryland watermen, suggested that age-related macular degeneration was not associated with cumulative exposure to either UV-A or UV-B (West et al., 1989). Darzins and colleagues (1997) did not find any association between light exposure and a higher risk of AMD development after examining 409 cases and comparing them with 286 control subjects resident in Newcastle, Australia. In their study, sensitivity to sunlight and glare of the participants was characterised, and sun exposure was determined from detailed histories, validated against avoidance or sun-seeking expected behaviour. This was supported by a population-based study in the UK of Khan and colleagues (2006). They compared 446 cases with end stage AMD and 283 spouse controls and based their evaluation of AMD on stereoscopic colour fundus photographs as well as clinical examination. A study by Delcourt and colleagues (2001) did not support a deleterious effect of sunlight exposure in AMD either. Their study included 2584 residents of the town of Sète, France. Early and late

AMD was assessed using an international classification system on the basis of 50 degree colour fundus photographs.

Cruickshanks and colleagues (1993) did not find an association between light exposure and early age-related maculopathy in 2649 women. However, they reported that the light exposure was associated with increased retinal pigment in men after adjusting for the time spent outdoors and age. The amount of leisure time spent outdoors in summer was found to be significantly associated with exudative macular degeneration and late maculopathy. The presence of AMD was determined by grading of stereoscopic colour fundus photographs.

Analysis performed by Taylor and colleagues (1990) to determine whether ocular exposure to violet light (400 to 450 nm), blue light (400 to 500 nm), or all visible light (400 to 700 nm) was associated with AMD, showed that high levels of exposure to blue and visible light late in life may be important in causing AMD. Their analysis included detailed histories of ocular sun exposure in 838 watermen who worked on the Chesapeake Bay. They assessed the presence and severity of AMD based on stereo macular photographs. The findings were further confirmed by the same group in further analysis of the correlation between exposure to light and development of AMD based on the group of watermen (Taylor et al., 1992).

The Beaver Dam Eye Study on the relationship between iris colour, hair colour, and skin sun sensitivity (Tomany et al., 2003) performed on a population of 4926 adults (range, 43-86 years of age at baseline) living in Beaver Dam, Wisconsin, showed that people with brown eyes were significantly more likely to develop soft indistinct drusen compared with people with blue eyes. People with brown eyes exhibited a significantly lower likelihood to develop retinal pigment epithelial depigmentation than blue-eyed individuals. Hair and iris colour were found to be associated with the 10-year incidence of pigmentary abnormalities, whereas iris colour appears to be inconsistently related to the 10-year incidence of early AMD lesions and the progression of the disease. Age-related

maculopathy status was assessed by grading stereoscopic colour fundus photos with the Wisconsin Age-Related Maculopathy Grading System. A recent study by Hirakawa and his group (Hirakawa et al., 2008) showed significantly more facial wrinkling and less facial hyperpigmentation present in late age-related macular degeneration cases when compared with controls. The study of Japanese men aged ≥50 years (67 controls and 148 with AMD separated into groups of early (n=75) and late (n=73) AMD) was based on early and late AMD association with facial wrinkle length and area of hyperpigmentation, considered to be associated with exposure to sunlight (measured by imaging with computer-based image analysis). It supports the hypothesis that sunlight is an important factor in the progression of late AMD.

1.5.6 **Processes underlying development of AMD**

As discussed in the previous sections AMD is a multifactorial disease with a strong genetic component predisposition. Although the pathology of AMD is still unclear, increasing evidence suggests that it may involve chronic inflammation (reviewed by Barouch and Miller, 2007). It is speculated that constituents of drusen present in predisposed individuals may cause an inflammatory response, resulting in secondary damage to the RPE and changes in regulation of growth factors leading to choroidal neovascularisation (Swaroop et al., 2009).

It has been considered that the constituents of drusen may stimulate the local activation of the complement system, resulting in further growth of drusen (Barouch and Miller, 2007). In the protection of host cells from pathogens, removing debris, and enhancing immune responses, activated complement CFH leads to destruction of foreign or damaged cells by the membrane attack complex (reviewed by (Barouch and Miller, 2007). Alterations of CFH could result in the destruction of normal and intact ocular cells.

The RPE is considered as the primary site of dysfunction, culminating in the retinal degeneration and neovascularisation of the retina associated with AMD

(Beatty et al., 2000). A correlation between AMD and RPE lipofuscin content has been reported, but a cause-and-effect relationship between retinal lipofuscin accumulation and the development of AMD has not been established (Katz, 2002). Lipofuscin accumulation causes the increased risk of damage to the RPE, which plays a pivotal role for the maintaining the proper function of photoreceptor cells. As mentioned before, increased levels of lipofuscin are correlated with photoreceptor cell loss, leading to visual impairment (Katz and Robison, 1986; Gao and Hollyfield, 1992; Curcio et al., 1993). It was observed that lipofuscin distribution in the retina is similar to the distribution of changes characteristic for AMD, and the contribution of its toxic effects to development of AMD is likely (Boulton et al., 2004).

Rapid rhodopsin regeneration is related to the release of ATR from regenerated rhodopsin before its reduction, and accumulation of the retinoid within the photoreceptor outer segments, allowing it to induce oxidative damage. There is a great need to find the implications of photobleaching of rhodopsin and its regeneration, leading to retinal photodamage and accumulation of (photo)toxic components in the RPE. It will allow us to understand the initial damage in severe retinal diseases, including AMD. It is hypothesised that the initial damage may be induced by ATR released from visual pigment, which propagates in the course of time as a result of the formation of non-degradable products (lipofuscin) in the RPE. Eventually, clinically recognised changes develop in the retina, which are classified as AMD.

A summary of AMD pathogenesis, where initial steps involve generation of reactive oxygen species, is presented in Figure 1.9.

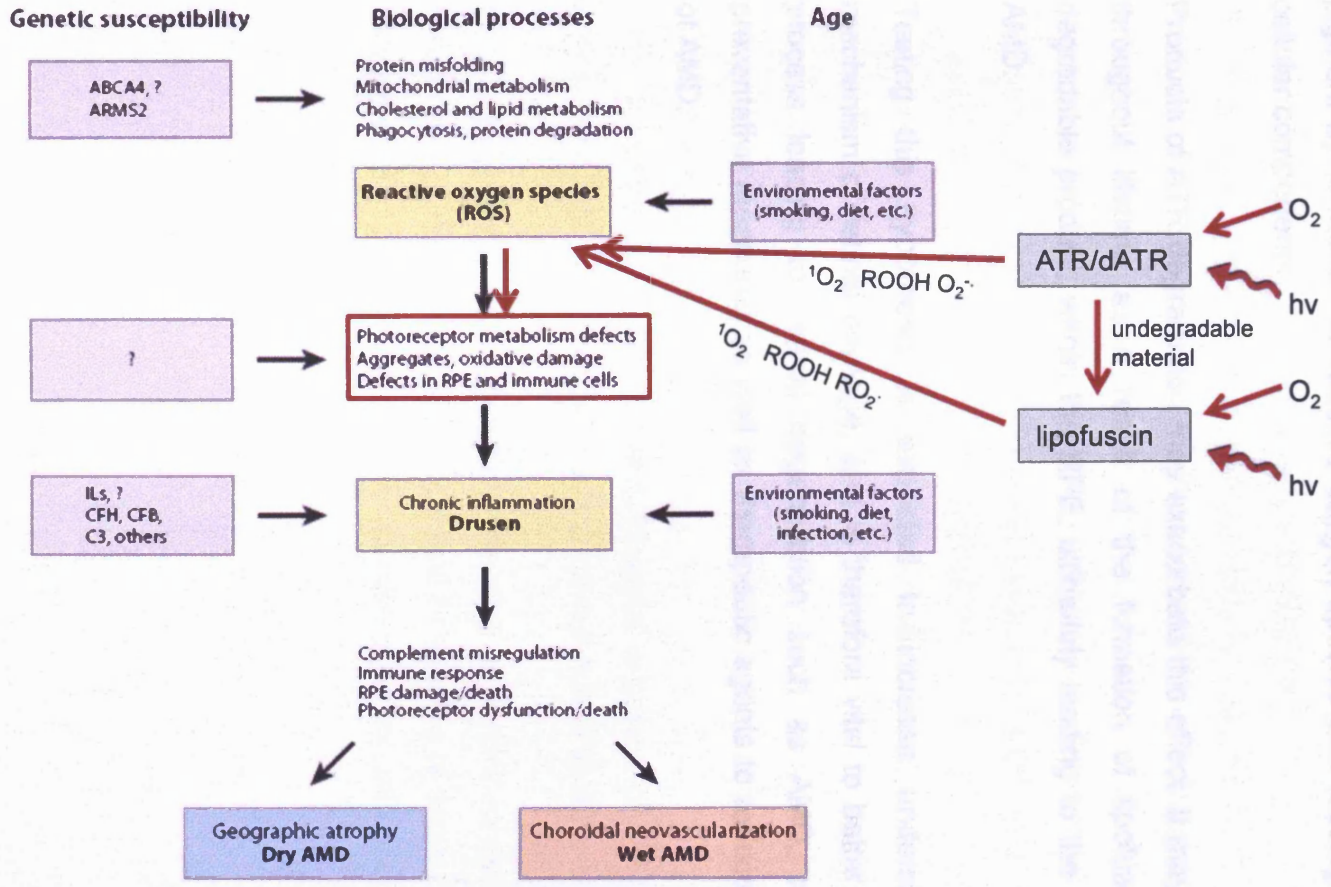

Figure 1.9 A model of AMD pathogenesis (adapted from Swaroop et al., 2009). Red arrows indicate the pathways tested in the thesis. Wavy arrows = light (hv).

1.6 **Hypothesis**

There is strong evidence implicating photobleaching of rhodopsin and its regeneration leading to photodamage to the retina as well as the accumulation of (photo)toxic components in the RPE. The implications are crucial for understanding the initial damage in severe blinding diseases such as AMD. It is hypothesised that the initial damage is induced by ATR released from the visual pigment by formation of reactive oxygen species and leading to oxidation of cellular components.

Products of ATR degradation may exacerbate this effect. It may be propagated throughout lifetime as a result of the formation of lipofuscin - the non-degradable product, within the RPE, ultimately leading to the development of AMD.

Testing this hypothesis is expected to increase understanding of the mechanism of retinal damage, and is therefore vital to better understand the process leading to retinal degeneration such as AMD, and to develop preventative measures as well as therapeutic agents to reduce the prevalence of AMD.

1.7 Aims of this project

The overall aim of this project is to gain insight into the role of the visual pigment in the oxidative stress in the retina causing retinal damage. To achieve this, the study is divided into several specific objectives:

- assess the kinetics of ATR hydrolysis after rhodopsin bleaching and ROL formation at room temperature and physiologically-relevant conditions
- investigate the ability of ATR to generate singlet oxygen depending on its position in opsin and the presence of ATP/NADPH
- assess the susceptibility of POS lipids to oxidation
- investigate the effects of ATR and products of its degradation (dATR) on RPE cell function and viability
- determine whether selected antioxidants: α-tocopherol, ROL, retinyl ascorbate, ascorbyl palmitate, N-acetyl-cysteine, glutathione and vitamin B_6 can prevent (photo)toxic effects of ATR and dATR
- determine the ability of ATR and dATR to generate singlet oxygen depending on excitation wavelength
- assess the ability to photosensitise singlet oxygen generation and rate constants of singlet oxygen quenching by selected compounds tested in the (photo)toxicity study
- investigate the effect of simultaneous exposure of the RPE to POS +/- ATR and +/- light on cell viability and accumulation of lipofuscin-like deposits

The investigations are needed to develop a further understanding of the mechanism of retinal (photo)damage and of the role of exposure to light in the development of age-related macular degeneration and retinal blindness.

Chapter 2

Materials and methods

All chemicals were purchased from Sigma, UK, unless stated otherwise.

2.1 POS preparations

2.1.1 Extraction of bovine retinas from fresh eyes

Freshly enucleated bovine eyes were obtained from an abattoir. To extract the retinas, the anterior portions of the eyes were removed by circumferential incision. Then the vitreous was discarded and the retina was gently detached and dissected by cutting at the optic nerve.

2.1.2 Dark-adapted frozen bovine retinas and fresh retinas

Frozen dark-adapted retinas were obtained from Wanda Lawson Co. (Lincoln, Nebraska, USA). They were stored at -80°C and thawed by overnight storage at 4°C just before isolation of POS.

Fresh bovine retinas were obtained from an abattoir. Retinas were isolated from eyes after muscle and fat were removed from the orbit. An incision was made in the orbit, using a scalpel, and the anterior segment and vitreous were removed using scissors. The retina was gently detached from the eye cup and cut at the optic nerve. Retinas were either used immediately to isolate POS or refrigerated, and POS were isolated within 12 hours.

2.1.3 Photoreceptor outer segments isolation

Photoreceptor outer segments were isolated under dim red light on ice according to the modified technique of Papermaster (Papermaster, 1982). The procedure described below was performed on 50 retinas. 15 ml of homogenisation medium (see Table 2.1) was added to 25 retinas, and the retinal mixtures were passed through a Teflon hand-held 50 ml homogeniser three times. The retinal mixture was then homogenised with a second 50 ml homogeniser three times. The homogenate was decanted into cold centrifuge tubes. These steps were repeated for the remaining 25 retinas. The

homogenate was centrifuged at 1500 × g for 4 min at 4°C (U-32R; BOECO, Germany; Hettich Zentrifugen 1617 rotor).

	Fresh retina (34% w/w)	Frozen retina (30% w/w)
42% sucrose	191 g	162 g
1 M NaCl	13 ml	13 ml
0.1 M $MgCl_2$	0.4 ml	0.4 ml
1 M Tris-acetate	1 ml	1 ml
Add ddH_2O to obtain:	230 g	226 g

Table 2.1 Composition of homogenisation media for POS isolation from fresh or frozen bovine retinas.

The supernatant was decanted into cold centrifuge tubes while the pellet was re-homogenised with a further 15 ml of homogenisation medium then homogenised as above. The homogenate was centrifuged at 1500 × g for 4 min at 4°C (U-32R; BOECO, Germany; Hettich Zentrifugen 1617 rotor).

The final volume of the supernatant was determined before being transferred to a cold 500 ml conical flask. Two volumes of 0.01 M Tris-acetate buffer (ice cold, pH 7.4) were added slowly whilst stirring. The POS were then pelleted at 1800 × g for 10 min at 4°C. The pellet was re-suspended in 1.10 g/ml sucrose solution (Tab. 2.2). Sucrose gradients were prepared using ice-chilled 1.15 g/ml and 1.11 g/ml solutions of sucrose.

The re-suspended pellet was passed consecutively through 18- and 21-gauge needles rapidly ejecting the homogenised solution against the wall of the plastic tube. Crude POS suspended in 1.10 g/ml sucrose were then gradually layered onto the sucrose gradient. The gradients were then spun at 100000 × *g* for 30 minutes at 4 °C in an ultracentrifuge (Sorvall Ultra-Pro 80, Sorvall Products, L.P., Newtown, Connecticut).

POS were located in the interface sucrose solutions. The POS were removed using a sterile Pasteur pipette, recovered by dilution with 0.01 M Tris-acetate and sedimented at 70000 × *g* for 20 minutes in the ultracentrifuge.

	Density ($g \cdot ml^{-1}$)		
	1.10	**1.11**	**1.15**
42% sucrose (g)	31.2	34.2	46.5
0.1 M $MgCl_2$ (µl)	50	50	50
1 M Tris-acetate (µl)	50	50	50
Add ddH_2O to obtain (g):	55	55.5	57.5

Table 2.2 Composition of sucrose solutions used for sucrose gradient during POS isolation from bovine retinas.

For POS isolated for long-time exposure of cells to POS, sterile conditions were maintained throughout. All solutions were filtered with a 2 µm filter and pre-chilled, and ice was used to ensure samples were maintained at a temperature of ~4 °C.

2.1.4 Isolation of photoreceptor outer segment discs

Isolation of POS discs was performed under dim red light, on ice, according to Smith and Litman, 1982. Pelleted POS were re-suspended in 5% Ficoll and kept under argon for at least 30 minutes before overnight incubation. After incubation, the suspension of burst POS was layered with double distilled cold water. After 2 hours of ultracentrifugation at 100000 × *g* at 4°C, the discs were collected from the 5% Ficoll water interface. The remaining pellet was collected separately. The obtained discs were suspended in the appropriate medium for further experiments, ultracentrifuged at 70000 × *g* for 25 minutes and re-suspended in the same medium.

2.1.5 Determination of concentration of rhodopsin in POS and POS discs

To determine the concentration of rhodopsin, the absorption spectrum was measured before and after complete bleaching of rhodopsin (Schadel *et al.*, 2003). Spectra were recorded with a UV-VIS U-2800 spectrophotometer (Hitachi High Technologies, Tokyo, Japan). To bleach the sample it was exposed for 1 minute to green light (see Fig. 2.1). The irradiance was 2.2 mW/cm^2.

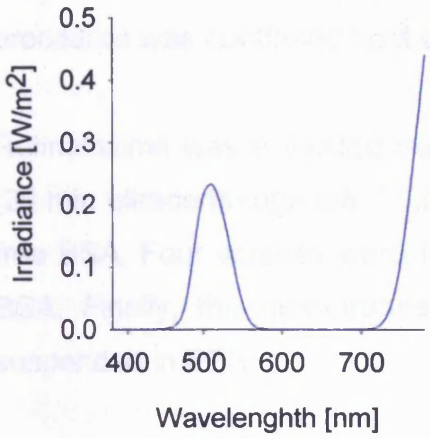

Figure 2.1 Radiance spectrum of green light used for bleaching of rhodopsin.

The rhodopsin concentration was determined from the difference in absorption at 500 nm before and after complete bleaching, using for the extinction coefficient, ε = 40,600 $M^{-1}cm^{-1}$ (Schadel et al., 2003). To decrease light scattering, Triton X-100 was added at a final concentration of 2%.

2.1.6 Isolation of opsin membrane

Retinoids were depleted from POS discs membranes according to Sachs (Sachs, Maretzki and Hofmann, 2000). The extraction was carried out in the presence of hydroxylamine (10 mM), by extraction of the photoisomerised chromophore with fatty acid-free bovine serum albumin.

Washed POS membranes were vigorously mixed in 30 ml ice-cold buffer, 10 mM sodium phosphate, pH 7.0, containing 10 mM hydroxylamine and fatty acid-free bovine serum albumin (2%). The suspension placed in cell culture

flasks was then bleached using green light for 4 min, then 30s on ice. Membranes were pelleted by centrifugation (30,000g, 20 min), and were resuspended in 10 mM sodium phosphate buffer, pH 6.5, containing 5 M urea (35 ml) with a glass/glass homogeniser. After 10 min of incubation on ice, 35 ml phosphate buffer (10 mM, pH 6.5) containing fatty acid-free bovine serum albumin (2%) was added to the suspension, which was vigorously mixed before centrifugation. It was centrifuged for 20 min, 30,000 g at 4°C. The pellet was suspended in the same buffer, stored in 4°C overnight and the isolation procedure was continued next day.

Retinaloxime was extracted from the membrane-bound opsin by three washes (20 min ultracentrifugation, 30,000 g) with the same buffer containing fatty acid-free BSA. Four washes were then carried out with the buffer alone to remove BSA. Finally, the membranes were washed with PBS, centrifuged and re-suspended in PBS.

2.1.7 Determination of opsin concentration in POS and POS discs

Opsin concentration was determined in samples using 1% n-dodecyl β-D-maltoside as a detergent. It was calculated from opsin absorption at 280 nm, using extinction coefficient ε = 81,200 $M^{-1}cm^{-1}$ (Heck *et al.*, 2003).

2.1.8 Transmission electron microscopy (TEM) for testing purity of POS discs

All reagents used for preparation of TEM specimens were purchased from Agar Scientific (UK) unless stated otherwise.

POS discs were isolated according to the procedure described above. After final centrifugation with 5% Ficoll and with a layer of water, both phases – Ficoll/water interphase and a pellet were collected separately. They were centrifuged to obtain pellets.

Pellets were fixed using a mixture of glutaraldehyde and osmium tetroxide buffered with 0.05 M imidazole (Sigma, UK), pH 7.4 (1 part 2.5% glutaraldehyde + 2 parts of 1% osmium tetroxide, both in 0.05 M imidazole) for 1 hour at 4 °C. The pellet was scraped from the side periodically to make sure that there was full penetration of the fixative. Following fixation, pellets were broken up and centrifuged. Then, they were embedded in 3% (w/v) agar (Difco Laboratories, MI, USA). Agar was heated first to allow dissolving, then cooled prior to embedding of samples. Total immersion in the agar was ensured by scraping pellets from the side. Once the agar was solidified, all samples were removed from the vials and cut to remove excess agar from around the specimens. Thanks to this procedure, several small pieces of embedded pellets were provided for each treatment. An excess fixative was removed by washing 4 times for 10 minutes each with dH_2O. Then samples were stained with 0.5% aqueous uranyl acetate for 60 minutes in the dark at 4°C.

Following staining, samples were dehydrated in a graded series of ethanol concentrations (Scientific, UK) for 10 minutes each: 30%, 50%, 70%, 80%, 90% and 3 x 100%. After dehydration, specimens were incubated in propylene oxide 2 times for 10 minutes each. Then, they were infiltrated with resin overnight at room temperature in a fume hood – a 1:1 mixture of propylene oxide and araldite mix (composed of 5g araldite CY 212: 5g DDSA : 0.15g BDMA). After overnight incubation, samples were transferred into fresh resin (i.e. araldite mixture without propylene oxide) in plastic moulds and embedded for 48 hours at 60°C. After that, the resin became solid thanks to its polymerisation.

An Ultracut microtome (Reichert-Jung E, Austria) with ultrathin sections (60 – 90 nm) was used to cut sections. They were collected on pure or pioloform coated copper grids. Sections underwent counterstaining first with 2% uranyl acetate for 10 minutes, washed briefly twice in dH_2O, then in Reynold's lead citrate for 5 minutes, again followed by two brief washes in dH_2O. Sections were examined with a transmission electron microscope (Philips EM400T; Eindhoven, Netherlands) operated at 80 kV accelerating voltage.

Representative images of both phases – interphase and pellet were taken.

2.2 ATR fate in POS

Fluorescence spectra and kinetics were recorded using an F-4500 fluorescence spectrophotometer (Hitachi High-Technologies, Tokyo, Japan).

2.2.1 Monitoring of ATR position in opsin *via* fluorescence measurements

Regeneration of *iso*rhodopsin was tested by the addition of 9-*cis*-retinal in ethanol to bleached POS discs with completely hydrolysed ATR, at selected concentrations. Formation of *iso*rhodopsin was assessed by the presence of the absorption peak at 478 nm, characteristic for *iso*rhodopsin (Fan at al., 2003).

To monitor the position of ATR in opsin after bleaching of rhodopsin, the quenching effect of ATR on intrinsic tryptophan fluorescence was employed. The emission spectrum of intrinsic tryptophan fluorescence were recorded between 305 and 400 nm using excitation wavelength 295 nm, at 21 and 37 °C. For time-resolved records, fluorescence emission was monitored at 335 nm.

The kinetic data were fitted to a single-exponential growth model $F = F_0 + A(1-e^{-kt})$ to calculate the observed rate (k), initial values (F_0) and maximum fluorescence values (A) using SigmaPlot.

The lifetime of Meta II (τ) was calculated using the following equation:

$$\tau = 1/k$$

Equation 2.1 Equation used to calculate the lifetime of Meta II. k – rate of decay, τ – lifetime

The half-life $t_{1/2}$ was evaluated by using the equation below.

$$t_{1/2} = \tau \ln(2)$$

Equation 2.2 Equation used to calculate the half-life $t_{1/2}$.

To test the influence of halothane on tryptophan fluorescence, emission of the amino acid was monitored after addition of halothane at selected

concentrations. The influence of halothane on *iso*rhodopsin formation was determined by addition of 9-*cis*-retinal to bleached POS discs in the presence of halothane.

2.2.2 Monitoring of formation of ROL *via* fluorescence measurements

To monitor the formation of ROL in POS discs, the fluorescence emission spectra of ROL were recorded between 350-550 nm and wavelength of 324 nm was used as the excitation wavelength. For time-resolved records fluorescence emission was monitored at 490 nm. The kinetic data were fit to a single-exponential growth model to calculate all parameters as mentioned above.

ROL concentration was determined based on the observed fluorescence intensity and regression coefficients of calibration curves for NADPH and synthetic ROL suspended in ethanol and incorporated in POS discs. ROL at various concentrations was also incorporated into Triton X micelles and calibration curve was determined for comparative purposes.

Calculations were carried out using following equation:

$$F_{obs} = \Delta c \, (\Phi_{NADPH} + \Phi_{ROL})$$

Equation 2.3 Equation used to calculate concentraton of ROL. F_{obs} . observed fluorescence value, F_{obs} . observed fluorescence value, Δc – amplitude of ROL concentration, Φ_{NADPH} – regression coefficient for NADPH, Φ_{ROL} - regression coefficient for ROL.

2.3 Measurements of singlet oxygen formation

2.3.1 Instrumentation

Time-resolved detection of characteristic singlet oxygen phosphorescence at 1270 nm was used to monitor formation of transient products. A nitrogen-cooled germanium detector (North Coast, CA, USA) was employed, coupled to an Agilent digitising scope (Infiniium 54830B DSO, Agilent, Santa Clara, CA, USA) interfaced with a Risc PC computer (Acorn, Swadlincote, Derbyshire) (Fig. 2.2).

To excite the studied sample a 5 ns laser pulse from a Q-switched Nd-YAG laser (Surelite II, Continuum, Santa Clara, CA, USA) equipped with an optical parametric oscillator (Panther OPO, Continuum, Santa Clara, CA, USA) was used. The sample was excited with selected wavelength. Rose bengal (Acros, UK) was used as a standard singlet oxygen sensitiser.

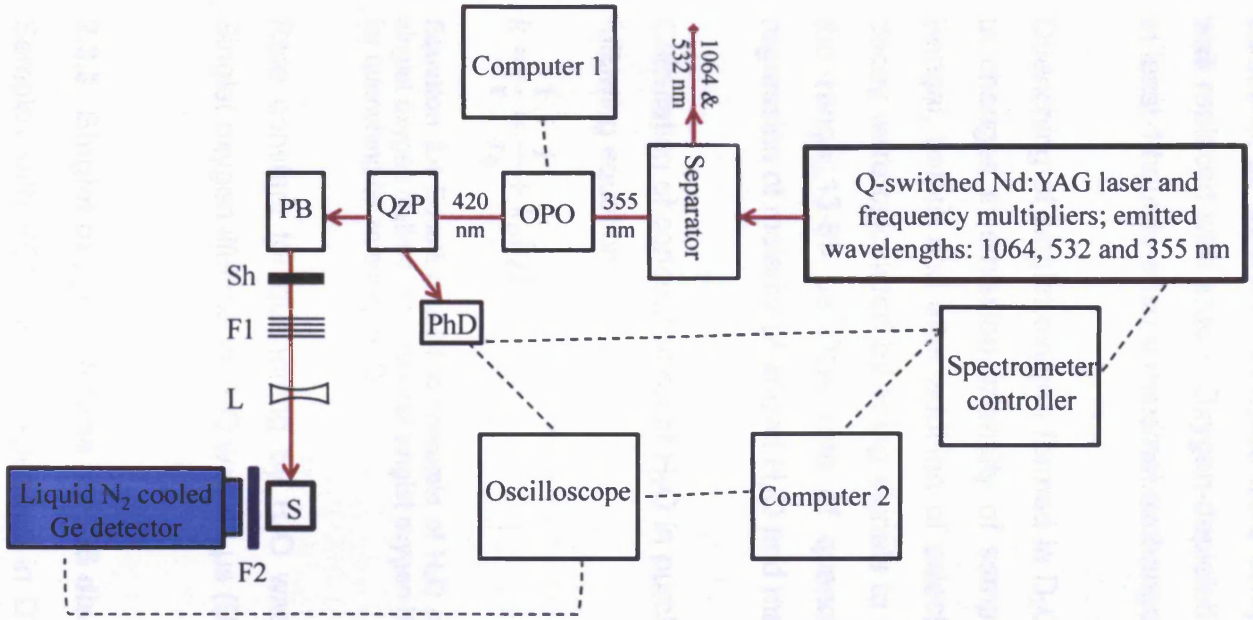

Figure 2.2 Schematic diagram of apparatus for singlet oxygen detection. **OPO** – optical parametric oscillator; **QzP** – quartz plate; **PB** – Pellin Broca prism; **Sh** – shutter; **F1** – neutral density filters for regulation of laser intensity (optional); **L** – diverging lens (optional); **S** – sample in a quartz cell; **F2** – an interference filter with transmission maximum at 1260 nm and Si filters cutting off stray below 1100 nm; **PhD** – photodiode (for measuring relative laser pulse energy); dark red line = laser beam path.

2.3.2 Singlet oxygen in oxygen-rich and oxygen-depleted solutions and quenching effect of H_2O

To determine the singlet oxygen yield in oxygen-rich and oxygen-depleted solutions, air-saturated samples were compared with samples in which oxygen was replaced with argon. Oxygen-depleted samples were kept under argon for at least 1 hour to ensure maximal exchange of oxygen and argon.

Quenching of singlet oxygen formed in D_2O was determined by measurements of changes in emission intensity of samples with a known sensitiser – rose Bengal, before and after addition of selected concentrations of H_2O. Rates of decay were calculated by fitting signals to a single exponential decay model in the range 13-69 μs. The rate of quenching was calculated from a linear regression of molarity of added H_2O and matching rate constants of decay.

Calculation of concentration of H_2O in purchased D_2O was carried out using the following equation:

$$k = \frac{1}{\tau} = \frac{1}{\tau_0} + k_Q[Q]$$

Equation 2.4 Equation used to calculate of H_2O present in D_2O. k – total rate of decay, τ – singlet oxygen lifetime, τ0 – natural singlet oxygen lifetime in a given solvent, kQ – rate constant for quenching by an acceptor Q.

Rate constant for quenching by H_2O was 3887 $M^{-1}s^{-1}$ (Sousa et al., 2008). Singlet oxygen lifetime in D_2O was 68 μs (Deadwyle et al., 1997).

2.3.3 Singlet oxygen lifetime in POS discs suspended in D_2O and H_2O

Samples with POS discs suspended in D_2O were compared with samples in H_2O solutions. Kinetics were analysed as described in the section below. Rate constants of decays and amplitudes for all three components of decays were compared.

To reveal the effect of H_2O on the analysed exponents, a sample with POS discs suspended in D_2O was used and singlet oxygen signals were measured

before and after addition of selected concentrations of H_2O. The analysis was carried out as described above.

2.3.4 Formation of singlet oxygen depending on ATR position and exogenous components

POS discs were isolated as described in section 2.1.3 and 2.1.4. Concentration of rhodopsin and opsin was determined prior to any further processing. Samples were sonicated just before measurements to minimise light scattering and ensure samples homogeneity.

In experiments testing dependency on exogenous retinoids, the components were dissolved in acetone and added to samples at a desired final concentration (final concentration of ethanol did not exceed 1.5%). ATP and NADPH were diluted in D_2O and added at the required concentration (final dilution of sample ≤1.5%).

All obtained signals were fitted in SigmaPlot to a three exponential decay function using equation below:

$$I = A_1 \times e^{-k_1 t} + A_2 \times e^{-k_2 t} + A_3 \times e^{-k_3 t} + A$$

Equation 2.5 Equation used to fit singlet oxygen kinetics. t = time, A_1, A_2, A_3 = amplitudes for short-lived (A_1), middle-lived (A_2) and long-lived (A_3) exponent, k_1, k_2, k_3 = rates constant for short-lived (k_1), middle-lived (k_2) and long-lived (k_3) exponent, A = initial emission intensity.

The final analysis included amplitudes and rate constants for all components separately and as their sum unless otherwise stated.

2.3.5 Photosensitising of singlet oxygen by ATR and dATR

ATR and dATR solutions were prepared in benzene. Samples were excited with 355 and 422 nm to reveal differences between singlet oxygen yields depending on the absorption spectrum.

Measurements were taken in concentration- and absorbance-matched samples. All signals were fitted with a single exponential model, using the following equation:

$$I = A \times e^{-kt} + A_0$$

Equation 2.6 Equation used to fit kinetics of singlet oxygen photosensitised by ATR and dATR. A_0 = initial emission intensity, t – time, I = emission intensity at t → ∞, k = rate constant of decay.

Yields of singlet oxygen was determined for each sample in triplicates and compared. Average laser intensity was calculated and all values were normalised taking into consideration the ratio between actual and relative laser energy.

Quantum yield of singlet oxygen was determined by comparing the intensity values with that obtained from a known sensitiser (ATR in benzene in the experiments), using the following equation:

$$\Phi_s = \frac{\Phi_{ATR}}{\text{slope}_{ATR}} \bullet \text{slope}_s$$

Equation 2.7 Equation used to calculated quantum yields of singlet oxygen. Φ - quantum yield, s – sample, ATR - all-*trans*-retinal, slope - slope of fitted initial emission intensity values.

Yields of singlet oxygen within a determined range of light were calculated using the following equation:

$$\varphi = \Phi_{1O_2} \times IAbs$$

Equation 2.8 Equation to calculate total singlet oxygen yield (φ_t). Φ_{1O2} – quantum yield of singlet oxygen; I_{Abs} – integrated absorbance calculated as a sum of absorbance in the range 390 – 600 nm.

Proportion of absorbed light by ATR and dATR are calculated as a function of the absorbance and irradiance spectrum of light used for irradiation, based on following calculations:

$$A = \log\frac{I_0}{I_t} = \log\frac{I_0}{I_0 - I_A} \rightarrow I_A = I_0 - \frac{I_0}{10^A} = I_0\left(1 - \frac{1}{10^A}\right)$$

Equation 2.9 Equation used to determine the value of absorbed light. A – absorbance, I_0 – initial intensity of light, I_t - transmitted intensity of light, I_A - absorbed intensity of light.

Assuming that I_0 is similar for both ATR and dATR, the intensities of absorbed light can be compared using the following proportion:

$$\frac{I_A^{ATR}}{I_A^{dATR}} = \frac{1-10^{-A_{ATR}}}{1-10^{-A_{dATR}}}$$

Equation 2.10 Equation used to calculate the ratio between absorbed light by ATR and dATR. A – absorbance.

Singlet oxygen yield for samples with different absorbance at indicated wavelength was normalised to the absorbed light using the following proportion:

$$\frac{I_{A_1}}{I_{A_2}} = \frac{1-10^{-A_1}}{1-10^{-A_2}}$$

Equation 2.11 Equation used to normalise yields of singlet oxygen for samples with different absorbance at selected wavelengths.

Laser intensity was reduced using neutral density filters (Figure 2.3 A). The reduction in transmission per filter was ~15 and ~12 % at the laser excitation wavelengths of 355 and 422 nm, respectively. Figure 2.3 B shows the expected relative laser intensity over the range of filter numbers used in these experiments.

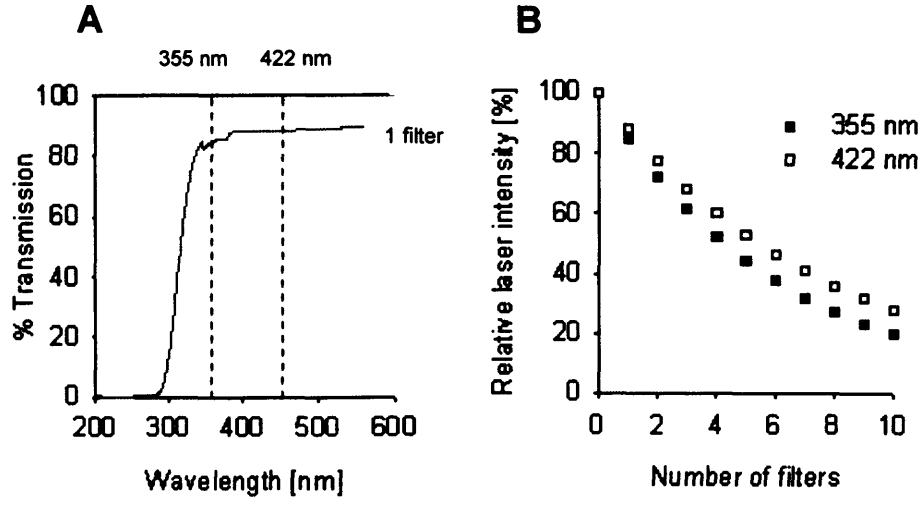

Figure 2.3 Effects of neutral density filters on light transmission. (A) Transmission spectra with either air only or with 1 filter; (B) calculated relative laser energy at 355 and 422 nm with 0 to 10 filters in the light path.

2.3.6 Quantum yield and quenching of singlet oxygen by selected compounds

Formation of singlet oxygen was determined in samples with ATR, ROL and retinyl ascorbate. All absorbance-matched compounds were dissolved in acetone. Singlet oxygen signals were monitored depending on the laser energy changed by using neutral density filters. Yields of singlet oxygen were calculated as slopes of initial emission intensity values for all three components and compared.

Rates of singlet oxygen quenching were determined in solutions of retinyl ascorbate, ascorbyl palmitate and ROL. Acetone solutions of tested components were added at indicated concentrations to a solution of rose bengal as a standard sensitiser. The final concentration of added acetone was <10% of the initial volume.

All signals were fitted to a single exponential model in SigmaPlot as described in section 2.3.5. Rates of decay were calculated and compared. The rate of singlet oxygen quenching was calculated as a slope of rate constants dependent on the concentrations of the quenchers.

Singlet oxygen yield for samples with different absorbance at a selected wavelength was normalised as described in the section above.

2.4 Oxidation of lipids

2.4.1. Extraction of lipids from POS

Lipids from POS were extracted using a modified Folch's method (Folch *et al.*, 1957; Rozanowska *et al.*, 2004). 0.5 ml suspension of POS in PBS was added to 0.8 ml chloroform/methanol (2:1 v/v; both Fisher Scientific, UK) and vortexed briefly, then centrifuged. Formation of an upper polar phase enriched with methanol/PBS, a protein-enriched interphase, and a lower chloroform-enriched phase was observed as shown in Figure 2.4. All phases were removed and

analysed separately. Chloroform enriched-phases were used to analyse lipids peroxidation.

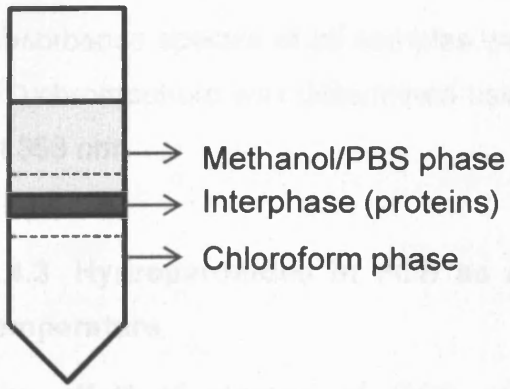

Figure 2.4 Diagrammatic representation of the layers formed in chloroform/ methanol extraction of proteins and lipids from photoreceptor outer segments.

2.4.2. Idometric assay to determine hydroperoxides in lipids

Detection of hydroperoxides was based on their reaction with iodide quantitatively and in a stoichiometric proportion as shown on the scheme below (Jessup at al., 1994).

$$ROOH + 2H^+ + 2I^- \rightarrow ROH + H_2O + I_2$$

Equation 2.12 Scheme of reaction of of hydroperoxides with iodide.

The I_2 can be estimated by determination of triiodide (I^{3-}) in the excess of iodide (see reaction below).

$$I_2 + I^- \rightarrow I^{3-}$$

Equation 2.13 Scheme of triiodide (I^{3-}) in the excess of iodide.

All steps were carried out at room temperature. Solutions were freshly prepared and kept under argon for at least 30 minutes before they were used. All samples and solution were saturated with argon during the whole procedure.

Acetic acid/chloroform (3:2 v/v) and 0.02 ml of potassium iodite (KI; 1.2 g/ml) in water were added to samples kept in Eppendorf tubes followed by saturation with Argon and vortexing. Samples were incubated for 10 minutes. The reaction

was stopped by addition of 0.9 ml of 5% cadmium acetate in water. All samples were centrifuged (1 min, ~800 × g).

Absorbance spectra of all samples were measured against water. The triiodide (I^{3-}) chromophore was determined using its extinction coefficient 22,500 $M^{-1}cm^{-1}$ at 353 nm.

2.4.3 Hydroperoxides in POS as a function of incubation time at room temperature

The effect of storage of POS at room temperature was evaluated by assessment of the level of hydroperoxides in POS stored at room temperature at selected time points (0-60 minutes).

2.4.4 Hydroxyperoxides in lipids in POS as a function of ATR position

The test the influence of ATR on lipid peroxidation, POS were bleached with green light as described in Section 2.1.5 and kept at room temperature at selected time intervals until the extraction of lipids was performed. Unbleached POS were compared with POS just after (1.5 min), 8, 10 and 20 minutes after rhodopsin bleaching. In addition, samples with bleached rhodopsin 20 minutes after bleaching were irradiated with white light (see Section 2.6.3 for irradiance spectrum) for 10 and 20 minutes and compared with those kept in the dark. To test the influence of ATR conversion to ROL on the level of hydroperoxides, samples with hydrolysed ATR were compared with samples with addition of NADPH and/or ATP at the same concentration as rhodopsin.

2.5 Cell culture

2.5.1 ARPE-19 cell line

The ARPE-19 cell line was cultured for future experiments. The cell line was obtained from the American Type Collection (ATCC). Its origin is cells cultured from a 19 year old donor. ARPE-19 cells have been shown to exhibit several,

but not all, functional and structural properties of human RPE (Dunn et al., 1996). They are characterised by normal karyology, polarised distribution of cell surface markers and they express CRALBP and RPE-65, both of which are synthesised by differentiated RPE *in vivo* (Dunn et al., 1996).

2.5.1.1 Maintenance of cells

Cells were cultured in a 1:1 mixture of Dulbecco's Eagle's medium and Ham's F12 medium (DMEM:F12, GIBCO, UK). The medium was supplemented with antibiotics (100 µg/mL streptomycin, 100µg/mL kanamycin and 60µg/mL penilicin; Sigma, UK), fungizone (1.25 µg/mL amphotericin; GIBCO, UK) and 10% v/v heat-inactivated fetal calf serum (FCS; BioSera). As soon as cells reached confluence, the concentration of FCS was decreased to 2%. Cells were maintained in 75 cm^2 at 37°C in a humidified incubator containing 5% CO_2 and 95% air.

2.5.1.2 Subculturing

Cell culture medium was aspirated and cells were washed with freshly made PBS. Detachment of the cells was carried out by addition of 2 ml of 0.25% (w/v) Trypsin (Sigma, UK) and 0.02% EDTA (Sigma, UK) in PBS and incubation at 37°C for 2 minutes. An inverted microscope was used to confirm detachment of the cells. Trypsin was deactivated by addition of growth medium with 10% FCS and cells were split from 1:3 up to 1:6 surface ratios.

2.5.1.3 Long-term storage

For long-term storage, cells were trypsinised as described in section 2.5.1.2. Medium with 10% FCS was added to flasks and cells were transferred to 15 ml centrifuge tubes and centrifuged at 700 × g for 5 minutes. Obtained supernatant was removed. Cells were suspended in FCS with 10 % v/v dimethylsulphoxide (DMSO) and put in cryovials and frozen. Cells were initially kept in an isopropanol cryostorage box at -80 °C before being transferred to liquid nitrogen storage.

2.6 (Photo)toxicity of ATR and degraded ATR

2.6.1 Degradation of ATR

ATR was degraded by exposure of ATR suspended in benzene to white light ~12 mW/cm^2 (see figure below).

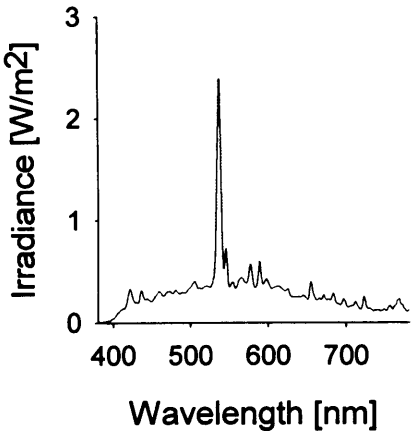

Figure 2.5 Radiance spectrum of white light used for degradation of ATR.

For time-dependent degradation of ATR, solutions of ATR were exposed for 0, 10, 30, 60, 90 and 120 minutes to the light. Spectra were recorded before and after irradiation. The level of degradation was estimated by assessment of an increase in absorption of shorter wavelengths (at 325 nm) after ATR degradation. The contribution of products of ATR degradation was calculated using the equation below:

$$A_{325DP} = A_{325dATR} - A_{380dATR} \times A_{325ATR}/A_{380ATR}$$

Equation 2.0.84 Equation used to calculate absorbance of degradation products (DP) mixture with the remaining ATR (dATR) at 325 taking into account the contribution of the remaining ATR. A – absorbance; subscripts: DP – degradation products of ATR, ATR – all-*trans*-retinal, dATR – mixture of degradation products and remaining all-*trans*-retinal, numbers – wavelengths at which absorbance was measured/calculated expressed in nm.

2.6.2 Liposome preparation

A lipid film of DMPE and DMPC, as 1,2-dimyristoyl-*sn*-glycero-3-phosphoethanolamine and 1,2-dimyristoyl-*sn*-glycero-3-phosphocholine, respectively (Avanti Polar lipids, Alabaster, AL, USA), was formed using a rotary

vacuum evaporator (Büchi, Flawil, Switzerland). The sample flask was maintained at 37 °C and rotated under argon (Pureshield, BOC, UK), and the pressure was gradually decreased to 250 mbar as the solvent evaporated. Once it was ensured that the lipid film was dry and solvent-free, waste chloroform was removed from the system, and the pressure was reduced to 40 mbar then left for at least 60 minutes (under argon, dark, room temperature). For liposomes with ATR or degraded ATR (dATR), selected amounts of retinoid suspended in benzene was added to dry film of phospholipid followed by reducing the pressure to a final value of 40 mbar and left for at least 1 hour.

To form liposomes, phosphate buffered saline (PBS) was added gradually to the flask containing the lipid, lipid with ATR or with dATR film, and the film was rehydrated using a combination of rotation and warming to a temperature about 10 °C higher than the transition temperatures for DMPC and DMPE (23 and 50 °C, respectively). To ensure formation of uniformly-sized liposomes, freshly prepared liposomes were sonicated. Samples were stored under argon at -20 °C.

2.6.3 Exposure of cells to ATR or dATR, and light

ATR and degraded ATR solutions were made in DMSO, and diluted further to concentrations between 0.0025 and 1 M. They were diluted five hundred times in D-PBS to required concentrations of ATR and dATR in 0.2% DMSO (see individual chapters).

ARPE-19 cells grown in 24-well plates were rinsed twice with D-PBS, then ATR or dATR solutions were added to the wells (1ml/well).

The same procedure was applied to ATR and dATR incorporated in liposomes with 1,2-dimyristoyl-*sn*-glycero-3-phosphocholine (DMPC).

Light exposure was performed with a Sol lamp (Hönle UV Ltd, Birmingham; see Figure 2.4). Heat and UV filters (Lee Heat Shield and #226 Lee U.V. respectively; Lee Filters, UK) were placed above the lamp in all experiments.

Irradiance spectra of the light to which cells were exposed are shown in Figure 2.3.

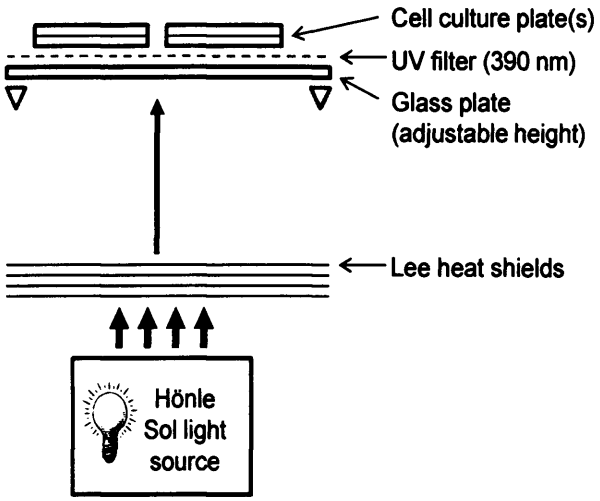

Figure 2.6 Experimental setup for light exposure experiments, with cells illuminated from below.

Cells on plates were exposed to the light for 1 hour. For dark experiments, plates were wrapped in black and silver foil and placed above the lamp to mimic temperature and air conditions experienced by light-exposed cells. Spectral irradiance of the light source between 380 and 780 nm was measured in each experiment using a handheld spectroradiometer (Specbos 1201 with JETI LiMeS software; Glen Spectra, UK) to ensure consistency. Additionally temperature was monitored too. If required, the light intensity was altered before each exposure by adjusting the height of the glass plate relative to the lamp.

A one hour exposure was followed by aspiration of solutions of ATR and dATR, cells were washed twice with D-PBS, then returned to the incubator with normal growth medium containing 2% FCS for a 24 hour incubation prior to processing.

2.7 Protective role of antioxidants

2.7.1 Exposure to ATR and dATR with antioxidants

ARPE-19 cells were exposed to ATR, dATR and antioxidants with the same procedure applied as in the section above.

Two concentrations of ATR and dATR were used to test the protective role of antioxidants – 0.05 and 0.1 mM, respectively, unless otherwise stated. Solutions of ATR and dATR were made in DMSO and then suspended in D-PBS.

Hydrophilic antioxidants (N-acetyl-cysteine (NAC), glutathione (GSH) and Vitamin B_6) were dissolved in PBS and added to solutions of ATR and dATR to obtain the required concentrations. ROL and α-tocopherol were suspended in DMSO and added together with ATR and dATR to get a final concentration of DMSO 0.2%. PE was incorporated in liposomes suspended in D-PBS (for protocol see section 2.5.2).

2.7.2 Cytotoxicity assays

2.7.2.1 Microscopy for cell morphology

Cells were visualised using an Olympus IX70 inverted microscope configured for phase contrast imaging. Images were obtained using a Spot RT colour CCD camera and Spot Advanced software (Diagnostic Instruments Inc, UK).

2.7.2.2 MTT assay

Living cells can reduce 3-(4,5-dimethylthiazol-2-yl)-2,5-diphenyl tetrazolium bromide (MTT) to formazan. Crystals of formazan can be dissolved and their absorbance measured. This provides a rapid test of cell viability (Mosmann, 1983) and can be a method to measure mitochondrial activity (Martínez-Martos et al., 2000).

Cells on 24-well plates exposed to ATR, or dATR with or without antioxidants were washed with D-PBS after post-incubation in fresh medium. A solution of 0.5 mg/ml MTT in PBS was prepared. 1 ml of MTT was added to each well and incubated at 37 °C for 1 hour. After incubation, the MTT solution was removed and formazan crystals were dissolved in acidified isopropanol (200 µl/well of isopropanol with 0.04 M HCl). Plates were left for 1-2 minutes for crystals to dissolve. The absorbance was measured at 590 nm in a microplate reader (BioTek ELx800). A reference filter at 690 nm was used and absorbance values at this wavelength were substracted off the absorbance at 590 nm. Background measurements were taken in cells exposed only to acidified isopropanol (i.e. no ATR/dATR, no antioxidants, no MTT).

For all experiments mitochondrial activity was calculated as a percentage of the control – cells not treated with any of the components tested under the same conditions (the same plate).

2.7.2.3 Monitoring of membrane integrity

Propidium iodide is widely used for evaluation of cell death as it cannot cross the intact cell membrane of live cells. It can penetrate cell membranes of dead or dying cells. PI binds to DNA allowing nuclei of cells with compromised membranes to be visualised.

Cells were exposed to ATR and dATR, in the dark and exposed to light at 13 mW/cm^2. After exposure, cells were washed with PBS and incubated for 2 or 24 hours with fresh medium and 2% FCS before labelling. Following incubation, cells were labelled for 15 minutes at 37 °C with 1 µg/ml PI in PBS. 3 µg/ml Hoechst 33342 was used as a co-labelling agent to allow the total number of cells to be counted. Cells were washed with PBS and imaged immediately with the Olympus IX70 inverted microscope. There were two filter sets used – one optimised for red emission (for PI; excitation 510 – 550 nm; longpass emission filter > 590 nm) and for blue emission (for Hoechst; excitation 330 – 385 nm; longpass emission filter > 420 nm).

2.8 The effect of exposure of RPE to POS +/- ATR and light

2.8.1 Feeding RPE with POS +/- ATR, +/- light

POS were isolated from frozen bovine retinas isolated under sterile conditions. The number of POS/ml and rhodopsin/opsin concentration was determined prior to feeding. The number of POS used for feeding was 1×10^7 POS/ml. ATR diluted in ethanol was added to the POS at three different concentrations: the same as opsin, twice and 3.5 greater than the opsin concentration (3.5 times greater concentration than opsin corresponds to the maximum concentration of free ATR in the retina) . The final concentration of ethanol that cells were exposed to did not exceed 0.5%.

Confluent ARPE-19 cells were used for the experiments. Feeding was carried out every day with fresh POS added. Each treatment was done in triplicate. Cells kept in the dark were compared with cells exposed to white light (see Fig. 2.3 for irradiance spectrum). Irradiation was preceded by removing the excess of POS and washing twice with D-PBS. The same procedure was applied to cells kept in the dark to provide the same conditions for comparison. After exposure to light, fresh POS were applied and incubated for about 24 hours. Controls were fed with medium only (DMEM:F12 medium containing 2%FCS).

A two-week exposure was followed by quantification of fluorescence using light microscopy and spectrofluorometry.

2.8.2 Microscopy of cells fed with POS +/- ATR, +/- light

After a two-week exposure to POS +/- ATR cells were washed with PBS. Fluorescence was visualised using an Olympus IX70 inverted microscope configured for fluorescence imaging. Images were obtained using a Spot RT colour CCD camera and Spot Advanced software (Diagnostic Instruments Inc, UK) with a filter optimized for blue emission (excitation 330 – 385 nm; longpass emission filter > 420 nm).

2.8.3 Quantification of fluorescence in RPE fed with POS +/- ATR, +/- light

Fluorescence imaging of cells was followed by quantification of fluorescence by spectrofluorometry. Cells were solubilised in 2% Triton X-100 – 1ml/well with triplicates combined into one sample. Fluorescence was monitored with two excitation wavelengths: 360 and 488 nm.

All spectra were corrected based on emission spectra of known components with fluorescent properties – fluorescein and 9,10-diphenylanthracene. Their fluorescence emission spectra were recorded and compared with established corrected spectra from literature. Both spectra were normalized to the same maxima values and the ratio between the actual and corrected spectrum was calculated. Ratio values were used to determine corrected spectra for all measurements.

Maxima of fluorescence spectra were determined and calculated for both excitation wavelengths in indicated samples.

2.8.4 Lipofuscin

2.8.4.1 Isolation of lipofuscin

Donors' eyes without corneas were received from Bristol Eye Bank with permission given for research use. Only details of age, sex and cause of death given were given without any personal information.

Dissection was started with the separation of the anterior segment of the eye by circumferential incision posterior to the ora serrata. The vitreous was detached and gently removed. The neuroretina was detached from the underlying RPE and removed by cutting off of the optic disk. The eye cup was washed with 1 ml of phosphate buffered saline (PBS). Detachment of the RPE was obtained by gentle washing of the RPE/choroid complex with a fine camel hair brush with addition of fresh PBS (1 ml). The same step was repeated once. The cell

suspension was transferred to a cryovial (Nalgene, Rochester, NY, USA) with a sterile Pasteur pipette (Copan Innovations, Murrieta, CA, USA) before being stored at -80 °C until needed for further use.

To increase the yield of lipofuscin isolated, in some cases whole complex of RPE/Bruch's membrane was removed and stored at -80 °C until needed. To obtain the RPE, isolated complexes were trypsinised with 0.25% (w/v) trypsin + 0.02% EDTA (both Sigma) in PBS and incubated at 37 °C for 30 minutes with mechanical mixing every several minutes during incubation. After incubation with trypsin, suspensions of cells were separated from the tissues by using small sieves. They were centrifuged at 70000 × *g* 20 minutes at 4°C.

Trypsinisation of the remaining tissues was repeated three times. To ensure all cells of RPE were detached from the remaining tissues it was washed three times with PBS.

Trypsinised RPE and previously isolated, thawed RPE suspensions were combined and pooled in different age groups: <47 years, 65-75 years and >80 years (15-25 pairs of eyes per group). They were treated separately for the rest of the procedure.

Lipofuscin granules were isolated from the RPE cell extracts according to the Boulton and Marshall method (1985). The suspensions were homogenised through 18-gauge needles (BD Microlance, Oxford, UK) several times. Then the tips of needles were cut off with pliers. An aperture in the tip of the needles was formed and samples were homogenised repeatedly with gradually decreased diameters of the gap. Homogenates were transferred onto 15 ml centrifuge tubes (Sterilin, Staffs, UK) and centrifuged at 100 *g* (Boeco U-32R, Hamburg, Germany) for 7 mins at 4°C to remove cellular debris. The supernatant was removed and stored on ice while the pellet was further homogenised with the same method as described above and the centrifugation repeated at 100 *g* for 7 mins at 4°C.

The supernatant was centrifuged at 7000 *g* (Sorvall Ultra-Pro 80) for 10 mins at 4°C to form a pellet of pigment. All samples were stored overnight at 4°C and the procedure was continued on the following day.

The pigment was resuspended in 0.25 M sucrose and homogenised with a 18 G syringe. The tip of the needle was cut off and homogenisation was repeated with decreasing size of the aperture. Homogenised samples were layered on a discontinuous sucrose density gradient (1.0, 1.2, 1.4, 1.6125 and 2.0 M). The gradient was centrifuged at 103000 *g* for 1 hr at 4°C.

Material accumulated between 0.25 and 1.0 M sucrose was collected isolated using a sterile Pasteur pipette. Phase between 1.0 and 1.4 M sucrose (upper layer) was collected and purified separately (Fig. 2.7). The rest of the interphases were collected and frozen at -80°C.

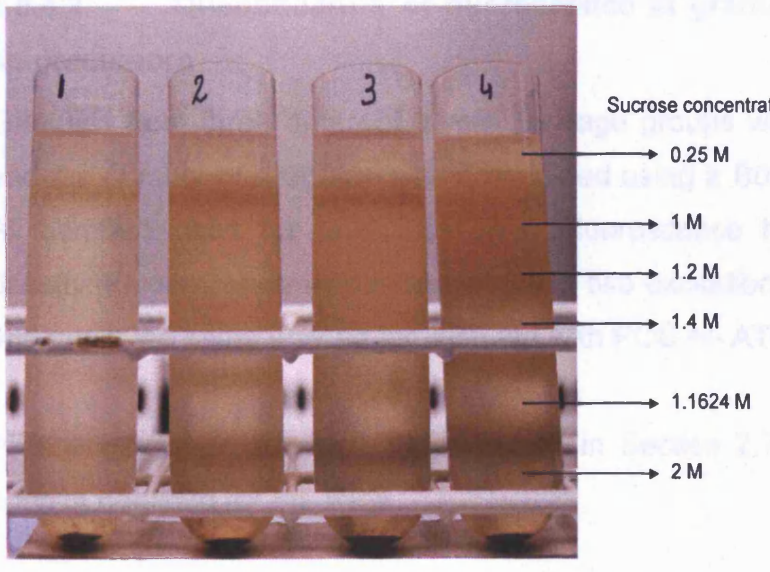

Figure 2.7 Sucrose gradients with indicated sucrose concentrations and centrifuged retinal pigment. Layer between 1 and 1.4 M sucrose was used for purification of lipofuscin granules. Samples from different age groups: 1: <47 years, 2: 51-64 with 76-79 years (not included in further experiments and analysis), 3: 65-75 years and 4: >80 years.

All the granules were diluted in PBS and centrifuged at 7000 *g* for 15 mins and 4°C to create pellets for all samples. On the following day all samples were re-suspended in 0.25 M sucrose and were further homogenised through an 18 G

syringe in the same way as before. The suspensions were layered onto a modified discontinuous density sucrose gradient (1.0, 1.2, 1.4 and 1.6125 M sucrose) and the centrifugation step repeated separately for the upper and lower layers. Purification of the upper layer gave one layer; it was isolated and the washing step in PBS was repeated. Centrifugation of gradient with the lower layer resulted in purification of three layers: 0.25/0.1 M sucrose, 1.0/1.2 M sucrose and 1.2/1.4 M sucrose. The first one was added to the upper phase, isolated before, and washed with PBS again. The middle phase was believed to be a precursor of lipofuscin and was collected and washed in PBS separately. Lipofuscin accumulating at the 1.2 and 1.4 M interphase was collected and washed in the same way as described before.

All samples were re-suspended in 2 ml PBS and yield was determined by counting on a haemocytometer (Bürker, Sigma, UK).

2.8.4.2 Quantification of fluorescence in granules of lipofuscin and its precursors

Granules from three different layers and age groups were suspended in PBS and the number of granules was determined using a Bürker counting chamber. All samples used for quantification of fluorescence had the same granule density. Fluorescence was monitored with two excitation wavelengths: 360 and 488 nm in the same way as for RPE fed with POS +/- ATR.

All spectra were corrected as described in Section 2.7.3 and compared with spectra obtained for the RPE.

2.8.5 Transmission electron microscopy (TEM) for monitoring accumulation of inclusion bodies in cells

A two-week feeding of cells with POS was followed by cell trypsinisation, washing with PBS and centrifugation of cells to obtain pellets.

Samples were prepared as described in section 2.1.8 with Sőrensen Phosphate Buffer (as a standard buffer used in TEM procedure) used instead of 0.05 M imidazole. Sőrensen Phosphate Buffer was prepared by mixing 81.8 ml of 68 mM sodium phosphate dibasic and 18.2 ml of 68 mM potassium phosphate monobasic.

Representative images were taken and analysed using ImageJ.

2.9 Statistical analysis

Normalisation of data and calculation of means and SD/SEM were carried out using Microsoft Office Excel 2007. Linear regression was carried out using SigmaPlot 9.0. All further statistical analyses were carried out using Excel 2007 or SPSS 16. Tables of *P*-values for all post-tests carried out after significant ANOVA tests, and for one-sample, t-tests and other selected comparisons are included in Appendices.

Chapter 3

Fate of ATR after bleaching of the visual pigment

3.1 Introduction

Absorption of light by visual pigments is essential for visual perception, but it also makes the retina susceptible to light-induced damage. As described in the General Introduction section, the absorption of a photon by rhodopsin is followed immediately by isomerisation of the visual pigment chromophore, 11-*cis*-retinal, to ATR and then by a series of conformational changes of the protein, and hydrolysis of the Schiff-base bond between ATR and protein. Comparison of photochemical properties of free ATR and different Schiff bases of ATR indicate that, in contrast to its Schiff bases, free ATR is a potent photosensitiser. While it is well documented that the presence of rhodopsin is essential to make the retina susceptible to damage induced by visible light, it still remains unclear what mechanism is responsible for that susceptibility.

As already discussed in the General Introduction, upon hydrolysis of ATR from metarhodopsin II, ATR is channelled to the opsin "exit" site where it remains non-covalently bound until being enzymatically reduced to ROL and/or released to the disc membrane when 11-*cis*-retinal binds to opsin and regenerates rhodopsin. It is expected that depending on the position of ATR within opsin or disc membrane, its photosensitising properties can vary, as well as the proximity of different targets of oxidation. Therefore, the first aim of this project was to adapt the methodology developed by Schadel and colleagues (Schadel et al., 2003) to monitor as a function of time after photobleaching of visual pigments: a) ATR hydrolysis, b) its position within opsin and/or POS discs, and c) its conversion to ROL.

While the time-course of ATR trafficking in bovine POS discs has been determined by Schadel and colleagues at room temperature, it can be expected that at physiological temperature, where the diffusion, membrane fluidity, and chemical reactivity are likely to be greater than at 20°C, these kinetics will be faster. Therefore, the second aim was to determine the kinetics of ATR hydrolysis and reduction to ROL at a physiologically-relevant temperature of 37°C.

3.2 Experimental design

3.2.1 Test of the purity of POS discs

As described in the Methods section, isolation of POS discs involves a final step of centrifugation with a layer of Ficoll and water (2.1.4). It results in POS discs located between Ficoll and a water layer (the interface) and on the bottom of centrifuge tubes as a pellet. It was necessary to test the disruption of POS and purity of obtained POS discs since pure POS discs were crucial in experiments in which cofactors of the retinoid cycle were tested. Separated discs allow for easy access of hydrophilic co-factors to membrane-associated enzymes, while lack of contamination by other organelles minimises the risk that those co-factors and added retinoids will interact with other than the desired organelles.

3.2.2 *Iso*rhodopsin generation in POS discs

Due to the high content of polyunsaturated fatty acids, iron ions and photosensitisers, POS are highly susceptible to oxidation, which is likely to affect protein structure and enzymatic activity. Therefore, bleaching of rhodopsin and the ability to form *iso*rhodopsin upon addition of 9-*cis*-retinal was used as a test of POS suitability for further measurements.

Initially dark-adapted, frozen, bovine retinas were used to isolate POS discs (Section 2.1.2) in order to obtain high yields of rhodopsin in isolated material. Further experiments were performed with POS discs isolated from fresh bovine retinas and POS discs isolated just after delivery of eyes (Section 2.1.2). Results presented were obtained using POS discs from fresh retinas unless otherwise stated.

Opsin depleted of all retinoids was isolated (Section 2.1.6) in order to assess the effect of exogenously added retinoids with known, controlled concentrations.

3.2.3 Monitoring of isomerisation of 11-*cis*-retinal and ATR hydrolysis

As already described in the Introduction section, rhodopsin undergoes changes through a cycle of uptake of its chromophore, 11-*cis*-retinal, by the apoprotein opsin and release of ATR formed after photoisomerisation of the chromophore resulting from absorption of light (Hubbard and Wald, 1952). Exposure of rhodopsin to light leads to isomerisation of 11-*cis*-retinal to ATR, and formation of the active form of rhodopsin – metarhodopsin II (Meta II). At this stage the Schiff base linkage between Lys^{296} and ATR is still intact, but deprotonated. Isomerisation can be monitored by recording the changes in the absorption spectrum of POS discs before and after rhodopsin bleaching. In order to monitor absorption spectra, all samples with POS discs were isolated and prepared in such a way as to minimise light scatter (absorbance values for long wavelengths >800 nm close to 0). Sonication was applied when necessary.

Decay of Meta II coincides with hydrolysis of the Schiff base linkage between ATR and channelling of ATR in the opsin to the opsin "exit" site, where it remains non-covalently bound. It has been shown that hydrolysis of ATR from opsin is accompanied by a significant increase in intrinsic tryptophan (Trp) fluorescence after release of ATR from the active site (reviewed by Heck at al., 2003).

Schadel and colleagues (2003) reported that measuring of Trp fluorescence in POS discs provides a method of monitoring the fate of ATR after rhodopsin bleaching. There are five tryptophan residues in total (positions 35, 126, 161, 175, and 265) in the primary structure of bovine rhodopsin and they are located on different helices (Lin and Sakmar 1996). 11-*cis*-retinal is tightly packed within the bundle of transmembrane (TM) helices of the protein and restricted along the axis of the retinal polyene chain by TM helices H5 and H7 (Ahuja at al., 2009). Its binding site is enclosed on the extracellular side of rhodopsin in the dark state by the second intradiscal loop (EL2). Trp265 is conserved in all visual pigments and is located on helice 6 in the closest position to the retinal chromophore.

Monitoring of ATR position in opsin was performed according to Schadel's experiment (Schadel at al., 2003) to determine the kinetics of ATR hydrolysis and channelling upon rhodopsin regeneration depending on selected factors under the same laboratory conditions as conditions for further experiments (including singlet oxygen production discussed in the next chapter) (Section 2.2.1). As mentioned before, Schadel and colleagues monitored the kinetics of Trp changes after rhodopsin bleaching and tested the influence of the addition of retinoids such as ATR and 9-*cis*-retinal on the changes of Trp fluorescence intensity.

The measurements were taken at room temperature similar to that as in experiments described by Schadel et al. (2003) and, in addition at 37 °C as physiologically-relevant conditions. The temperature was typically 21°C, however, occasional unstability in thermal conditions within the laboratory caused the temperature to fluctuate between 19-21°C (referred in the text simply as 21°C). Stirring with a magnetic stirrer was adjusted for all measurements to ensure homogeneity of samples during monitoring.

3.2.4 Fate of ATR after rhodopsin regeneration

Regeneration of bleached rhodopsin results in the release of ATR from the "exit site" to the inner leaflet of the disc membrane upon binding (Heck et al., 2003). Schadel and colleagues reported a rapid, biphasic decrease in intrinsic Trp fluorescence upon addition of 11-*cis*-retinal to opsin membranes (Schadel et al., 2003).

In the experiments, the absorption spectrum before and after addition of 9-*cis*-retinal to bleached POS discs and fluorescence measurements before and after rhodopsin bleaching allowed monitoring of *iso*rhodopsin regeneration and ATR release from the opsin exit site, respectively.

Using Trp fluorescence as a tool to monitor ATR position and rhodopsin regeneration, it has been shown that halothane, one of the anesthetics, may

compete with the ligand 11-*cis*-retinal, potentially blocking rhodopsin regeneration (Ishizawa at al., 2002). Ishizawa and colleagues (2002) provided evidence that halothane contacts Trp265 lining the ligand binding activity in the TM core of rhodopsin. It is unclear, however, whether or not binding of halothane to opsin leads to the release of ATR from the opsin "exit" site to the disc membrane. If so, it would provide a convenient way of inducing ATR release and comparing its photosensitising properties at the opsin "exit" site and in the disc membrane without a need of introducing other retinoids, which make data analysis more convoluted.

On the other hand, if halothane does not induce ATR release from the opsin "exit" site, it can explain its protective action against white light-induced damage (Keller et al., 2001), but not against blue-light-induced damage. Protection against damage induced by white light may involve preventing rhodopsin regeneration and therefore breaking a cycle of absorption of light by rhodopsin and ATR accumulation in POS disc membranes. However, it does not protect from photosensitizing effects of 11-*cis*-retinal delivered to POS discs unable to bind to the opsin active site. This would suggest that halothane may be used to prevent 11-cis- and 9-*cis*-retinal from generating rhodopsin/*iso*rhodopsin, thus allowing assessment of the photosensitizing properties of these and other selected retinoids in POS disc lipid membranes with inhibited rhodopsin regeneration (see Methods section 2.2.1 for details).

3.2.5 Reduction of ATR to ROL

In contrast to ATR, ROL fluoresces so its formation can be easily monitored. In rods reduction of ATR to ROL is catalysed by photoreceptor retinol dehydrogenase (prRDH) using NADPH as a cofactor (as discussed in the Introduction section) and therefore is concomitant with a decrease in NADPH fluorescence with a maximum at ~450 nm and an increase in ROL fluorescence with a maximum at ~490 nm, providing a means to monitor ATR reduction (Schadel at al., 2003).

ATR can be reduced either while being still in the "exit" site of opsin or after being released to the disc membrane upon rhopdopsin/*iso*rhopdopsin generation. Once in the disc membrane, ATR binds via a Schiff base to an abundant phospholipid PE forming NRPE. ATP-binding cassette transporter rim protein (ABCR) is involved in transporting NRPE from the inner leaflet to the outer leaflet of the disc membrane, where ATR becomes accessible for enzymatic reduction. Thus, it can be expected that in discs with *iso*rhodopsin, enzymatic reduction of ATR to ROL will be facilitated in the presence of ATP.

Formation of ROL from ATR depends on the presence of NADPH/ATP, and can be monitored simply from its intrinsic fluorescence as it has been done both *in vitro* (MacDonald and Ong, 1987; Loew et al., 2001; Gonzalez-Fernandez et al., 2009) and *in vivo* (Kaplan, 1985; Tsina et al., 2004; Chen *at al.,* 2005; Chen *at al.,* 2009). Monitoring of ROL formation was used to assess the kinetics of ATR reduction (as described in the Methods section).

To determine conditions under which ATR is reduced to form ROL, kinetics of increase in ROL fluorescence were monitored after photobleaching of POS discs suspension in the presence and absence of NADPH, ATP, and/or 9-*cis*-retinal. NADH was tested as an alternative, control cofactor. Measurements were taken at 19-21°C and 37°C. Parameters of measurements were adjusted to minimise the contribution of NADPH emission to the fluorescence measured (Methods Section 2.2.1).

3.3 Results

3.3.1 Purity of POS discs isolated from bovine retinas

TEM imaging of POS disc revealed substantial differences in purity of POS discs between discs located in the interface and the pellet (representative images shown in Fig. 3.1). The interface was characterised by the presence of separated discs. Although some discs in the pellet were also separated, some

appeared to remain attached to other discs. Additionally, discs from the pellet were distinctively contaminated with other cellular components such as cellular membrane (green arrow in Fig. 3.1; purple arrows show various contaminations). POS discs from the interface only were used for further experiments.

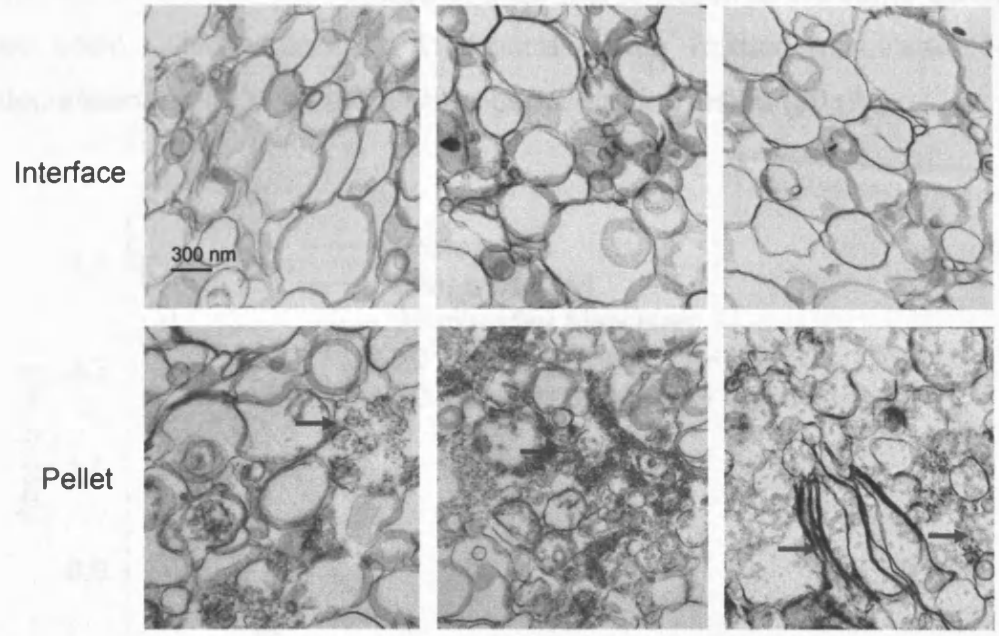

Figure 3.1 Representative TEM images of POS discs collected from two different parts of Ficoll/water phases: Ficoll/water interface and pellet.

3.3.2 Generation of *iso*rhodopsin in POS discs from frozen and fresh retinas

Addition of 9-*cis*-retinal to bleached POS discs isolated from dark adapted frozen retinas did not result in formation of *iso*rhodopsin (see Fig. 3.2), based on a lack of an absorption peak at 478 nm, characteristic for *iso*rhodopsin (Fan *at al.,* 2003). *Iso*rhodopsin was not present even after addition of 9-*cis*-retinal in concentrations two times greater than the initial concentration of rhodopsin.

POS discs obtained from fresh retinas, on the other hand, exhibited the ability to generate *iso*rhodopsin upon addition of 9-*cis*-retinal, as indicated in Fig. 3.3 by an absorption peak at 478 nm. There was an absorption peak at 478 nm characteristic for *iso*rhodopsin. Figure 3.4 A shows absorption spectra for

unbleached and bleached POS discs with and without 9-*cis*-retinal added exogenously at different proportions to opsin/rhodopsin. There was a peak observed at 487 nm that increased in amplitude with increasing concentration of 9-*cis*-retinal. The yield of *iso*rhodopsin formed was proportional to the amount of the retinoid, but did not mirror the concentration of added retinoid (as shown on Fig. 3.4 B). The percentage of 9-*cis*-retinal added at the same concentration as opsin, which becomes incorporated into *iso*rhodopsin, was 54% and decreased to ~40% for the highest concentration tested (20 μM).

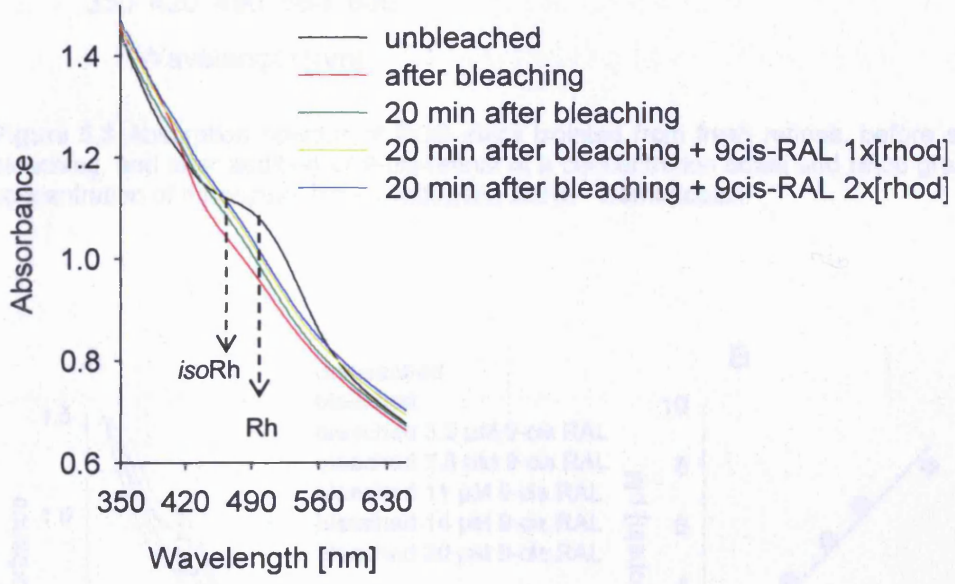

Figure 3.2 Absorption spectra of POS discs isolated from dark adapted, frozen retinas, before and just after bleaching and after addition of 9-*cis*-retinal at a concentration equal and twice greater than the concentration of rhodopsin. Rh – rhodopsin, *iso*Rh - *iso*rhodopsin.

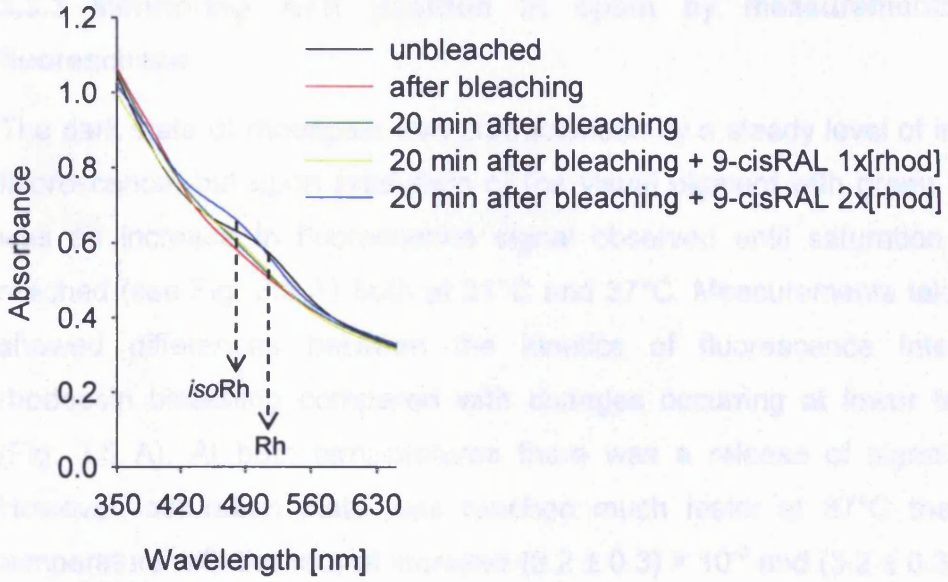

Figure 3.3 Absorption spectra of POS discs isolated from fresh retinas, before and just after bleaching, and after addition of 9-*cis*-retinal at a concentration equal and twice greater than the concentration of rhodopsin. Rh – rhodopsin, *iso*Rh - *iso*rhodopsin.

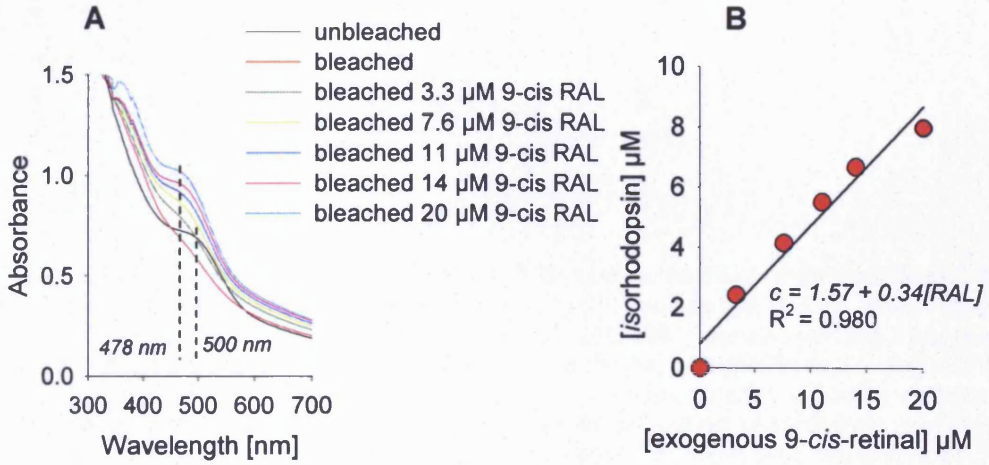

Figure 3.4 Formation of isorhodopsin. **A** - Absorption spectra of POS discs isolated from fresh retinas, before and just after bleaching and after addition of 9-*cis*-retinal at selected concentrations. Concentration of rhodopsin and opsin in POS discs 3.3 µM and 7.6 µM, respectively. **B** - Dependency of *iso*rhodopsin concentration formed after addition of selected concentrations of exogenous 9-*cis*-retinal to POS discs containing 3.3 µM rhodopsin and 7.6 µM opsin.

3.3.3 Monitoring ATR position in opsin by measurements of Trp fluorescence

The dark state of rhodopsin was characterised by a steady level of intrinsic Trp fluorescence, but upon irradiation of the visual pigment with green light, there was an increase in fluorescence signal observed until saturation state was reached (see Fig. 3.5 A) both at 21°C and 37°C. Measurements taken at 37°C showed differences between the kinetics of fluorescence intensity after rhodopsin bleaching compared with changes occurring at lower temperature (Fig. 3.5 A). At both temperatures there was a release of signal observed. However, saturation state was reached much faster at 37°C than at room temperature with the rate of increase $(8.2 \pm 0.3) \times 10^{-3}$ and $(3.2 \pm 0.3) \times 10^{-3}$ s^{-1}, respectively (Tab. 3.1).

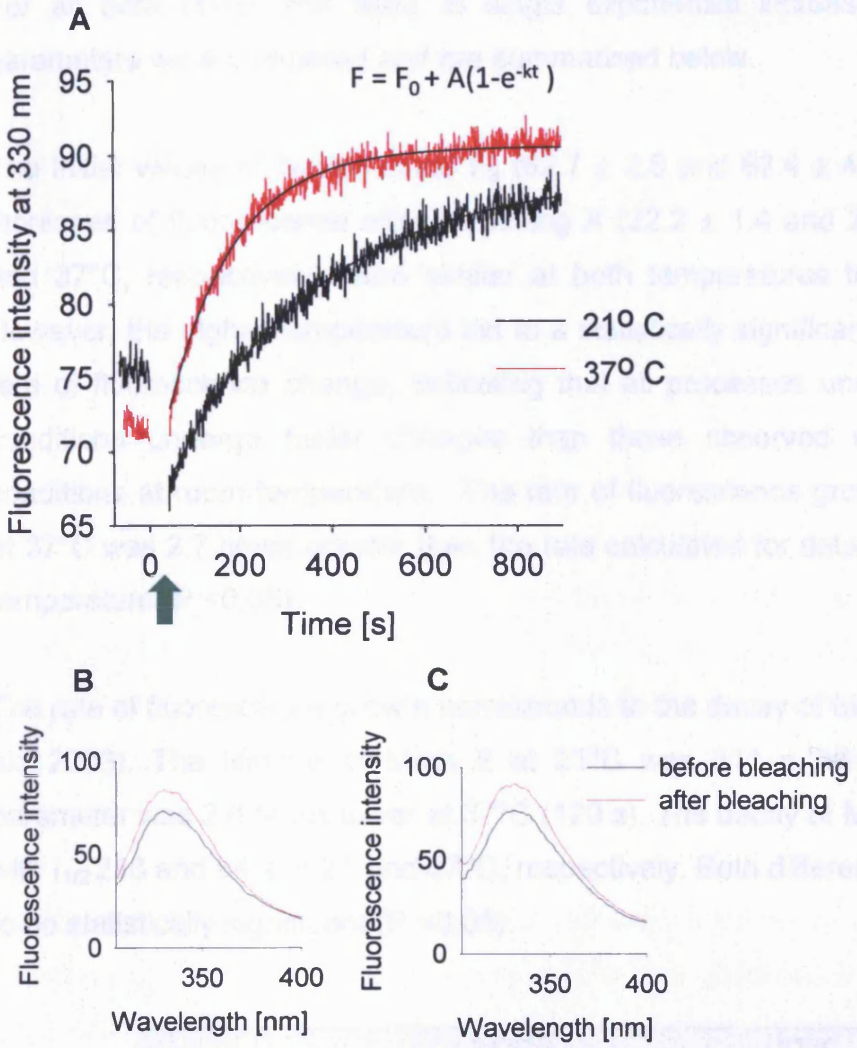

Figure 3.5 A – Time-dependent changes of fluorescence emission monitored at 330 nm before and after bleaching with green light of 1 μM rhodopsin in POS discs measured at 21 °C (black kinetics) and 37 °C (red kinetics); excitation wavelength 295 nm; green arrow indicates rhodopsin bleaching; black, smooth lines correspond to a fitted equation. Green arrow refers to rhodopsin bleaching with green light. **B**, **C** - Fluorescence emission spectra recorded in the range 305-400 nm before and after complete bleaching of rhodopsin and hydrolysis of ATR from the active site of rhodopsin (approximately 17 minutes after bleaching) at 21 (**B**) and 37 °C (**C**); excitation wavelength 295 nm.

For all data taken and fitted to single exponential increase to maximum, parameters were compared and are summarised below.

The initial values of fluorescence F_0 (62.7 ± 2.8 and 63.4 ± 4.8) and maximal increases of fluorescence after bleaching A (22.2 ± 1.4 and 24.3 ± 1.7 for 21 and 37°C, respectively) were similar at both temperatures tested ($P > 0.05$). However, the higher temperature led to a statistically significant increase of the rate of fluorescence change, indicating that all processes under physiological conditions undergo faster changes than those observed under laboratory conditions at room temperature. The rate of fluorescence growth (k) observed at 37°C was 2.7 times greater than the rate calculated for data taken at a lower temperature ($P < 0.05$).

The rate of fluorescence growth corresponds to the decay of Meta II (Schadel et al., 2003). The lifetime of Meta II at 21°C was 311 s, whereas the same parameter was 2.6 times lower at 37°C (120 s). The decay of Meta II proceeded with $t_{1/2}$ 216 and 84 s at 21 and 37°C, respectively. Both differences were shown to be statistically significant ($P < 0.05$).

	21°C		37°C
F_0	62.7 ± 2.8		63.4 ± 4.8
A	22.2 ± 1.4		24.3 ± 1.7
k [s^{-1}]	$(3.2 \pm 0.3) \times 10^{-3}$	*	$(8.2 \pm 0.3) \times 10^{-3}$
τ [s]	311 ± 30	*	120 ± 4
$t_{1/2}$ [s]	216 ± 20	*	84 ± 3

Table 3.1 Comparison of parameters for time-dependent changes of Trp fluorescence in POS discs with 1 μM rhodopsin at 21 and 37°C. Fitted to $F = F_0 + a(1-e^{-kt})$; mean ± SD; number of repeated measurements (n) = 3. F_0 – initial fluorescence intensity, A – increase of fluorescence after bleaching, k – rate constant of decay, τ – lifetime, $t_{1/2}$ - half-life. The symbol "*" represents statistically significant difference of parameters between 21 and 37°C.

3.3.4 The influence of different retinoids on tryptophan fluorescence in POS discs

3.3.4.1 The effect of the addition of ATR

Addition of exogenous ATR to bleached POS discs with completely decayed Meta II or opsin deprived of retinoids resulted in a decrease of Trp fluorescence (Fig. 3.6 and 3.7).

After bleaching of rhodopsin in POS discs there was an increase of fluorescence signal characterised by exponential growth, with a rate constant of (3.6 ±0.1) × 10^{-3} s^{-1}. Addition of ATR resulted in a biphasic quenching effect on Trp fluorescence (Fig. 3.6). The initial quenching process was completed within ~30 s. The following decay of Trp fluorescence was adequately fitted by a single exponential decay with a rate constant of (9.4 ±0.6) ×10^{-3} s^{-1}, followed by a linear decay.

Addition of ATR to opsin deprived of retinoids resulted in a rapid, biphasic decrease of Trp fluorescence, similar to the one observed in POS discs with completely hydrolysed ATR (Fig. 3.7). The initial phase of quenching proceeded with a rate constant of (8.1±0.1) ×10^{-2} s^{-1}. It was completed within about 30 s, and was followed by a linear decrease until a plateau state was reached. Illumination of the sample did not result in a substantial change of observed signal. However, when observed over a longer time scale, illumination of the sample led to a further decrease of signal, suggesting photooxidative damage of the monitored amino acid.

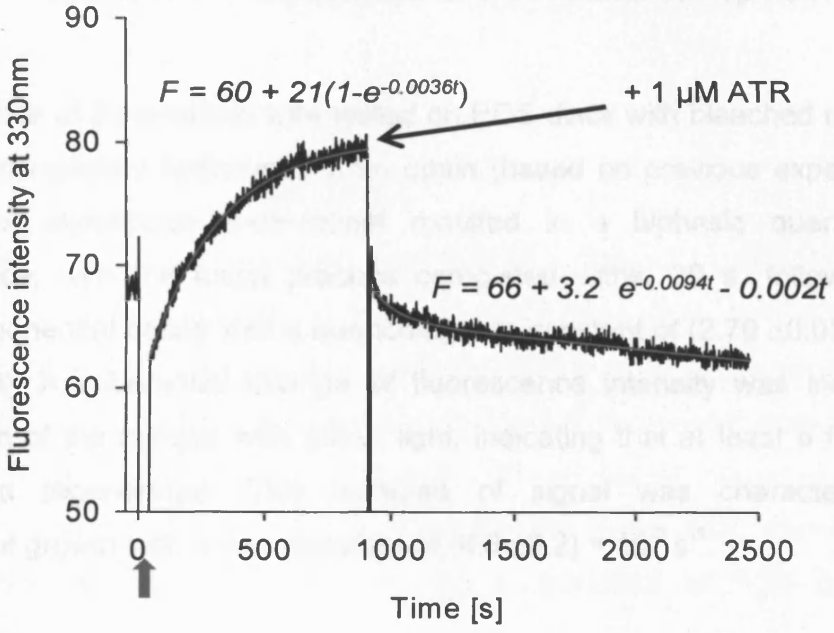

Figure 3.6 Time-dependent changes of tryptophan fluorescence in POS discs before and after bleaching of 1 µM rhodopsin and after addition of 1 µM ATR; 21°C; excitation wavelength 295 nm. Green arrow indicates rhodopsin bleaching. Red lines correspond to a fitted equation.

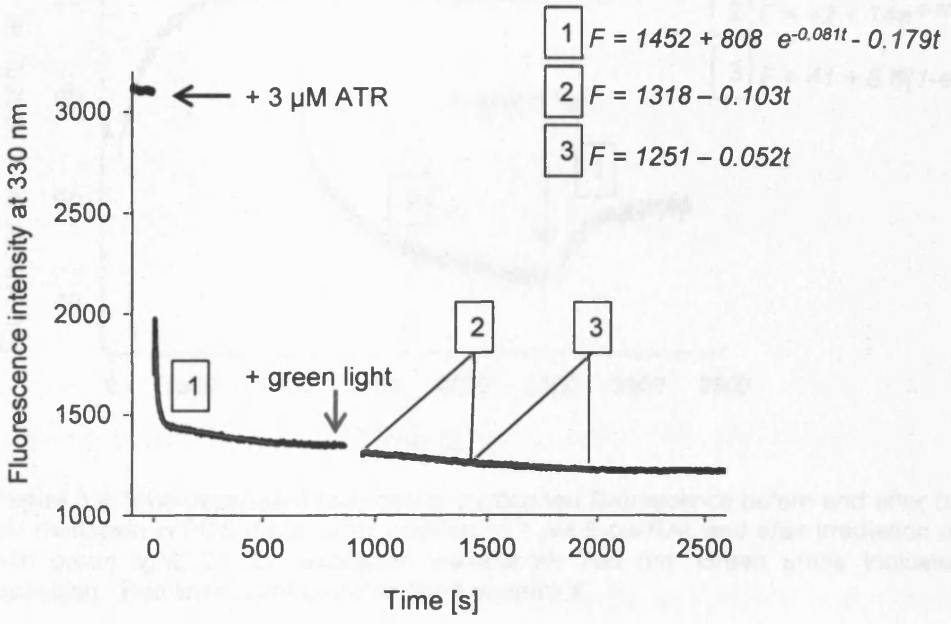

Figure 3.7 Time-dependent changes of tryptophan fluorescence in POS with 3 µM opsin deprived from retinoids before and after addition of 3 µM ATR and after irradiation with green light; 21°C; excitation wavelength 295 nm. Red lines correspond to fitted equations.

3.3.4.2 The effect of the addition of 9-*cis*-retinal on Trp fluorescence in POS

The influence of 9-*cis*-retinal was tested on POS discs with bleached rhodopsin and ATR completely hydrolysed from opsin (based on previous experiments). Addition of exogenous 9-*cis*-retinal resulted in a biphasic quenching of fluorescence, with the initial process completed within 20 s, followed by a further exponential decay with a quenching rate constant of (2.70 ±0.03) $\times 10^{-3}$ s^{-1} (Fig. 3.8). A substantial change of fluorescence intensity was induced by illumination of the sample with green light, indicating that at least a fraction of opsin was regenerated. The increase of signal was characterised by exponential growth with a rate constant of (6.6 ±0.2) $\times$ 10^{-3} s^{-1}.

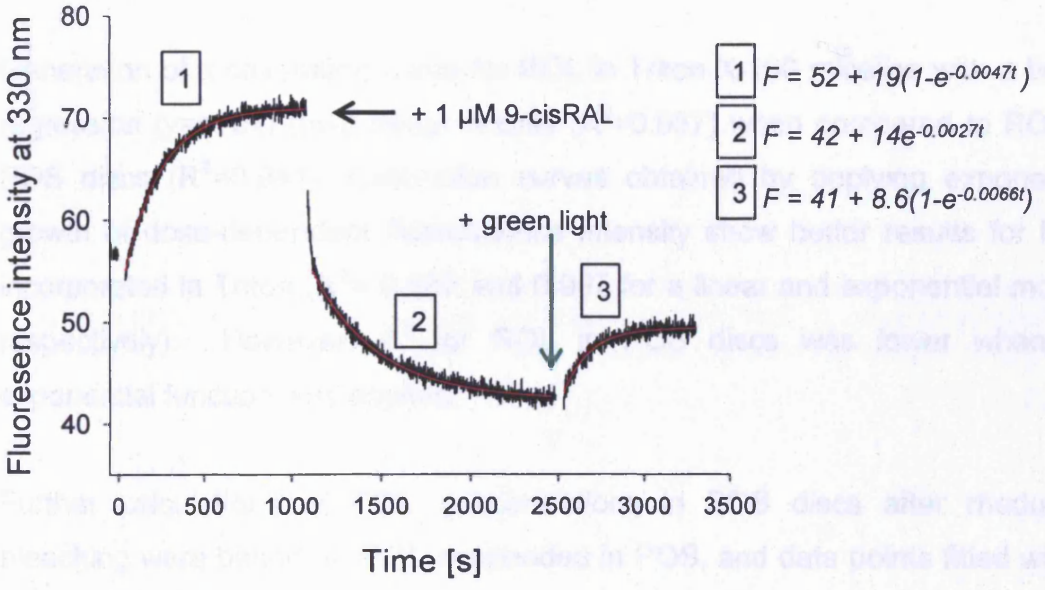

Figure 3.8 Time-dependent changes of tryptophan fluorescence before and after bleaching of 1 µM rhodopsin in POS discs, after addition of 1 µM 9-*cis*-RAL and after irradiation of the sample with green light; 21 °C; excitation wavelength 295 nm. Green arrow indicates rhodopsin bleaching. Red lines correspond to fitted equations.

3.3.5 Formation of ROL in POS discs monitored by measurements of its fluorescence intensity

3.3.5.1 Calibration curve of ROL

A calibration curve was used to quantify ROL obtained in POS discs after rhodopsin bleaching based on its fluorescence values. ROL was incorporated into either Triton X-100 micelles or photoreceptor outer segment discs and suspended in PBS in order to determine its yield of fluorescence as a function of concentration in different environments. Fluorescence intensity of ROL in POS discs was lower than fluorescence for the same ROL concentrations observed in micelles, indicating that the environment of POS discs may influence its fluorescence.

Generation of a calibration curve for ROL in Triton X-100 micelles with a linear regression (y=a+bx) gave better results (R^2=0.987) when compared to ROL in POS discs (R^2=0.941). Calibration curves obtained by applying exponential growth of dose-dependent fluorescence intensity show better results for ROL incorporated in Triton (R^2= 0.987 and 0.997 for a linear and exponential model, respectively). However, R^2 for ROL in POS discs was lower when an exponential function was applied.

Further calculations of ROL concentrations in POS discs after rhodopsin bleaching were based on ROL suspended in POS, and data points fitted with a linear regression.

Concentration-dependent fluorescence spectra of NADPH and calibration curve fitted to a linear regression are presented in Figure 3.10 A and B, respectively.

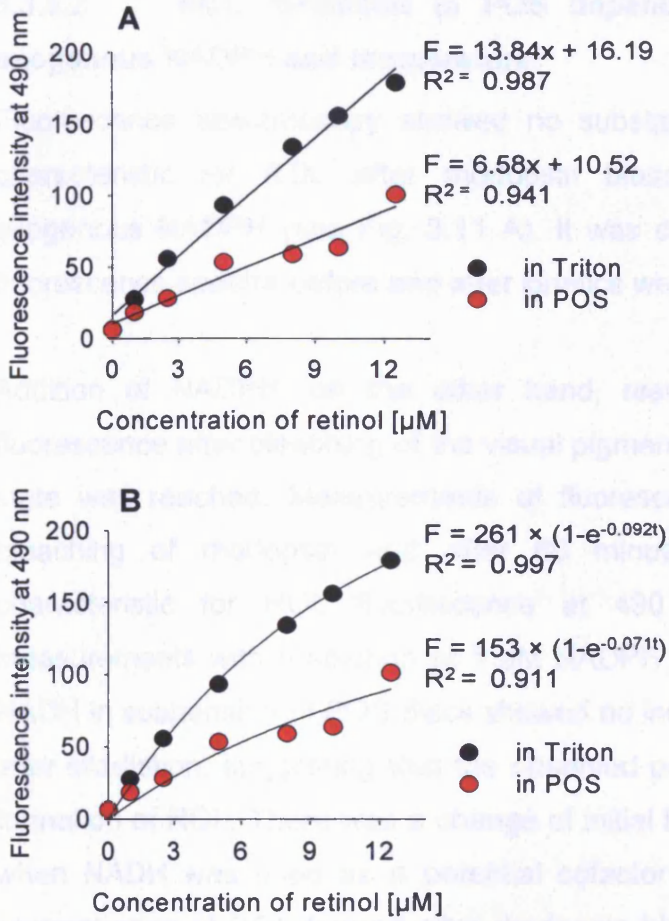

Figure 3.9 Calibration curves for ROL fluorescence at different concentrations of ROL dissolved in Triton X-100 and suspended in ethanol and incorporated into POS. **A** - data points fitted to a linear regression; **B** - data points fitted to a single exponent. Excitation wavelength of 295 nm.

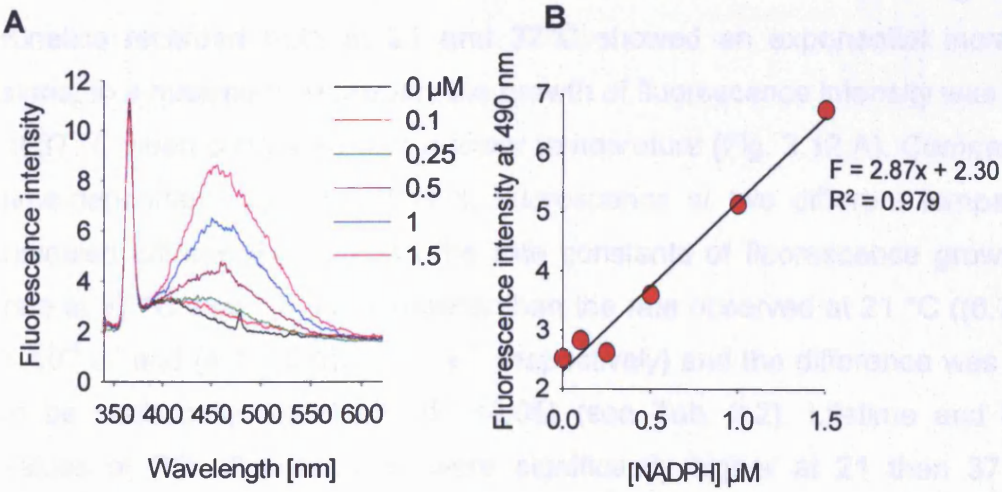

Figure 3.10 Fluorescence of NADPH. **A** – Emission spectra of NADPH at indicated concentrations. **B** - Calibration curves for NADPH fluorescence after solubilisation in PBS. Excitation wavelength of 295 nm.

3.3.5.2 ROL formation in POS dependening on the presence of exogenous NADPH and temperature

Fluorescence spectroscopy showed no substantial changes in fluorescence characteristic for ROL after rhodopsin bleaching in POS discs without exogenous NADPH (see Fig. 3.11 A). It was confirmed by measurements of fluorescence spectra before and after kinetics were recorded (Fig. 3.11 E).

Addition of NADPH, on the other hand, resulted in an increase in ROL fluorescence after bleaching of the visual pigment (Fig. 3.11 A) until a saturation state was reached. Measurements of fluorescence spectra recorded before bleaching of rhodopsin and after 60 minutes revealed an increase of characteristic for ROL fluorescence at 490 nm (Fig. 3.12 B). Control measurements with a solution of 1 µM NADPH in PBS and a sample of 1 µM NADH in suspension of POS discs showed no increase in fluorescence intensity after irradiation, suggesting that the observed process is a NADPH-dependent formation of ROL. There was a change of initial fluorescence intensity observed when NADH was used as a potential cofactor (Fig. 3.11 A). Calculations of concentration of ROL formed after rhodopsin bleaching and hydrolysis of ATR was ~0.97 µM.

Kinetics of ROL fluorescence was also monitored at 37 °C (see Fig. 3.12 A). Kinetics recorded both at 21 and 37°C showed an exponential increase of signal to a maximum. However, the growth of fluorescence intensity was greater at 37 °C when compared with a lower temperature (Fig. 3.12 A). Comparison of time-dependent changes of ROL fluorescence at two different temperatures revealed differences between the rate constants of fluorescence growth. The rate at 37 °C was 1.4 times greater than the rate observed at 21 °C ($(6.7 \pm 0.6) \times 10^{-4}\ s^{-1}$ and $(4.7 \pm 0.6) \times 10^{-4}\ s^{-1}$, respectively) and the difference was proved to be statistically significant ($P < 0.05$) (see Tab. 3.2). Lifetime and half-life values of ROL fluorescence were significantly higher at 21 than 37 °C ($P > 0.05$). Both initial values of fluorescence and the maximal increases of fluorescence after bleaching (A) were found to be significantly different for both 21°C and 37°C ($P < 0.05$).

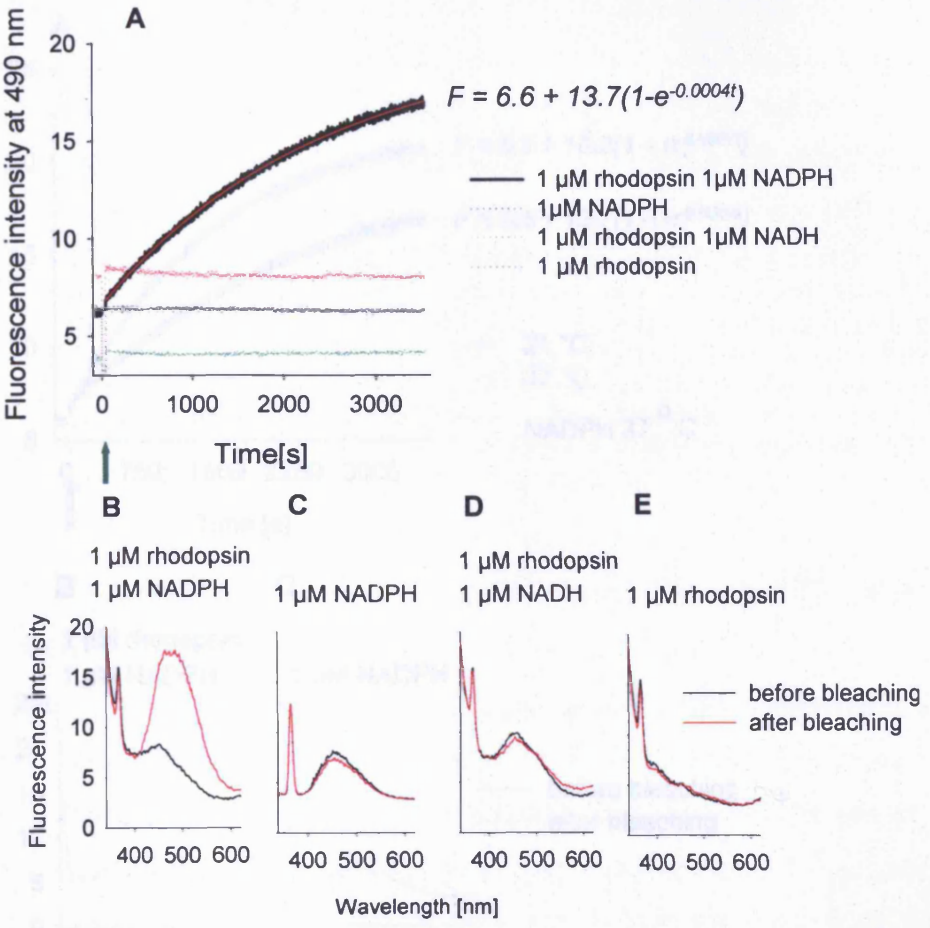

Figure 3.11 ROL fluorescence in POS discs monitored at 21°C. **A** – Time-dependent changes of fluorescence emission monitored at 490 nm before and after bleaching with green light of 1 µM rhodopsin in POS discs; control measurements involved samples with 1 µM NADPH only, POS discs with 1 µM rhodopsin with addition of 1 µM NADH and without addition of exogenous components; Samples kept at temperature of 21 °C; excitation wavelength of 324 nm; green arrow indicates rhodopsin bleaching; smooth red line indicates the kinetics fitted to a single exponential rise to a maximum $F = F_0 + A(1-e^{-kt})$. **B, C, D, E** - Fluorescence emission spectra recorded in the range 340-620 nm before and after complete bleaching of rhodopsin and hydrolysis of ATR from the active site of rhodopsin (60 minutes after bleaching) in the same samples as in 3.11 A. Excitation wavelength of 324 nm.

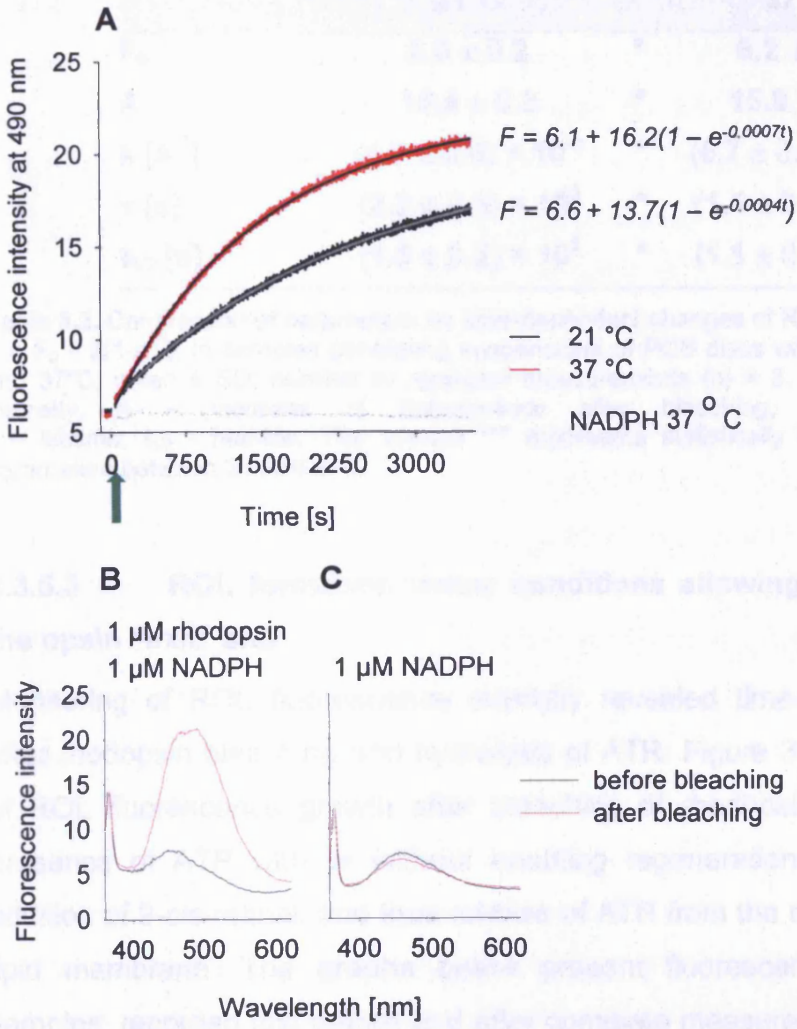

Figure 3.12 Comparison of ROL fluorescence in POS discs monitored at 21 and 37°C. **A** – Representative time-dependent changes of ROL fluorescence monitored at 490 nm before and after bleaching of POS discs with 1 µM rhodopsin and 1 µM NADPH measured at 21 and 37 °C; measurement with 1 µM NADPH as a control; excitation wavelength 324 nm; green arrow indicates rhodopsin bleaching. Red line corresponds to fitted equations. **B, C** - Representative fluorescence emission spectra of ROL in the range 340 - 620 nm at 37°C before and after complete bleaching of rhodopsin (60 minutes after bleaching) in POS discs with 1 µM rhodopsin and 1 µM NADPH (B); 1 µM NADPH as a control (C).

	21°C		37°C
F_0	**6.8** ± 0.2	*	**6.2** ± 0.1
A	**13.4** ± 0.3	*	**15.8** ± 0.6
k [s^{-1}]	**(4.7** ± 0.6) × 10^{-4}	*	**(6.7** ± 0.6) × 10^{-4}
τ [s]	**(2.2** ± 0.3) × 10^3	*	**(1.5** ± 0.1) × 10^3
$t_{1/2}$ [s]	**(1.5** ± 0.2) × 10^3	*	**(1.1** ± 0.1) × 10^3

Table 3.2. Comparison of parameters for time-dependent changes of ROL fluorescence fitted to $F = F_0 + a(1-e^{-kt})$; in samples containing suspensions of POS discs with 1 μM rhodopsin at 21 and 37°C; mean ± SD; number of repeated measurements (n) = 3. F_0 – initial fluorescence intensity, A – increase of fluorescence after bleaching, k – rate constant, τ – lifetime, $t_{1/2}$ - half-life. The symbol "*" represents statistically significant difference of parameters between 21 and 37°C.

3.3.5.3 ROL formation under conditions allowing ATR release from the opsin "exit" site

Monitoring of ROL fluorescence intensity revealed time-dependent changes after rhodopsin bleaching and hydrolysis of ATR. Figure 3.13 A shows kinetics of ROL fluorescence growth after bleaching of rhodopsin depending on the presence of ATP with or without enabling regeneration of isorhodopsin by addition of 9-*cis*-retinal, and thus release of ATR from the opsin "exit" site to the lipid membrane. The graphs below present fluorescence spectra for the samples, recorded just before and after complete measurements of kinetics (60 minutes). Addition of 9-*cis*-retinal with or without ATP to the same sample resulted in a decrease of the difference between the fluorescence intensity before and after rhodopsin bleaching, with 9-*cis*-retinal alone having the greatest effect (Fig. 3.13 B, C, D).

The initial fluorescence value (F_0) was higher in samples with NADPH only when compared to samples with 9-*cis*-retinal with or without ATP (see Tab. 3.3) and the differences were found to be statistically significant ($P < 0.05$; Fig. 3.14). The highest initial increase of fluorescence within bleaching time (F_1) was observed in samples with exogenous NADPH present and regenerated *iso*rhodopsin (0.98 ±0.01). The amplitude of fluorescence reached the lowest value of 1.71 ± 0.01 in samples with NADPH and regenerated *iso*rhodopsin, suggesting that regeneration of the pigment led to

releasing of ATR to the inner leaflet of POS discs where it cannot be reduced to ROL. Addition of ATP to the same sample resulted in an increase of the A value, indicating that the presence of cofactor for ABCR protein allowed ATR to be accessible to retinol dehydrogenase. The difference between the sample with and without addition of ATP was statistically significant ($P < 0.05$; Fig. 3.14). The rate of fluorescence increase in samples with NADPH and regenerated *iso*rhodopsin was similar in all samples compared.

13-*cis*-retinal, when compared with 9-*cis*-retinal, had a considerably smaller effect on the kinetics of fluorescence changes in the presence of ATP (Fig. 3.15 A, B, C, D, E, F). Initial values of fluorescence (F_0) were found to be similar in the presence of NADPH and ATP with or without 13-*cis*-retinal (Tab. 3.5; Fig. 3.15). F_0 for samples with regenerated *iso*rhodopsin was the lowest when compared with two other samples (7.18 ±0.49). The differences were not found to be significant ($P > 0.05$; Fig. 3.16 A). An initial decrease of fluorescence signal was significantly different between samples: -0.006 ± 0.008 and -0.021 ± 0.001 for 9-*cis* and 13-*cis*-retinal, respectively ($P < 0.05$), with only samples containing 13-*cis*-retinal being significantly different from the control sample. Increase of fluorescence intensity after rhodopsin bleaching and hydrolysis of ATR was significantly higher in samples with addition of 13-*cis*-retinal (4.02 ± 0.01) in comparison with 9-*cis*-retinal (2.52 ± 0.27) ($P < 0.05$). There were no significant differences in the constant rates between the samples ($P > 0.05$).

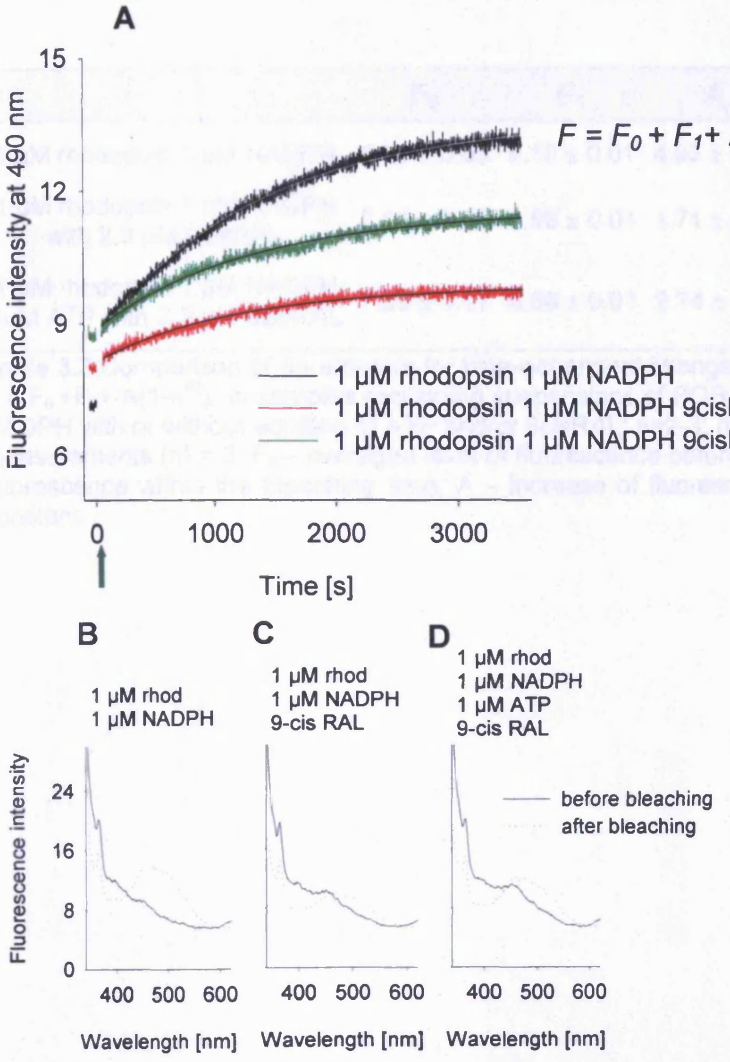

Figure 3.13 A - Time-dependent changes of ROL fluorescence monitored at 490 nm before and after bleaching of POS discs with 1 µM rhodopsin and 1 µM NADPH, 1 µM rhodopsin and 1 µM NADPH with regenerated isorhodopsin by addition of 9-*cis*-retinal and 1 µM rhodopsin and 1 µM NADPH with regenerated *iso*rhodopsin and 1 µM ATP; measured at 21 °C; excitation wavelength of 324 nm. Green arrow indicates rhodopsin bleaching; black/grey, smooth lines correspond to a fitted equation. **B**, **C**, **D** - Fluorescence emission spectra of ROL in the range 340 - 620 nm before and after complete bleaching of rhodopsin (60 minutes after bleaching) in POS discs with 1 µM rhodopsin and 1 µM NADPH (**B**), 1 µM rhodopsin and 1 µM NADPH with regenerated *iso*rhodopsin by addition of 9-*cis*-retinal (**C**) and 1 µM rhodopsin and 1 µM NADPH with regenerated isorhodopsin and 1 µM ATP (**D**); measured at 21 °C; excitation wavelength 324 nm.

	F_0	F_1	A	k [s^{-1}]
1 μM rhodopsin 1 μM NADPH	**8.66** ± 0.06	**0.19** ± 0.01	**4.96** ± 0.06	(**7** ± 1)×**10**$^{-4}$
1 μM rhodopsin 1 μM NADPH with 2.3 μM 9*cis*RAL	**7.11** ± 0.03	**0.98** ± 0.01	**1.71** ± 0.01	(**8** ± 1)×**10**$^{-4}$
1 μM rhodopsin 1 μM NADPH 1uM ATP with 2.3 μM 9*cis*RAL	**7.99** ± 0.07	**0.88** ± 0.01	**2.74** ± 0.05	(**7** ± 1)×**10**$^{-4}$

Table 3.3 Comparison of parameters for time-dependent changes of ROL fluorescence fitted to $F = F_0 + F_1 + A(1-e^{-kt})$; in samples containing suspensions of POS discs with 1 μM rhodopsin and NADPH with or without addition of ATP and/or 9cisRAL; n=2-3; mean ± SD; number of repeated measurements (n) = 3. F_0 – averaged level of fluorescence before bleach, F_1 – initial increase of fluorescence within the bleaching time, A – increase of fluorescence after bleaching, k – rate constant.

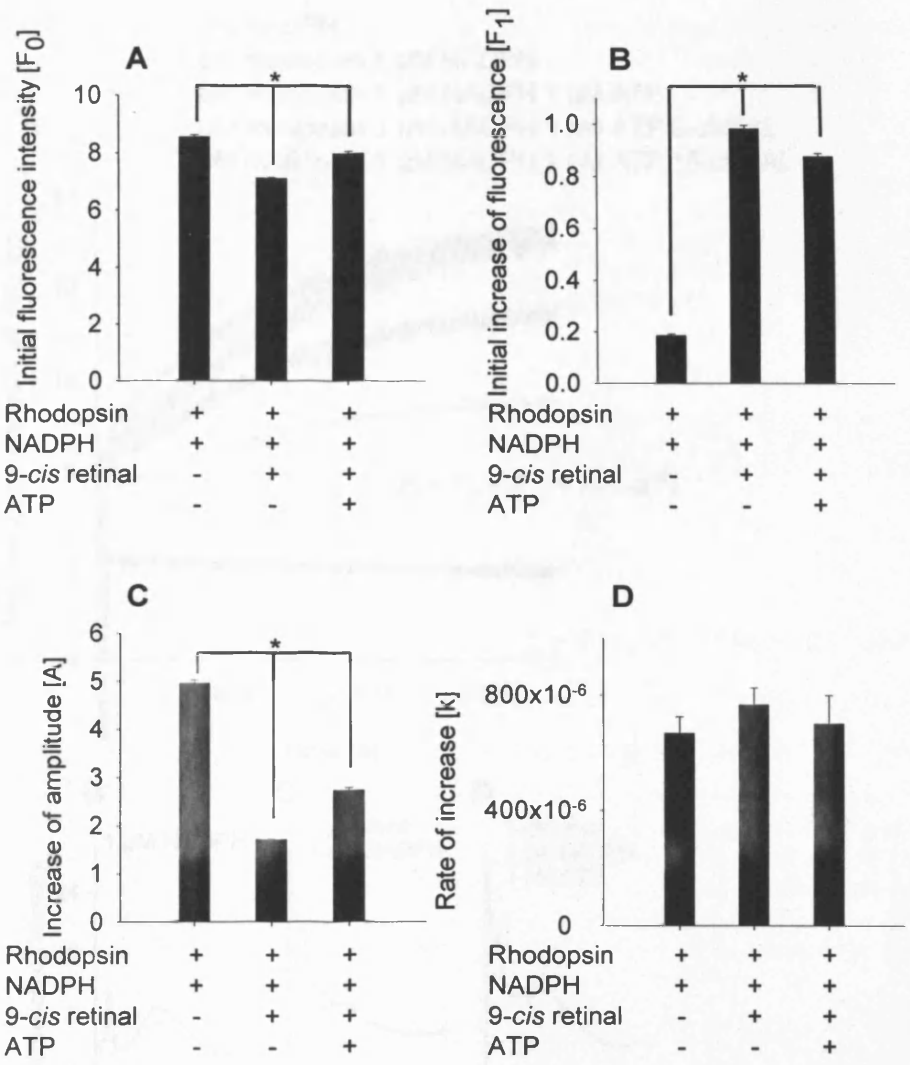

Figure 3.14 Comparison of parameters for time-dependent changes of ROL fluorescence fitted to $F = F_0 + F_1 + A(1-e^{-kt})$ (n=3) in samples containing suspensions of POS discs with 1 μM rhodopsin and 1 μM NADPH with or without addition of 9-*cis* RAL and ATP. A – initial fluorescence intensity; B – initial fluorescence intensity within bleaching time; C – amplitude of fluorescence before and after measurement; D – rate of fluorescence intensity increase. The symbol "*" represents statistically significant difference of parameters between indicated samples.

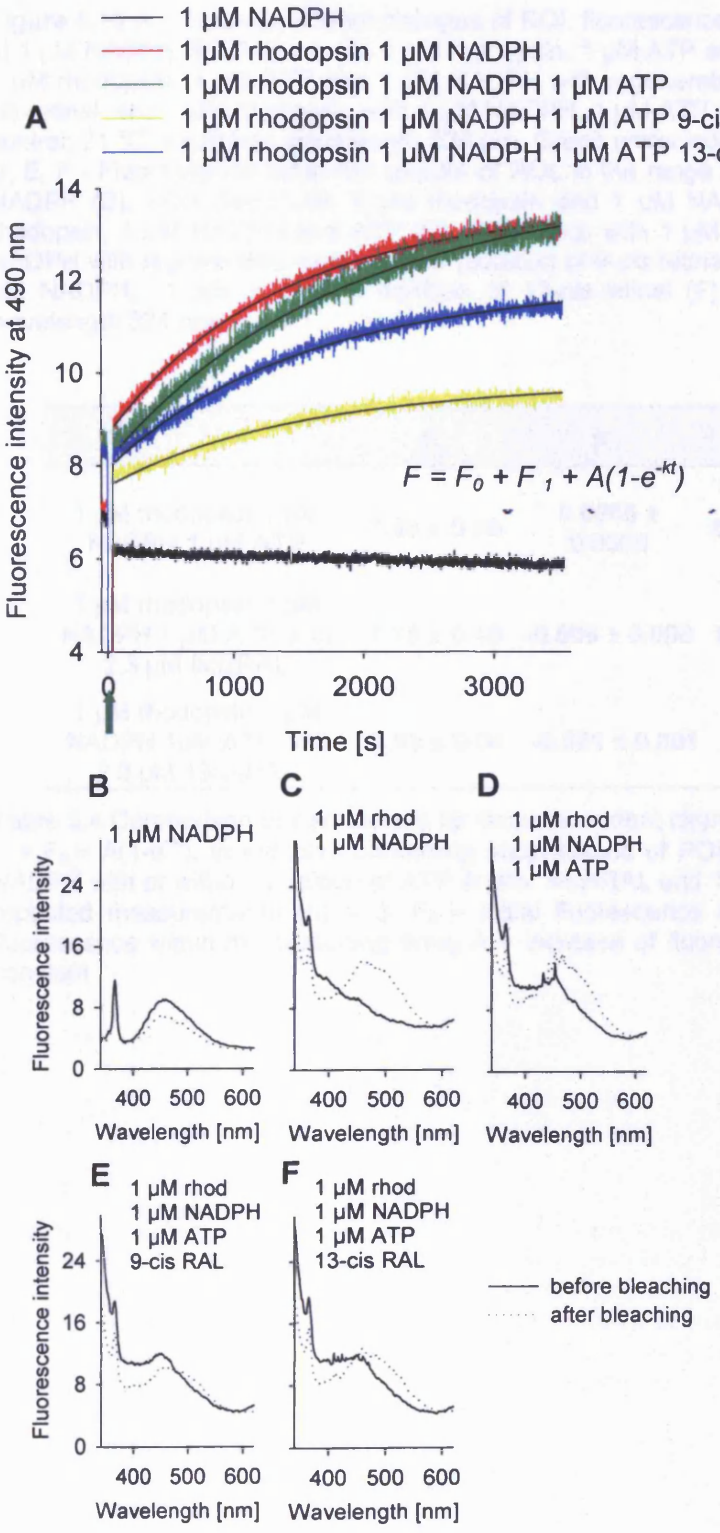
A
1 µM NADPH
1 µM rhodopsin 1 µM NADPH
1 µM rhodopsin 1 µM NADPH 1 µM ATP
1 µM rhodopsin 1 µM NADPH 1 µM ATP 9-cisRAL
1 µM rhodopsin 1 µM NADPH 1 µM ATP 13-cisRAL
Fluorescence intensity at 490 nm
14
12
10
8
6
4
0
1000
2000
3000
Time [s]
$F = F_0 + F_1 + A(1-e^{-kt})$
B
1 µM NADPH
C
1 µM rhod
1 µM NADPH
D
1 µM rhod
1 µM NADPH
1 µM ATP
Fluorescence intensity
24
16
8
0
400 500 600
Wavelength [nm]
E
1 µM rhod
1 µM NADPH
1 µM ATP
9-cis RAL
F
1 µM rhod
1 µM NADPH
1 µM ATP
13-cis RAL
before bleaching
after bleaching

Figure 3.15 A - Time-dependent changes of ROL fluorescence monitored at 490 nm in solution of 1 μM NADPH, POS discs with 1 μM rhodopsin, 1 μM ATP and 1 μM NADPH, POS discs with 1 μM rhodopsin, 1 μM ATP and 1 μM NADPH with regenerated isorhodopsin by addition of 9-cis-retinal and 1 μM rhodopsin with 1 μM NADPH, 1 μM ATP with addition of 13-*cis*-retinal as a control; 21 °C; excitation wavelength 324 nm. Green arrow indicates rhodopsin bleaching. **B, C, D, E, F** - Fluorescence emission spectra of ROL in the range 340 - 620 nm in solution of 1 μM NADPH (B), POS discs with 1 μM rhodopsin and 1 μM NADPH (C), POS discs with 1 μM rhodopsin, 1 μM NADPH and ATP (D), POS discs with 1 μM rhodopsin, 1 μM ATP and 1 μM NADPH with regenerated *iso*rhodopsin (addition of 9-*cis*-retinal) (E) and 1 μM rhodopsin with 1 μM NADPH, 1 μM ATP with addition of 13-*cis*-retinal (F) as a control; 21 °C; excitation wavelength 324 nm.

	F_0	F_1	A	k [s^{-1}]
1 μM rhodopsin 1 μM NADPH 1 μM ATP	**7.89** ± 0.03	**0.0066** ± 0.0006	**6.20** ± 0.02	(**53** ±6) ×10^{-5}
1 μM rhodopsin 1 μM NADPH 1 μM ATP with 2.3 μM 9*cis*RAL	**7.18** ± 0.49	**-0.006** ± 0.008	**2.52** ± 0.27	(**50** ±10) ×10^{-5}
1 μM rhodopsin 1 μM NADPH 1uM ATP with 2.3 μM 13*cis*RAL	**7.93** ± 0.04	**-0.021 ± 0.001**	**4.02** ± 0.01	(**55** ±5) ×10^{-5}

Table 3.4 Comparison of parameters for time-dependent changes of ROL fluorescence fitted to $F = F_0 + A(1-e^{-kt})$; in samples containing suspensions of POS discs with 1 μM rhodopsin and NADPH with or without addition of ATP and/or 9-*cis*RAL and 13-*cis*RAL; mean ± SD; number of repeated measurements (n) = 3. F_0 – initial fluorescence intensity, F_1 – initial increase of fluorescence within the bleaching time, A – increase of fluorescence after bleaching, k – rate constant.

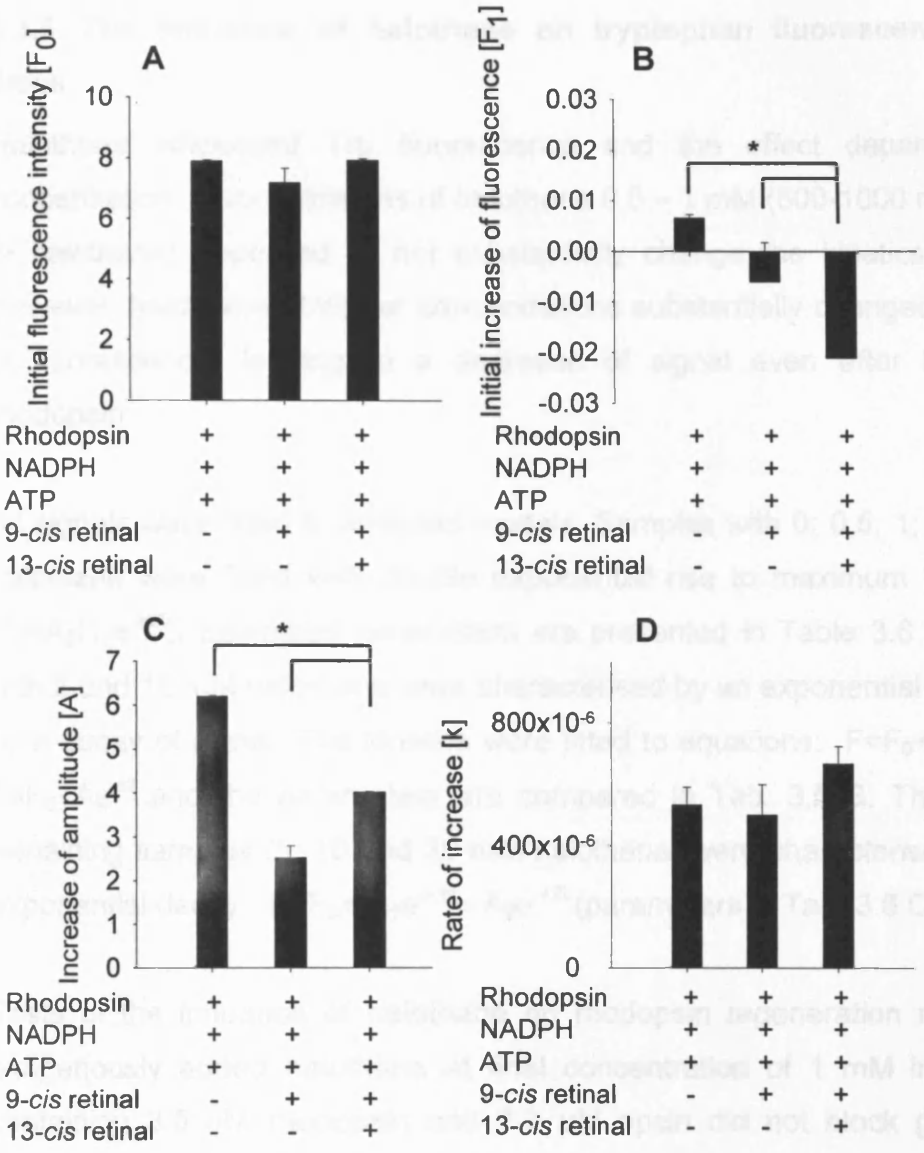

Figure 3.16 Comparison of parameters for time-dependent changes of ROL fluorescence fitted to $F = F_0 + F_1 + A(1-e^{-kt})$ (n=3) in samples containing suspensions of POS discs with 1 μM rhodopsin and 1 μM NADPH with or without addition of 9-*cis*RAL and ATP, 13-*cis*RAL as a control. A – initial fluorescence intensity; B – initial fluorescence intensity within bleaching time; C – amplitude of fluorescence before and after measurement; D – rate of fluorescence intensity increase. The symbol "*" represents statistically significant difference of parameters between indicated samples.

3.3.6 The influence of halothane on tryptophan fluorescence in POS discs

Halothane influenced Trp fluorescence and the effect depended on its concentration. Concentrations of halothane 0.5 – 1 mM (500-1000 molar excess of halothane) appeared to not substantially change the kinetics (Fig. 3.17). However, halothane at higher concentrations substantially changed the kinetics of fluorescence, leading to a decrease of signal even after bleaching of rhodopsin.

All signals were fitted to selected models. Samples with 0; 0.5; 1; 4 and 8 mM halothane were fitted with double exponential rise to maximum $F=F_0+A_1(1-e^{-k1t})+A_2(1-e^{-k2t})$. Estimated parameters are presented in Table 3.6 A. Samples with 2 and 15 mM halothane were characterised by an exponential rise followed by a decay of signal. The kinetics were fitted to equations: $F=F_0+A(1-e^{-kt})$ and $F=F_0+Ae^{-kt}$ and the parameters are compared in Tab. 3.5 B. The kinetics of remaining samples (5; 10 and 20 mM halothane) were characterised by double exponential decay - $F=F_0+ A_1e^{-k1t}+ A_2e^{-k2t}$ (parameters in Tab. 3.6 C).

Tests of the influence of halothane on rhodopsin regeneration revealed that exogenously added halothane at final concentration of 1 mM in POS discs containing 3.5 μM rhodopsin and 7.7 μM opsin did not block generation of *iso*rhodopsin upon addition of 8 μM 9-*cis*-retinal (Fig. 3.18). There was a peak observed characteristic for *iso*rhodopsin based on which its concentration was assessed as 5.6 μM.

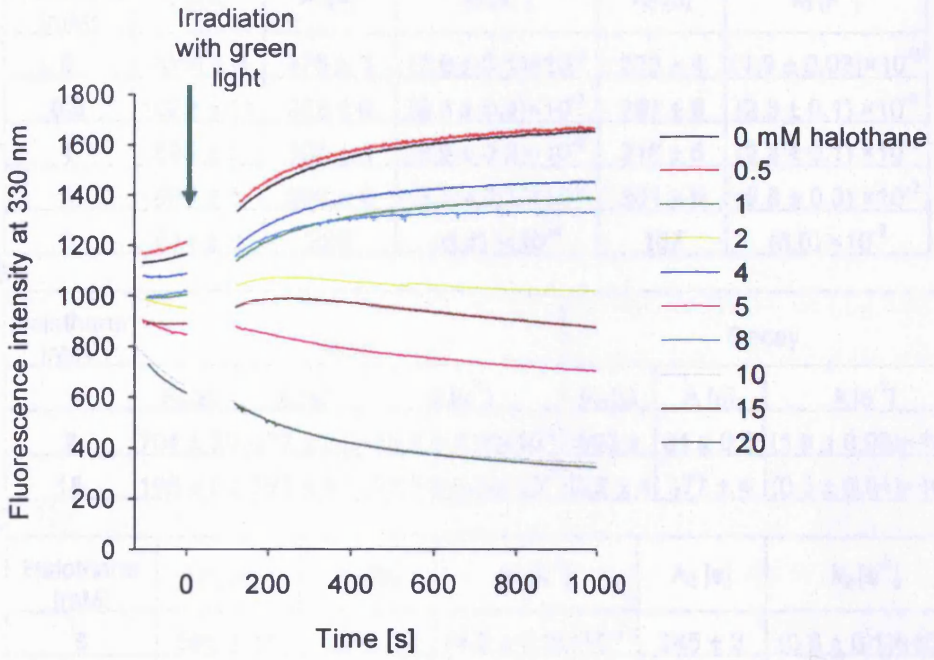

Figure 3.17 Time-dependent changes of tryptophan fluorescence before and after bleaching of 1 µM rhodopsin in POS discs with or without halothane added exogenously at different concentrations; 21 °C; excitation wavelength 295 nm.

A

Halothane [mM]	F_0 [s]	A_1[s]	k_1 [s^{-1}]	A_2 [s]	k_2 [s^{-1}]
0	1044 ± 4	375 ± 3	(7.9 ± 0.1)×10^{-3}	279 ± 4	(1.9 ± 0.03)×10^{-3}
0.5	1029 ± 11	383 ± 6	(9.4 ± 0.3)×10^{-3}	287 ± 8	(2.3 ± 0.1) ×10^{-3}
1	886 ± 5	306 ± 4	(8.6 ± 0.2)×10^{-3}	216 ± 6	(2.3 ± 0.1) ×10^{-3}
4	897 ± 6	265 ± 8	(3.3 ± 0.1)×10^{-3}	301 ± 5	(9.8 ± 0.3) ×10^{-3}
8	944 ± 5	220	(6.8))×10^{-3}	167	(6.8) ×10^{-3}

B

Halothane [mM]	Rise			Decay		
	F_0 [s]	A [s]	k [s^{-1}]	F_0 [s]	A [s]	k [s^{-1}]
2	704 ± 38	372 ± 37	(18.4 ± 0.9)×10^{-3}	993 ±	81 ± 0.6	(1.6 ± 0.03)×10^{-3}
15	196 ± 60	796 ± 60	(25.7 ± 0.6)×10^{-3}	622 ± 4	377 ± 4	(0.5 ± 0.01)×10^{-3}

C

Halothane [mM]	F_0 [s]	A_1 [s]	k_1 [s^{-1}]	A_2 [s]	k_2 [s^{-1}]
5	595 ± 11	102 ± 10	(4.2 ± 0.3)×10^{-3}	245 ± 2	(0.8 ± 0.1)×10^{-3}
10	294 ± 2	296 ± 4	(5.7 ± 0.1)×10^{-3}	156 ± 3	(1.2 ± 0.1) ×10^{-3}
20	275 ± 1	209 ± 3	(7.2 ± 0.2)×10^{-3}	250 ± 3	(1.6 ± 0.04) ×10^{-3}

Table 3.5 Comparison of parameters of fitted kinetics of Trp fluorescence in POS discs with or without addition of halothane at indicated concentrations. Kinetics fitted to following equations: **A:** double exponential rise to maximum: $F= F_0+A_1(1-e^{-k1t})+A_2(1-e^{-k2t})$ (0; 0.5; 1; 4; 8 mM halothane); **B**: exponential rise: $F=F_0+A(1-e^{-kt})$ and exponential decay: $F=F_0+Ae^{-kt}$ (2 and 15 mM halothane); C: double exponential decay: $F=F_0+ A_1e^{-k1t}+ A_2e^{-k2t}$ (5; 10; 20 mM halothane).

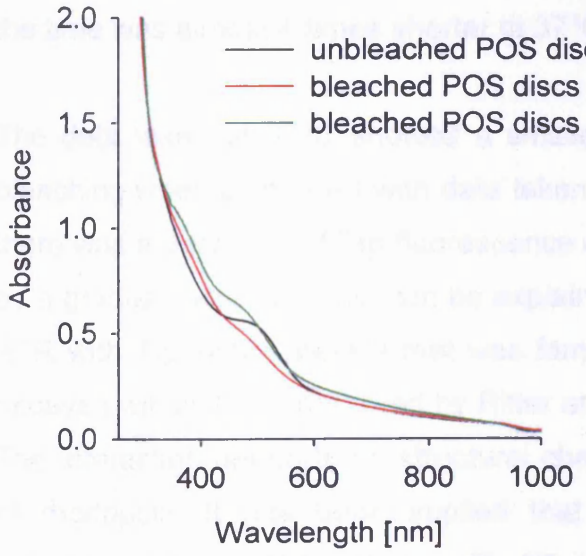

Figure 3.18 Absorption spectra of POS discs with unbleached and bleached 3.5 µM rhodopsin and 1 mM halothane (molar proportion 285:1) and after addition of 9-*cis*-retinal to generate *iso*rhodopsin.

3.4 Discussion

Tryptophan fluorescence in POS discs after rhodopsin bleaching

The obtained data confirmed the findings of Schadel and colleagues (2003) showing that photobleaching of the visual pigment results in a release of ATR from the active site of the protein and a gradual increase of fluorescence signal until the state of saturation is reached (approximately 15-20 minutes). However, the time needed to achieve half of the maximum of ATR hydrolysis was shorter in our experiments in comparison with results obtained by Schadel (~217 s and ~330 s, respectively; for measurements recorded at 21°C). Also, the percentage growth of fluorescence signal after bleaching of rhodopsin based on initial and final fluorescence value was lower (~30%) in comparison with their results (~70%). The observed difference may result from a possible presence of already bleached rhodopsin and hydrolysed ATR in our samples and higher fluorescence intensity to begin with.

The rate of ATR hydrolysis was significantly higher at 37°C than at 21°C. It took about 4 minutes for ATR to be hydrolysed in 50% of maximal value, whereas the time was almost 4 times shorter at 37°C (~1 min).

The data taken at 37°C showed a smaller increase of Trp fluorescence after bleaching when compared with data taken at 21°C. It needs to be stressed that there was a decrease of Trp fluorescence observed just after bleaching followed by a gradual increase. This can be explained by a possible closer interaction of ATR with Trp within Meta II that was formed after bleaching of rhodopsin and decayed within 10^2 s (reviewed by Ritter at al., 2008) than with Trp in rhodopsin. The interaction depends on structural changes occurring upon photoactivation of rhodopsin. It has been implied that retinal transformation can lead to rearrangement of TM helices with H6 undergoing rotation upon rhodopsin activation (Altenbach at al., 2008). It is consistent with a theory suggesting that the retinal moves towards H6 and the β-ionone ring is placed in the H5-H6

interface (see Fig. 3.18 A). Although the distance between Trp265 and retinal is greater in activated rhodopsin than in the inactive state, the conformational changes could possibly lead to an interaction between retinal and local tryptophan residue. This could subsequently lead to the changes in tryptophan fluorescence observed. Borhan and colleagues suggested a different model (Borhan at al., 2000), in which isomerisation is followed by retinal moving towards H6 and a change of the helix H4 position upon photoactivation. Different proposals also suggest that the β-ionone ring does not change its position when Meta II is formed (Spooner at al., 2004; Salom at al., 2006).

Crocker and colleagues (Crocker et al., 2006) proposed a model in which formation of metarhodopsin II results in a loss of the retinal C20–Trp265 contact, but a new contact is created with the C19 methyl group (Fig 3.19 B I and II). They showed that the retinal moves toward H5 in metarhodopsin II. This in conjunction with the formation of Trp–C19 contact, may imply that rhodopsin activation is followed by a significant movement of the Trp265 side-chain. A recent study by Ahuja and colleagues (Ahuja at al., 2009) confirmed these findings. Trp265 moves upon rhodopsin activation into a more hydrophilic environment changing its orientation. Interaction between helices H3-H5 and H4-H5 seemed to change in the formation of Meta II, reflecting an increased retinal-protein interaction in H3 and H5. All suggested structural transformations may lead to a specific interaction between Trp residues and retinal in activated rhodopsin.

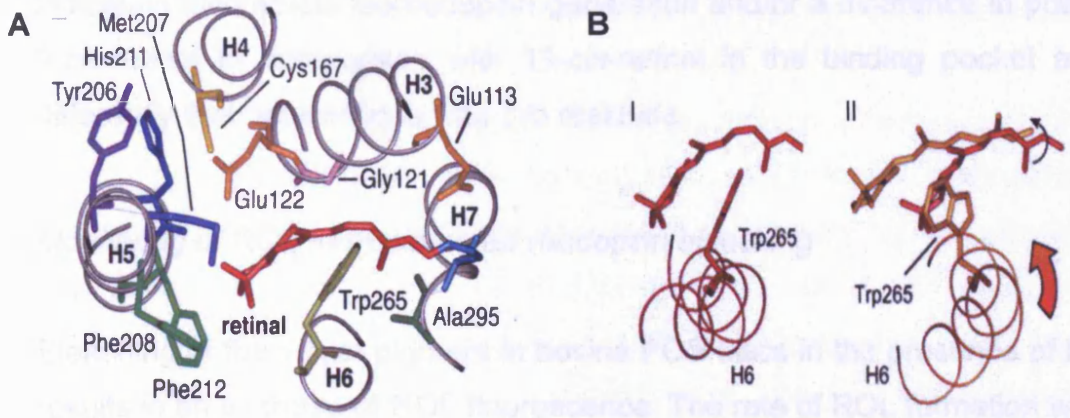

Figure 3.19 Structure of the retinal binding site in rhodopsin. **A** - View of the rhodopsin crystal structure showing transmembrane helices H3-H7 and the position of key amino acids including Trp265 (adapted from Ahuja et al., 2009). **B** - Model for structural transformation in rhodopsin (I – crystal structure of rhodopsin showing the position of the 11-*cis* retinal relative to Trp265 and H6) and metarhodopsin II (II - model of metarhodopsin II showing the positions of H6, the all-*trans* retinal and Trp265). Adapted from Crocker et al., 2006.

The influence of exogenous retinoids on intrinsic Trp fluorescence

Addition of exogenous ATR to opsin devoid of any endogenous retinoids or after the decay of Meta II leads to a decrease in intrinsic Trp fluorescence (Fig. 3.6 and 3.7). The decrease in POS discs with hydrolysed ATR follows a complex time course with a rapid part completed within ~30 s followed by an exponential decrease with a lifetime of 100 s and a slow linear decay. The linear decay observed after addition of ATR to POS discs with completely decayed Meta II could be explained by slow re-arrangements of opsin as well as photooxidation of tryptophan molecules. The kinetics indicate a formation of a complex different than regenerated rhodopsin. No changes in protein fluorescence after illumination of opsin with exogenous ATR indicates that this retinoid cannot regenerate rhodopsin, which is also consistent with the results of Schadel and colleagues (2003).

Similarly, a rapid decrease of signal followed by a further exponential decrease is observed upon addition of 9-*cis*-retinal to opsin after the complete decay of Meta II (Fig. 3.7). However, irradiation of samples led to a subsequent increase of signal indicating that the retinoid used can generate isorhodopsin. Fluorescence intensity did not reach the same level as before bleaching,

indicating incomplete *iso*rhodopsin generation and/or a difference in position of 9-*cis*-retinal in comparison with 11-*cis*-retinal in the binding pocket affecting differently their interactions with Trp residues.

Monitoring of ROL formation after rhodopsin bleaching

Bleaching of the visual pigment in bovine POS discs in the presence of NADPH results in an increase of ROL fluorescence. The rate of ROL formation was 1.43 times greater at 37°C than at 21°C. The time needed to reach a steady-state of ROL fluorescence was about 60 minutes measured at 37°C. It took longer than 60 minutes after bleaching for the level of ROL to reach a maximum at 21°C (data taken between 0 and 3600 s). Chen and colleagues (2005 and 2009) found that in frog and mouse retinas ROL fluorescence reached a maximum after 30-40 and about 60 minutes, respectively at room temperature. The results presented in this thesis seem to be closer to results of experiments performed on mice, suggesting some similarity in the kinetics of ROL formation characteristic for these two different species.

Comparison of rates for ROL formation and ATR hydrolysis monitored by Trp fluorescence measurements revealed that the reduction of ATR was 6.9 and 12.3 times slower than the decay of Meta II at 21 and 37 °C, respectively. It may be suggested that because of this large difference between the rates of ATR hydrolysis from opsin and its reduction, there seems to be an inherent risk of ATR accumulation upon exposure of POS to light. The rate of ATR reduction in samples with ATR being in the "exit" site of rhodopsin was higher than the rate in samples with generated *iso*rhodopsin and ATP present as a substrate for ABCR protein. The highest rate of reduction was observed in samples with *iso*rhodopsin formed without exogenous ATP, but the amplitude of ROL fluorescence (final concentration of ROL) reached the lowest level when compared with two other samples. It may suggested that only ATR which ended up at the outer leaflet was reduced and was better accessible to prRDH when compared with the opsin exit site. It can be concluded that the reduction of ATR is one of the limiting steps in the process of ATR removal.

The influence of halothane on ATR hydrolysis and isorhodopsin generation

Measurements of kinetics of tryptophan fluorescence after addition of halothane revealed that halothane at low concentrations (0.5 and 1 mM) showed no substantial effect on Trp fluorescence kinetics, whereas, higher concentrations influenced the changes of Trp fluorescence after rhodopsin bleaching. The percentage decrease of Trp fluorescence in our experiments upon addition of 15 mM halothane was about 80% when compared with 0.5 and 1 mM halothane. Results for higher concentrations of halothane are in agreement with data shown by Ishizawa and colleagues (2002). In their experiments, bleached and regenerated POS discs at a rhodopsin concentration of 0.5 µM were used with increasing concentration of halothane in the range of 0-15 mM (proportion 1:0 – 1:30000 mol/mol) to show the changes of Trp fluorescence after addition of halothane. They reported an 80% decrease of Trp fluorescence intensity in bleached rod disc membranes after addition of up to 15 mM halothane.

A possible explanation for the differences between the published results and ours is that halothane is highly volatile. The accuracy and desirable concentrations of halothane in samples were an upper limit and could be questionable. This could also explain a discrepancy of selected samples regarding the concentration-dependent influence of halothane on Trp fluorescence changes in POS discs (Fig. 3.16).

In our experiments, halothane was found to be unable to prevent *iso*rhodopsin formation after addition of 9-*cis*-retinal. There has been evidence shown by Ishizawa (2002) that halothane binds to the endogenous ligand binding site in rhodopsin and can act as a competitor for the ligand retinal. Based on the lack of a preventive effect on the formation of *iso*rhodopsin shown in this thesis, it may be questionable that binding of halothane to bleached opsin with ATR at the exit site causes a conformational change in protein and a release of ATR into disc membranes.

Another explanation for the lack of a preventive effect on the formation of *iso*rhodopsin may be provided by the experimental set-up. As Keller and colleagues reported (2001), inhibition of rhodopsin regeneration by halothane is reversible. Anesthetised mice exhibited remarkable, almost complete inhibition of metabolic regeneration of rhodopsin. However, animals were anesthetised constantly during exposures. Termination of anaesthesia just after bleaching resulted in the start of rhodopsin regeneration as soon as 15 minutes thereafter, suggesting that time is needed to clear the halothane from the retina. In our experiments it was impossible to provide a constant access of halothane to samples. Taking into consideration that the time between rhodopsin bleaching and generation of *iso*rhodopsin was longer than 15 minutes in our experiments, it may be suggested that halothane was removed from the POS discs, thus allowing for *iso*rhodopsin generation.

In summary, this chapter provided necessary detailed data on ATR hydrolysis and ROL formation for further experiments including singlet oxygen formation.

Chapter 4

Singlet oxygen formation in POS discs

4.1 Introduction

As discussed in the Introduction section, ATR has been suggested to be one of the several chromophores acting as a photosensitiser of damage in the retina occurring through oxidative damage (Delmelle 1977; Delmelle 1978). Already in 1977 Delmelle suggested that ATR may play an important role in the process and reported that illumination of ATR molecules leads to production of singlet oxygen, which in turn induces peroxidation of retinal lipids and damage to the lipid membrane (Delmelle, 1977; Delmelle, 1978). However, it is not clear at which point on its pathway following its formation upon absorption of light by rhodopsin, ATR can efficiently photosensitise formation of singlet oxygen.

In this chapter, the efficiency of singlet oxygen generation by ATR will be evaluated and discussed depending on whether it forms a Schiff base with Lys296, is non-covalently bound to opsin, or is released to the lipid membrane in the free form or bound to PE. It is also expected that reduction of ATR to ROL may affect the yield of singlet oxygen (as described in the Introduction section). Thus, experiments were carried out to monitor singlet oxygen generation in POS before and after rhodopsin bleaching in the presence or absence of NADPH and/or ATP to assess the correlation between the yields of singlet oxygen generation with the binding state of ATR and its position in opsin/POS.

4.2 Experimental design

As described in the Methods section (2.3.1) photogeneration and decay of singlet oxygen was monitored by time-resolved detection of phosphorescence at 1270 nm. Time-resolved detection of $^1O_2$ enabled measurements of singlet oxygen lifetimes and yields as a function of time. This was crucial to assess the ability of ATR to produce singlet oxygen as a function of its position after rhodopsin bleaching and the influence of the quenchers.

4.2.1 Singlet oxygen lifetime in oxygen-rich and oxygen-depleted suspensions of POS discs and quenching effect of H_2O

Since availability of oxygen determines generation of singlet oxygen, samples with oxygen replaced with argon are expected to exhibit lower yields of generated singlet state of oxygen. The initial concentration of singlet oxygen formation is expected to be lower in samples depleted of oxygen in comparison with samples saturated with air but the rate of decay is expected to be the same (Section 2.3.2).

Comparison of singlet oxygen signals in D_2O with several different concentrations of H_2O allows for determining the singlet oxygen quenching rate constant of H_2O. The lifetime of $^1O_2$ varies from ~3.5 μs in water to 68 μs in deuterated water (Zebger et al., 2004). Thus, presence of H_2O or D_2O in samples with POS discs is expected to influence the lifetime of singlet oxygen which diffuses out of the POS disc membrane (Method section 2.3.2). Replacing H_2O with D_2O in POS discs was expected to be incomplete and therefore, a calibration curve of the rates of singlet oxygen decay as a function of concentration of H_2O was determined in order to assess the concentration of H_2O in POS discs.

4.2.2 Singlet oxygen in POS discs as a function of ATR position in opsin

The yield of singlet oxygen was measured as described in the Methods section (Section 2.3.4) for samples with POS discs before and after rhodopsin bleaching at different time points, selected based on the kinetics of hydrolysis of ATR. Singlet oxygen yield was also assessed in POS discs with ATR removed from the exit site of opsin by delivery of 9-*cis*-retinal and generation of *iso*rhodopsin. Lack of blocking effect of halothane on *iso*rhodopsin generation made it questionable whether halothane induces a conformation change of opsin, leading to the release of ATR to the disc membrane. Thus, to evaluate the ability of ATR to produce singlet oxygen after being released to the inner leaflet of disc membrane, and to compare it with the yields of $^1O_2$ obtained for ATR in the "exit" site of rhodopsin, it was necessary to add 9-*cis*-retinal. As not

all 9-*cis*-retinal added was binding to the opsin active site generating *iso*rhopdopsin, samples with added 9-*cis*-retinal were compared with samples after addition of 13-*cis*-retinal, which exhibits similar absorption and photosensitizing properties as 9-*cis*-retinal but does not generate *iso*rhodopsin. Concentrations of added 9-*cis*-retinal and 13-*cis*-retinal were equal to the concentration of opsin in POS discs (7.6 μM). As not all added 9-*cis*-retinal binds to opsin forming *iso*rhodopsin, additional control experiments were performed with a concentration of 3.45 μM 13-*cis* retinal equal to the concentration of 9-*cis*-retinal, which was not used for *iso*rhodopsin formation upon addition of 7.6 μM 9-*cis*-retinal (see Section 4.3.4). Concentration of ATR (4.15 μM) refers to assumed ATR released after *iso*rhodopsin formation with 7.6 μM 9-*cis*-retinal.

Yields of singlet oxygen generated by 9-*cis*-, 13-*cis*-retinal and ATR were assessed at the same concentration as used in experiments with POS discs in order to determine their ability to produce singlet oxygen. Two solvents with different polarities were used to compare the ability to generate $^1O_2$ by the retinal isomers in different environments.

As described in the Introduction section, ATR can form complexes with various amines including PE – an abundant phospholipid present in POS membranes. Since Schiff base formation between retinal and PE occurs on a long time scale (0.107 $mM^{-1}h^{-1}$ for synthetic PE and retinal in chloroform; Plack and Pritchard, 1969), singlet oxygen formation was monitored as a function of time between 0 and 80 minutes after rhodopsin bleaching with addition of exogenous ATR. It was expected that formation of a complex between ATR and PE would lead to a suppression of photosensitising properties of ATR and a decrease in singlet oxygen yield.

All samples were sonicated just before measurements were made to ensure homogeneity and to minimise scattering. Conditions of sample bleaching were the same as described in Methods section (2.1.5).

It was expected that there would be different lifetimes of singlet oxygen observed in POS discs. The position and environment of ATR would also influence the generation of singlet oxygen. The lifetime of singlet oxygen in the protein- and lipid-rich environment of the POS membrane is expected to be different to the lifetime in an aqueous environment for singlet oxygen molecules which diffuse out of the membrane.

All signals were fitted to the three exponential decay model as described in the Methods section 2.3.4. Yields of singlet oxygen for each sample were calculated separately. Final analysis involved also a comparison of sums of amplitudes of all three components or percentage difference referring to either unbleached samples or samples immediately after bleaching as 100%.

4.2.3 Singlet oxygen generation in POS discs as a function of pH

As described in the Introduction section, the decay of Meta I/Meta II formed just after rhodopsin bleaching occurs by direct dissociation into opsin and free ATR, or to Meta III – a storage form of rhodopsin (Bartl and Vogel, 2007). The conversion strictly depends on pH and favours the first pathway at acidic to neutral pH, whereas the latter one is more often at alkaline pH. Therefore, generation of singlet oxygen in POS discs after rhodopsin bleaching was expected to vary depending on the ratio of formed Meta III and Meta II decaying to opsin and ATR. Samples at pH 4.5 were expected to be characterised by greater ability to generate singlet oxygen than samples at higher pH (7.8), in which decay of MetaI/MetaII would predominantly occur via formation of Meta III.

4.2.4 NADPH and ATP effect on singlet oxygen in POS discs

To reveal any possible changes in singlet oxygen yield under conditions facilitating reduction of ATR to ROL, that is in the presence of NADPH or both NADPH and ATP with regenerated *iso*rhodopsin, measurements were taken for samples with completely hydrolysed ATR (20 minutes after start of bleaching

unless otherwise stated) with or without the enzyme co-factors. 9-*cis*-retinal was used to generate *iso*rhodopsin, whereas 13-*cis*-retinal was used for comparative purposes, as it has been shown not to be able to generate *iso*rhodopsin, but exhibits similar optical absorption and photosensitising properties as 9-*cis*-retinal (Rotmans and Kropf, 1975).

4.3 Results

4.3.1 Singlet oxygen lifetime in oxygen-rich and oxygen-depleted suspensions and quenching effect of H_2O

Comparison of air- and argon-saturated samples with POS discs showed a similarity of signals (Fig. 4.1). However, analysis of the parameters of kinetics revealed no substantial differences between rate constants of decays and the amplitudes of signals (Tab. 4.1). Depletion of oxygen from lipids in a suspension of lipid vesicles in aqueous medium is rather inefficient, therefore, additional tests were performed to determine whether the observed emission is due to $^1O_2$ phosphorescence or phosphorescence of other components of POS discs.

As mentioned in the Experimental design, singlet oxygen has a characteristic lifetime of 3.5 µs in water, which is extended to 68 µs in deuterated water. However, as commercially available D_2O already contains some H_2O and once open can further absorb H_2O from the air, it was necessary to determine $^1O_2$ lifetime in D_2O used for these experiments using a well characterised photosensitiser, rose bengal.

Figure 4.2 A shows selected signals of formation and decay of infrared luminescence, obtained after photo-excitation of the sample with rose bengal suspended in D_2O before and after addition of H_2O at indicated concentrations. In the absence of H_2O, singlet oxygen lifetime was ~40 µs. There was a decrease in signal intensity with increasing concentration of H_2O. Calculations of rate constants of decay and singlet oxygen lifetime for all measurements revealed a dose dependent decrease of $^1O_2$ lifetime in the sample with added

H_2O when compared with an initial value of ~40 µs (Fig. 4.2 B). Singlet oxygen lifetime in the given D_2O was lower than the literature value (~40 µs compared with 68 µs), suggesting the presence of H_2O. Based on the determined rate of singlet oxygen quenching by H_2O, the initial concentration of H_2O in D_2O was estimated to be 2.4 M.

The signal of infrared emission from POS discs samples suspended in D_2O without addition of H_2O appeared to be higher than signals after addition of selected concentrations of H_2O (Fig. 4.3 A). Control measurements done by addition of the same volume of D_2O as the greatest volume of H_2O to compensate for the dilution factor did not reveal any changes, indicating that H_2O does lead to a decrease in signal amplitude and lifetime (Fig. 4.3 B). However, analysis of parameters of exponential decays revealed no substantial changes in rates of decay and singlet oxygen yields for all components of kinetics with or without constrained parameter for one of the rate constants of decay (Tab. 4.2 A, B, C, D). All fitted curves were fitted reasonably well ($R^2 \geq 0.992$) and gave similar residuals (Fig. 4.3 C). Also fitting of obtained signal kinetics with or without constrained parameters did not reveal any significant changes of $^1O_2$ lifetimes with increasing concentration of H_2O.

Comparison of POS discs suspended in H_2O with discs suspended in D_2O (Fig. 4.4) revealed a decrease in amplitude for middle- and long-lived exponent, but there was no substantial change in any of the rates constant of decay (Tab. 4.3).

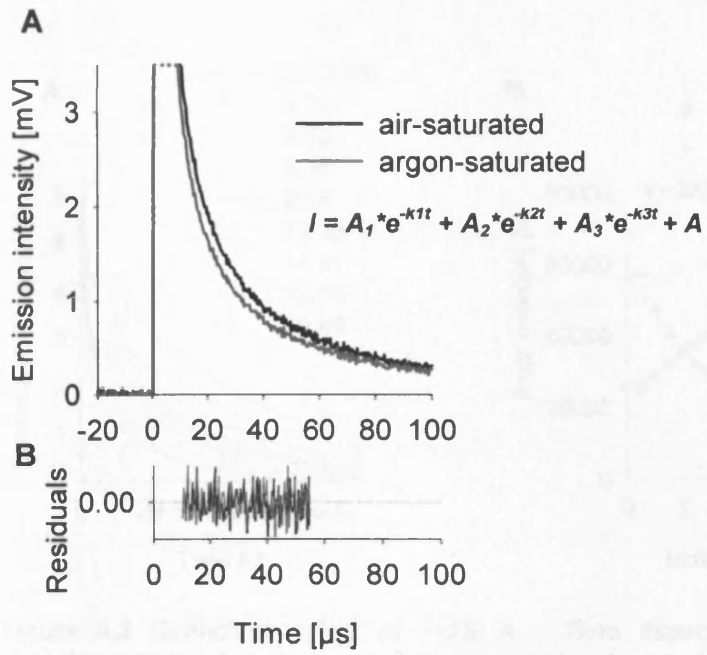

Figure 4.1 Comparison of time dependent changes of infrared phosphorescence in sample with air- and argon-saturated POS discs. A - Comparison of time dependent changes of infrared phosphorescence induced by a 5 ns laser pulse in sample with air- and argon-saturated POS discs. Excitation wavelength of 355 nm. Blue smooth lines correspond to data fitted to the equation. B - Residuals within the range used for fitting a three exponential decay.

POS discs	A_1	A_2	A_3
Air-saturated	**7.4** ±1.7	**2.4** ±1.3	**1.3** ±1.3
Argon-saturated	**9.4** ±1.8	**2.5** ±1.1	**0.8** ±1.1
	k_1 [s^{-1}]	k_2 [s^{-1}]	k_3 [s^{-1}]
Air-saturated	(**2.2**±0.4)×10^5	(**0.5** ±0.2)×10^5	(**0.5** ±0.4)×10^5
Argon-saturated	(**2.4** ±0.3)×10^5	(**0.5** ±0.2)×10^5	(**0.5** ±0.7)×10^5

Table 4.1 Comparison of parameters of fitted three exponential decay: $I = A_1*e^{-k1t} + A_2*e^{-k2t} + A_3*e^{-k3t} + A$ for air- and argon-saturated samples with POS discs. A –initial amplitudes of infrared phosphorescence for the shortest (A_1), middle (A_2) and longest (A_3) lived exponent. B – rate constants of the decay of infrared phosphorescence for the short- (k_1), middle- (k_2) and long- (k_3) lived exponent. Excitation wavelength of 355 nm. Errors correspond to SD of fitted parameters.

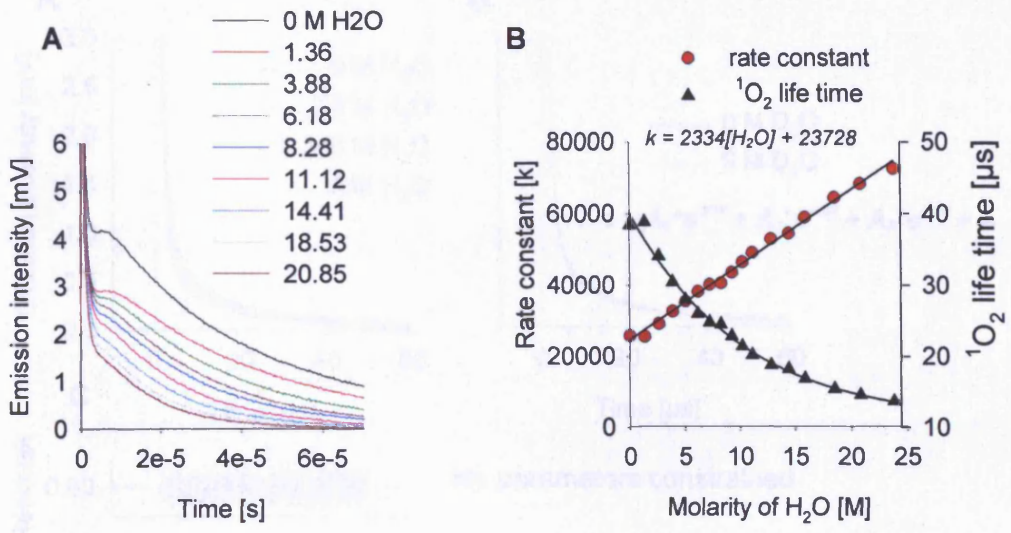

Figure 4.2 Quenching effect of H_2O. **A** - Time dependent changes of singlet oxygen phosphorescence induced by a 5 ns laser pulse in sample with rose begal solution in D_2O before and after addition of indicated concentrations of H_2O. **B** – Calculated rates constant of decay and singlet oxygen lifetimes for indicated concentrations of H_2O in the sample with rose bengal suspended in deuterated water. Excitation wavelength of 355 nm.

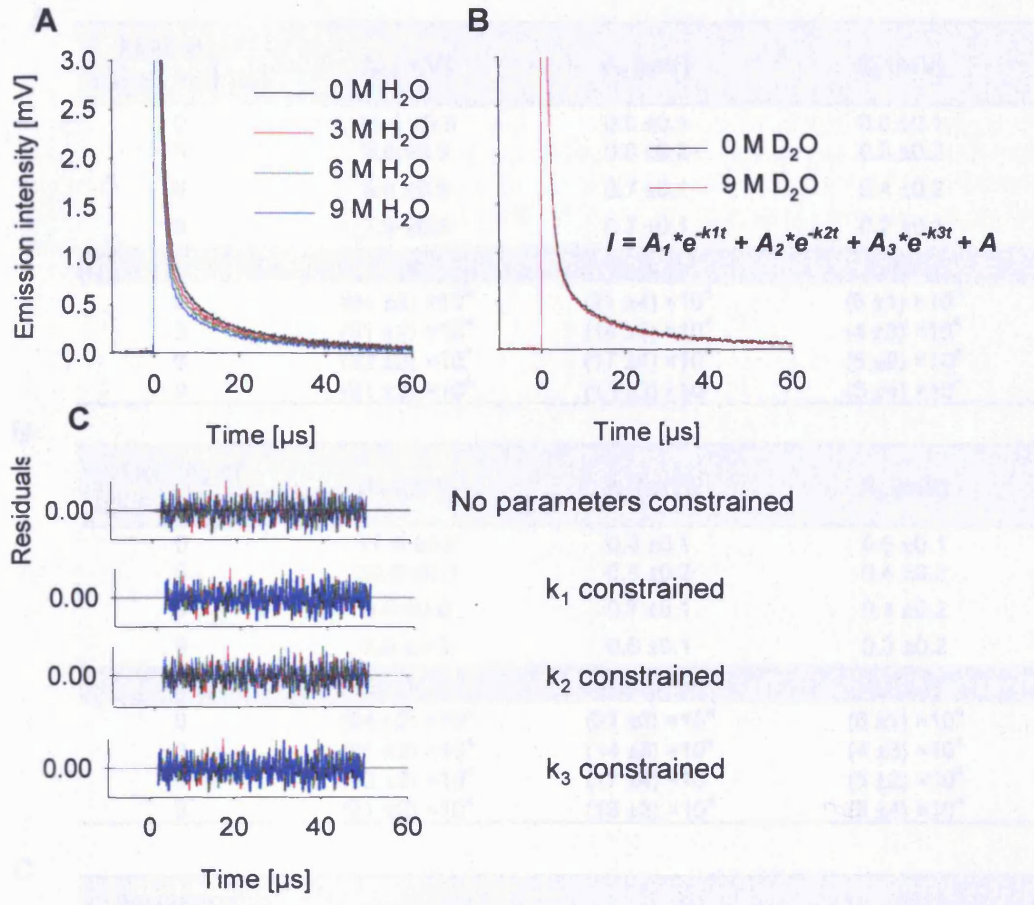

Figure 4.3 Comparison of time dependent changes of singlet oxygen phosphorescence in the sample with POS discs suspended in D_2O before and after adding indicated concentration of H_2O (**A**). To account for the dilution factor, the same concentration of D_2O was added as that corresponding to the highest concentration of added H_2O (**B**). Excitation wavelength of 355 nm. **C** – Residuals for fitted kinetics with or without constraining of parameters.

A

Molarity of added H_2O [M]	A_1 [mV]	A_2 [mV]	A_3 [mV]
0	11.8 ±0.3	0.9 ±0.1	0.6 ±0.1
3	9.9 ±0.3	0.8 ±0.2	0.3 ±0.2
6	9.0 ±0.3	0.7 ±0.1	0.4 ±0.2
9	7.9 ±0.3	0.7 ±0.1	0.2 ±0.1
	k_1 [s^{-1}]	k_2 [s^{-1}]	k_3 [s^{-1}]
0	(94 ±2) ×10^4	(21 ±4) ×10^4	(6 ±1) ×10^4
3	(91 ±2) ×10^4	(14 ±3) ×10^4	(4 ±3) ×10^4
6	(92 ±3) ×10^4	(17 ±4) ×10^4	(5 ±2) ×10^4
9	(91 ±2) ×10^4	(13 ±3) ×10^4	(3 ±4) ×10^4

B

Molarity of added H_2O [M]	A_1 [mV]	A_2 [mV]	A_3 [mV]
0	11.8 ±0.3	0.9 ±0.1	0.6 ±0.1
3	10.0 ±0.3	0.8 ±0.2	0.4 ±0.2
6	9.0 ±0.3	0.7 ±0.1	0.4 ±0.2
9	8.0 ±0.3	0.6 ±0.1	0.3 ±0.2
	k_1 [s^{-1}]	k_2 [s^{-1}]	k_3 [s^{-1}]
0	(94 ±2) ×10^4	(21 ±3) ×10^4	(6 ±1) ×10^4
3	(91 ±2) ×10^4	(14 ±3) ×10^4	(4 ±3) ×10^4
6	(92 ±3) ×10^4	(17 ±4) ×10^4	(5 ±2) ×10^4
9	(91 ±2) ×10^4	(13 ±3) ×10^4	(3 ±4) ×10^4

C

Molarity of added H_2O [M]	A_1 [mV]	A_2 [mV]	A_3 [mV]
0	11.8 ±0.3	0.9 ±0.1	0.6 ±0.1
3	10.0 ±0.3	0.7 ±0.1	0.5 ±0.2
6	9.0 ±0.3	0.7 ±0.1	0.4 ±0.2
9	8.0 ±0.3	0.5 ±0.1	0.4 ±0.2
	k_1 [s^{-1}]	k_2 [s^{-1}]	k_3 [s^{-1}]
0	(94 ±2) ×10^4	(21 ±4) ×10^4	(6 ±1) ×10^4
3	(91 ±2) ×10^4	(14 ±3) ×10^4	(4 ±3) ×10^4
6	(92 ±3) ×10^4	(17 ±4) ×10^4	(5 ±2) ×10^4
9	(91 ±2) ×10^4	(13 ±3) ×10^4	(3 ±4) ×10^4

D

Molarity of added H_2O [M]	A_1 [mV]	A_2 [mV]	A_3 [mV]
0	11.8 ±0.3	0.9 ±0.1	0.6 ±0.1
3	10.0 ±0.3	0.7 ±0.2	0.4 ±0.2
6	9.0 ±0.3	0.7 ±0.1	0.4 ±0.2
9	8.0 ±0.3	0.6 ±0.2	0.3 ±0.2
	k_1 [s^{-1}]	k_2 [s^{-1}]	k_3 [s^{-1}]
0	(94 ±2) ×10^4	(21 ±4) ×10^4	(6 ±1) ×10^4
3	(91 ±2) ×10^4	(14 ±3) ×10^4	(4 ±3) ×10^4
6	(92 ±3) ×10^4	(17 ±4) ×10^4	(5 ±2) ×10^4
9	(91 ±2) ×10^4	(13 ±3) ×10^4	(3 ±4) ×10^4

Table 4.2 Comparison of signal amplitudes and rates of decay for signals fitted to a three exponential decay model: $I = A_1*e^{-k1t} + A_2*e^{-k2t} + A_3*e^{-k3t} + A$ for bleached samples with POS discs before and after addition of H_2O. A_1, k_1 – amplitude and rate of decay of the short-lived component; A_2, k_2 – amplitude and rate of decay of the middle-lived component; A_3, k_3 –amplitude and rate of decay of the long-lived component. A – no parameters constrained; B – constraints: $92 \times 10^4 < k_1 < 96 \times 10^4$; C – constraints: $17 \times 10^4 < k_2 < 24 \times 10^4$; D – constraints: $5 \times 10^4 < k_3 < 7 \times 10^4$. Excitation wavelength of 355 nm. Errors correspond to SD of fitted parameters.

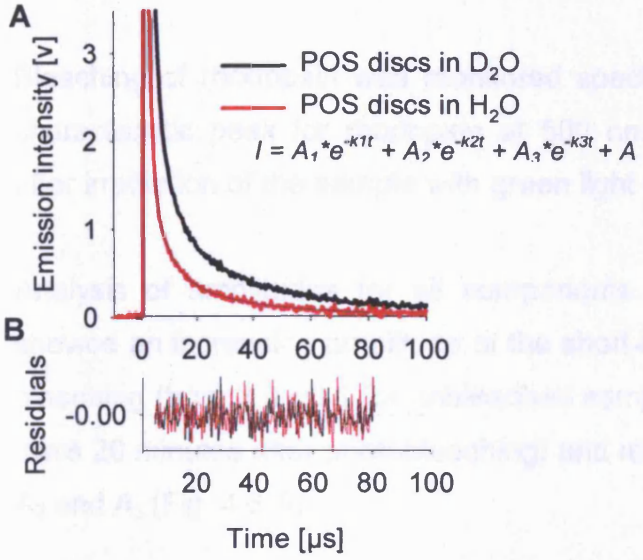

Figure 4.4 Comparison of time dependent changes of singlet oxygen phosphorescence in the sample with POS discs suspended in D_2O and H_2O. **A** - Comparison of time dependent changes of singlet oxygen phosphorescence induced by a 5 ns laser pulse in the sample with POS discs suspended in D_2O and H_2O. Excitation wavelength of 355 nm. Blue smooth lines correspond to data fitted to the equation. **B** - Residuals within the range used for fitting a three exponential decay.

POS discs in:	A_1 [mV]	A_2 [mV]	A_3 [mV]
D_2O	**27.9** ±5.5	**3.0** ±0.4	**1.1** ±0.1
H_2O	**31.9** ±34	**1.7** ±0.3	**0.6** ±0.1
	k_1 [s^{-1}]	k_2 [s^{-1}]	k_3 [s^{-1}]
D_2O	(61 ±6) $\times 10^4$	(15 ±2) $\times 10^4$	(3 ±5) $\times 10^4$
H_2O	(88 ±25) $\times 10^4$	(17 ±4) $\times 10^4$	(4 ±1) $\times 10^4$

Table 4.3 Comparison of parameters for fitted kinetics of phosphorescence observed in samples with POS discs suspended in D_2O and H_2O. Excitation wavelength of 355 nm. Errors correspond to SD of fitted parameters.

4.3.2 Singlet oxygen formation in POS depending on ATR position

Singlet oxygen traces obtained for POS discs with rhodopsin and bleached rhodopsin after selected times after photobleaching are presented in

Fig. 4.5 A. There was an increase of signal observed after rhodopsin bleaching with the highest signal for POS discs bleached and stored at room temperature for 20 minutes. A three exponential decay was applied as a model for fitting all signals as shown in the figure for unbleached samples. The accuracy of kinetics fitting was confirmed by a symmetrical distribution of residuals relative to the coordinate axis (shown on figure below).

Bleaching of rhodopsin was monitored spectrophotometrically and revealed a characteristic peak for rhodopsin at 500 nm and disappearance of the peak after irradiation of the sample with green light (Fig. 4.5 C).

Analysis of amplitudes for all components of the three exponential decays showed an increasing amplitude of the short-lived decay in time after rhodopsin bleaching (from 3.9 ±0.1 for unbleached samples to 7.1 ±0.1 for bleached POS discs 20 minutes after photobleaching) and relatively small or lack of increase in A_2 and A_3 (Fig. 4.6 A).

Total sums of all three components of decay showed an increase of singlet oxygen yields after bleaching until a maximum was reached about 20 minutes after rhodopsin bleaching (Fig. 4.6 B). Averaged total yield of singlet oxygen was 4.4 ±0.1mV and increased to 6.9 ±0.1 mV when half of the ATR molecules were hydrolysed from the active site of rhodopsin (4.33 minutes after bleaching). The maximum yield was observed 20 minutes after rhodopsin bleaching and reached a value of 7.8 ±0.1 mV.

The total yield of singlet oxygen was significantly lower just after bleaching than for the signal observed after more than 8 minutes ($P < 0.05$; Fig. 4.6 B). Samples with bleached rhodopsin after 4.33 and 8 minutes exhibited a significantly lower ability to generate singlet oxygen than samples 10 and more minutes after bleaching. The ability to generate singlet oxygen was significantly lower 10 minutes after rhodopsin bleaching than after 20 minutes ($P < 0.05$)

There were no substantial changes in singlet oxygen lifetimes for all three analysed components of exponential decays depending on the duration following rhodopsin bleaching and ATR position (Fig. 4.6 C).

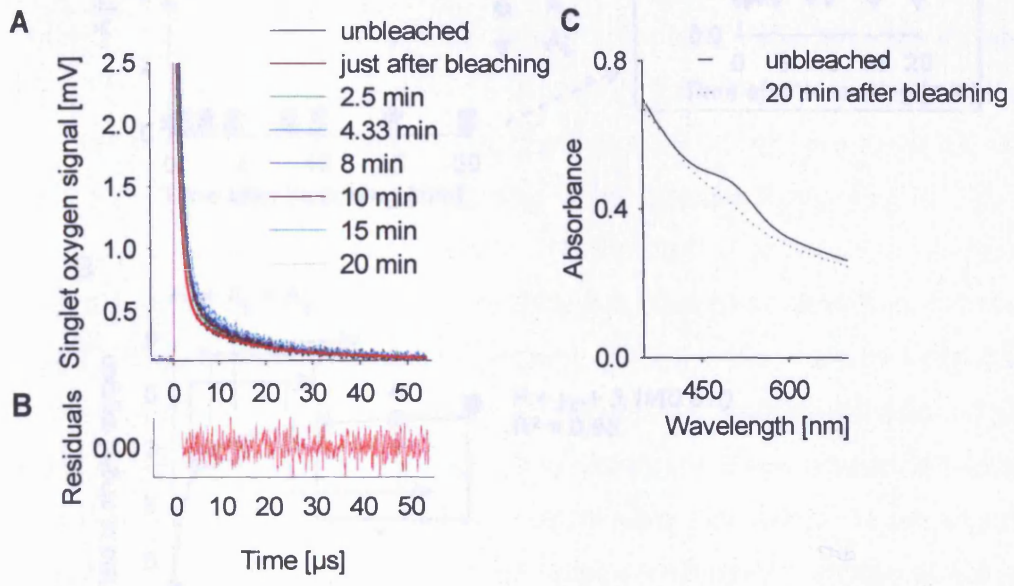

Figure 4.5 Formation of singlet oxygen in POS discs depending on ATR position in opsin. A - Time dependent changes of singlet oxygen phosphorescence kinetics for unbleached and bleached POS discs with ~3 µM rhodopsin at different time points after rhodopsin bleaching (1min, 30 s (just after bleaching) – 20 min). Signal for unbleached POS discs fitted to a three exponential decay $I = A_1*e^{-k1t} + A_2*e^{-k2t} + A_3*e^{-k3t} + A$ (red dotted ine) with residuals presented below. B – Bleaching of rhodopsin determined spectrophotometrically by measurements of absorption spectra of (smooth line) and bleached POS discs after 20 minutes after irradiation (dotted line).

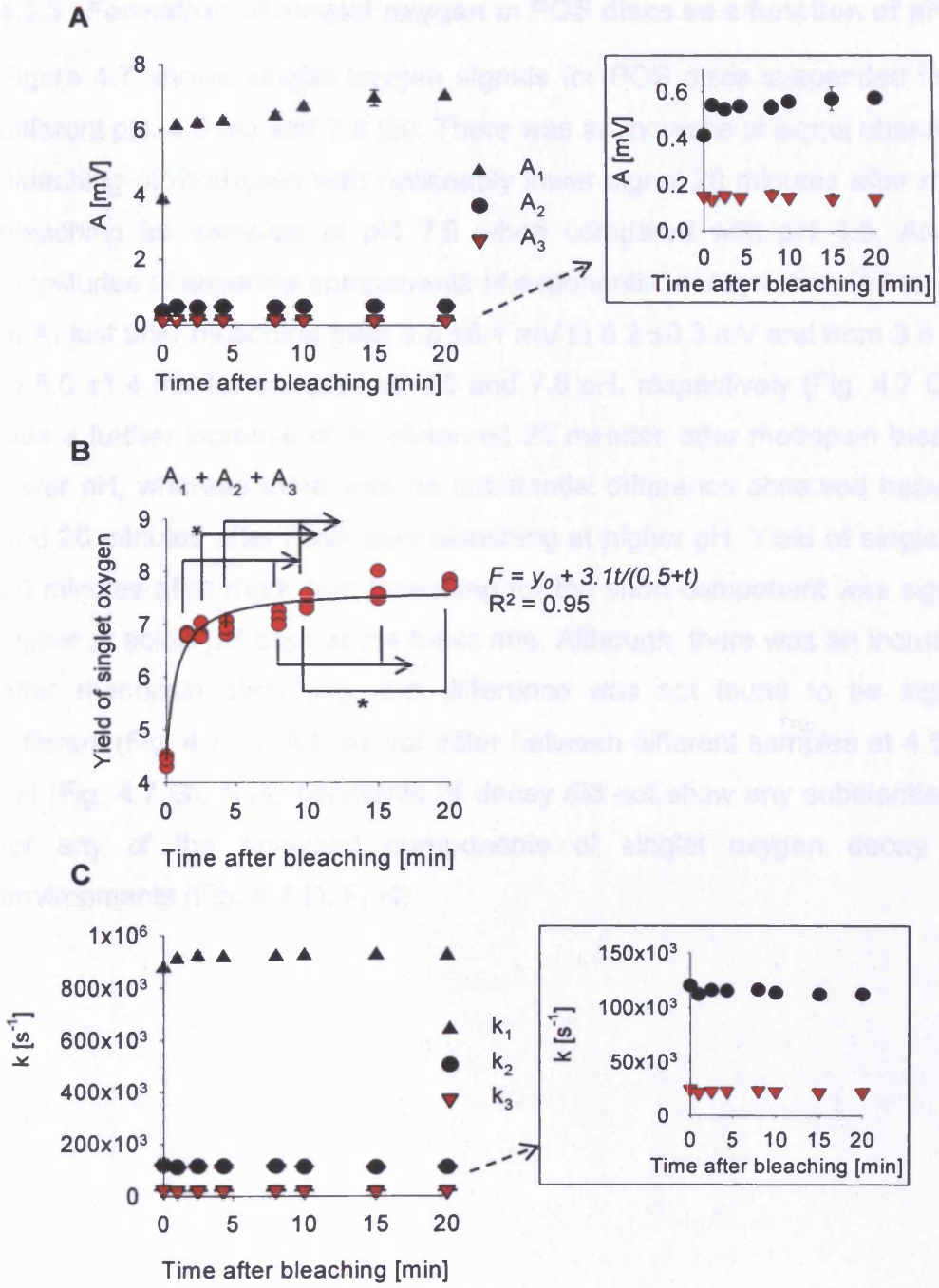

Figure 7.6 Singlet oxygen yields (amplitudes A) and rates of decay (k) obtained for POS discs before and after rhodopsin bleaching at different times following irradiation. Each time point was in triplicate. Kinetics of singlet oxygen phosphorescence fitted to an equation: $I = A_1 * e^{-k1t} + A_2 * e^{-k2t} + A_3 * e^{-k3t} + A$. **A** – amplitudes calculated from three exponential decays: A_1 – the short-lived, A_2- middle-lived and A_3 – long-lived. All points in triplicates. Error bars = SD. **B** – sums of yields of singlet oxygen for three exponential decays for selected time points after bleaching. Data points fitted to the equation: I = A + a*t/(b+t). The asterix sign indicates statistically significant differences between samples. **C** – rate constant of decay calculated from three exponential decays: k_1 – the short-lived, k_2- middle-lived and k_3 – long-lived. All points in triplicates. Error bars = SD.

4.3.3 Formation of singlet oxygen in POS discs as a function of pH

Figure 4.7 shows singlet oxygen signals for POS discs suspended in D_2O at different pH: 4.5 (A) and 7.8 (B). There was an increase of signal observed after bleaching of rhodopsin with noticeably lower signal 20 minutes after rhodopsin bleaching for samples at pH 7.8 when compared with pH 4.5. Analysis of amplitudes of separate components of exponential decays revealed an increase of A_1 just after bleaching from 3.3 ±0.1 mV to 5.2 ±0.3 mV and from 3.6 ±0.1 mV to 5.0 ±1.4 mV for samples at 4.5 and 7.8 pH, respectively (Fig. 4.7 C). There was a further increase of A_1 observed 20 minutes after rhodopsin bleaching at lower pH, whereas there was no substantial difference observed between one and 20 minutes after rhodopsin bleaching at higher pH. Yield of singlet oxygen 20 minutes after rhodopsin bleaching for the short component was significantly higher at acidic pH than at the basic one. Although, there was an increase of A_2 after rhodopsin bleaching, the difference was not found to be significantly different (Fig. 4.7 E). A3 did not differ between different samples at 4.5 and 7.8 pH (Fig. 4.7 G). Rate constants of decay did not show any substantial change for any of the analysed components of singlet oxygen decay in both environments (Fig. 4.7 D, F, H).

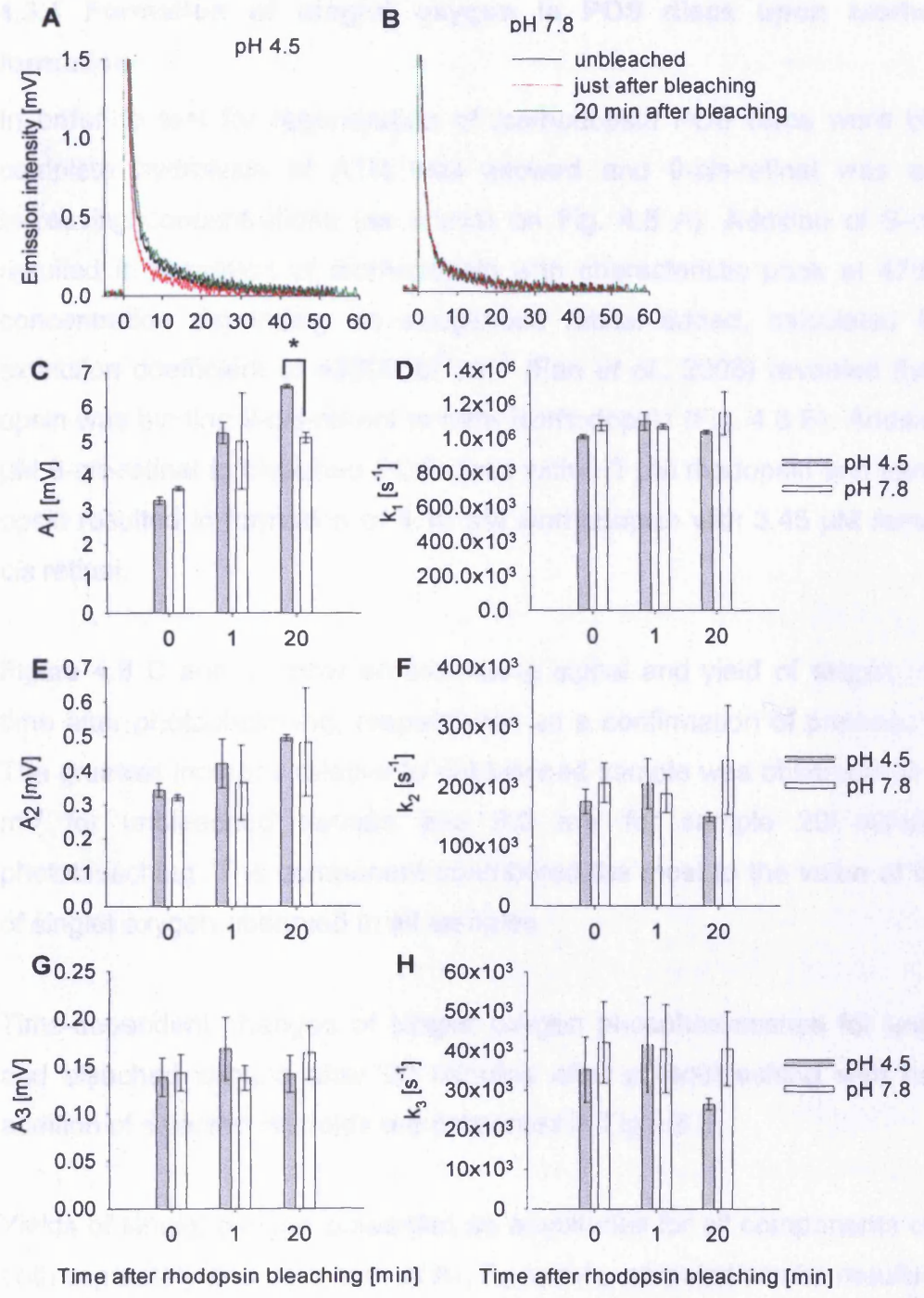

Figure 4.7 Signals of singlet oxygen observed in POS discs before and after rhodopsin bleaching as a function of pH. **A** - - Time dependent changes of singlet oxygen phosphorescence kinetics for unbleached and bleached POS discs with ~3 μM rhodopsin just after and 20 minutes after rhodopsin bleaching. **C, E, G** – amplitudes for short- (C), middle- (E) and long- (G) decays for signals measured before and after rhodopsin bleaching. **D, F, H** – rates of decay for short- (D), middle- (F) and long- (H) decays for signals measured before and after rhodopsin bleaching. Excitation wavelength of 355 nm.

4.3.4 Formation of singlet oxygen in POS discs upon *iso*rhodopsin formation

In order to test for regeneration of *iso*rhodopsin POS discs were bleached, complete hydrolysis of ATR was allowed and 9-*cis*-retinal was added at increasing concentrations (as shown on Fig. 4.8 A). Addition of 9-*cis*-retinal resulted in formation of *iso*rhodopsin with characteristic peak at 478 nm. Its concentration depending on exogenous retinal added, calculated from the extinction coefficient of 43000 $M^{-1}cm^{-1}$ (Fan *et al.*, 2008) revealed that not all opsin was binding 9-*cis*-retinal to form *iso*rhodopsin (Fig. 4.8 B). Addition of 7.6 µM 9-*cis*-retinal to bleached POS discs with 3.3 µM rhodopsin and total 7.6 µM opsin resulted in formation of 4.15 µM *iso*rhodopsin with 3.45 µM remaining 9-*cis* retinal.

Figure 4.8 C and D show an increasing signal and yield of singlet oxygen in time after photobleaching, respectively, as a confirmation of previous findings. The greatest increase relative to unbleached sample was observed for A_1 – 2.6 mV for unbleached sample and 6.0 mV for sample 20 minutes after photobleaching. The component contributed the most to the value of final yield of singlet oxygen observed in all samples.

Time-dependent changes of singlet oxygen phosphorescence for unbleached and bleached sample after 20 minutes after photobleaching with or without addition of selected retinoids are presented in Fig.4.8 E.

Yields of singlet oxygen presented as amplitudes for all components of decays both separately and as a sum of A_1, A_2 and A_3, revealed similar results for POS discs with addition of 3.45 and 7.6 µM 13-*cis*-retinal – an increase of about 10% of final yield when compared with bleached sample (Fig. 4.8 F). There was a 20% increase of signal in samples with 9-*cis*-retinal added at concentration of 7.6 µM when compared with the same concentration of 13-*cis*-retinal. Addition of 4.15 µM ATR resulted in the same increase of signal as observed in sample with exogenous 7.6 µM 9-*cis*-retinal.

Analysis of singlet oxygen yields samples of 9-*cis*-, 13-*cis*-retinal and ATR at the same concentrations as used in previous experiments, in solvents with different polarities showed substantially higher values for samples diluted in benzene except for ATR when compared with acetone (Fig. 4.7). ATR exhibited similar yield of singlet oxygen both in acetone and benzene – 2.27 ±0.05 and 2.25 ±0.02, respectively. 9-*cis*-retinal was characterised by 1.4 and 1.2 higher yields of singlet oxygen than 13-*cis*-retinal at the same concentration in acetone and benzene, respectively. The lowest yield of singlet oxygen was observed in samples with 3.45 μM 13-*cis*-retinal - 0.170 ±0.01 and 0.55 ±0.03 in acetone and benzene, respectively.

The interaction between ATR and PE was tested by monitoring of singlet oxygen in samples with and without addition of exogenous ATR as a function of time and the results are shown in Figure 4.9 A. Analysis of amplitudes of three different components of exponential decay showed differences in A_1 and A_2, depending on time after rhodopsin bleaching and the presence of exogenous ATR (Fig. 4.9 B and C). Yields of singlet oxygen were greater in samples with exogenous ATR present when compared with the same samples without addition of ATR. A_1 and A_2 seemed to reach the maximum after 80 minutes for samples without exogenous ATR, whereas the highest values for sample with the exogenous retinoid were observed after 40 minutes. There were no substantial changes observed in the amplitude A_3 (4.9 D). Total yields of singlet oxygen reflect the values of A_1 since it has the greatest contribution to the total amplitude for singlet oxygen (4.9 E).

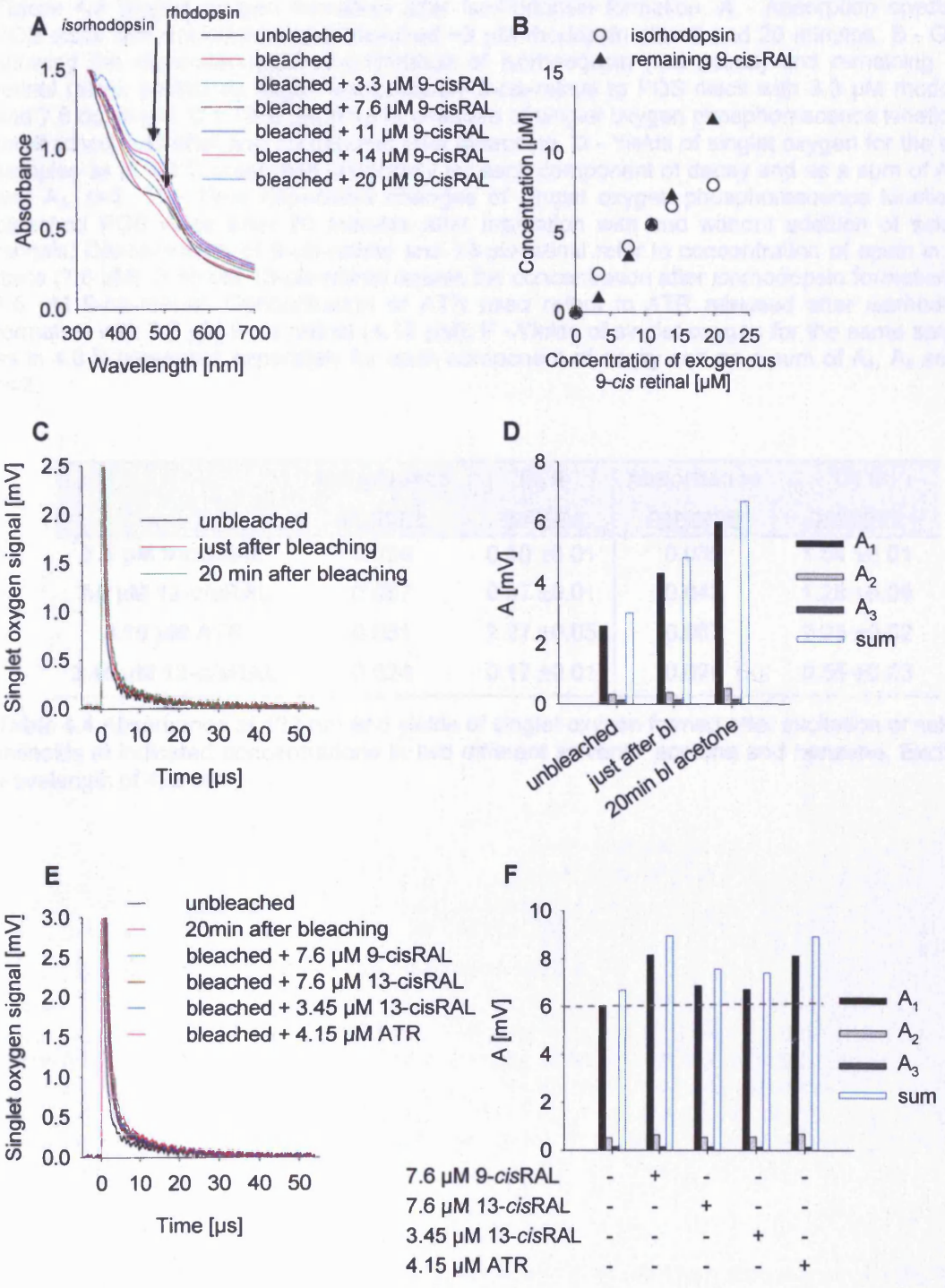
A
isorhodopsin
rhodopsin
unbleached
bleached
bleached + 3.3 µM 9-cisRAL
bleached + 7.6 µM 9-cisRAL
bleached + 11 µM 9-cisRAL
bleached + 14 µM 9-cisRAL
bleached + 20 µM 9-cisRAL
Absorbance
Wavelength [nm]
B
isorhodopsin
remaining 9-cis-RAL
Concentration [µM]
Concentration of exogenous 9-cis retinal [µM]
C
Singlet oxygen signal [mV]
unbleached
just after bleaching
20 min after bleaching
Time [µs]
D
A [mV]
A1
A2
A3
sum
unbleached
just after bl
20min bl acetone
E
Singlet oxygen signal [mV]
unbleached
20min after bleaching
bleached + 7.6 µM 9-cisRAL
bleached + 7.6 µM 13-cisRAL
bleached + 3.45 µM 13-cisRAL
bleached + 4.15 µM ATR
Time [µs]
F
A [mV]
A1
A2
A3
sum
7.6 µM 9-cisRAL
7.6 µM 13-cisRAL
3.45 µM 13-cisRAL
4.15 µM ATR

Figure 4.8 Singlet oxygen formation after *iso*rhodopsin formation. **A** - Absorption spectra of POS discs with unbleached and bleached ~3 μM rhodopsin after 0 and 20 minutes. B - Graph showing the dependency of concentration of isorhodospin (red points) and remaining 9-*cis* retinal (black points) on added exogenously 9-*cis*-retinal to POS discs with 3.3 μM rhodopsin and 7.6 opsin μM. **C** - Time dependent changes of singlet oxygen phosphorescence kinetics for unbleached, just after and 20 minutes after bleaching. **D** - Yields of singlet oxygen for the same samples as in 4.8 C presented separately for each component of decay and as a sum of A_1, A_2 and A_3. n=2. E – Time dependent changes of singlet oxygen phosphorescence kinetics for bleached POS discs after 20 minutes after irradiation with and without addition of selected retinals. Concentration of 9-*cis*-retinal and 13-*cis*-retinal refer to concentration of opsin in POS discs (7.6 μM). 3.45 μM 13-*cis*-retinal equals the concentration after *iso*rhodopsin formation with 7.6 μM 9-*cis*-retinal. Concentration of ATR used refers to ATR released after *iso*rhodopsin formation with 7.6 μM 9-*cis* retinal (4.15 μM). F –Yields of singlet oxygen for the same samples as in 4.8 E presented separately for each component of decay and as a sum of A_1, A_2 and A_3. n=2.

	Absorbance acetone	**$^1O_2$ Φ acetone**	**Absorbance benzene**	**$^1O_2$ Φ benzene**
7.6 μM 9-*cis*RAL	0.024	0.50 ±0.01	0.035	1.54 ±0.01
7.6 μM 13-*cis*RAL	0.057	0.37 ±0.01	0.043	1.28 ±0.05
4.15 μM ATR	0.051	2.27 ±0.05	0.067	2.25 ±0.02
3.45 μM 13-*cis*RAL	0.024	0.17 ±0.01	0.020	0.55 ±0.03

Table 4.4 Absorbance at 422 nm and yields of singlet oxygen formed after excitation of selected retinoids at indicated concentrations in two different solvents: acetone and benzene. Excitation wavelength of 422 nm.

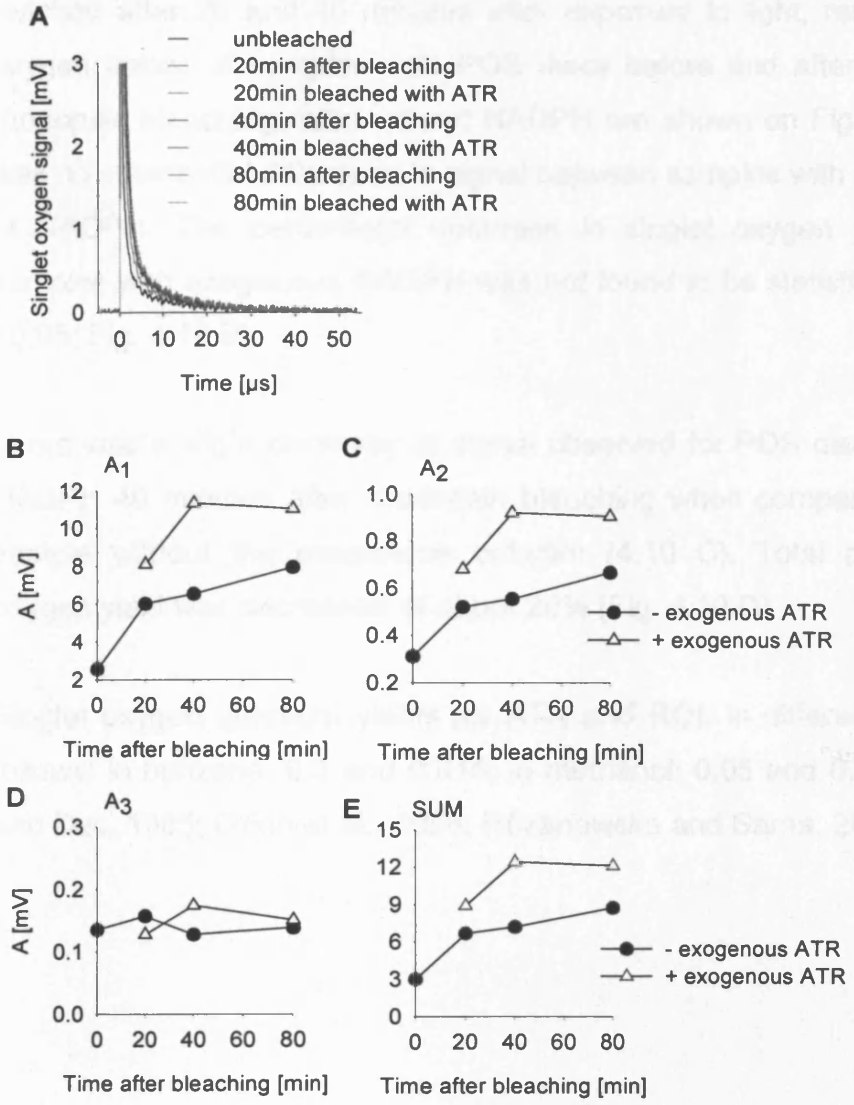

Figure 4.9 Singlet oxygen production in POS depending on time after bleaching and presence of exogenous ATR. **A** - Time dependent changes of singlet oxygen phosphorescence kinetics for unbleached and bleached POS discs after 20, 40 and 80 minutes after irradiation with and without addition of 4.15 µM ATR. **B, C, D, E** – Yields (amplitudes) of singlet oxygen for the same samples as in graph 4.9 A; amplitudes for the short- (B), middle- (C), long- (D) exponent and sums of A_1, A_2 and A_3 (E). n=1.

4.3.5 Formation of singlet oxygen depending on the presence of NADPH

Comparison of singlet oxygen production in samples with or without NADPH allowed the effect of ATR reduction and formation of ROL with different physicochemical properties to be assessed.

Based on results showing kinetics of ROL formation after rhodopsin bleaching discussed in Chapter 3, about 75% and 95% of maximum ROL concentration is

reached after 20 and 40 minutes after exposure to light, respectively. Singlet oxygen traces of samples with POS discs before and after 20 minutes after rhodopsin bleaching, with without NADPH are shown on Figure 4.10 A. There was no substantial difference in signal between samples with or without addition of NADPH. The percentage decrease in singlet oxygen yield observed in samples with exogenous NADPH was not found to be statistically significant ($P > 0.05$; Fig. 4.10 B).

There was a slight decrease of signal observed for POS discs with addition of NADPH 40 minutes after rhodopsin bleaching when compared with the same sample without the exogenous cofactor (4.10 C). Total percentage singlet oxygen yield was decreased of about 20% (Fig. 4.10 D).

Singlet oxygen quantum yields for ATR and ROL in different solvents are as follows: in benzene: 0.3 and 0.015; in methanol: 0.05 and 0.03 (Bhattacharyya and Das, 1985; Dillon et al., 1996; Różanowska and Sarna, 2005).

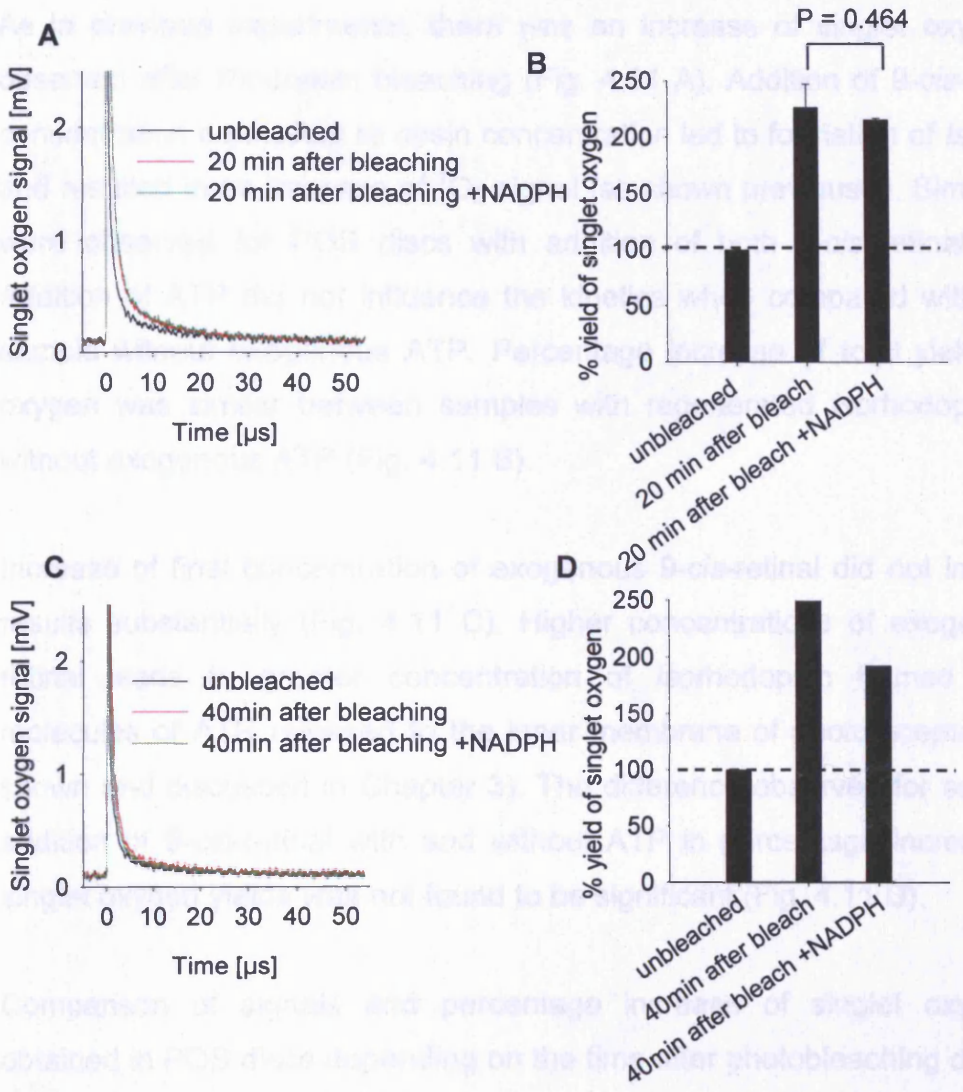

Figure 4.10 Singlet oxygen formation in POS discs depending on NADPH. **A** - Time dependent changes of singlet oxygen phosphorescence kinetics for unbleached and bleached POS discs with ~3 µM rhodopsin after 20 minutes after bleaching with and without NADPH. Total yields of singlet oxygen calculated as a sum of A_1, A_2 and A_3. **B** - Yields of singlet oxygen in samples mentioned above presented as percentage increase related to unbleached sample as 100%. Bars represent SD. n=3. **C** - Time dependent changes of singlet oxygen phosphorescence kinetics for unbleached and bleached POS discs with ~3 µM rhodopsin after 40 minutes after bleaching with and without NADPH. **D** - Yield of singlet oxygen in samples mentioned in 4.10 C. Total yields of singlet oxygen calculated as a sum of A_1, A_2 and A_3. n=1.

4.3.6 Formation of singlet oxygen depending on the presence of ATP

ATP was expected to exhibit an effect on singlet oxygen signal in samples with generated *iso*rhodopsin in which ATR is released at least in part to the inner leaflet of segments discs. The presence of ATP would allow ABCR protein to take the action and transport ATR-PE adduct to the cytoplasmic site allowing the reduction to ROL to take place.

As in previous experiments, there was an increase of singlet oxygen signal observed after rhodopsin bleaching (Fig. 4.11 A). Addition of 9-*cis*-retinal at a concentration equivalent to opsin concentration led to formation of *iso*rhodopsin and resulted in an increase of $^1O_2$ signal (as shown previously). Similar kinetics were observed for POS discs with addition of both 9-*cis* retinal and ATP. Addition of ATP did not influence the kinetics when compared with the same sample without exogenous ATP. Percentage increase of total yield of singlet oxygen was similar between samples with regenerated *iso*rhodopsin with or without exogenous ATP (Fig. 4.11 B).

Increase of final concentration of exogenous 9-*cis*-retinal did not influence the results substantially (Fig. 4.11 C). Higher concentrations of exogenous 9-*cis* retinal leads to greater concentration of *iso*rhodopsin formed and more molecules of ATR released to the inner membrane of photoreceptor discs (as shown and discussed in Chapter 3). The difference observed for samples with addition of 9-*cis*-retinal with and without ATP in percentage increase of total singlet oxygen yields was not found to be significant (Fig. 4.11 D).

Comparison of signals and percentage increase of singlet oxygen yields obtained in POS discs depending on the time after photobleaching did not show substantial changes (Fig. 4.11 E and F). Extension of time to 40 minutes after bleaching resulted in a slight increase of singlet oxygen yield. Formation of *iso*rhodopsin in sample with the same incubation time resulted in a substantial increase of the total amplitude. The presence of NADPH in the same sample seemed to coincide with about 30% decrease of the signal.

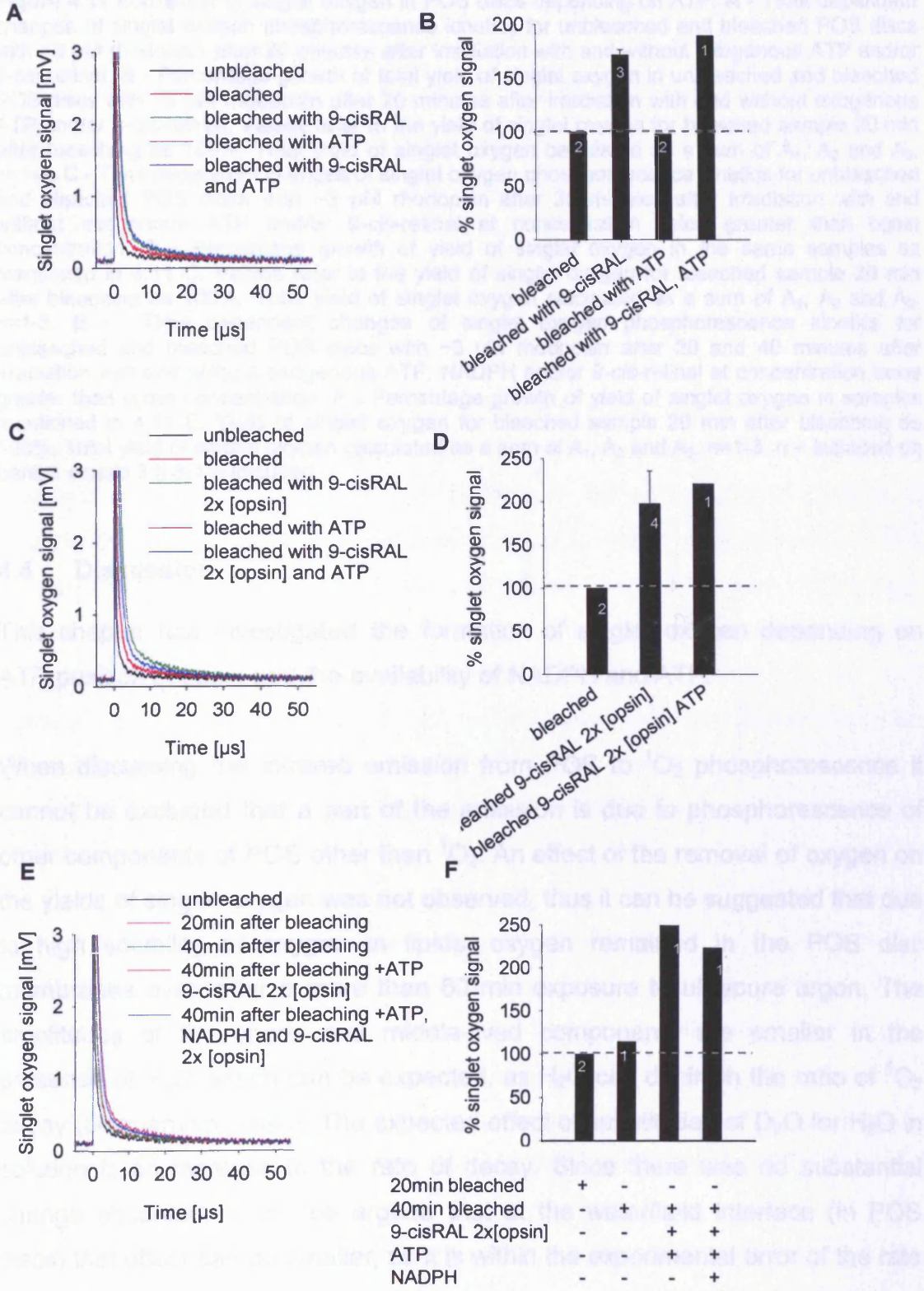
A
Singlet oxygen signal [mV]
Time [µs]
unbleached
bleached
bleached with 9-cisRAL
bleached with ATP
bleached with 9-cisRAL and ATP
B
% singlet oxygen signal
bleached
bleached with 9-cisRAL
bleached with ATP
bleached with 9-cisRAL, ATP
C
Singlet oxygen signal [mV]
Time [µs]
unbleached
bleached
bleached with 9-cisRAL 2x [opsin]
bleached with ATP
bleached with 9-cisRAL 2x [opsin] and ATP
D
% singlet oxygen signal
bleached
bleached 9-cisRAL 2x [opsin]
bleached 9-cisRAL 2x [opsin] ATP
E
Singlet oxygen signal [mV]
Time [µs]
unbleached
20min after bleaching
40min after bleaching
40min after bleaching +ATP 9-cisRAL 2x [opsin]
40min after bleaching +ATP, NADPH and 9-cisRAL 2x [opsin]
F
% singlet oxygen signal
20min bleached
40min bleached
9-cisRAL 2x[opsin]
ATP
NADPH

Figure 4.11 Formation of singlet oxygen in POS discs depending on ATP. **A** - Time dependent changes of singlet oxygen phosphorescence kinetics for unbleached and bleached POS discs with ~3 μM rhodopsin after 20 minutes after irradiation with and without exogenous ATP and/or 9-*cis*-retinal. **B** - Percentage growth of total yield of singlet oxygen in unbleached and bleached POS discs with ~3 μM rhodopsin after 20 minutes after irradiation with and without exogenous ATP and/or 9-*cis*-retinal. Values refer to the yield of singlet oxygen for bleached sample 20 min after bleaching as 100%. Total yield of singlet oxygen calculated as a sum of A_1, A_2 and A_3. n=1-3. **C** - Time dependent changes of singlet oxygen phosphorescence kinetics for unbleached and bleached POS discs with ~3 μM rhodopsin after 20 minutes after irradiation with and without exogenous ATP and/or 9-*cis*-retinal at concentration twice greater than opsin concentration. **D** - Percentage growth of yield of singlet oxygen in the same samples as mentioned in 4.11 C. Values refer to the yield of singlet oxygen for bleached sample 20 min after bleaching as 100%. Total yield of singlet oxygen calculated as a sum of A_1, A_2 and A_3. n=1-3. **E** - Time dependent changes of singlet oxygen phosphorescence kinetics for unbleached and bleached POS discs with ~3 μM rhodopsin after 20 and 40 minutes after irradiation with and without exogenous ATP, NADPH and/or 9-*cis*-retinal at concentration twice greater than opsin concentration. F - Percentage growth of yield of singlet oxygen in samples mentioned in 4.11 E. Yield of singlet oxygen for bleached sample 20 min after bleaching as 100%. Total yield of singlet oxygen calculated as a sum of A_1, A_2 and A_3. n=1-3. n – included on bars; it equals 3 if SD is included.

4.4 Discussion

This chapter has investigated the formation of singlet oxygen depending on ATR position in opsin and the availability of NADPH and ATP.

When discussing the infrared emission from POS to $^1O_2$ phosphorescence it cannot be excluded that a part of the emission is due to phosphorescence of other components of POS other than $^1O_2$. An effect of the removal of oxygen on the yields of singlet oxygen was not observed, thus it can be suggested that due to high solubility of oxygen in lipids, oxygen remained in the POS disc membranes even after a more than 60 min exposure to ultrapure argon. The amplitudes of the short- and middle-lived components are smaller in the presence of H_2O, which can be expected, as H_2O can diminish the ratio of $^1O_2$ decay (Darmanyan, 1993). The expected effect of substitution of D_2O for H_2O in solution is an increase in the rate of decay. Since there was no substantial change observed, it can be argued that at the water/lipid interface (in POS discs) that effect can be smaller, so it is within the experimental error of the rate of decay.

Monitoring of singlet oxygen formation – its yields and lifetime, in POS discs is determined by various environments that the tested photosensitiser may be

exposed to. Lack of any effect of H_2O on the lifetimes of singlet oxygen detected in POS discs suspended in D_2O suggest that most molecules of oxygen in singlet state undergo deactivation and/or interact with molecules within the lipid membrane, so the observed long-lived component of $^1O_2$ phosphorescence originating from the water environment is negligible. The two other components are determined by various environments of the membranes – the lipids and proteins embedded in the lipid membrane, the majority of which is opsin.

Photobleaching of rhodopsin resulted in a growth in signal of singlet oxygen as a function of time until a maximum was reached after about 20 minutes. This seemed to reflect the hydrolysis of ATR from the active site of opsin and channelling to the exit site. The time needed to reach a maximum of ATR molecules hydrolysed from the active site (about 15 minutes) was shorter than the time needed to reach the maximum of total yield of singlet oxygen generation in POS discs after rhodopsin bleaching (about 20 minutes). However, the difference in total singlet oxygen between 15 and 20 minutes after rhodopsin bleaching was not statistically significant. It can be stated that ATR in the exit site of opsin generates higher levels of singlet oxygen than when it is bound in the active site.

As mentioned in the Experimental design section (Section 4.2.3), generation of singlet oxygen in POS discs after rhodopsin bleaching was expected to vary depending on the ratio of formed Meta III and Meta II decaying to opsin and ATR, related to pH. Samples at pH 4.5 exhibited significantly higher yield of singlet oxygen for the shortest exponent when compared with samples at pH 7.8, which favours formation of Meta III preventing from hydrolysis of ATR.

Release of ATR to the disc membrane upon formation of *iso*rhodopsin led to a further increase of signal. However, as it was shown, not all molecules of exogenous 9-*cis*-retinal are used to bind to opsin and generate *iso*rhodopsin, so the increase may be ascribed at least in part to the singlet oxygen formed by free 9-*cis*-retinal. Testing the influence of remaining 9-*cis*-retinal by comparing it

with the same concentration of 13-*cis*-retinal allowed to test whether free ATR in the lipid membrane contributes to the increase in $^1O_2$ phosphorescence, and revealed a substantial decrease of singlet oxygen yield in samples with addition of 13-*cis*-retinal in comparison with samples with added 9-*cis*-retinal. Addition of ATR at the concentration that equalled the amount of ATR released after addition of 7.6 μM 9-*cis*-retinal resulted in the same yield as for samples with regenerated *iso*rhodopsin.

Microheterogeneity of the samples may also affect the obtained signals. The yield of decay of $^1O_2$ via phosphorescence was different in different environments. As shown in the Results section, there were differences between the amplitudes of short- and middle-lived exponential decays with a negligible effect of the long-lived exponent (Fig.4.8).

The highest efficiency of singlet oxygen generation was observed for samples with regenerated *iso*rhodopsin and ATR being released to the inner leaflet of the membrane. A similar value of total yield of singlet oxygen was obtained for sample addition of ATR at the same concentration as the expected concentration of released ATR after *iso*rhodopsin formation. The control signal for samples with addition of 13-*cis*-retinal at the same concentration as 9-*cis*-retinal showed an ~18% decrease in the amplitude for the total $^1O_2$ yield when compared with 9-c*is*-retinal.

It was expected that upon release of ATR to the lipid membrane, its binding to PE would diminish the yield of photosensitised generation of singlet oxygen. Experiments on the interaction between ATR and PE revealed a decrease (from 5.2 mV to 3.4 mV) in the difference in the amplitude of singlet oxygen phosphorescence between samples 40 min and 80 minutes after rhodopsin bleaching, when samples with and without addition of exogenous ATR were compared. It may suggest that formation of ATR-PE adducts may lead to a decrease of ATR-induced singlet oxygen generation.

Surprisingly, there was no substantial change in singlet oxygen yield in the presence of exogenous NADPH when 75% of ATR was expected to be converted to ROL. The absorption spectrum of ROL was shifted towards shorter wavelengths in comparison to ATR, so it can be expected that a considerably smaller number of incident photons of 355/422 nm light were absorbed. However, ROL is also able to generate singlet oxygen. It is known that formation of singlet oxygen is strictly solvent-dependent. As mentioned in the Results section, the quantum yield of singlet oxygen from ROL is higher in polar media than in non-polar solvents (Section 4.3.5). Therefore, polarity of the environment for ATR and ROL in POS discs will determine the yield of singlet oxygen observed. Singlet oxygen formation could take place with similar yield for both ROL and ATR in the polar environment of water or at the interface of POS disc membranes and water. As previously mentioned, both ROL and ATR exhibit similar quantum yields of singlet oxygen generation in methanol. It could possibly explain why there were no substantial differences between samples without NADPH and samples where formation of ROL was allowed by addition of the cofactor (Fig. 4.10).

Our results also suggest that there is no change in the yield of singlet oxygen produced by ATR upon *iso*rhodopsin formation and in the presence of ATP. The presence of ATP would allow ABCR protein to flip the complex between ATR and PE to the outer leaflet of the disc membrane. It can be suggested that ATR located in the inner leaflet of disc membrane upon rhodopsin formation is able to yield similar amounts of singlet oxygen as when situated in the outer leaflet when it is accessible to the dehydrogenase enzyme. It also needs to be stressed that POS discs are extremely susceptible to oxidative stress. It is possible that at the stage when experiments were performed, proteins in POS discs were already changed in a way that led to a decrease in their enzymatic activities.

In summary, the yield of ATR-induced singlet oxygen generation increased upon rhodopsin bleaching and ATR hydrolysis. *Iso*rhodopsin formation and release of ATR to the disc membrane resulted in a further increase of signal.

ATP and NADPH were not found to exhibit a substantial effect on the yield of singlet oxygen formed in POS discs with completly hydrolysed ATR.

Chapter 5

Oxidation of lipids in POS

5.1 Introduction

As discussed in the General Introduction, the retina, photoreceptors in particular, is rich in polyunsaturated lipids such as docosahexaenoate extremely susceptible to oxidation and is exposed to high levels of oxygen due to the high metabolic requirements of the whole process of (photo)transduction. Additionally, the retina contains widely known photosensitisers, such as ATR in photoreceptors and lipofuscin in the RPE. Thus, the combination of those factors with regular and high fluxes of light that the retina is constantly exposed to, may result in the formation of reactive oxygen species such as singlet oxygen and free radicals (Delmelle 1977; Delmelle 1978; Boulton at al., 1993; Różanowska at al., 1995). As shown in Chapter 4, production of singlet oxygen in POS discs depends on the position of ATR determined upon rhodopsin bleaching. ATR produces $^1O_2$ with greater ability when it is in the "exit site" of rhodopsin. Rhodopsin regeneration exacerbates this effect. Lack of a significant difference in singlet oxygen between POS discs with and without ATR reduction to ROL, discussed in Chapter 4, may suggest that ROL is also involved in formation of $^1O_2$.

Singlet oxygen may react with lipids leading to the formation of lipid hydroperoxides:

$$^1O_2 + LH \rightarrow LOOH$$

Equation 5.1 Scheme of reaction of singlet oxygen with lipid molecule. $^1O_2$ – singlet oxygen, LH – unsaturated lipid molecule, LOOH – lipid hydroperoxide.

Lipids hydroperoxides become a source of free radical chain of lipid peroxidation after being decomposed by redox active metal ions, such as iron, leading to the formation of more free radicals:

$$LOOH + Me^{n+} \rightarrow LO^{\bullet} + Me^{(n-1)+}$$

Equation 5.2 Scheme of reaction of lipid hydroperoxide with oxidised form of metal ion. LOOH – lipid hydroperoxide, Me^{n+} and $Me^{(n-1)}$ – oxidised and reduced form of metal ion, respectively, $LO^{\bullet}$ - lipid alcoxyl radical.

$$LOOH + Me^{(n-1)+} \rightarrow LOO^{\bullet} + Me^{n+}$$

Equation 5.3 Scheme of reaction of lipid hydroperoxide with reduced form of metal ion. LOOH – lipid hydroperoxide, Me^{n+} and $Me^{(n-1)}$ – oxidised and reduced form of metal ion, respectively, $LOO^{\bullet}$ - lipid peroxyl radical.

Iron ions have been shown to be present in the retina and accumulate with age (He et al., 2007). They also have been suggested to be a source of oxidants in the pathogenesis of AMD (He et al., 2007).

Free radicals formed as a result of the decomposition of lipid hydroperoxides can initiate a chain-reaction with a characteristic ability of one radical to induce the oxidative modifications of a large number of other lipid molecules – phospholipids containing polyunsaturated fatty acids (PUFA) in particular (reviewed by Catalá 2006). Peroxidation is divided into three steps presented schematically below.

$$LH + R^{\bullet} \rightarrow L^{\bullet} + RH \text{ (initiation)}$$

Equation 5.4 Scheme of initiation of lipid peroxidation. LH – unsaturated lipid molecule, $R^{\bullet}$ - a free radical, $L^{\bullet}$ - lipid radical.

$$L^{\bullet} + O_2 \rightarrow LOO^{\bullet} \text{ (formation of peroxyl radical)}$$

Equation 5.5 Scheme of formation of peroxyl radical. $L^{\bullet}$ - lipid radical, $LOO^{\bullet}$ - lipid peroxyl radical.

$$LH + LOO^{\bullet} \rightarrow L^{\bullet} + LOOH \text{ (propagation)}$$

Equation 5.6 Scheme of the propagation of lipid peroxidation. LH – unsaturated lipid molecule, $LOO^{\bullet}$ - lipid peroxyl radical, $L^{\bullet}$ - lipid radical, LOOH – lipid hydroperoxide.

Lipid hydroperoxide is the first, relatively stable product of the chain reaction. If lipid peroxidation undergoes continuous initiation, a termination reaction occurs, yielding non-radical products (NRP):

$$LOO^{\bullet} + LOO^{\bullet} \rightarrow NRP \text{ (termination)}$$

Equation 5.7 Scheme of the termination of lipid peroxidation. $LOO^{\bullet}$ - lipid peroxyl radical, NRP – non-radical products.

Lipid hydroperoxides may lead to the formation of a large variety of different secondary products of lipid peroxidation, such as short and long chain aldehydes (Porter, 1990). In the presence of metal ions or at high temperature, they readily undergo decomposition to alcoxy radicals – unstable products ultimately undergoing decomposition to low molecular weight carbonyl compounds, short-chain hydroxycabons and alcohols (Choe, 2008). Some of the products of unsaturated fatty acids oxidation include hydroxynonenal (HNE) and hydroxyhexenal (HHE), which can form covalent adducts with retinal proteins (reviewed by Organisciak and Vaughan, 2010).

Large concentrations of polyunsaturated lipids such as DHA and certain amino acid residues in the proteins present in the outer retina are extremely susceptible to the damaging effect of reactive species formed after exposure to light. It has been shown that exposure to light may result in the formation of oxidised lipids and modified proteins (Renganathan at al., 2003; Organisciak and Vaughan, 2010).

Apart from singlet oxygen, there are other reactive oxygen species formed or likely formed in the retina. Oxygen can be damaging in the dark due to the formation of superoxide radical anion as a result of mitochondrial respiration (Turrens, 1997). The protonated form of superoxide can act as a free radical initiating a chain of lipid peroxidation (Equation 5.4). Alternatively, superoxide can dismutate to hydrogen peroxide (Equation 5.8), which, in turn, may be involved in Fenton type reactions, where hydrogen peroxide interacts with a reduced form of metal ion such as Cu(I) or Fe(II), resulting in oxidation of the metal ions accompanied by decomposition of the hydrogen peroxide to the extremely oxidizing hydroxyl radical ($OH^{\bullet}$) and hydroxyl anion (Equation 5.9).

$$O_2^{-\bullet} + O_2^{-\bullet} + 2H^+ \rightarrow H_2O_2 + O_2$$

Equation 5.8 Scheme of dismutation of superoxide to hydrogen peroxide. $O_2^{-\bullet}$ – superoxide, H_2O_2 – hydrogen peroxide.

$$H_2O_2 + Me^{(n-1)+} \rightarrow HO^{\bullet} + HO^{-} + Me^{n+}$$

Equation 5.9 Scheme of the reaction of hydrogen peroxide with the reduced form of metal ion. H_2O_2 – hydrogen peroxide, Me^{n+} and $Me^{(n-1)}$ – oxidised and reduced form of metal ion, respectively, $HO^{\bullet}$ - hydroxyl radical, HO^{-} - hydroxyl anion.

Both ATR and ROL have been shown to generate superoxide radicals in the dark as a result of interaction with metal ions (Dillon et al., 1996; Murata and Kawanishi, 2000; Pawlak et al., 2003).

The aim of the experiment was to quantify levels of hydroperoxides in lipids in photoreceptor outer segments depending on the ATR position in opsin. It was expected that bleaching of rhodopsin and ATR hydrolysis would lead to an increase in oxidative modifications of lipids, and that it would be further exacerbated upon exposure to light.

5.2 Experimental design

5.2.1 Isolation of photoreceptor outer segments (POS) and extraction of lipids and proteins

Due to the high susceptibility of POS to oxidation, the main concern was the freshness of bovine eyes used for isolation of POS. To minimise unwanted changes in samples, POS were isolated from fresh bovine retinas (just after they were delivered from the abattoir) and the time of storage was minimised (Method section 2.1.2 and 2.1.3). Lipids were extracted as described in the Methods section. All samples were prepared with the same content of lipids (the same concentration and volume of POS suspension) in duplicates or triplicates (Methods section 2.4.1), used just after extraction or stored at -80 °C under argon.

5.2.2 Hydroperoxides in POS as a function of incubation time at room temperature

To test the effect of storage of POS at room temperature, samples were kept for different periods of time at 21°C to reveal changes in the level of hydroperoxides determined in lipid fraction by iodometric assay. The initial LOOH levels in POS were monitored in order to reveal any changes over a period of time 0-60 minutes (Method Section 2.4.3).

5.2.3 Evaluation of hydroxyperoxides in lipids in POS as a function of ATR position

There were different treatments applied to POS with completely hydrolysed ATR before extraction of lipids to allow the influence of rhodopsin bleaching and subsequent irradiation to be assessed. It was expected that ATR hydrolysis will lead to initiation of lipids peroxidation. To test the hypothesis, POS were kept in the dark as a control, or bleached with green light and kept at room temperature until extraction at selected time intervals (Method section 2.4.4). Samples 8, 10 and 20 minutes after rhodopsin bleaching refer to 75%, 90% and 100% of hydrolysed ATR from opsin. To test how photoexcitation of hydrolysed ATR affects lipids, samples with bleached rhodopsin and ATR completely hydrolysed were irradiated with white light for 10 and 20 minutes (irradiance of ~12 mW/cm^2) and compared with those kept in the dark (Method section 2.4.4). To test whether conversion of ATR to ROL results in a difference in the level of hydroperoxides, samples with hydrolysed ATR were compared with samples where ROL formation was enabled by addition of NADPH and/or ATP (for samples with ATR released from the opsin "exit" site) (Method Section 2.4.4).

5.3 Results

5.3.1 Assessment of the initial level of hydroperoxides in POS and its changes depending on time of incubation at room temperature

Testing the level of triiodide in POS stored at room temperature for various periods of time revealed that there was an initial increase of hydroperoxides observed already at about 5 minutes of storage at room temperature, followed by a gradual decrease to a level of hydroperoxides at 40 min that was similar to the initial level. Samples stored at room temperature for longer than 40 minutes showed lower levels of LOOH than at time zero (Fig. 5.1), indicating that hydroperoxides were not stable over a longer time interval of POS exposure to room temperature. It needs to be stressed that the kinetics of hydrolysis of ATR and its reduction to ROL occur on a time scale up to minutes at room temperature.

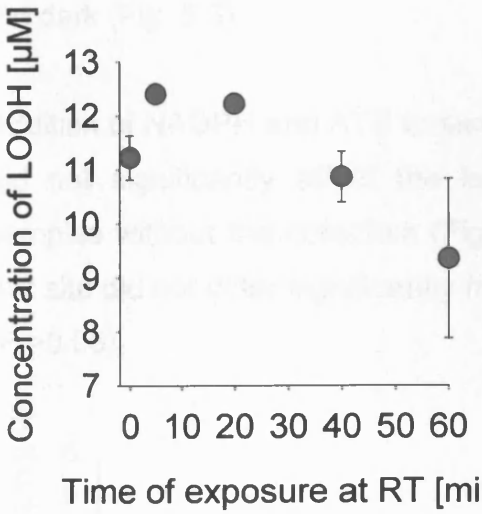

Figure 5.1 Concentration of hydroperoxides (LOOH) [µM]/1.4 mg of opsin in POS kept at room temperature for different periods of time up to 60 minutes. Time 0 min corresponds to lipids extracted just after transferring POS from 4 to 21°C. Bars=SD.

5.3.2 Assessment of the level of hydroperoxides in POS depending on the position of ATR

The level of hydroperoxides in POS before and after bleaching (Fig. 5.2) was lower than the level determined in the previous experiment (Fig. 5.1), in which even the lowest level of LOOH was 9.4 μM.

The decrease in the concentration of LOOH just after bleaching when compared with unbleached sample was not found to be significant ($P > 0.05$). The level of LOOH was similar for unbleached samples and for samples after 8 and 10 minutes following bleaching (see Fig. 5.2). There was no substantial difference between unbleached sample and bleached POS with ATR completely hydrolysed (20 min bleached) ($P > 0.05$).

Irradiation of bleached POS with white light did not lead to a significant change of LOOH when compared with the initial sample and the same samples kept in the dark (Fig. 5.3).

Addition of NADPH and ATP to samples with ATR released to the opsin exit site did not significantly affect the level of the LOOHs compared to bleached samples without the cofactors (Fig. 5.4). Samples with ATR released from the exit site did not differ significantly from samples with completely hydrolysed ATR ($P > 0.05$).

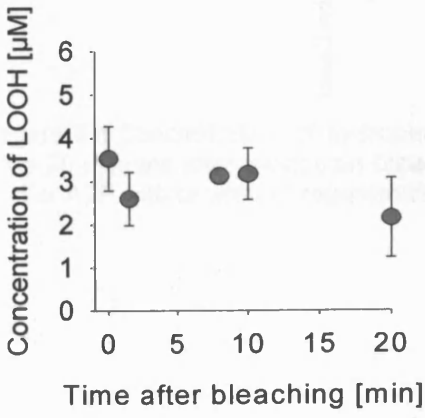

Figure 5.2 Concentration of hydroperoxides (LOOH) [μM]/1.4 mg opsin in POS before and after rhodopsin bleaching at different time points. 0 min refers to unbleached POS. Bars=SD.

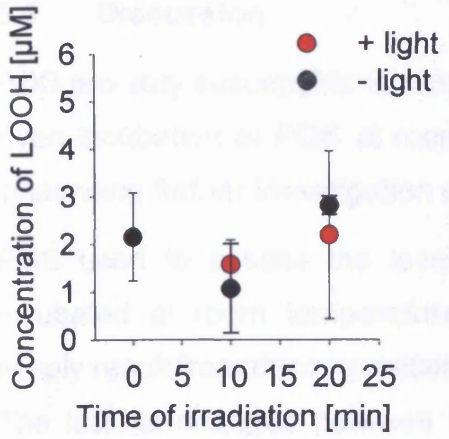

Figure 5.3 Concentration of hydroperoxides [µM]]/1.4 mg opsin in POS after 20 minutes after rhodopsin bleaching (0 min irradiation time) and irradiated samples for 10 and 20 minutes. Bars=SD.

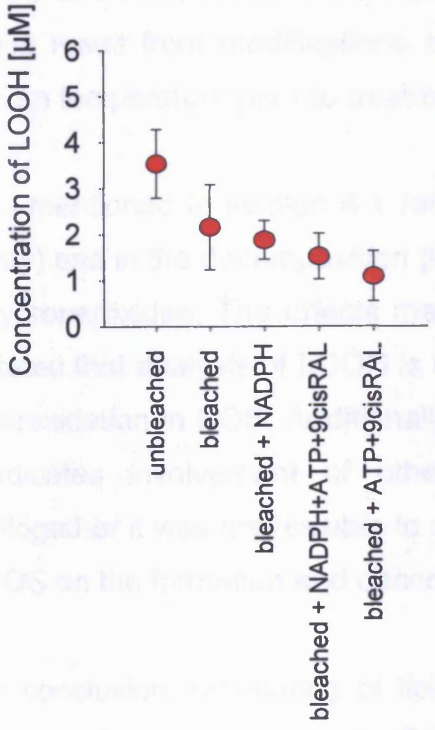

Figure 5.4 Concentration of hydroperoxides [µM]]/1.4 mg opsin in unbleached POS and POS after 20 minutes after rhodopsin bleaching compared with bleached POS with addition NADPH and/or ATP with or without regeneration of *iso*rhodopsin. Bars=SD.

5.4 Discussion

POS are very susceptible to oxidative damage as shown in the Results section. Even incubation of POS at room temperature leads to oxidative modifications, influencing further investigation of lipid peroxidation.

POS used to assess the level of LOOH depending on ATR position were incubated at room temperature prior to treatment. Thus, the changes may simply result from decomposition and/or newly formed LOOH.
The lack of changes between bleached POS kept in the dark and bleached POS exposed to white light may be due to decomposition of LOOH being compensated for by newly formed LOOH. Any observed changes in bleached POS when compared with bleached POS with addition of ATP and NADPH may also result from modifications of LOOH depending on the incubation time at room temperature prior to treatments.

As mentioned in section 4.1 retinoids play a role in both the formation (direct way) and in the decomposition (indirect role by redox cycling of iron ions) of lipid hydroperoxides. The effects may compensate for each other, hence it can be stated that analysis of LOOH is not an optimal way to assess a progress of lipid peroxidation in POS. Additionally, the high background level of hydroperoxides indicates involvement of other processes initiating lipid peroxidation, so altogether it was not feasible to assess the direct effect of the position of ATR in POS on the formation and decomposition of LOOH.

In conclusion, monitoring of lipid hydroperoxides is not an optimal method to assess lipid peroxiation in POS. POS lipids are extremely susceptible to oxidative changes and formed hydroperoxides undergo decomposition on the time scale of minutes.

Chapter 6

(Photo)toxicity of ATR and dATR and protective role of antioxidants

6.1 Introduction

As discussed in Chapter 4, formation and hydrolysis of ATR in POS can lead to the formation of singlet oxygen, indicating possible harmful effects on biological molecules and structures. To further investigate the actual effect of ATR on cells, experiments were carried out to reveal changes in mitochondrial activity and morphology of cells in the presence of ATR. As described in the Introduction section, it has been shown that ATR is a labile compound and undergoes a rapid degradation upon irradiation under aerobic conditions leading to the formation of oxidations products absorbing at shorter wavelengths. Thus, toxicity of degraded ATR was also tested in the experiments.

It has been shown that there are protective components preventing from oxidative stress caused by reactive oxygen species and toxic compounds such as aldehydes. One of the endogenous, protective components in photoreceptors and/or the RPE is PE and low-molecular retinal antioxidants: Vitamins E and B_6, glutathione (GSH) and ROL. Other antioxidants include synthetic compounds which can be obtained as a dietary supplement or are being developed as an antioxidant treatment – NAC, retinyl ascorbate (RA-AsA) and ascorbyl palmitate (AsA-Pal).

PE has been shown to have a substantial protective effect against retinal damage (Różanowska et al., 2003). It can form complexes with aldehydes, changing their physicochemical properties and protecting other molecules from being modified at the same time. A similar property is exhibited by one of the forms of $VitB_6$ – pyridoxamine, in which its amine group can also react with aldehydes. It has been shown to inhibit the formation of advanced glycation products and the chemical modification of proteins during lipid peroxidation reactions and during experimentally induced diabetes (Onorato et al., 2000; Stitt et al., 2002). Another form of the vitamin B_6 – pyridoxal, can be involved in competitive binding with amine groups of amino acids of proteins, resulting in protection of biologically important components. It has been also shown to be an effective inhibitor of advanced glycation products (Higuchi et al., 2006). A

recent study indicated that supplementation with one of the VitB forms (pyridoxine hydrochloride) may reduce the risk of AMD (Christen et al., 2009).

Protection from free radicals and singlet oxygen, on the other hand, can be obtained by direct antioxidant action of Vitamin E, retinoids (ROL), RA-AsA and AsA-Pal. Vitamin E – α-tocopherol, is one of the low-molecular-weight antioxidants. It also has been shown to prevent non-enzymatic lipid peroxidation (Guajardo et al., 1998). As an antioxidant, it has been shown to act in cell membranes, preventing the propagation of free radical reactions (Herrera and Barbas, 2001). In addition, protein kinase C-supressing and antiproliferative effects of α-tocopherol have been previously demonstrated (Engin, 2009). ROL exhibits antioxidant properties due to its polyene unit that can neutralise thiyl radicals, quench singlet oxygen and combine and stabilise peroxyl radicals (Palace et al., 1999). ROL was also found to be able to substantially inhibit non-enzymatic lipid peroxidation (Guajardo et al., 1998). RA-AsA was found to be a free radical scavenger and can be possibly used as a co-drug (Abdulmajed and Heard, 2004; Abdulmajed et al., 2005). It is a novel compound and its antioxidant potential has not been completely evaluated. Its chemical structure suggests that it might exhibit great antioxidant properties since it contains both a polyene chain, expected to retain ability to quench singlet oxygen as well as an ascorbate part, expected to act as both – $^1O_2$ quencher and a free radical scavenger. AsA-Pal has been shown to have potential as an antioxidant. It exhibits oxygen scavenging functions and is widely available and commercially used as an antioxidant in skincare (Cort, 1974; Kessler et al., 2002). Similarly to ascorbate anion, it scavenges reactive oxygen species but due to its palmitate part it can be incorporated into the lipid membrane and thus is expected to inhibit lipid peroxidation more efficiently than the hydrophilic ascorbate anion.

Antioxidant activities such as direct scavenging of free radicals have been attributed to GSH and NAC. GSH is a tripeptide of L-glutamine, L-cysteine, and glycine containing a sulfhydryl group. It is widely known as an antioxidant and plays several important roles. It directly quenches reactive free radicals. It may be involved in the action of one of the antioxidant enzymes - glutathione

peroxide (GPX). GPX reduces lipid hydroperoxides and hydrogen peroxide, which otherwise could initiate a chain of lipid or protein peroxidation or take part in a Fenton type reaction generating hydroxyl radicals (Brigelius-Flohe et al., 2003). GSH can also be a co-factor for glutathione S transferase (GST) – an enzyme important in detoxification, playing a key role in the detoxification of products of lipid peroxidation by conjugating them to GSH and thus making them water soluble, which enable their transport out of the cell (Berg et al., 2002; Hayes et al., 2005). NAC is a synthetic precursor of GSH as it provides cysteine, which is a limiting amino acid in synthesis of GSH. It exhibits antioxidant properties – it is capable of interacting with reactive oxygen species (ROS) (Aruoma at al., 1989).

The aim of this chapter was to determine the (photo)toxicity of ATR and dATR and to test possible protective agents against their harmful effects on cells.

6.2 Experimental design

In all experiments described in this chapter, MTT assay was performed ~24 hours following a 1 hour exposure to ATR or dATR +/- antioxidants, +/- light (2.7.2.2). Unless indicated otherwise, all results are presented as a mean from at least three independent experiments.

6.2.1 (Photo)toxicity of ATR and dATR

In order to assess the influence of ATR and dATR on cells, ARPE-19 cells were incubated with the retinoid in undegraded or degraded form (as described in the Method section 2.6.3). Light was the additional factor and cells kept in the dark were compared with cells exposed to white light. Figure 6.1 A shows the spectrum of light used for irradiation of ATR and cells in the actual experiments. The absorption spectrum of ATR before and after (photo)degradation is shown in Figure 6.1 B.

As described in the Method section 2.6.1, ATR was degraded in benzene as the reactivity of the solvent is relatively low and allows the possibility of influencing ATR degradation by the interaction with solvent to be minimised.

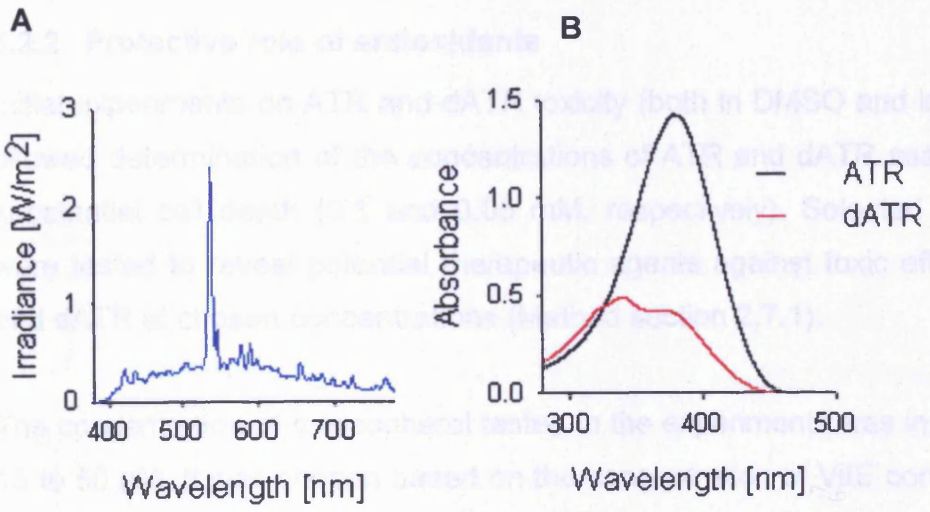

Figure 6.1 A - Irradiance spectrum of white light used for ATR degradation and exposure of cells; irradiance of ~12 mW/cm^2. B – Absorption spectra of ATR before irradiation (black line) and after 60 min exposure to white light (red line).

ATR degradation was tested at different times of degradation to reveal the time-dependent extent of changes in ATR. The increase in absorption at shorter wavelengths after ATR degradation was estimated as described in the Methods section 2.6.1.

For all further experiments, ATR was degraded for 1 hour with adjusted intensity of light to the same value of irradiance (~12 mW/cm^2). As described in the Method section 2.6.3, toxicity of ATR and dATR was tested both in DMSO and in liposomes to mimic *in vivo* conditions under which ATR and dATR would be present in POS membranes in close contact with the RPE.

To reveal the mechanism underlying the death of cells after exposure to ATR and dATR, labelling with propidium iodide together with Hoechst was performed (Method section 2.7.2.3). Labelling was carried out 2 and 24 hours post exposure. It was expected that if the uptake of PI would be observed

2 hours after exposure, the death of cells would be considered to occur via necrosis since apoptotic processes occur on a longer time scale. Assessment of cell death was based on the permeability of plasma membrane to PI and the shape of nuclei.

6.2.2 Protective role of antioxidants

Initial experiments on ATR and dATR toxicity (both in DMSO and in liposomes) allowed determination of the concentrations of ATR and dATR associated with substantial cell death (0.1 and 0.05 mM, respectively). Selected antioxidants were tested to reveal potential therapeutic agents against toxic effects of ATR and dATR at chosen concentrations (Method section 2.7.1).

The concentration of α-tocopherol tested in the experiments was in the range of 15 to 50 μM. It was chosen based on the concentration of VitE concentration in blood plasma of ~25 μM (Kinlay et al., 1999).

To study the effect of PE on dATR toxicity, liposomes were made with incorporated 1 mM and 0.5 mM dATR for experiments in the dark and light conditions, respectively. The concetration of dATR in the light conditions was lower since the toxicity of dATR in the light was expected to be exacerbated in comparison with the dark conditions. The molar percentage of DMPE in liposomes was based on published PE levels in rod outer segments – 35% of the total rod outer segment (ROS) phospholipids (Bazan et al., 1990). A concentration 1.8 times lower was also tested. 55% PE refers to the elevated level of PE observed in patients with Stargardt disease (Mata et al., 2000). The molar proportion of phospholipids to retinal was 10:1 and 20:1 in the dark and exposed to light liposomes, respectively.

Other antioxidants were tested at several concentrations in order to determine optimal conditions for protective effects.

6.3 Results

6.3.1 Phototoxicity of ATR and dATR for ARPE-19 cells depending on the level of ATR degradation

6.3.1.1 Degradation of ATR

Irradiation of ATR with white light resulted in a gradual formation of degradation products with an absorption spectrum shifted towards shorter wavelengths. Figure 6.2 A shows a representative absorption spectra recorded for ATR before and after irradiation lasting between 10 and 120 minutes. There was a decrease in absorption at 380 nm dependent on the length of time of irradiation, and an increase in absorption of shorter wavelengths shown by an increase of degradation products absorption at 325 nm, where the contribution of ATR was subtracted (Fig. 6.2 B).

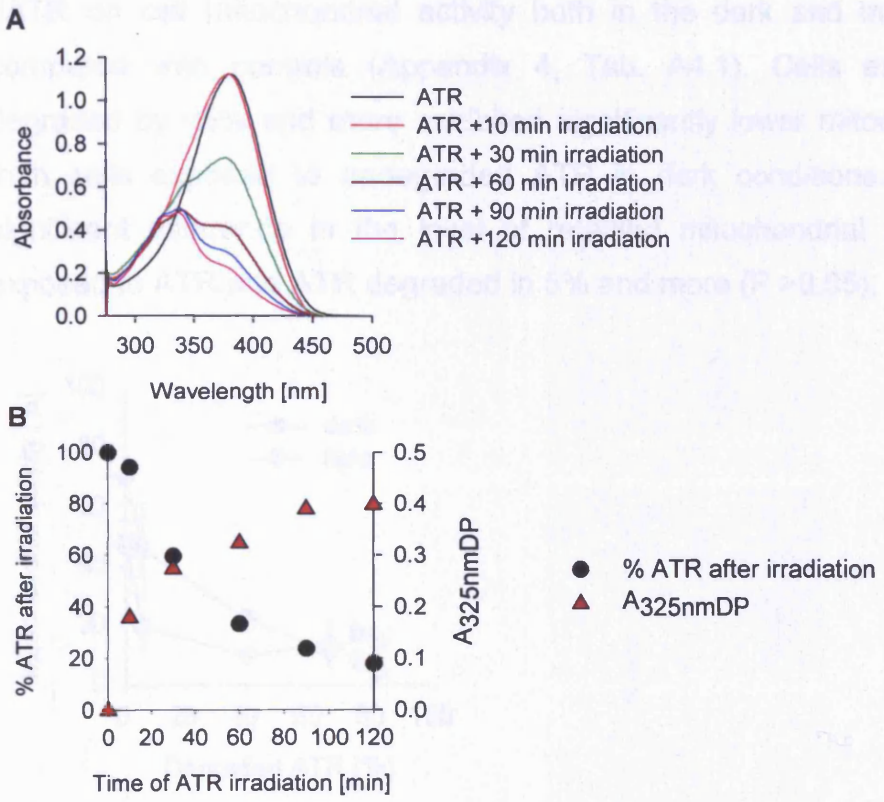

Figure 6.2 Photodegradation of ATR. **A** – Absorption spectra of ATR before and after indicated time of degradation. **B** – Dependence on the degradation time of the upper limit of ATR expressed as percentage of the initial concentration (calculations based on absorbance values at 380nm) and the absorbance of dATR at 325 nm with included contribution of ATR at 325 nm.

6.3.1.2 Effect of ATR and degraded ATR on mitochondrial activity

Both ATR and dATR appeared to be more harmful to cells in the light when compared with dark conditions.

Changes in mitochondrial activity of cells exposed to ATR occurred already when 5% of ATR underwent degradation (Fig. 6.3), but the difference when compared with the control was found to be significant only for cells exposed to light ($P < 0.05$). Loss of mitochondrial activity was observed to a higher extent with a greater degree of ATR degradation. A substantial decrease in mitochondrial activity occurred after exposure to ATR irradiated for 30 minutes (40% degraded ATR) and 10 minutes (5% degraded ATR) in the dark and when exposed to light, respectively, when compared with the control. Statistical analysis showed a significant difference between effects of ATR and

dATR on cell mitochondrial activity both in the dark and in the light when compared with controls (Appendix 4, Tab. A4.1). Cells exposed to ATR degraded by 65% and more exhibited significantly lower mitochondrial activity than cells exposed to undegraded ATR in dark conditions. There was no significant difference in the level of retained mitochondrial activity for cells exposed to ATR and ATR degraded in 5% and more (P >0.05).

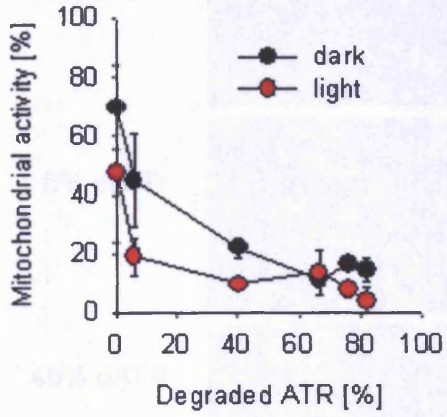

Figure 6.3 Toxicity of ATR depending on the level of its degradation. MTT results for cells exposed to 0.05 mM undegradaed ATR and ATR degraded at different degree of degradation with 0.05 mM initial concentration. During exposure to ATR/degraded ATR cells were kept in dark (dark) or exposed to white light (light). Bars = SEM. n = 3.

6.3.1.3 Effect of ATR and degraded ATR on cell morphology

There were changes of cell morphology observed after exposure of cells to ATR (Fig. 6.4). Exposure of cells to pre-irradiated ATR led to further morphological changes of cells as shown on Figure 6.4. Exposure of cells to 80% dATR resulted in cell shrinkage, loss of cell connections and cell loss. Elevation of some cells from the monolayer was also observed as a result of ATR and dATR exposure.

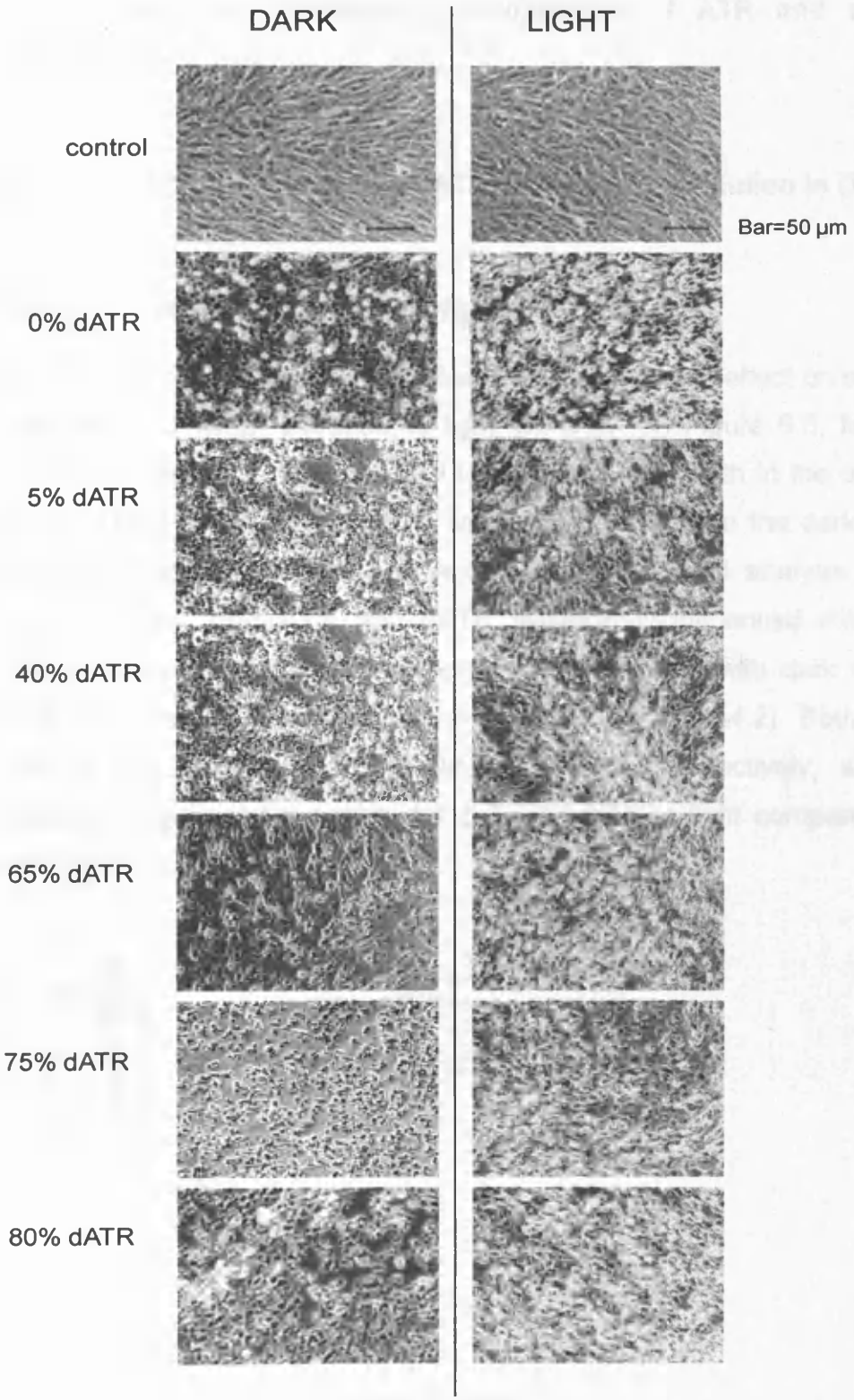

Figure 6.4 Effect of ATR and dATR on cell morphology. Phase contrast images of ARPE-19 cells taken 24 hours after exposure to 0.05 mM ATR and degraded ATR (initial concentration of 0.05 mM) at different percentage in relation to ATR. Cells exposed to ATR/dATR in the dark conditions (left column) and in the light (right column).

6.3.2 Concentration-dependent (photo)toxicity of ATR and dATR for ARPE-19 cells

6.3.2.1 Effects of ATR and dATR provided as a solution in DMSO

6.3.2.1.1 Mitochondrial activity

Both ATR and degraded ATR exhibited a dose-dependent effect on cell viability in the dark and when exposed to light, as show on Figure 6.5. MTT assay revealed that dATR is more harmful to cells than ATR both in the dark and in the light. LD50 for dATR in DMSO were 45 and 25 μM in the dark and light, respectively, while for ATR - 80 and 40 μM. Statistical analysis of results showed that 0.1 mM ATR and dATR significantly influenced mitochondrial activity of cells after exposure to light when compared with dark control (P-values for comparisons are shown in Appendix 4, Fig. A4.2). Both ATR and dATR at concentrations of 0.1 and 0.05 mM, respectively, significantly decreased mitochondrial activity for cells exposed to light compared to dark conditions ($P < 0.05$).

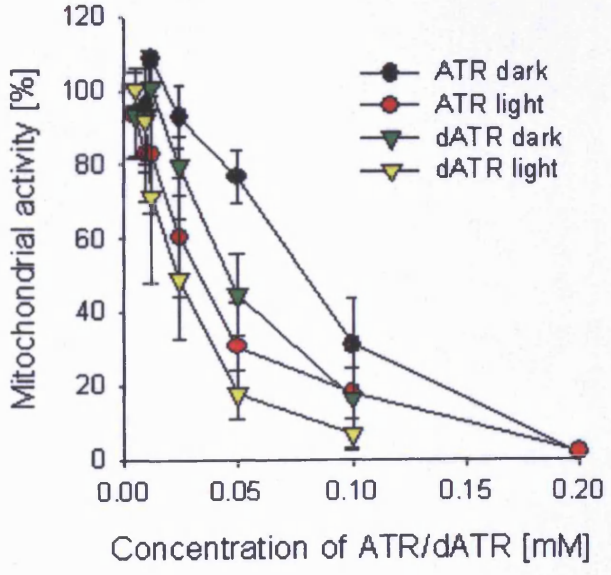

Figure 6.5 MTT results for cells exposed to ATR and dATR at indicated initial concentratons. Cells were kept in dark or exposed to white light. Cells not treated with ATR were used as control (100% mitochondrial activity). Bars = SEM. n = 3.

6.3.2.1.2 Cell morphology

Cells kept in the dark and exposed to the lowest concentrations tested up to 0.1 mM ATR showed no apparent morphological changes when observed by phase contrast microscopy (Fig. 6.6 A). Considerable changes were observed at concentrations of 0.1 mM and 0.2 mM, with cell shrinkage shown by bright areas in images caused by an increase in thickness of samples and difficulties in focusing.

Some cell detachment was also observed. Similar effect was observed in cells exposed to 0.05 mM dATR. Signs of morphological changes were already observed in cells exposed to the lowest concentrations of dATR tested (≥0.025 mM).

A damaging effect of ATR and dATR was observed at lower concentrations of ATR and dATR for cells exposed to light in comparison with cells kept in the dark (starting from 0.018 mM and 0.0125 for ATR and dATR, respectively). Exposure to higher concentrations of ATR and dATR resulted in cells shrinkage and detachment (Fig. 6.6 B).

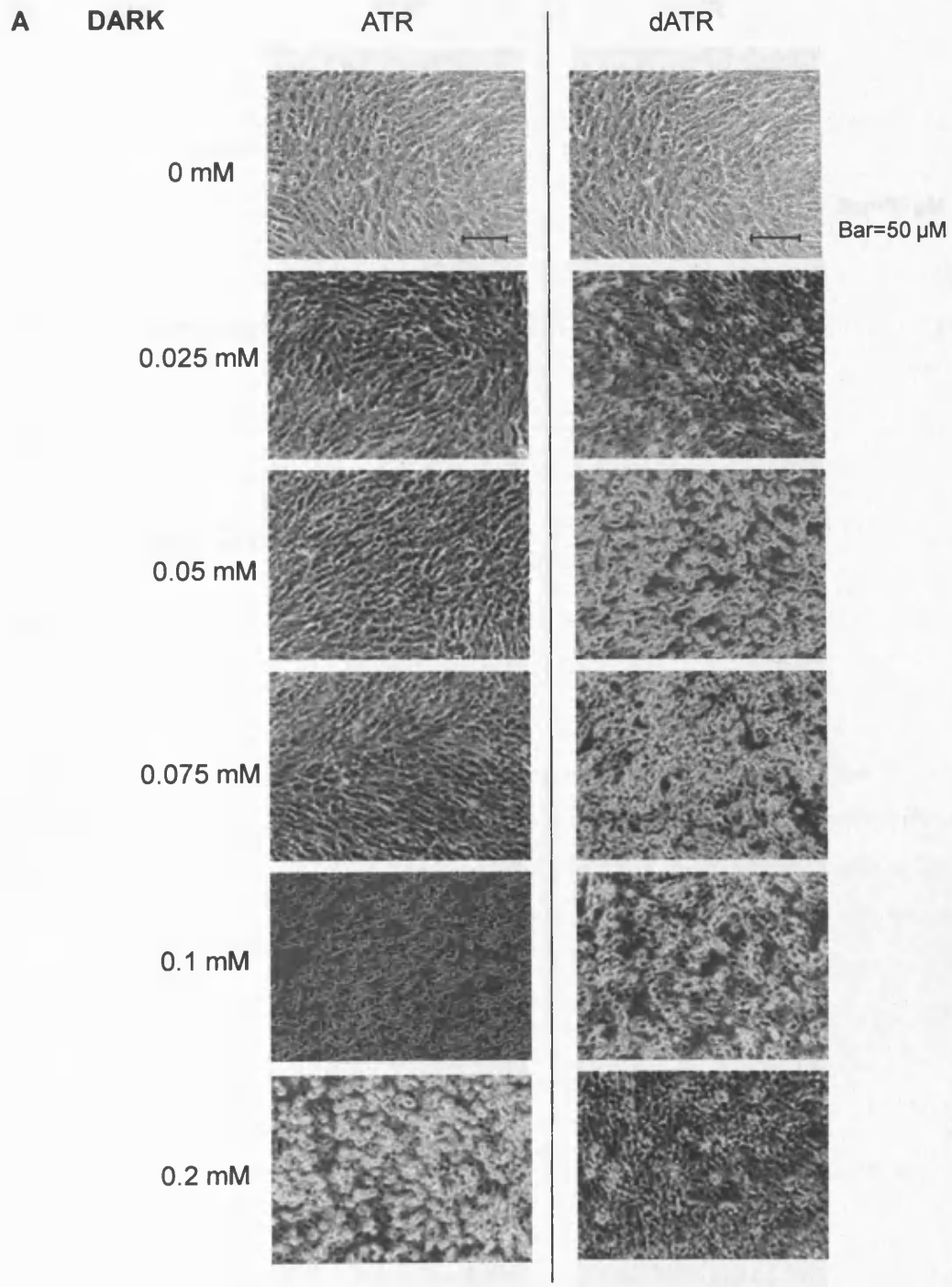
A
DARK
ATR
dATR
0 mM
0.025 mM
0.05 mM
0.075 mM
0.1 mM
0.2 mM
Bar=50 µM

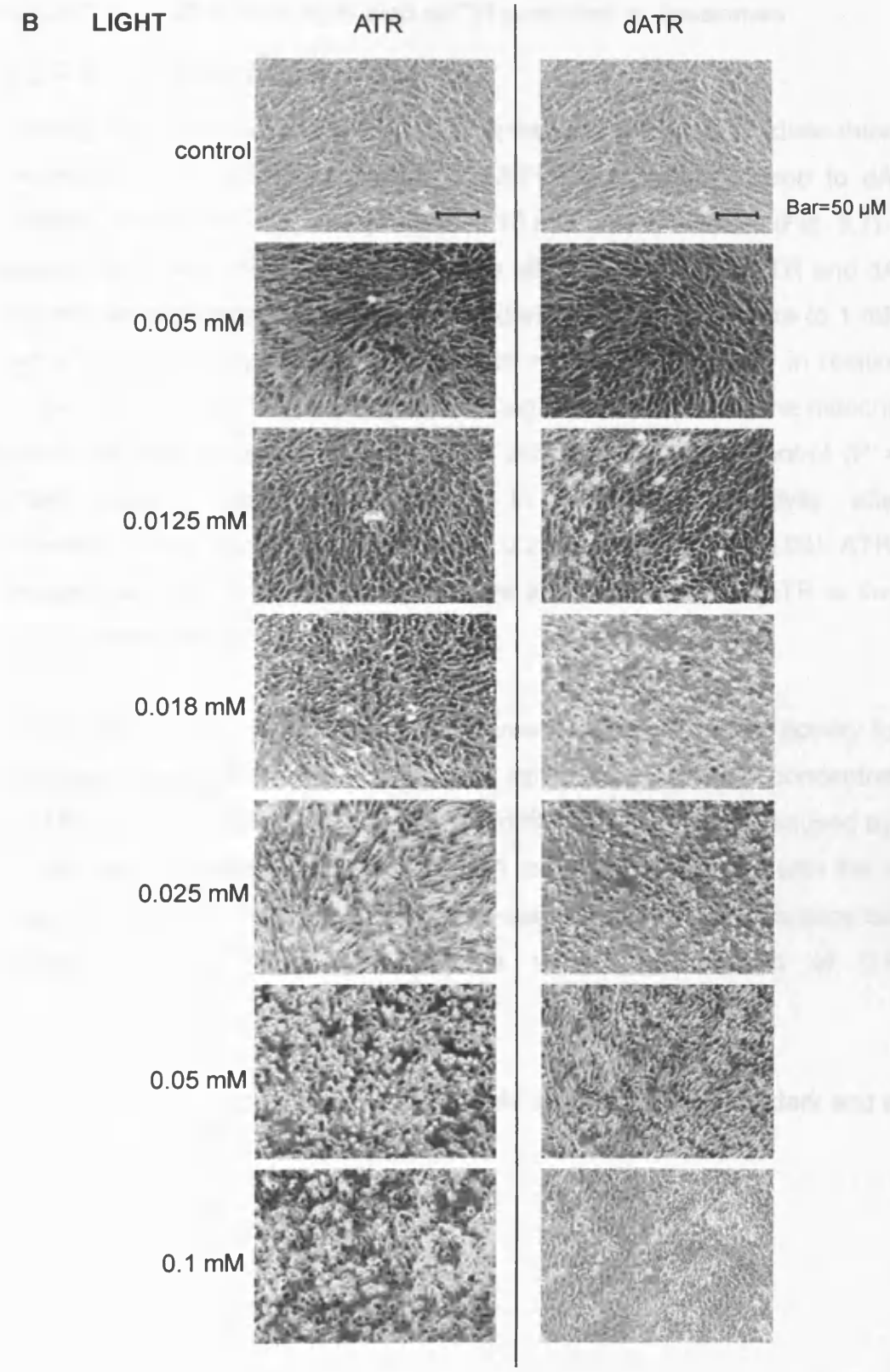

Figure 6.6 Effect of ATR and dATR on cell morphology. Phase contrast images of ARPE-19 cells taken 24 hours after exposure to ATR and degraded ATR at indicated concentrations. (A) Cells exposed to ATR/dATR in dark conditions; (B) cells exposed to ATR/dATR and light.

6.3.2.2 Effects of ATR and dATR provided in liposomes

6.3.2.2.1 Mitochondrial activity

Testing of cytotoxicity of dATR in liposomes showed a dose-dependent decrease in mitochondrial activity of ARPE-19 of cells exposed to dATR at different concentrations, incorporated in 10 mM DMPC vesicles (Fig. 6.7). There was a significant difference between the effect of 0.25 mM dATR and dATR at the highest concentration (1 mM) in the dark ($P < 0.05$). Exposure to 1 mM ATR led to a significantly smaller decrease of mitochondrial activity in relation to 1 mM ATR ($P < 0.05$). 0.1 mM ATR did not significantly influence the mitochondrial activity of cells exposed to light when compared with the control ($P > 0.05$). There was a significant decrease in mitochondrial activity after the concentration of dATR was increased to 0.25 and 0.5 mM ($P < 0.05$). ATR at the concentration of 0.5 mM seemed to have a similar effect as dATR at the same initial concentration.

There was a dose-dependent rapid decrease of mitochondrial activity for cells exposed simultaneously to dATR and light with increasing concentration of dATR (Fig. 6.7). There was a significant difference in the effect caused by dATR at the lowest concentration tested of 0.1 mM when compared with the highest one, 0.5 mM ($P < 0.05$; Fig 6.7). There was no significant difference between effects of dATR and ATR at the same concentration of 0.5 mM ($P > 0.05$).

LD50 for dATR in liposomes was 0.75 mM and 0.45 mM in the dark and in light, respectively.

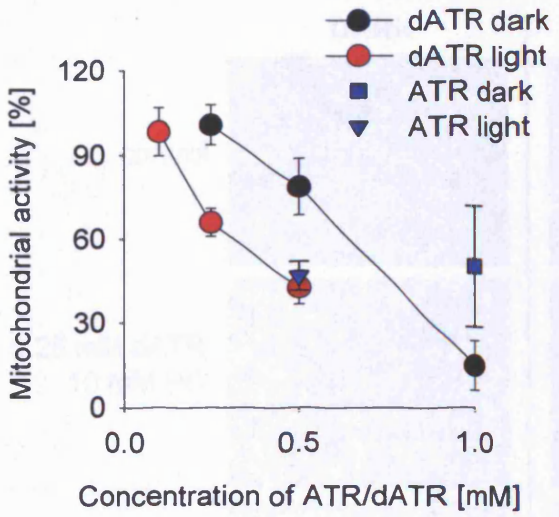

Figure 6.7 MTT result for cells exposed to ATR and dATR at selected concentrations, incorporated in liposomes containing 10 mM DMPC, in the dark and in light. Bars = SEM. n = 3.

6.3.2.2.2 Cell morphology

Figure 6.8 shows representative images of ARPE-19 cells exposed to ATR or ATR in liposomes made of 10 mM DMPC. There were morphological changes observed when cells were exposed to increasing concentrations of dATR in the dark starting from 0.25 mM. Features such as cell shrinkage, visible nuclei and cell detachment were characteristic for those cells. A similar effect was observed in cells exposed to light. Increasing concentration of dATR led to further changes of cell morphology.

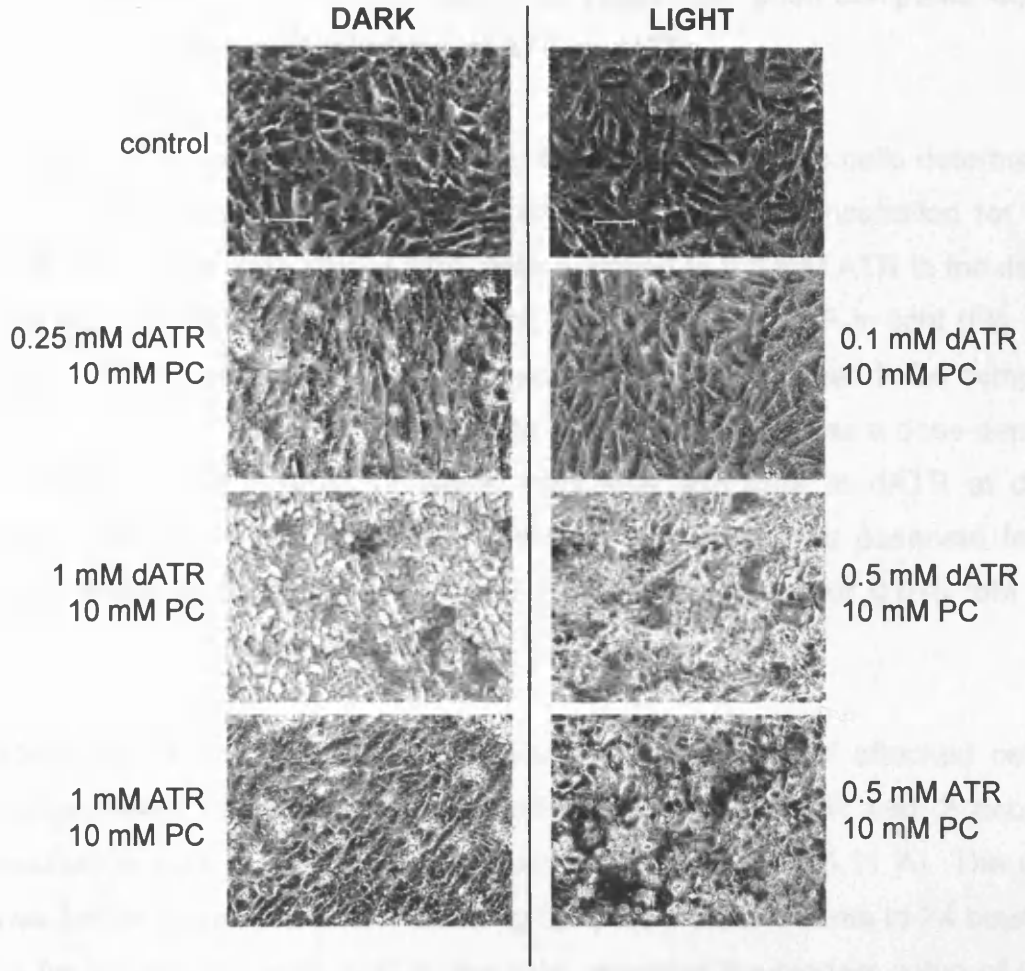

Figure 6.8 Effect of dATR on cell morphology. Phase contrast images of ARPE-19 cells taken 24 hours after exposure to ATR or degraded ATR at indicated concentrations in phosphatidylcholine (PC) liposomes. Cells exposed to dATR in dark conditions (left column) and in light (right column). Bars = 10 µm.

6.3.3 Propidium iodide labelling for plasma membrane integrity

Representative images of cells are presented in Fig. 6.9.

The highest number of viable cells which were attached to the cell culture dish and were impermeable to propidium iodite was observed for control cells and for cells exposed to the lowest concentrations of ATR and dATR in the dark (0.05 and 0.025 mM, respectively) assessed 2 hours after exposure (Fig. 6.10 A and C). An increase in concentration of ATR or dATR in darkness led to a decrease in the number of viable cells. Cells exposed to the highest concentrations of ATR and dATR (0.2 and 0.1 mM, respectively) and light were

characterised by the highest number of viable cells when compared with cells exposed to lower concentrations of ATR or dATR.

There was a substantial decrease in the number of viable cells determined 24 hours after exposure when compared with 2 hour post-incubation for control cells both in the dark and in light, cells exposed to 0.5 mM ATR in the dark, 0.1 mM ATR both in the dark and in light, and for 0.2 mM ATR in light (Fig. 6.10 B and D). The number of viable cells exposed to ATR seemed to be comparable both in the dark and after exposure to white light. There was a dose-dependent decrease in the number of viable cells after exposure to dATR at different concentrations in the dark. There were fewer viable cells observed following treatment with 0.05 mM dATR and light (similar value for 0.025 mM dATR) when compared with 0.1 mM dATR.

There was a dose-dependent increase in the number of attached cells with compromised membrane integrity after exposure to ATR and 2 hour post-incubation both in the dark and when exposed to light (6.11 A). The number was further increased after extending the post-incubation time to 24 hours (6.11 B) for 0.1 and 0.2 mM ATR in the light, reaching the highest value of 0.1 mM ATR.

Treatment with dATR led to an increase in PI labelled cells after exposure to 0.025 and 0.05 mM dATR both in the dark and in light with 2 hour post-incubation (Fig. 6.11 C) when compared with the same concentrations of ATR. The highest number of attached cells with impaired membrane integrity was observed after exposure of cells to 0.1 mM in the dark. The number of PI labelled cells after exposure to 0.05 and 0.1 mM dATR in the dark seemed to decrease 24 hours after exposure. There was an increase in the number of compromised cells for cells exposed to 0.025 and 0.1 mM dATR in light after 24 hours following exposure when compared with a shorter time of post-incubation.

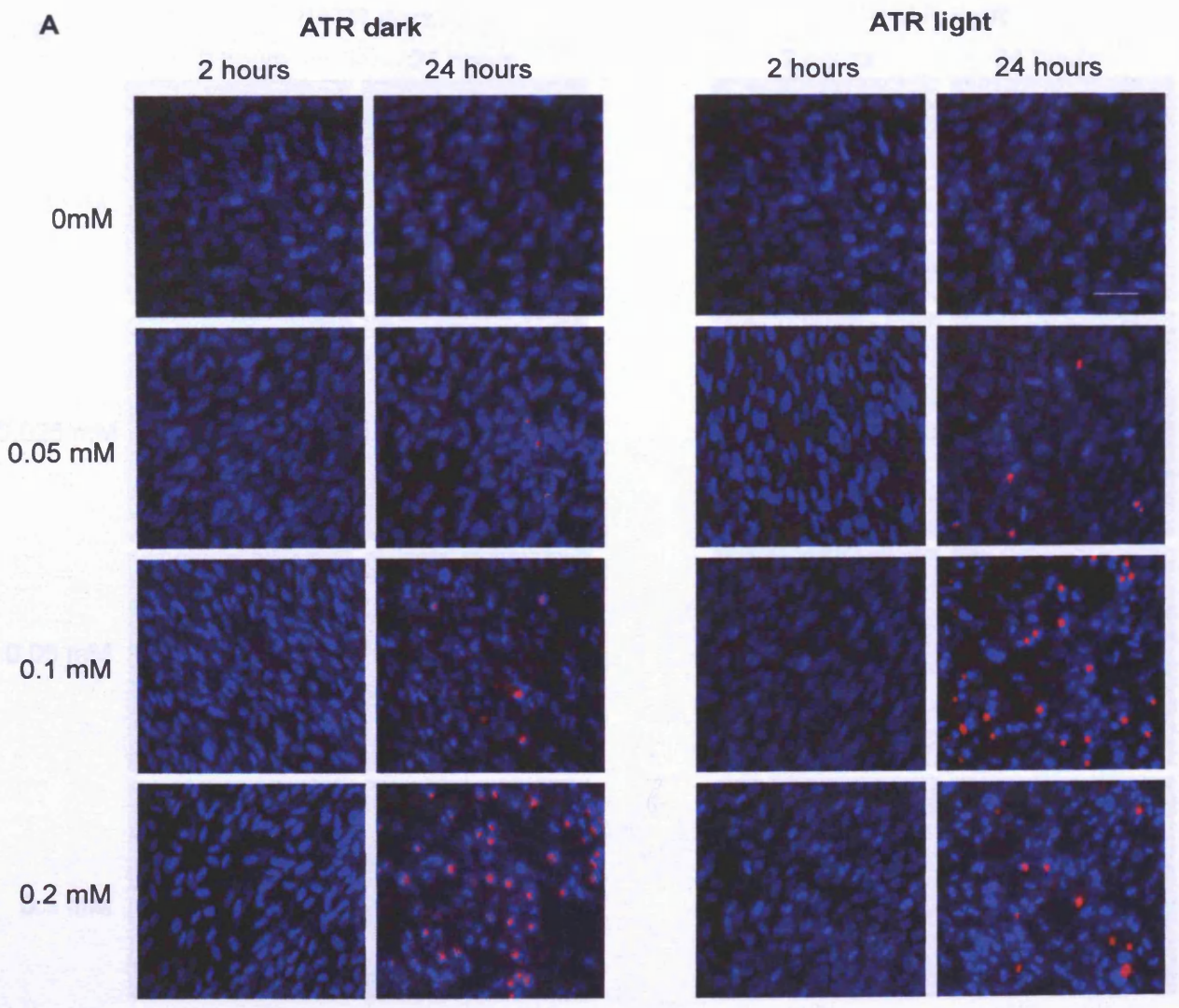
A
ATR dark
ATR light
2 hours
24 hours
2 hours
24 hours
0mM
0.05 mM
0.1 mM
0.2 mM

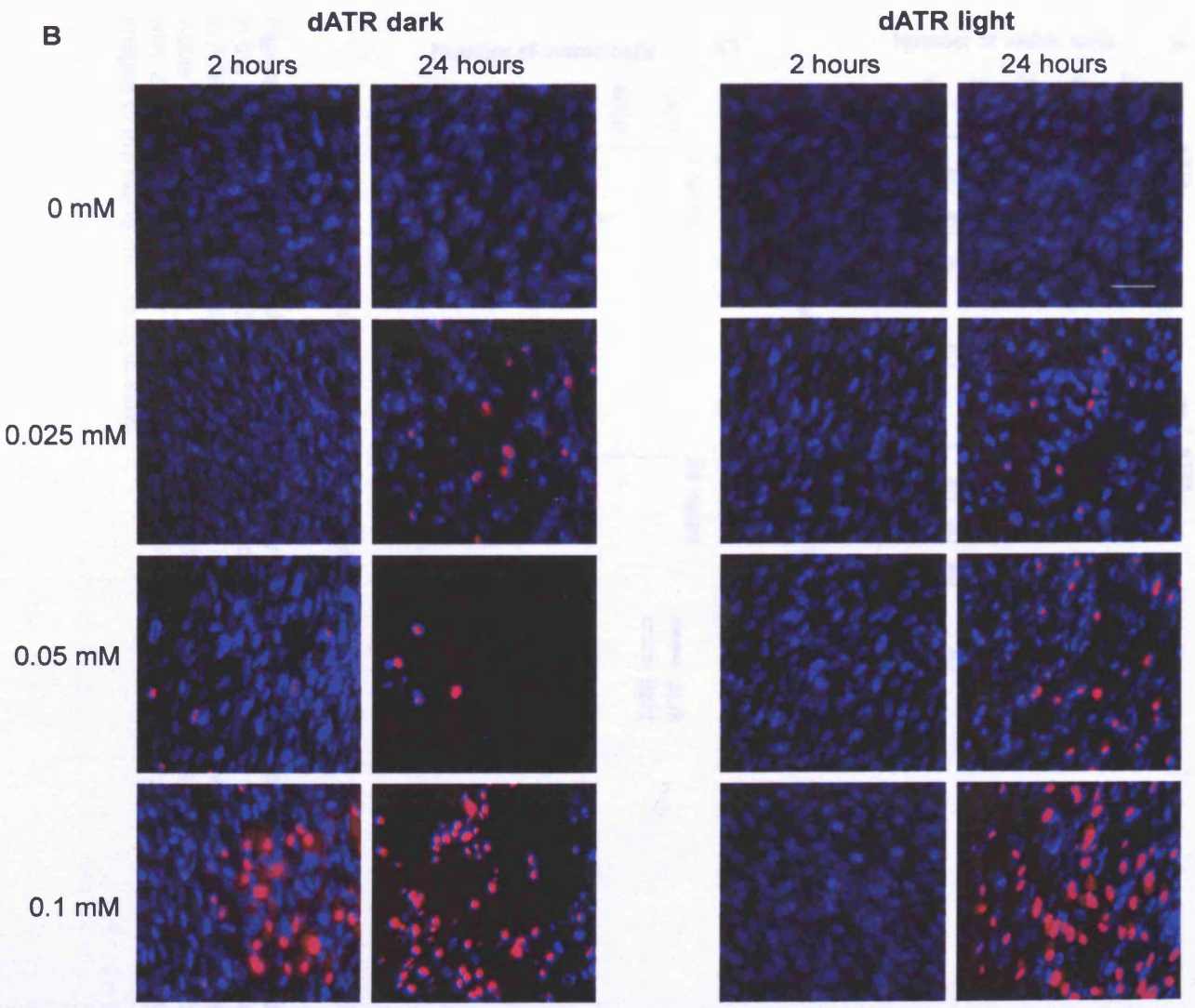
B
dATR dark
dATR light
2 hours
24 hours
2 hours
24 hours
0 mM
0.025 mM
0.05 mM
0.1 mM

Figure 6.9 Representative images of propidium iodide labelled cells after exposure to indicated concentrations of ATR (A) and dATR (B) in the dark or in light. Images were taken 2 and 24 hours after exposure. Bar = 50 μm.

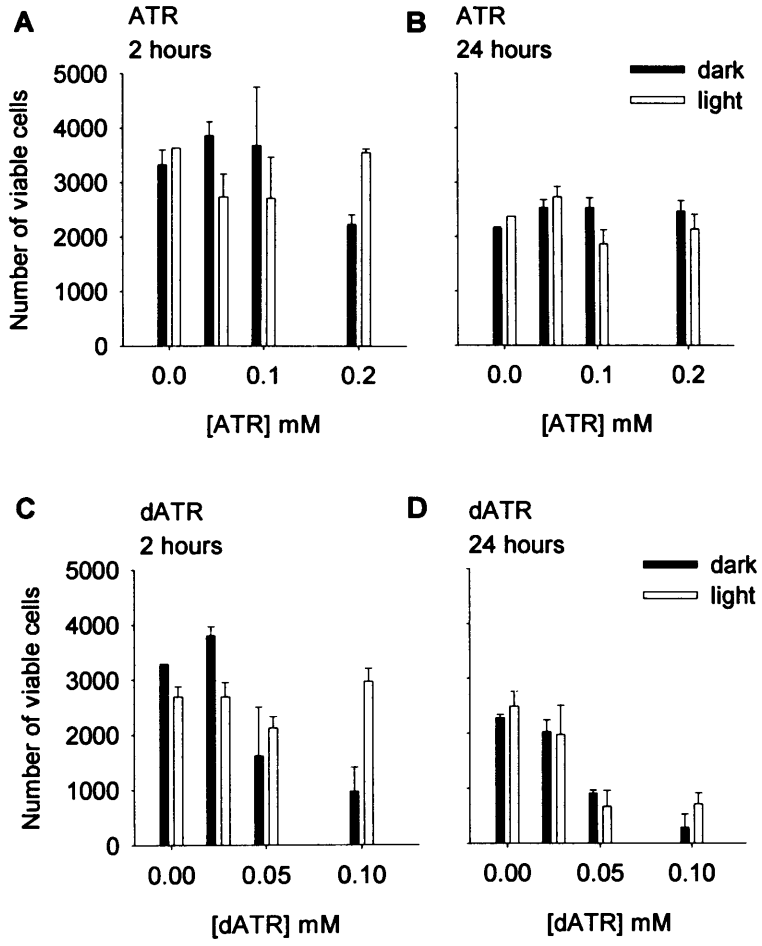

Figure 6.10 Number of viable cells after exposure to ATR or dATR, at indicated concentrations in the dark or in light 2 or 24 hour post-incubation. A, B – number of viable cells after exposure to ATR in the dark or exposed to light with 2 (A) or 24 (B) hour post-incubation. C, D - number of viable cells after exposure to dATR at indicated concentrations in the dark or exposed to light with 2 (C) or 24 (D) hour post-incubation. Calculations of means ± SD were based on 2-4 images of the same microscopic view.

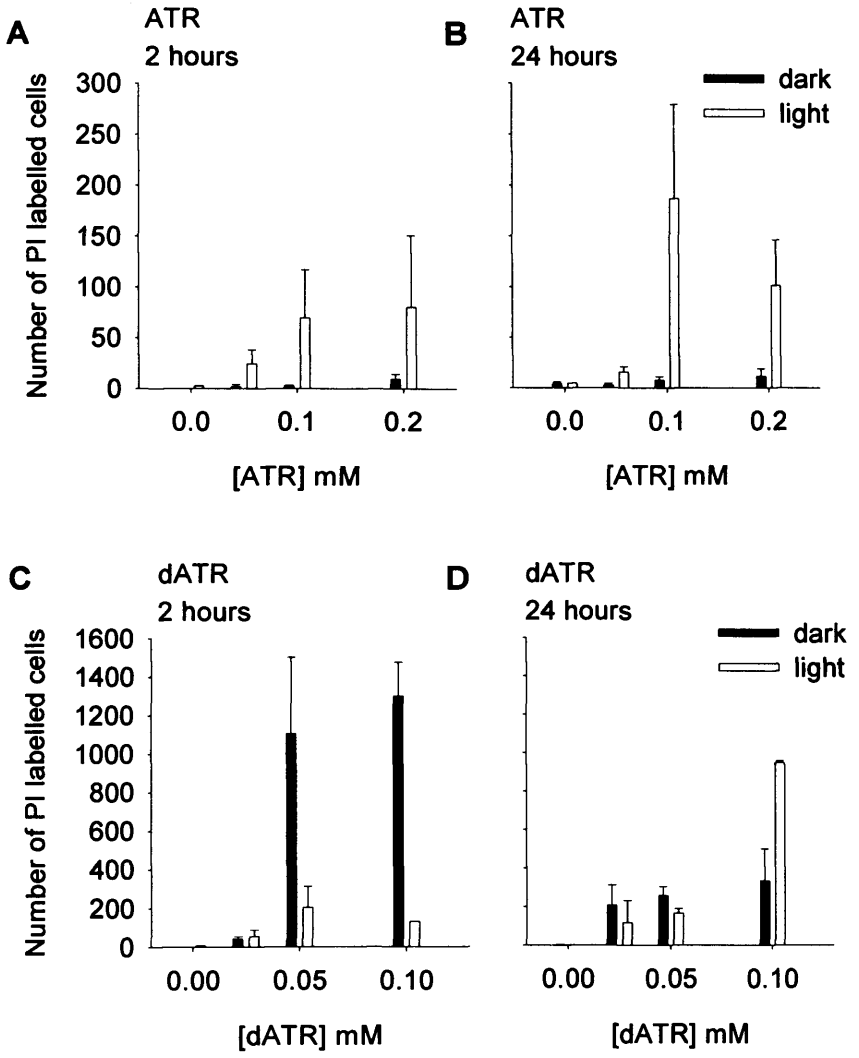

Figure 6.11 Number of PI labelled cells after exposure to ATR or dATR, at indicated concentrations in the dark or in light 2 or 24 hours post-incubation. A, B – number of PI labelled cells after exposure to ATR in the dark or exposed to light with 2 (A) or 24 (B) hour post-incubation. C, D - number of PI labelled cells after exposure to dATR at indicated concentrations in the dark or exposed to light with 2 (C) or 24 (D) hour post-incubation. Calculations of means ± SD were based on 2-4 images of the same microscopic view.

6.3.4 Effect of ROL on ATR and dATR (photo)toxicity

6.3.4.1 Mitochondrial activity

ROL exhibited a damaging effect on cells when exposed to ATR (Fig. 6.12). There was an additional ~20% loss of mitochondrial activity in the presence of 50 μM ROL both in the dark and in light in comparison with cells not exposed to ROL, but the decrease was not found to be statistically significant ($P > 0.05$). The loss was greater in the presence of 150 μM ROL and the difference was significant when compared with ATR only ($P < 0.05$).

There was an opposite effect observed when cells were exposed to dATR in the presence of ROL. ROL was found to have protective properties against dATR toxicity. ROL at a concentration of 150 μM rescued ~60% in the dark and the difference in mitochondrial activity was found to be statistically significant ($P < 0.05$). There was a further 20% increase of mitochondrial activity for cells exposed to dATR and 150 μM ROL + light and the difference was found to be significant ($P < 0.05$).

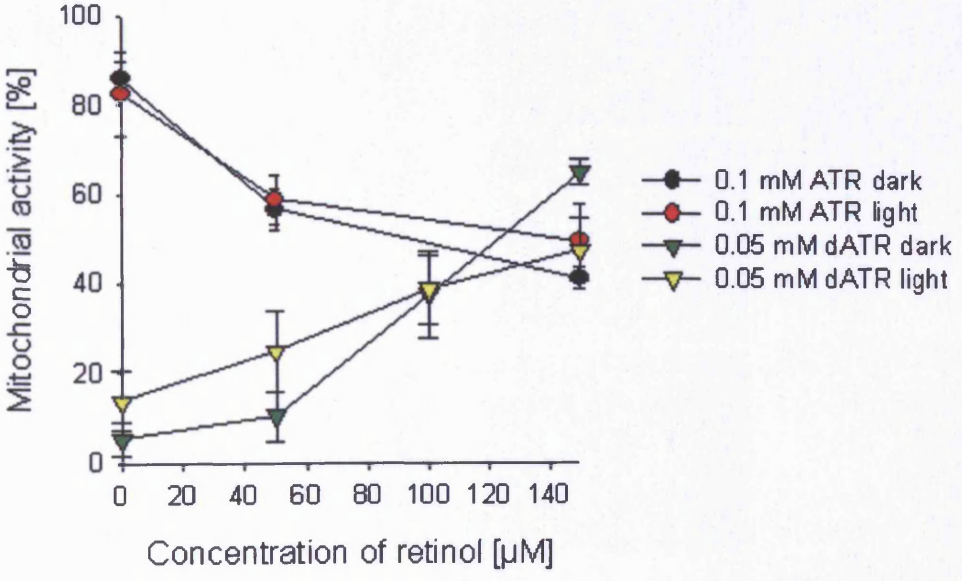

Figure 6.12 MTT results for ARPE-19 cells exposed to ATR or dTAR with or without ROL at indicated concentrations, in the dark or exposed to white light. Bars = SEM. n = 3.

6.3.4.2 Cell morphology

Results described in section 6.2.4.1 were confirmed by microscopic observations of cells (Fig 6.13). ATR in combination with ROL caused morphological changes of cells including cell detachment and shrinkage. ROL in the presence of dATR, on the other hand, partly rescued cells leading to a decrease in morphological changes of cells.

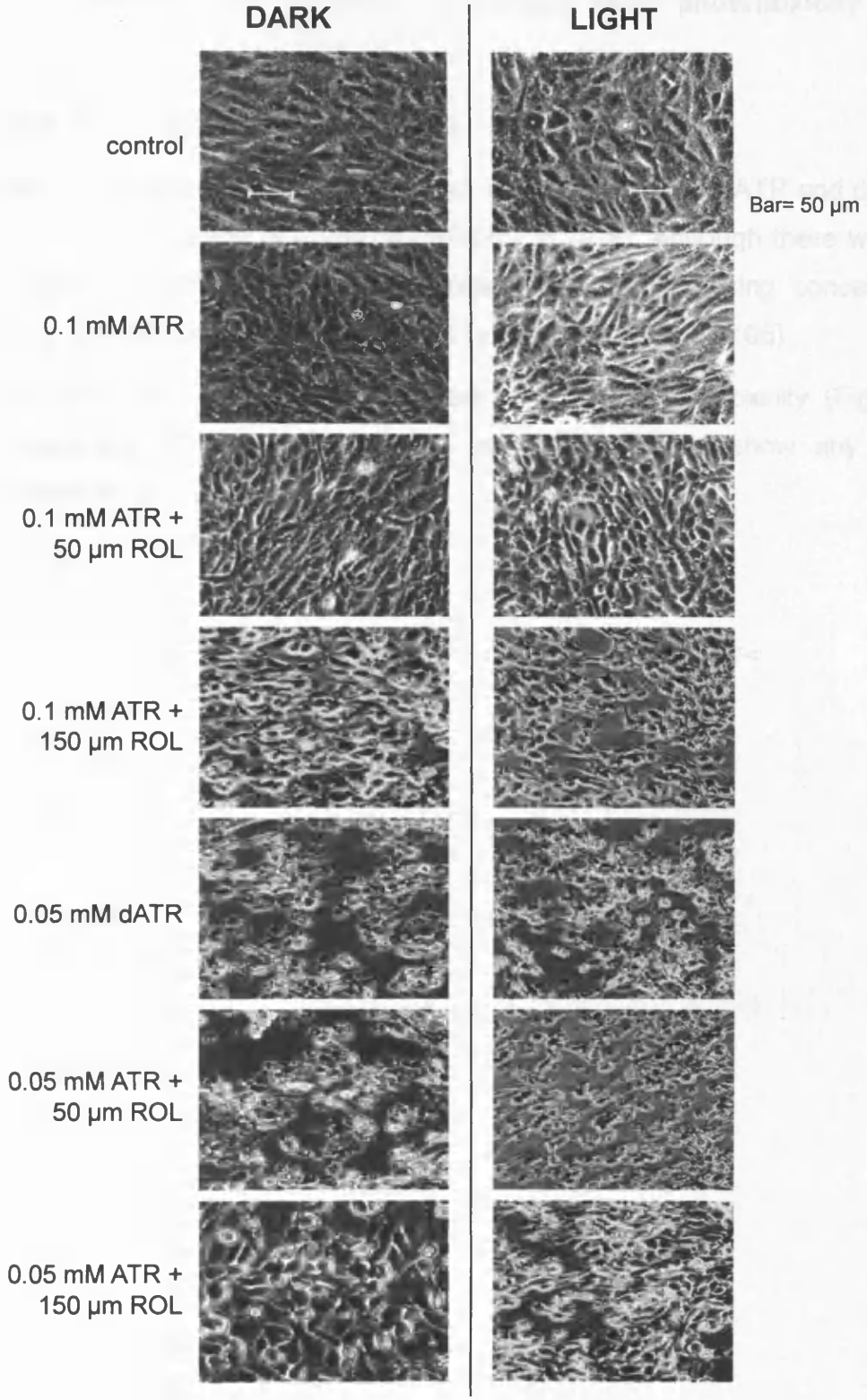

Figure 6.13 Effect of ATR and dATR in combination with ROL on cell morphology. Phase contrast images of ARPE-19 cells taken 24 hours after exposure to ATR and degraded ATR at indicated concentrations in with or without ROL at selected concentrations. Cells exposed to ATR/dATR with or without ROL in the dark conditions (left column) and in the light (right column).

6.3.5 Effects of NAC and GSH on ATR and dATR (photo)toxicity

6.3.5.1 Mitochondrial activity

NAC did not exhibit a protective effect for cells exposed to ATR and dATR in the concentration range of 0.05-0.5 mM (Fig. 6.14 A). Although there was a slight increase in mitochondrial activity observed with increasing concentration of NAC, the differences were not found to be significant ($P > 0.05$).

Also GSH did not protect cells from ATR and dATR toxicity (Fig. 6.14 B). Comparison of the effect of NAC and GSH did not show any significant differences ($P > 0.05$).

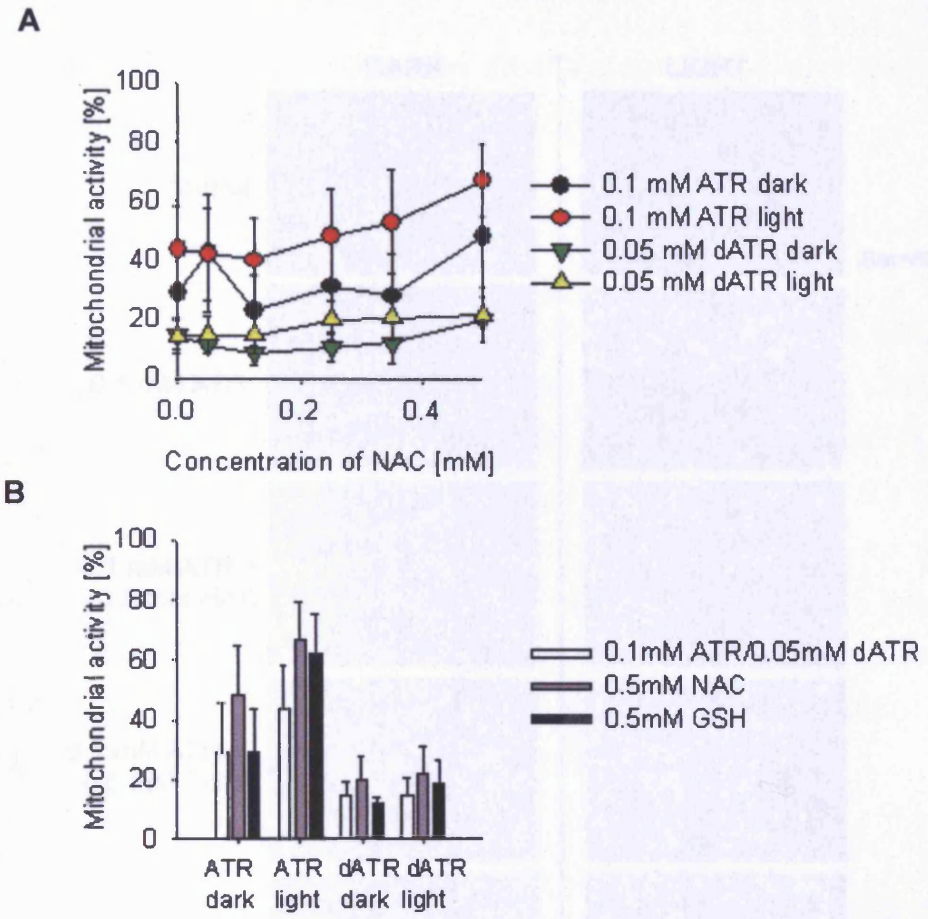

Figure 6.14 MTT results for ARPE-19 cells exposed to ATR or dTAR with or without NAC **(A)** and GSH **(B)** at selected concentrations. Bars = SEM. n = 3.

6.3.5.2 Cell morphology

There were no substantial differences in morphology of cells treated with ATR and/or dATR with or without NAC and GSH (Fig. 6.15).

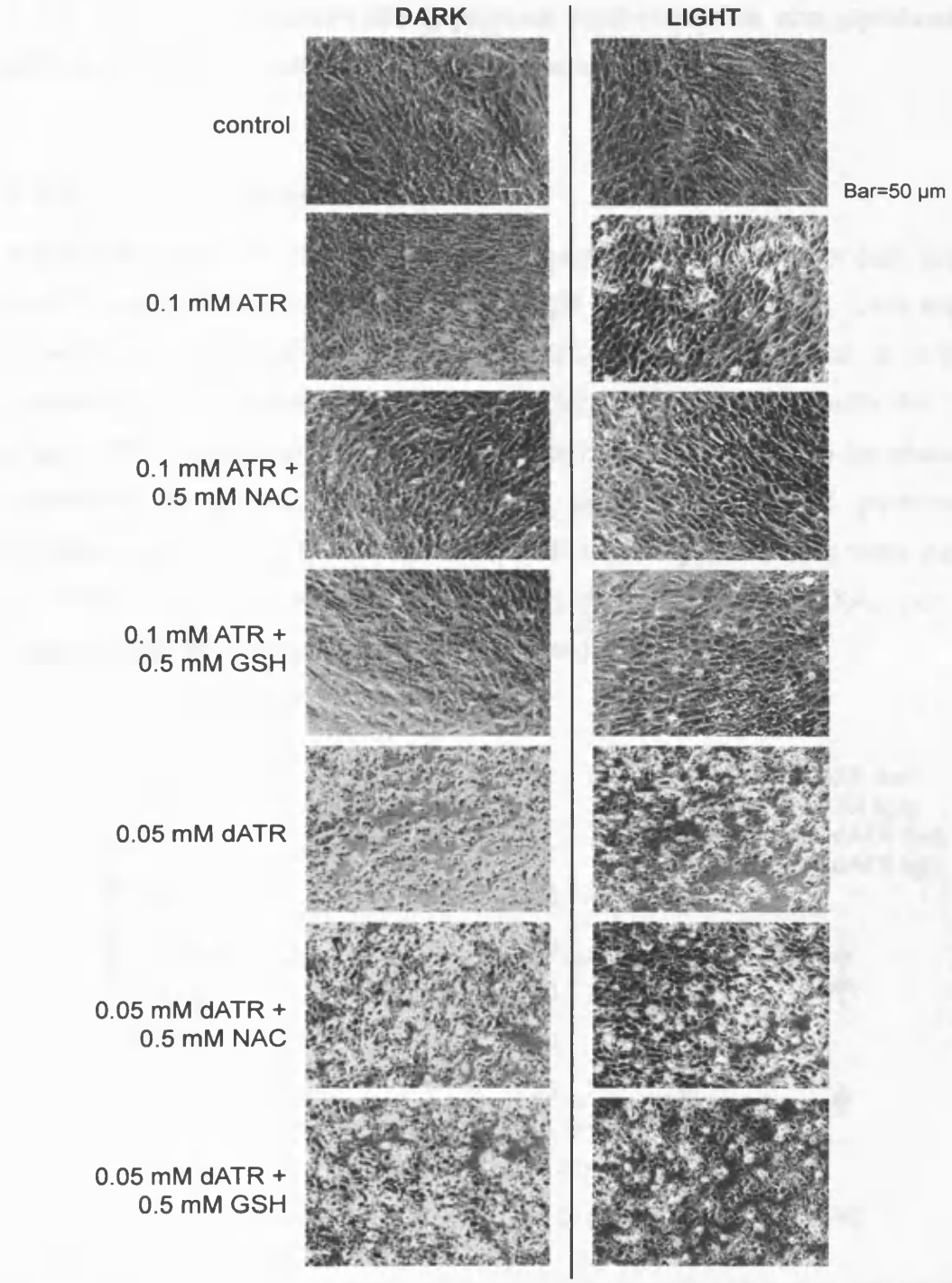

Figure 6.15 Effect of ATR and dATR in combination with NAC or GSH on cell morphology. Phase contrast images of ARPE-19 cells taken 24 hours after exposure to ATR and degraded ATR at indicated concentrations with or without NAC or GSH at selected concentrations. Cells exposed to ATR/dATR with or without NAC/GSH in dark conditions (left column) and in the light (right column).

6.3.6 Effects of Vitamin B6 (pyridoxal hydrochloride and pyridoxamine dihydrochloride) on ATR and dATR (photo)toxicity

6.3.6.1 MTT assay

None of the forms of Vitamin B_6 exhibited protective properties for cells exposed to ATR and dATR in the dark and in the light (Fig. 6.16 A and B). Cells exposed to ATR and pyridoxal hydrochloride (PXAL) at a concentration of 0.15 mM seemed to have higher mitochondrial activity when compared with the control (Fig. 6.16 A). None of the differences observed were found to be statistically significant ($P > 0.05$). There was no significant effect of pyridoxamine dihydrochloride (PXAM) on cell mitochondrial activity when cells were exposed to ATR in the dark and in the light (Fig. 6.16 B). Neither PXAL nor PXAL rescued cells after exposure to dATR in the dark and in the light.

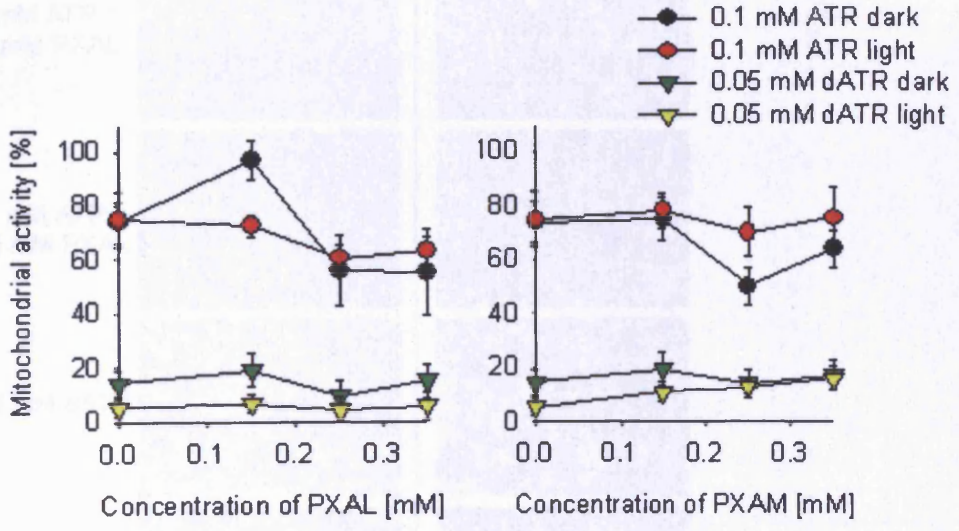

Figure 6.16 MTT results for ARPE-19 cells exposed to 0.1 mM ATR or 0.05 mM dATR in the dark or in visible light with or without pyridoxal – PXAL **(A)** or pyridoxamine – PXAM **(B)** at selected concentrations. Bars = SEM. n = 3.

6.3.6.2 Cell morphology

Cell morphology was not substantially influenced by the presence of PXAL or PXAM when compared with control cells (Fig. 6.17 A and B). Exposure of cells

to ATR and light in particular resulted in changes of cell morphology including cell loss. However, PXAM and PAL did not protect from the damaging effect.

There were no differences in cell morphology between cells exposed to dATR only and dATR with PXAL or PXAM.

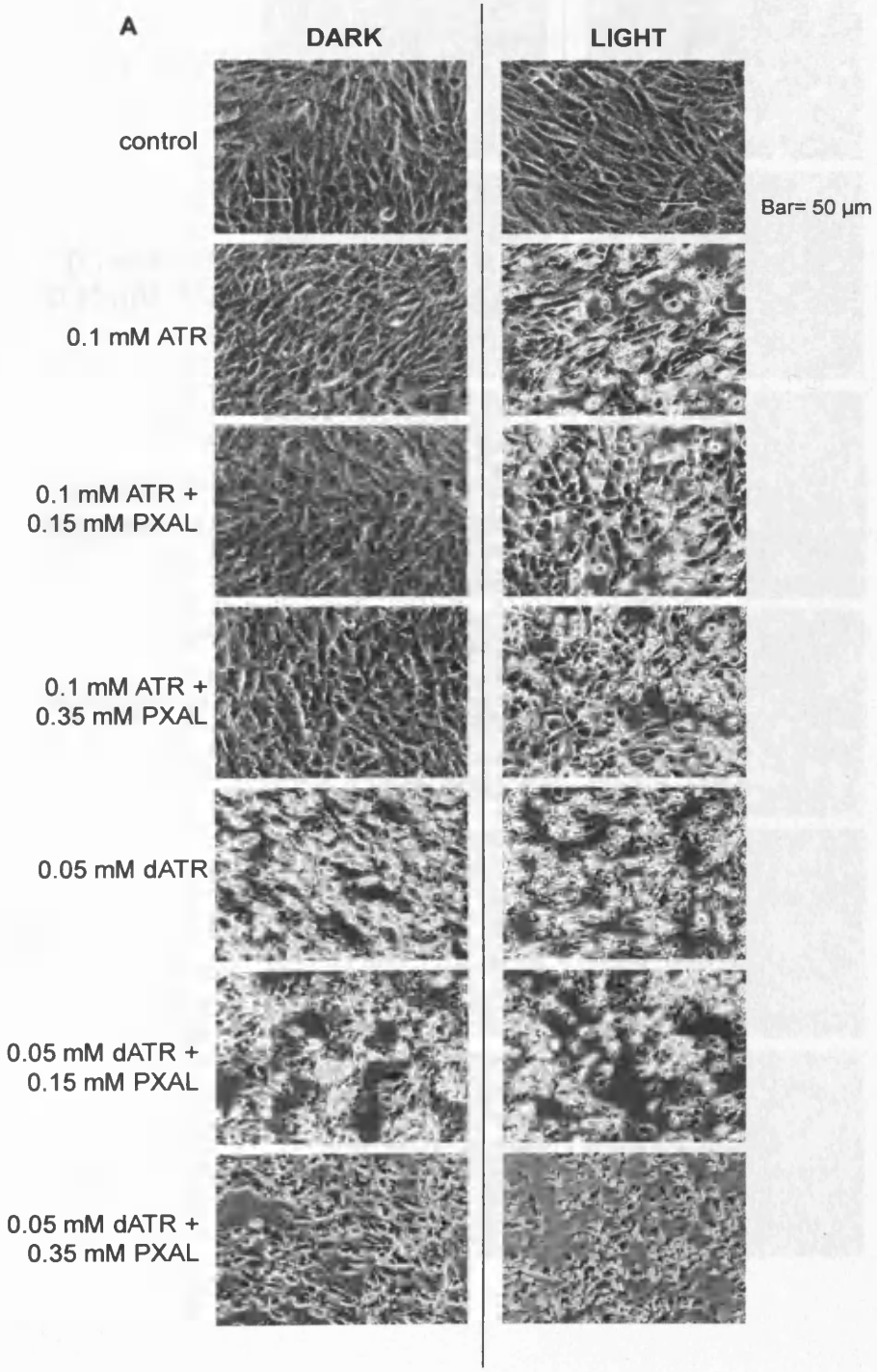

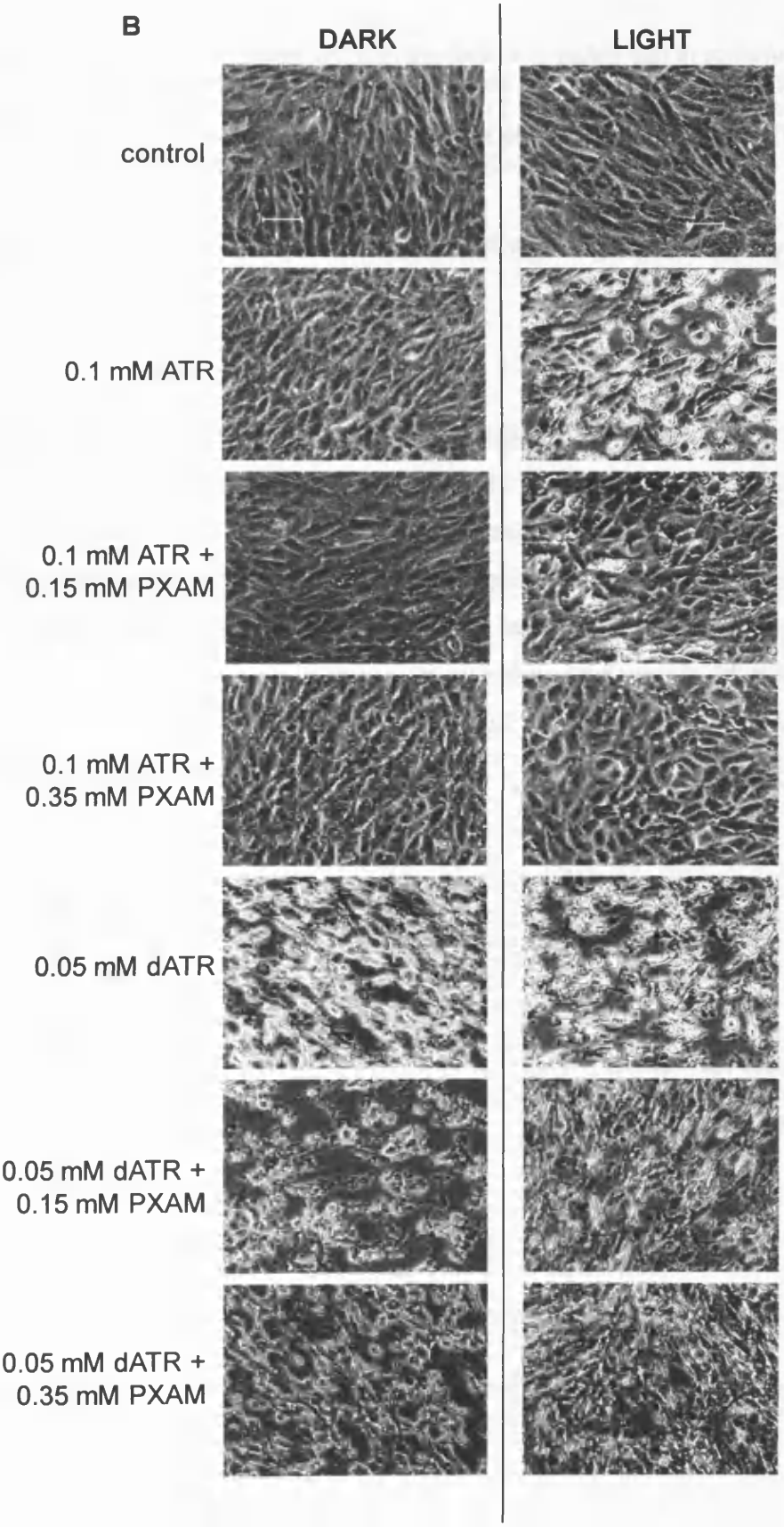
B
DARK
LIGHT
control
0.1 mM ATR
0.1 mM ATR +
0.15 mM PXAM
0.1 mM ATR +
0.35 mM PXAM
0.05 mM dATR
0.05 mM dATR +
0.15 mM PXAM
0.05 mM dATR +
0.35 mM PXAM

Figure 6.17 Effect of ATR and dATR in the dark or in visible light in combination with pyridoxal (A) or pridoxamine (B) on cell morphology. Phase contrast images of ARPE-19 cells taken 24 hours after exposure to ATR and degraded ATR at indicated concentrations with or without PXAL or PXAM at selected concentrations. Cells exposed to ATR/dATR with or without PXAL/PXAM in dark conditions (left columns) and in the light (right columns).

6.3.7 Effects of Vitamin E on ATR and dATR (photo)toxicity

6.3.7.1 Mitochondrial activity

There was no significant difference between cells exposed to ATR with or without addition of α-tocopherol (Fig. 6.18; $P > 0.05$). When cells were exposed to dATR, vitamin E seemed to protect cells from the damaging effect of dATR. 70% of cells were rescued when the highest concentration of VitE was applied in the dark and the effect was proven to be significant ($P < 0.05$). There was an increase in mitochondrial activity of cells with the same concentration of vitamin E and exposed to light, but the difference was not found to be significant ($P > 0.05$).

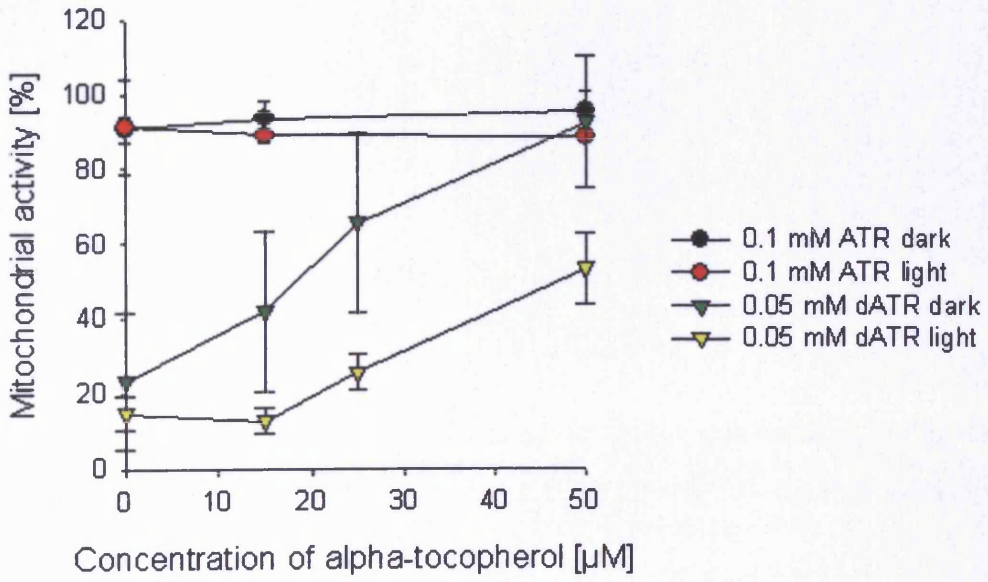

Figure 6.18 MTT results for ARPE-19 cells exposed to ATR or dTAR in the dark or in visible light with or without α-tocopherol at selected concentrations. Bars = SEM. n = 3.

6.3.7.2 Cell morphology

Cells kept in darkness and exposed to ATR and ATR+15μM α-tocopherol exhibit some morphological changes, while cells exposed to ATR+50μM α-tocopherol were comparable with control cells (Fig. 6.19). All cells exposed to light in the presence of ATR showed disruptions in the monolayer and elevated cells. α-tocopherol at highest concentration seemed to rescue some of the cells. However, analysis of the MTT results showed no significant differences (Fig. 6.18).

There was a substantial improvement in morphology of cells when α-tocopherol was present at the highest concentration for cells exposed to dATR in the dark but no apparent improvement in cells exposed to light.

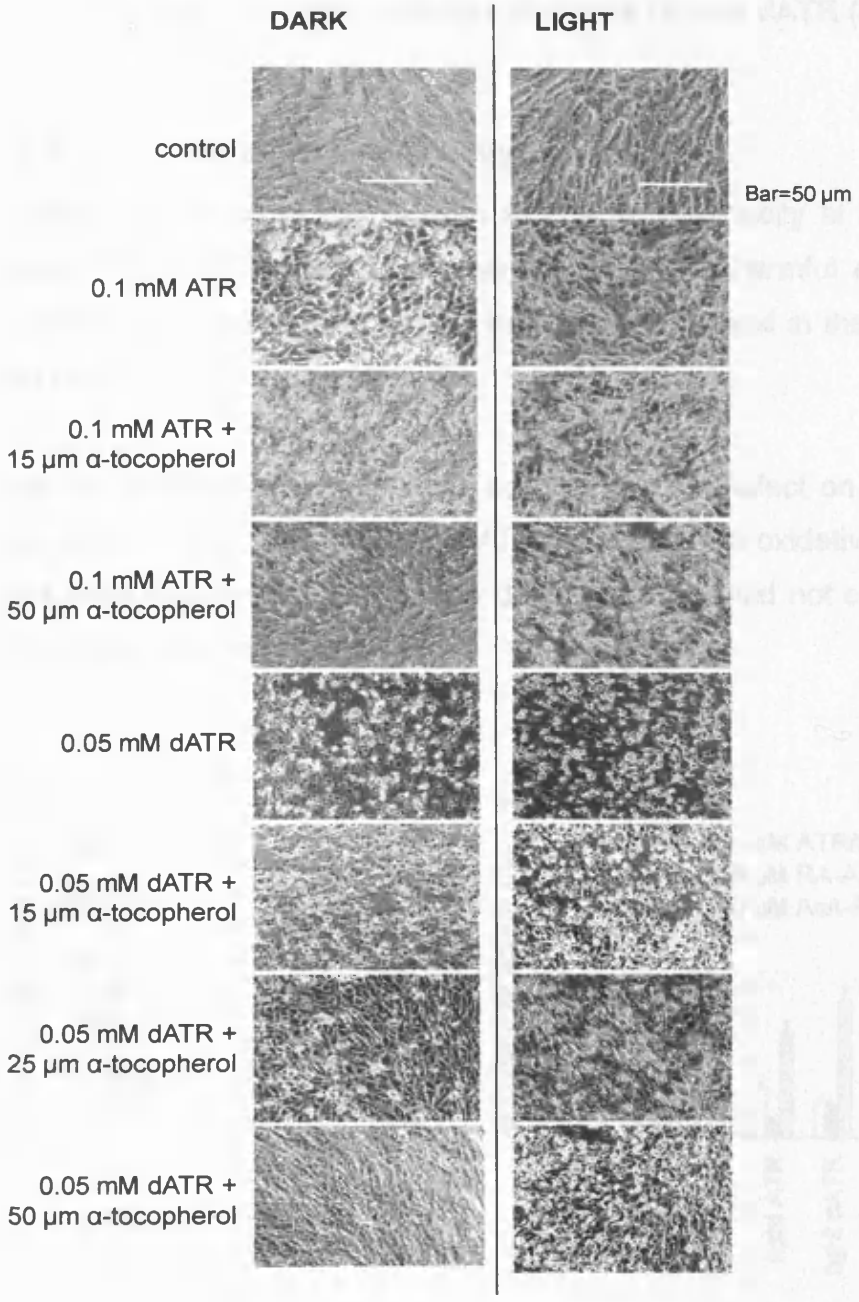

Figure 6.19 Effect of ATR and dATR in combination with alpha-tocopherol on cell morphology. Phase contrast images of ARPE-19 cells taken 24 hours after exposure to ATR and degraded ATR at indicated concentrations with or without alpha-tocopherol at selected concentrations. Cells exposed in dark conditions (left column) and in the light (right column).

6.3.8 Effects of RA-AsA and AsA-Pal on ATR and dATR (photo)toxicity

6.3.8.1 Mitochondrial activity

RA-AsA did not protect cells from ATR or dATR toxicity at the concentrations tested (Fig. 6.20 A and B). It seemed to have a harmful effect leading to a decrease of mitochondrial activity both in the dark and in the presence of ATR and dATR.

AsA-Pal exhibited a substantially better protective effect on cells against ATR and dATR in the light (Fig. 6.20 A). It exhibited pro-oxidative properties when cells were exposed to ATR in the dark, whereas it did not change cell viability when cells were exposed to dATR.

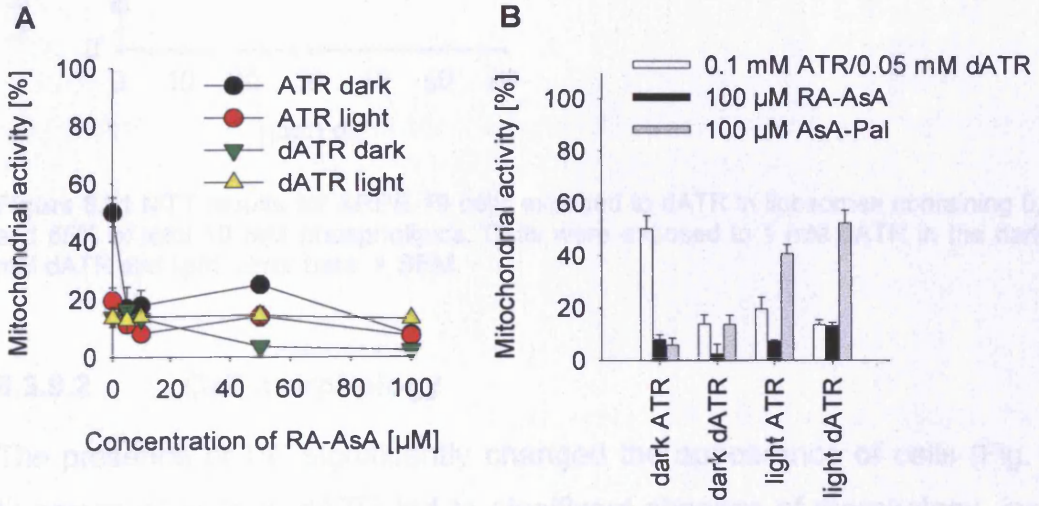

Figure 6.20 MTT results for ARPE-19 cells exposed to ATR or dTAR with or without (A) 100 µM RA-AsA and AsA-Pal or (B) RA-AsA at indicated concentrations. Error bars = SD; the results based on a single experiment with each treatment in triplicates.

6.3.9 Protective role of PE against ATR and dATR (photo)toxicity

6.3.9.1 Mitochondrial activity

Figure 6.21 shows a comparison of mitochondrial activity of cells exposed to 1 mM and 0.5 mM dATR in the dark and in the light. There was a great protective effect of PE observed at each of selected concentrations of PE. Even 20% PE significantly rescued all cells both in the dark and in light.

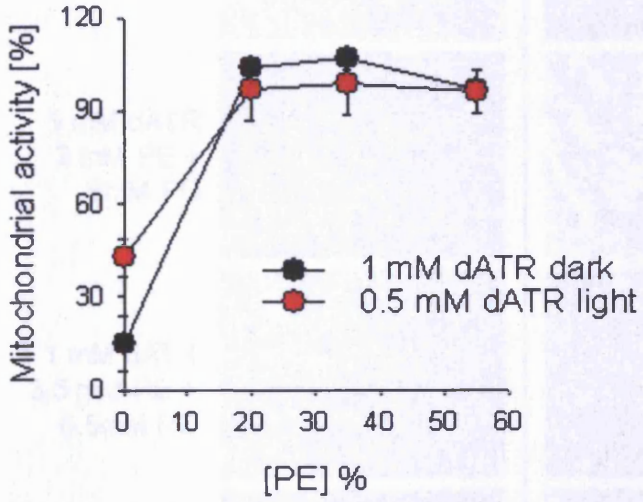

Figure 6.21 MTT results for ARPE-19 cells exposed to dATR in liposomes containing 0, 25, 35 and 55% of total 10 mM phospholipids. Cells were exposed to 1 mM dATR in the dark or 0.5 mM dATR and light. Error bars = SEM.

6.3.9.2 Cell morphology

The presence of PE significantly changed the appearance of cells (Fig. 6.22). Exposure of cells to dATR led to significant changes of morphology, including cell shrinkage and condensation of nuclei. The presence of PE even at the lowest concentration for cells incubated in darkness prevented cells from morphological changes. The lowest concentration of PE seemed to only partly protect cells exposed to light but at higher concentrations the monolayer appeared intact.

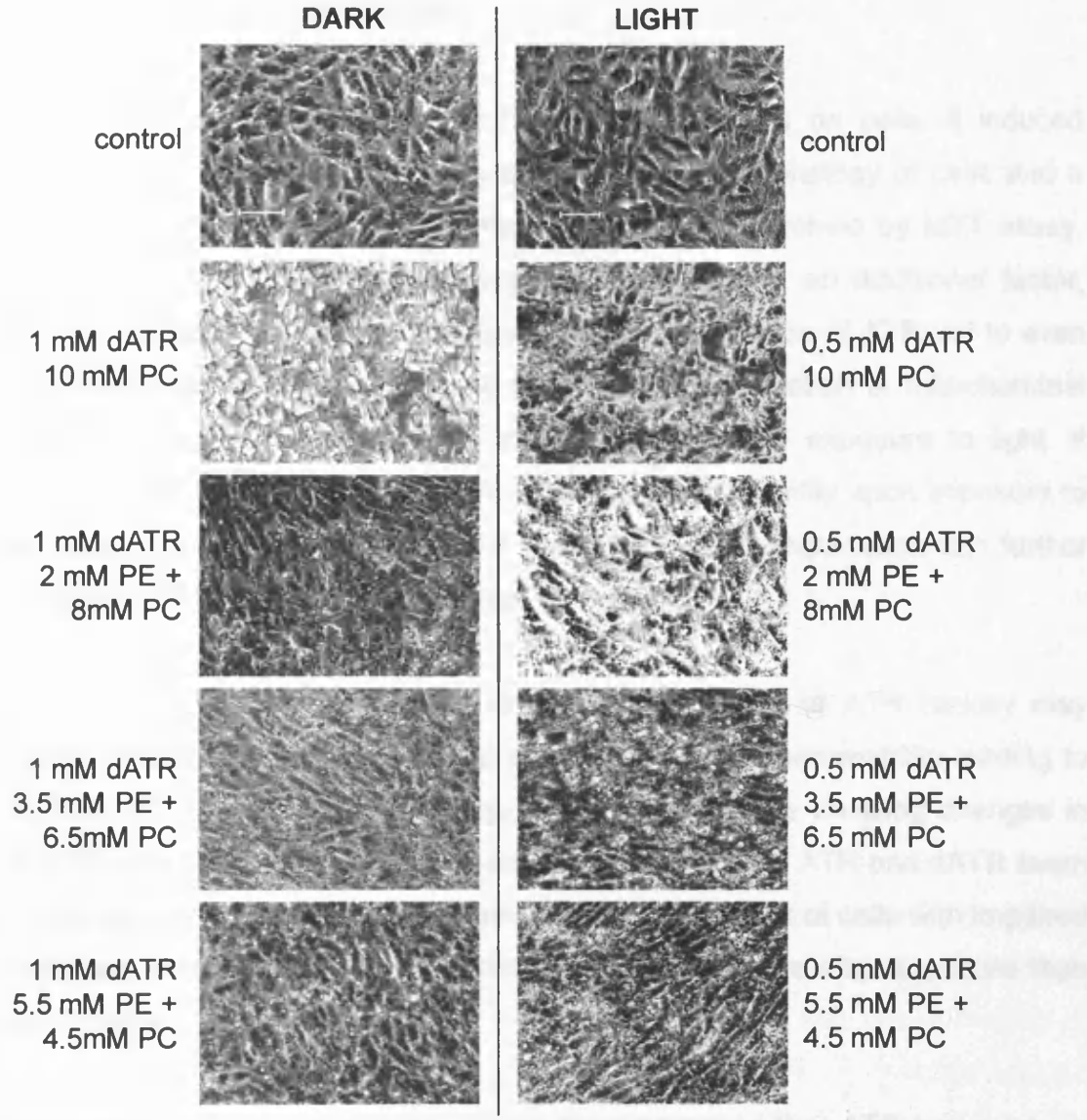

Figure 6.22 Effect of dATR in liposomes with or without PE. Phase contrast images of ARPE-19 cells taken 24 hours after exposure to degraded ATR in liposomes at indicated concentrations in the absence or presence of PE at selected concentrations. Cells exposed in dark conditions (left column) and in the light (right column). Control - cells not exposed to liposomes.

6.4 Discussion

The aim of this chapter was to further understand the response of cells to toxicity induced by ATR and products of its degradation both in DMSO and liposomes. Additionally, selected antioxidants were tested in order to determine possible ways of preventing from the harmful effects of ATR and dTAR.

(Photo)toxicity of ATR and dATR

As expected, ATR was proven to have harmful effects on cells. It induced ARPE-19 cell death, causing gross changes in the morphology of cells and a dose-dependent reduction in mitochondrial activity determined by MTT assay. The effect was intensified when exposure to light was an additional factor, confirming photosensitising properties of ATR. Degradation of ATR led to even more extensive changes of cell morphology and a reduction in mitochondrial activity, with the most deleterious effect occurring after exposure to light. It would suggest that degradation of ATR, which occurs readily upon exposure to light, does not stop the damage, but products of ATR degradation can further propagate deleterious changes caused by ATR.

Maeda and colleagues suggested that the mechanism of ATR toxicity may involve mitochondrial poisoning and plasma membrane permeability leading to activation of caspase and cell death (2009). Experiments showing changes in the POS membranes depending on time after exposure to ATR and dATR seem to be in agreement with these suggestions, as the number of cells with impaired membrane permeability was substantially higher 24 hours after exposure than after 2 hours.

As discussed in the Introduction, it has been proposed that ATR has a role in light-induced rhodopsin-dependent damage to the retina (proposed by Delmelle, 1978a, and reviewed by Różanowska and Sarna, 2005). The action spectrum of retinal photodamage determined for rats reared at cyclic dim light and exposed to low intensity light for relatively long periods of time was found to coincide with the absorption spectrum of rhodopsin (Noell et al., 1966; Williams and Howell, 1983). In their experiments, the maximum of retinal photodamage peaked at 500 nm, where rhodopsin reached a steady-state concentration (about 35% of the value in dark-adapted animals). Taking into consideration that the contribution of ATR to the absorption of photons at 500 nm is negligible, it needs to be stated that ATR cannot act as a photosensitiser under these conditions. The damaging effect observed in those experiments could be a

result of constant fluxes of 11-*cis*-retinal/ATR from and to outer segments. Retinals could exert their negative effect through imposing oxidative stress in OS without involvement of photosensitisation. It has been previously shown that ATR can cause oxidative damage to DNA and toxicity to cells in culture in the dark (Murata and Kawanishi S, 2000; Różanowski et al., 2003) and it has been confirmed by our experiments. This type of damage may be assumed to occur only in retinas with high content of rhodopsin, such as in animals reared in dark or dim light.

Experiments carried out on primates and rodents at higher intensities of light showed an increase in susceptibility to photodamage with decreasing wavelength to 320 nm (Gorgels and van Norren, 1995; Ham et al., 1982). As previously mentioned, ATR is a labile compound that can easily be degraded after exposure to light, leading to the formation of products with absorption spectra shifted towards shorter wavelengths (Różanowska and Sarna 2005).

It has been reported that the spectral characteristics of ATR in liposomes made of phosphatidylcholine or a mixture of phosphatidylcholine and PE (65:35 mol/mol) can reflect the wavelength dependence of initial levels of photooxidation of bovine dark-adapted outer segments, with the maximum at 370 nm (Różanowska et al., 2003; Różanowski et al., 2004). The action spectra of acute retinal photodamage (Gorgels and Vannorren, 1995; Ham et al., 1982) was similar to an action spectrum for OS bleached by exposure to room light before measurements exhibiting an increase of the photooxidation rates with decreasing wavelengths. These findings may support a view on ATR undergoing rapid photodegradation during photodamage to the retina and inducing formation of products absorbing shorter wavelengths of light, with photosensitising properties.

Protective role of antioxidants

A substantial protective role against dATR (photo)toxicity was observed only for PE. dATR (photo)toxicity was at least partly prevented by α-tocopherol and ROL.

ROL increased toxic effects of ATR when combined with ATR both in the dark and in the light, whereas there was a substantial increase in mitochondrial activity with increasing concentration of ROL in the presence of dATR. A possible explanation of these intriguing findings of increased toxicity observed in the presence of both ROL and ATR may be provided by the experimental setup using ARPE-19 cells with a disrupted retinoid cycle. It may also be suggested that rather than becoming esterified to the retinyl ester, ROL acts a substrate for cellular dehydrogenases, thus competing with retinal, degradation products of retinal and products of lipid peroxidation for enzymes responsible for detoxification of those products. Secondly, formation of cation radicals of retinal and ROL may be considered, as a result of interaction with metal ions and lipid-derived peroxyl radicals (Dillon et al., 1996; Murata and Kawanishi, 2000; Pawlak et al., 2003). It may be also suggested that cation radical of retinal can oxidise ROL, leading to the formation of cation radical of ROL, which undergoes rapid degradation forming similar products as dATR. Furthermore, dATR is unable to oxidise ROL in this manner so it can act as an antioxidant instead of contributing to the pool of toxic degradation products.

There was no protective effect of GSH and NAC observed when cells were exposed to ATR or dATR. Taking into consideration the chemical character of GSH, it might possibly remain outside the cells, not being able to protect them from the oxidative stress that the cells were exposed to in the lipophilic compartments. NAC may be absorbed by cells more easily than GSH (Meister, 1989; Arakawa and Ito, 2007). However, as a hydrophilic molecule, its protective action may be restricted again to the aqueous compartments. NAC can be used as a source of cysteine for synthesis of GSH inside the cells which then serves as cofactor of several antioxidant and detoxification enzymes

(Arakawa and Ito, 2007). However, the simultaneous time of exposure to NAC and ATR/dATR may not be sufficient for synthesis of GSH to occur.

Neither forms of Vitamin B_6 provided protection for cells after exposure to ATR or dATR in the dark or in the light. It is possible that both forms of vitamin B_6 might not be transported into cells, where the actual protective mechanisms may turn into action.

Lack of substantial toxicity of ATR made the assessment of a protective role of vitamin E impossible (Fig. 6.18). α-tocopherol at a physiological blood plasma concentration (about 25 µmol/L) partly rescued cells from dATR toxicity, although the effect was not found to be significant. Vitamin E at a concentration of 50 µM substantially rescued cell from dATR toxicity.

RA-AsA did not protect cells from toxicity caused by ATR and dATR. It exhibited pro-oxidative properties in the dark and light, leading to further damage of cells. A possible mechanism of toxicity of RA-AsA will be investigated and discussed in Chapter 8. AsA-Pal, in contrast, exhibited protective properties only when cells were exposed to light. It confirms its singlet oxygen scavenging properties.

In our experiments, PE was shown to be a great protective agent against both ATR and dATR toxicity in the dark and in the light. It confirms data on protective effects of PE against ATR (photo)toxicity reported by Różanowska and colleagues, showing that the presence of PE in liposomes containing ATR drastically reduced the susceptibility to photooxidation due to the decreased quantum yields of singlet oxygen generation of ATR bound to PE in comparison with free ATR (2003). Our results expand the protective role of PE also on products of ATR degradation. Assuming that PE accounts for ~35% of total rod outer segment (ROS) phospholipids (Bazan et al., 1990) and rhodopsin is the main protein (>90% of total protein; Palczewski, 2006), the molar ratio between rhodopsin (referring to a possible concentration of ATR hydrolysed after bleaching) and PE is ~ 1:20. The ratios tested in the described experiments with dATR were 1:10 and 1:20 in the dark and in the light, respectively. Results

showed that an even lower than physiological proportion of PE in relation to rhodopsin/released ATR is effective enough to provide significant protection against ATR and dATR toxicity. Phototoxicity of dATR can be prevented in the presence of PE at a concentration 1.8 times lower than the physiological one (20% PE of total phospholipids). It can be suggested that an elevated level of PE in patients with Stargardt's disease constitutes a protective mechanism against ATR and dATR (photo)toxicity.

In summary, both ATR and dATR were toxic to cells with dATR having an effect that is more deleterious. Exposure to light led to aggravation of their effects. RA-AsA, AsA-Pal, NAC, GSH and vitamin B_6 did not protect cells from ATR and dATR cytotoxicity. The toxic effect of dTAR was substantially prevented by PE and partially by ROL and α-tocopherol.

Chapter 7

Singlet oxygen photosensitised by ATR and dATR

7.1 Introduction

It was shown in Chapter 6 that ATR and dATR exhibit a damaging effect on the RPE with the more deleterious effect being exerted by dATR. One of the mechanisms of action of ATR and dATR could be via singlet oxygen production. It has been shown that ATR can generate singlet oxygen with relatively high quantum yields in various solvents (Krasnovsky and Kagan, 1979; Dillon et al., 1996; Rozanowska et al., 1998). It was also discussed in Chapter 6 that ATR is very susceptible to photodegradation, and exposure to light leads to the formation of products absorbing at shorter wavelengths than ATR (Baron et al., 1989; Yuzawa and Hamaguchi, 1995).

The aim of this chapter is to compare the ability of degraded ATR with ATR to produce singlet oxygen.

7.2 Experimental design

Yields of singlet oxygen were assessed for ATR and dATR at the same initial concentration. Quantum yields of ATR and dATR were determined for absorbance-matched samples of ATR and dATR (Methods section 2.3.5).
Results were obtained for two excitation wavelengths: 355 and 422 nm to reveal changes in the ability of ATR and dATR to produce singlet oxygen. Excitation wavelength of 355 nm may be relevant to physiological conditions for children - the lens in children can still partly transmit ultraviolet light with a transmission range centered at about 320 nm (Dillon et al., 2004). The range of light reaching the retina changes with age and covers the range from ~390 nm to ~780 nm for adults. Therefore, based on measured quantum yields, further calculations were performed to assess the contribution of ATR and dATR to singlet oxygen generation when excited by the whole spectrum of visible light. All calculated values are based on equations described in section 2.3.5.

7.3 Results

7.3.1 Singlet oxygen formation in samples with ATR and dATR upon excitation with 355 nm

Degradation of ATR led to a 51% decrease in maximum absorption at 380 nm. It was accompanied by a decrease in absorption at 355 nm from 0.350 to 0.180. The contribution of the degradation products to absorbance at 355 nm was 0.008 (calculated as described in the Methods section 2.3.5). The highest signal was observed for ATR (Fig. 7.1 B) and there was a 34% decrease in signal observed after ATR degradation (Fig. 7.1 B). The value of the yield of singlet oxygen fell from $(7.0 \pm 0.3)\times10^{-2}$ to $(4.6 \pm 0.2)\times10^{-2}$ upon degradation (Tab. 7.1). The ratio of absorbed photons by ATR and dATR (calculated as described in the Methods section) at 355 nm was 1.63, whereas the ratio of absorbance at 355 nm was 1.94.

Figure 7.1 shows absorption spectra of ATR, dATR and ATR with matched absorbance to dATR prior to singlet oxygen measurements. The yield of singlet oxygen was similar for absorbance matched samples of ATR and dATR ($(4.4 \pm 0.2)\times10^{-2}$ and $(4.6 \pm 0.2)\times10^{-2}$, Tab. 7.1) and therefore, there was no substantial difference between quantum yields of ATR and dATR with matched absorbance (0.30 ± 0.04 and 0.31 ± 0.01, respectively). Yields of singlet oxygen for ATR and dATR, taking into account the decreased efficiency of absorption of visible light (> 390 nm) after ATR degradation, was 3.73 ±0.50 and 0.97 ±0.03, respectively.

The lifetimes of singlet oxygen observed for samples were similar to the lifetime reported in literature for $^1O_2$ in benzene (30 µs; Scurlock and Ogilby, 1993) and the degradation did not affect singlet oxygen lifetime.

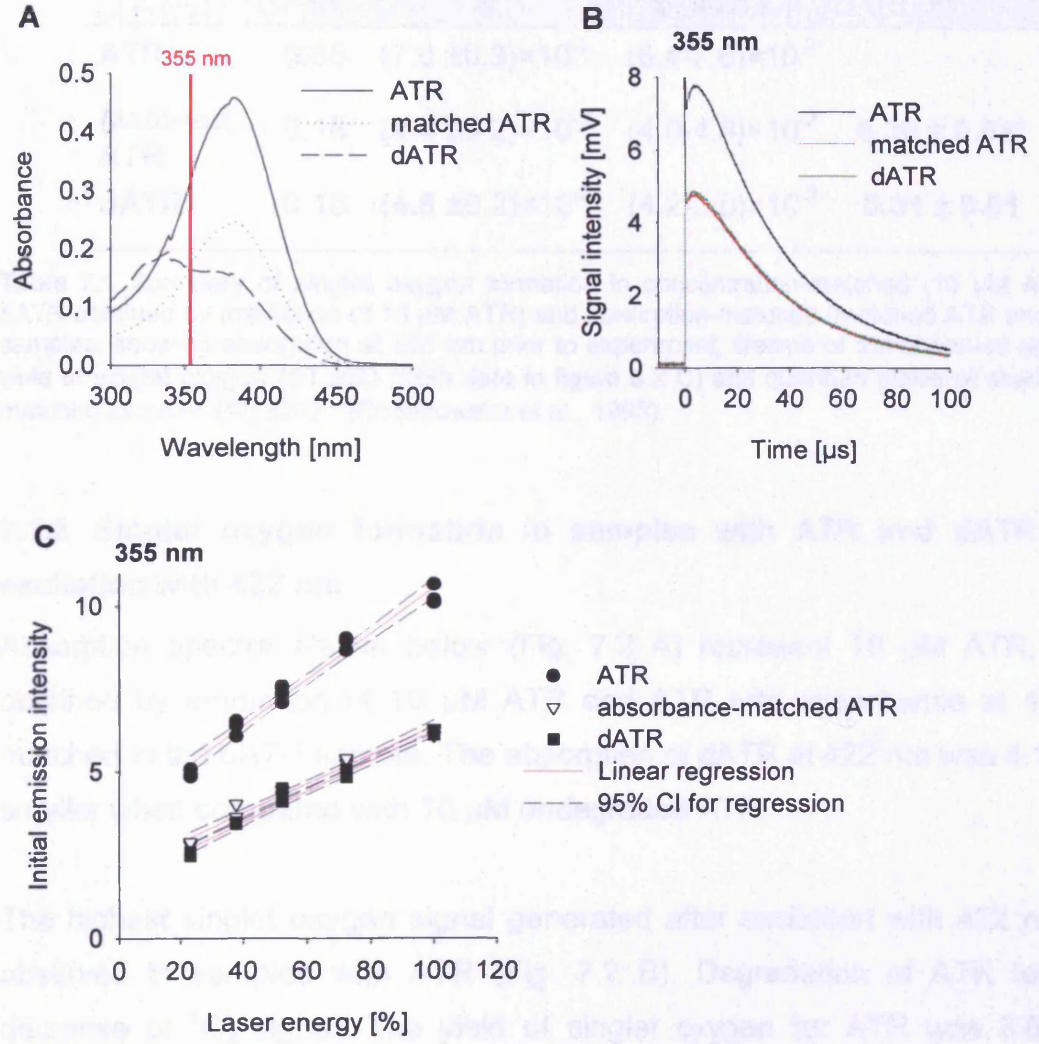

Figure 7.1 Formation of singlet oxygen in ATR and dATR upon excitation with 355 nm. **A** - Absorption spectra of 10 µM ATR, dATR obtained by degradation of 10 µM ATR and ATR with matched absorption at 355 nm. **B** - time-resolved infrared emission at 1270 nm for 10 µM ATR, dATR obtained by degradation of 10 µM ATR and ATR with matched absorption at 355 nm to that of dATR upon excitation with 355 nm at 100% laser energy. **C** – Linear regression of initial signal intensity values, based on 3 measurements for each chosen laser intensity. 95% confidence intervals of the linear regression are indicated by dashed lines.

	A_{355}	φ	φ: 95% CI	Φ
ATR	0.35	**(7.0** ±0.3)×10^{-2}	(6.4-7.6)×10^{-2}	
Matched ATR	0.18	**(4.4** ±0.2)×10^{-2}	(4.0-4.8)×10^{-2}	**0.30 ± 0.04***
dATR	0.18	**(4.6** ±0.2)×10^{-2}	(4.2-5.0)×10^{-2}	**0.31 ± 0.01**

Table 7.1 Summary of singlet oxygen formation in concentration-matched (10 μM ATR and dATR obtained by irradiation of 10 μM ATR) and absorption-matched (matched ATR and dATR) samples, showing absorption at 355 nm prior to experiment, lifetime of the observed signal (τ), yield of singlet oxygen (φ) ±SD (from data in figure 6.2 C) and quantum yields of absorbance-matched samples (Φ) ±SD. *(Różanowska et al., 1998).

7.3.2 Singlet oxygen formation in samples with ATR and dATR upon excitation with 422 nm

Absorption spectra shown below (Fig. 7.2 A) represent 10 μM ATR, dATR obtained by irradiation of 10 μM ATR and ATR with absorbance at 422 nm matched to the dATR sample. The absorption of dATR at 422 nm was 4.1 times smaller when compared with 10 μM undegraded ATR.

The highest singlet oxygen signal generated after excitation with 422 nm was observed in samples with ATR (Fig. 7.2 B). Degradation of ATR led to a decrease of $^1O_2$ signal. The yield of singlet oxygen for ATR was 3.6 times greater than the yield for dATR obtained by irradiation of ATR at the same initial concentration.

The yields of singlet oxygen for ATR and dATR with matched absorption at 422 nm were similar (Tab. 7.2). This was reflected in the regression shown in Figure 7.2 C. The results of the linear regression indicate a slightly shallower slope in samples containing absorbance-matched ATR, indicating possibly smaller yield of singlet oxygen. However, the 95% confidence intervals for the $^1O_2$ yields of dATR and matched ATR overlap, suggesting a non-significant difference.

Quantum yields of singlet oxygen for absorbance-matched samples did not differ significantly - 0.30 ± 0.04 and 0.33 ± 0.02 for ATR and absorbance-matched dATR, respectively. Yields of singlet oxygen for ATR and dATR taking into account the decreased efficiency in absorption of visible light

(> 390 nm) after ATR degradation was 3.73 ±0.50 and 1.06 ±0.06, respectively. It needs to be stated that the contribution of the mixture of products of ATR degradation to absorption in the range of light above 390 nm is unknown.

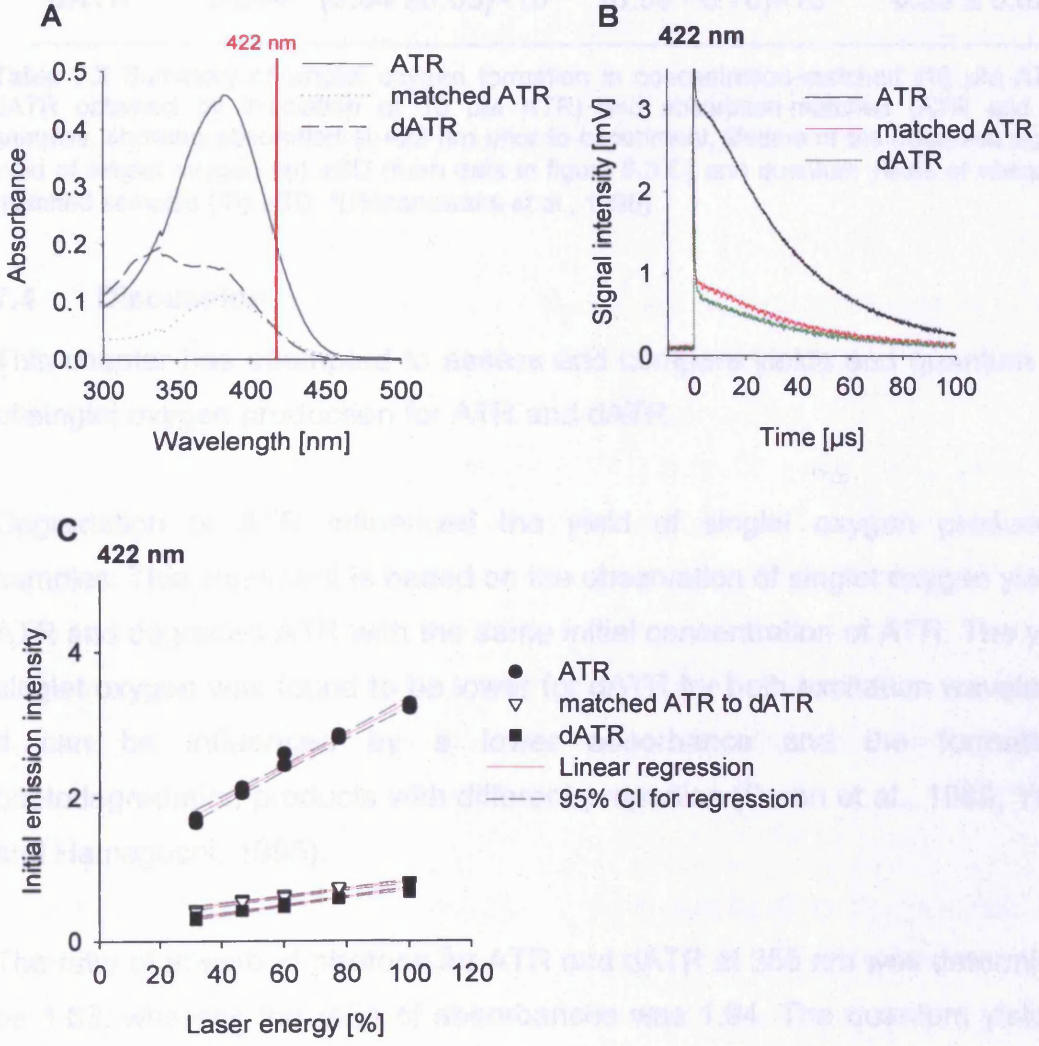

Figure 7.2 Formation of singlet oxygen in ATR and dATR upon excitation with 422 nm. **A** - Absorption spectra of 10 µM ATR, dATR obtained by degradation of 10 µM ATR and ATR with matched absorption at 422 nm. **B** - time-resolved infrared emission at 1270 nm for 10 µM ATR, dATR obtained by degradation of 10 µM ATR and ATR with matched absorption at 422 nm upon excitation with 422 nm at 100% laser energy. **C** – Linear regression of initial signal intensity values, based on 3 measurements for each chosen laser intensity. 95% confidence intervals of the linear regression are indicated by dashed lines.

	A_{422}	φ	φ: 95% CI	Φ
ATR	0.181	**(2.28** ±0.08)×10^{-2}	(2.11 - 2.45)×10^{-2}	
Matched ATR	0.049	**(0.54** ±0.03)×10^{-2}	(0.48 - 0.60)×10^{-2}	**0.30** ± 0.04*
dATR	0.044	**(0.64** ±0.03)×10^{-2}	(0.58 - 0.70)×10^{-2}	**0.33** ± 0.02

Table 7.2 Summary of singlet oxygen formation in concentration-matched (10 μM ATR and dATR obtained by irradiation of 10 μM ATR) and absorption-matched (ATR and dATR) samples, showing absorption at 422 nm prior to experiment, lifetime of the observed signal (τ), yield of singlet oxygen (φ) ±SD (from data in figure 6.3 C) and quantum yields of absorbance-matched samples (Φ) ±SD. *(Różanowska et al., 1998)

7.4 Discussion

This chapter has attempted to assess and compare yields and quantum yields of singlet oxygen production for ATR and dATR.

Degradation of ATR influenced the yield of singlet oxygen produced by samples. This statement is based on the observation of singlet oxygen yields for ATR and degraded ATR with the same initial concentration of ATR. The yield of singlet oxygen was found to be lower for dATR for both excitation wavelengths. It can be influenced by a lower absorbance and the formation of photodegradation products with different properties (Baron et al., 1989; Yuzawa and Hamaguchi, 1995).

The ratio of absorbed photons for ATR and dATR at 355 nm was determined to be 1.63, whereas the ratio of absorbances was 1.94. The quantum yield for a mixture of ATR+dATR formed after ATR degradation, was found to be the same as for ATR, thus the ratio of yields of singlet oxygen was expected to be the same as the ratio of absorbed photons. However, the proportion of singlet oxygen yields was 1.52, which indicates that degradation products of ATR exhibit a greater quantum yield than ATR on their own. Excitation of ATR and dATR with 422 nm light, on the other hand, showed significantly higher yields of singlet oxygen for ATR when compared with dATR at the same initial concentration.

The efficiency in absorption of visible light above 390 nm was 3.9 times lower for dATR when compared with ATR at the same initial concentration based on integrated absorption of ATR and dATR in the range 390 – 600 nm. The proportion of absorbed light of ATR and dATR with the same initial concentration of ATR is 3.65, indicating substantially higher efficiency of ATR absorption in the visible compared to ATR after (photo)degradation. As the quantum yields are the same, one might expect degradation products of ATR to be 3.65 times less efficient in generating $^1O_2$ than ATR when excited by whole spectrum of visible light.

Taking into consideration a lack of significant differences between quantum yields of singlet oxygen for dATR and ATR and a smaller efficiency in the absorption of visible light for dATR when compared with ATR it can be concluded that the damaging effect of ATR and dATR shown in Chapter 6 also involves other mechanisms than singlet oxygen. It has been shown that the toxicity occurs to a further extent when cells are exposed to dATR. It might be suggested that the presence of dATR requires elevated activity of antioxidants and detoxification enzymes such as glutathione transferase. This could lead to depletion of glutathione and other low-molecular weight antioxidants in cells, which in turn may facilitate further damaging effects.

In summary, the ability of products of ATR degradation to generate singlet oxygen was greater after exposure to UVA light (355 nm) than to blue light (422 nm). Excitation of both ATR and its degradation products with blue light resulted in formation of singlet oxygen with similar quantum yields.

Chapter 8

Singlet oxygen formation and quenching by selected components

8.2 Introduction

As discussed in Chapter 6, ROL has a potential protective role for cells under stress. It has been shown to have a protective effect for cells exposed to degraded ATR both in the dark and in light. However, ROL was harmful for cells in the presence of ATR. As shown in Chapter 4, there was no substantial decrease in singlet oxygen generation after reduction of ATR to ROL in POS discs. It has been shown that ROL exhibits the ability to photosensitise singlet oxygen. It may be suggested that ROL can also contribute to the formation of singlet oxygen, and comparison of quantum yield of singlet oxygen formation by ATR and ROL may provide an explanation for the lack of difference in singlet yield between samples with and without enabled reduction of ATR to ROL. There has been a discrepancy between the values of quantum yields determined for ROL by different authors. Ostrovskiĭ and Fedorovich (1994) reported similar quantum yields of singlet oxygen formation in methanol for both ATR and ROL - 0.20 and 0.22, respectively, measured by chemical methods. It was reported by Dillon and colleagues (1996) that the quantum yield of singlet oxygen for ROL in methanol was 0.03, whereas for ATR – it was 0.05. The quantum yield of ATR was different in non-polar solvents such as benzene – 0.15 (Różanowska and Sarna, 2005).

In experiments involving determination of the (photo)toxicity of ATR and dATR, RA-AsA exhibited pro-oxidative properties (Chapter 6). Thus, further investigation into the mechanism of action of RA-AsA was applied and included determination of the yield of singlet oxygen generated by RA-AsA in the same solvent as ATR and ROL.

As mentioned in Chapter 6, RA-AsA is a complex of ROL with ascorbate, both of which exhibit reasonably high rates of quenching for singlet oxygen, about 2-3 orders of magnitude greater than the rate of quenching of singlet oxygen by unsaturated lipids (Bhattacharyya and Das, 1985; Vever-Bizet et al., 1989; Bisby et al., 1999). AsA-Pal, also tested in this thesis, has been shown to quench singlet oxygen with the rate of 7.51×10^7 $M^{-1}s^{-1}$ in the benzene/methanol mixture (Lee et al., 1999). ROL was used for comparative purposes. The rate of

quenching has been reported to be in a range from 3.5×10^6 $M^{-1}s^{-1}$ in benzene to 6.0×10^6 $M^{-1}s^{-1}$ in methanol (Bhattacharyya and Das, 1985).

8.2 Experimental design

Singlet oxygen production was measured for absorbance-matched samples of ATR, ROL and RA-AsA and initial yields of singlet oxygen were compared (Method 2.3.6). Acetone was use a solvent for all tested components. The polarity of acetone is lower than the polarity of methanol and greater than the polarity of benzene (solvents used by other authors to determine quantum yield of singlet oxygen).

To better understand possible mechanisms of action for ROL and RA-AsA, yields of singlet oxygen were assessed for both compounds and compared with a photosensitiser for which the quantum yield of singlet oxygen is known, ATR. Additionally, their singlet oxygen quenching abilities were investigated to find a possible explanation for their protective effect. AsA-Pal was used for comparative purposes. The ability of selected components to quench singlet oxygen was investigated by measuring time-resolved singlet oxygen phosphorescence and measuring singlet oxygen lifetimes as a function of quencher concentration. Solubilities of the tested components were assessed by measuring their absorption spectra and testing the linearity of absorbance with concentration.

Rose Bengal was used as a standard sensitiser. The absorption spectrum of ~7 μM solution, used in the experiments, is presented below (Fig. 8.1).

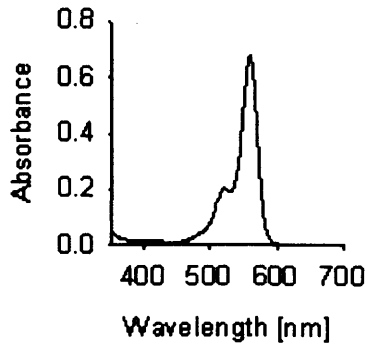

Figure 8.1 Absorption spectrum of ~7 μM rose bengal in acetone, used to assess rates of quenching of ROL, RA-AsA and AsA-Pal.

The laser light intensity was reduced by using neutral density filters (as described in the Methods section 2.3.5). The excitation wavelength used to determine the singlet oxygen quenching abilities of the tested components was 550 nm - a wavelength within the range of maximal absorption of rose bengal but out of the absorption range for the components tested.

Since absolute values of quantum yields of singlet oxygen are not available for any of the compounds tested in acetone, only quantum yields relative to ATR and then calculated yields of singlet oxygen produced if equimolar concentrations of ATR, ROL, RA-AsA could be compared.

8.3 Results

8.3.1 Singlet oxygen quantum yields for ATR, ROL, RA-AsA in acetone

Absorption spectra of absorbance-matched samples with ATR, ROL and RA-AsA are presented in Figure 8.2 A.

Figure 8.2 B shows comparison of infrared emission signals for samples with ATR, ROL and RA-AsA after excitation with a 5 ns laser pulse at 355 nm and 100% laser intensity. The ATR sample was characterised by the highest signal intensity, whereas the lowest one was observed in the sample with RA-AsA.

Figure 8.2 C, D and E show kinetics of emission intensity in samples with ATR (8.2 C), ROL (8.2 D) and RA-AsA (8.2 E) as a function of laser intensity.

Introduction of filters resulted in a linear decrease of signals in all samples in the whole range tested.

The signal oxygen lifetime, presented in Table 8.1, was comparable between samples containing ATR and ROL (44 and 39 μs, respectively). The obtained lifetime of singlet oxygen in acetone was similar to the one reported by Clennan and colleagues (1989) – between 38 and 43 μs. Results show a large difference between these two samples and the sample with RA-AsA for which the lifetime of observed signal was 9 μs. Table 8.1 also shows a summary of absorbance at 355 nm, singlet oxygen lifetimes, yields of singlet oxygen (from calculated regression slopes) and their confidence intervals.

The upper limit yield of singlet oxygen, calculated as described in the Methods section 2.3.6, for ATR was 1.7 and 3.5 times greater than for ROL and RA-AsA, respectively and the differences seemed to be significant. Excitation of RA-AsA resulted in formation of the smallest number of single oxygen molecules. The difference between RA-AsA was found to be significant when compared with the other samples based on 95% confidence intervals.

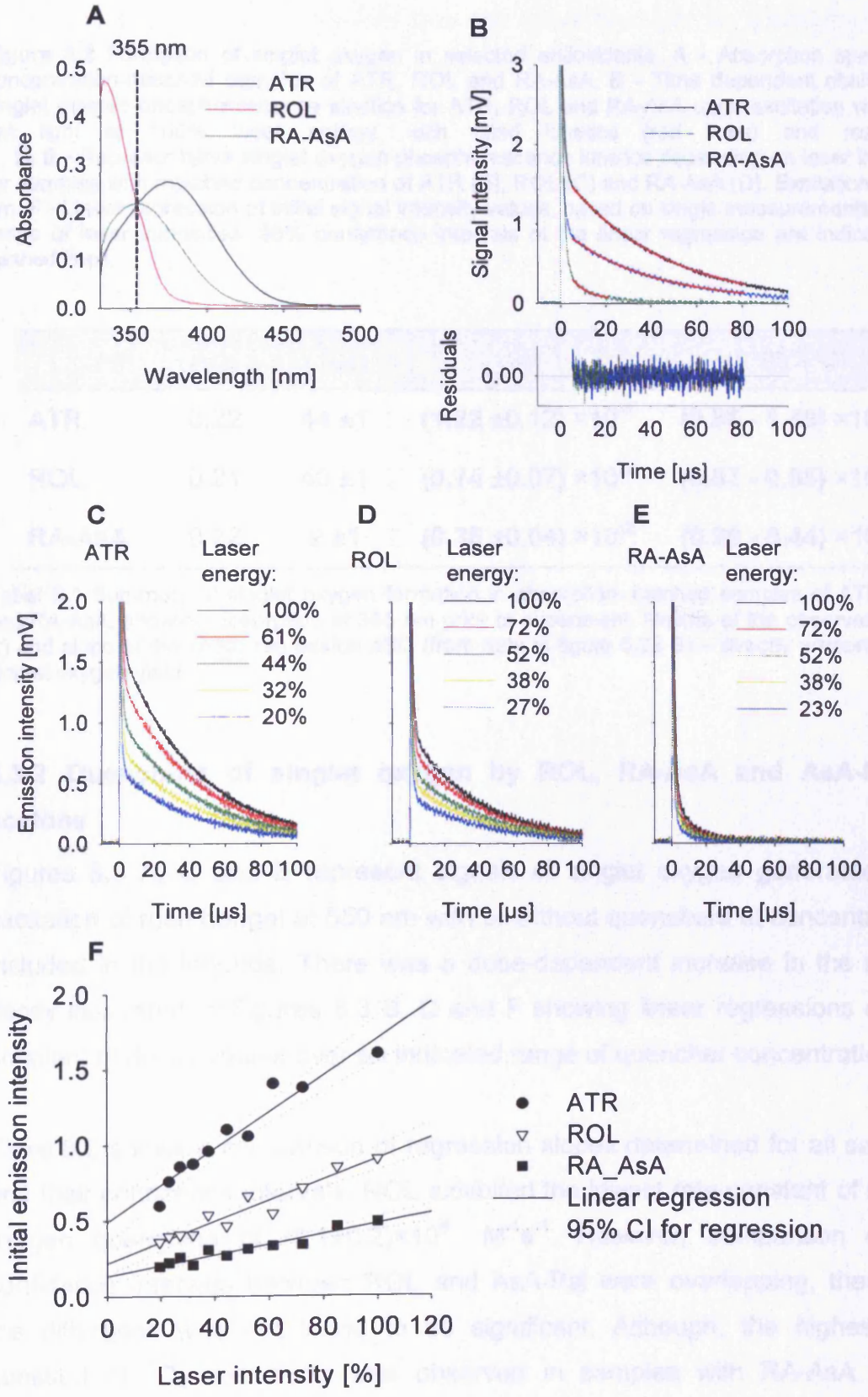
A
355 nm
ATR
ROL
RA-AsA
Absorbance
Wavelength [nm]
B
Signal intensity [mV]
Residuals
Time [µs]
C
ATR
Laser energy:
100%
61%
44%
32%
20%
Emission intensity [mV]
Time [µs]
D
ROL
Laser energy:
100%
72%
52%
38%
27%
Time [µs]
E
RA-AsA
Laser energy:
100%
72%
52%
38%
23%
Time [µs]
F
Initial emission intensity
Laser intensity [%]
ATR
ROL
RA_AsA
Linear regression
95% CI for regression

Figure 8.2 Formation of singlet oxygen in selected antioxidants. **A** - Absorption spectra of concentration-matched samples of ATR, ROL and RA-AsA. **B** - Time dependent changes of singlet oxygen phosphorescence kinetics for ATR, ROL and RA-AsA upon excitation with 355 nm light at 100% laser energy, with fitted kinetics (red lines) and residuals. **C, D, E** - Representative singlet oxygen phosphorescence kinetics depending on laser intensity for samples with matched concentration of ATR (B), ROL (C) and RA-AsA (D). Excitation at 355 nm. **F** - Linear regression of initial signal intensity values, based on single measurements over a range of laser intensities. 95% confidence intervals of the linear regression are indicated by dashed lines.

	A_{355}	τ (μs)	φ	φ: 95% CI
ATR	0.22	44 ±1	**(1.22** ±0.12) $\times 10^{-2}$	**(0.95 - 1.49)** $\times 10^{-2}$
ROL	0.21	40 ±1	**(0.74** ±0.07) $\times 10^{-2}$	**(0.53 - 0.85)** $\times 10^{-2}$
RA-AsA	0.22	9 ±1	**(0.35** ±0.04) $\times 10^{-2}$	**(0.26 - 0.44)** $\times 10^{-2}$

Tabel 8.1 Summary of singlet oxygen formation in absorption-matched samples of ATR, ROL and RA-AsA, showing absorption at 355 nm prior to experiment, lifetime of the observed signal (τ) and slope of the linear regression ±SD (from data in figure 5.22 B) – directly proportional to singlet oxygen yield.

8.3.2 Quenching of singlet oxygen by ROL, RA-AsA and AsA-Pal in acetone

Figures 8.3 A, C and E represent signals of singlet oxygen generated after excitation of rose bengal at 550 nm with or without quenchers at concentrations included in the legends. There was a dose-dependent increase in the rate of decay illustrated in Figures 8.3 B, D and F showing linear regressions of rate constant of decay values over an indicated range of quencher concentrations.

Table 8.2 shows a comparison of regression slopes determined for all samples and their confidence intervals. ROL exhibited the lowest rate constant of singlet oxygen quenching of $(3.1\pm0.2)\times10^{6}$ $M^{-1}s^{-1}$. However, comparison of the confidence intervals between ROL and AsA-Pal were overlapping, therefore, the difference was not found to be significant. Although, the highest rate constant of $^{1}O_2$ quenching was observed in samples with RA-AsA ($(18.9 \pm7.5)\times10^{6}$), the confidence interval for linear regression suggests no significant difference between RA-AsA and AsA-Pal or ROL. Low R^2 obtained for linear

regression for RA-AsA suggested that the solubility might be a limiting factor. However, analysis of concentration-dependent absorption of light for RA-AsA (Fig. 8.3 G and H) revealed a linear increase of absorbance at 355 nm, excluding the solubility of RA-AsA in acetone as a limiting factor for quenching of singlet oxygen.

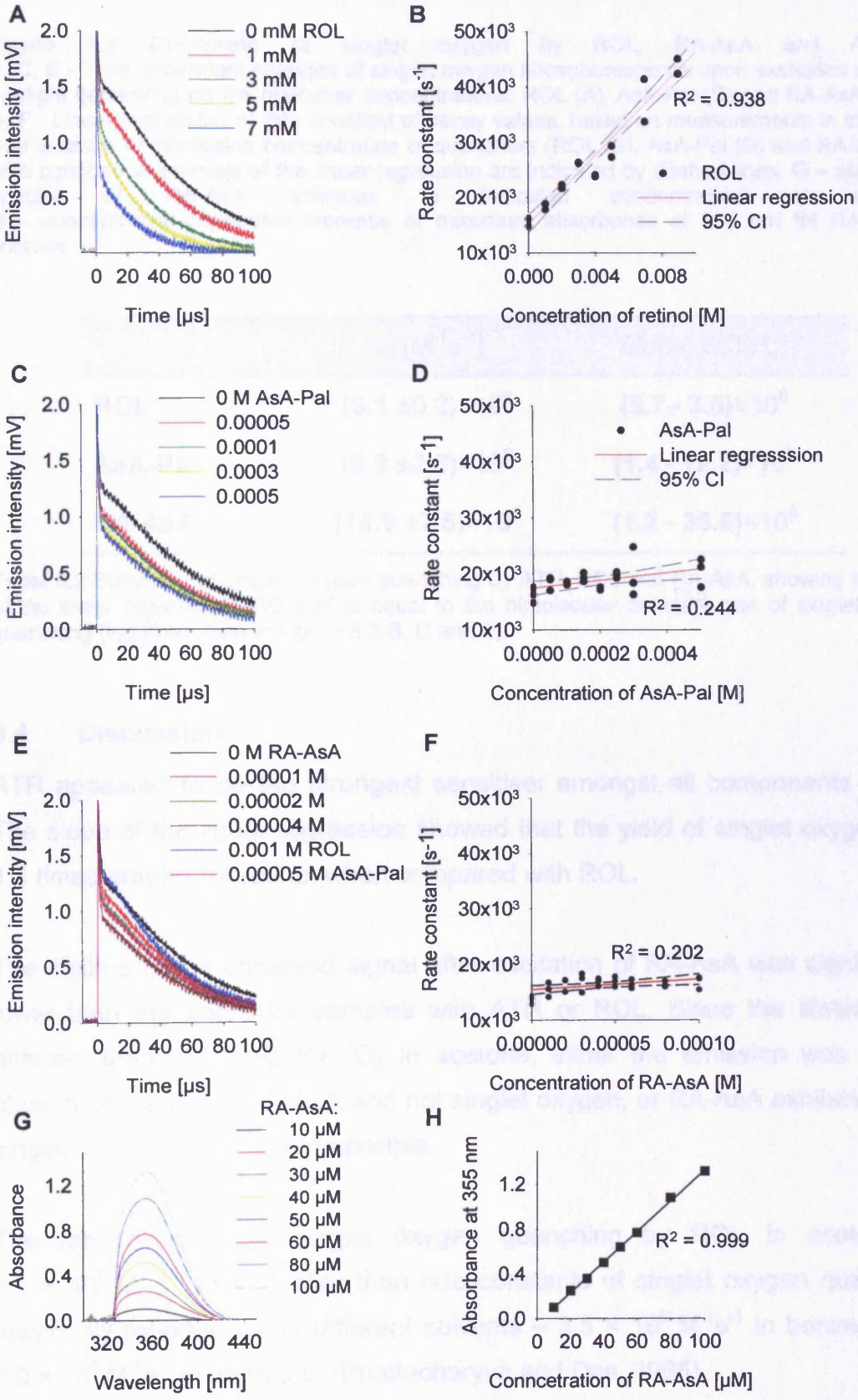
A
Emission intensity [mV]
2.0
1.5
1.0
0.5
0 20 40 60 80 100
Time [µs]
0 mM ROL
1 mM
3 mM
5 mM
7 mM
B
Rate constant [s-1]
50x10³
40x10³
30x10³
20x10³
10x10³
0.000 0.004 0.008
Concetration of retinol [M]
R² = 0.938
ROL
Linear regression
95% CI
C
Emission intensity [mV]
2.0
1.5
1.0
0.5
0.0
0 20 40 60 80 100
Time [µs]
0 M AsA-Pal
0.00005
0.0001
0.0003
0.0005
D
Rate constant [s-1]
50x10³
40x10³
30x10³
20x10³
10x10³
0.0000 0.0002 0.0004
Concentration of AsA-Pal [M]
AsA-Pal
Linear regresssion
95% CI
R² = 0.244
E
Emission intensity [mV]
2.0
1.5
1.0
0.5
0.0
0 20 40 60 80 100
Time [µs]
0 M RA-AsA
0.00001 M
0.00002 M
0.00004 M
0.001 M ROL
0.00005 M AsA-Pal
F
Rate constant [s-1]
50x10³
40x10³
30x10³
20x10³
10x10³
0.00000 0.00005 0.00010
Concentration of RA-AsA [M]
R² = 0.202
G
Absorbance
1.2
0.8
0.4
0.0
320 360 400 440
Wavelength [nm]
RA-AsA:
10 µM
20 µM
30 µM
40 µM
50 µM
60 µM
80 µM
100 µM
H
Absorbance at 355 nm
1.2
0.8
0.4
0.0
0 20 40 60 80 100
Conncetration of RA-AsA [µM]
R² = 0.999

Figure 8.3 Quenching of singlet oxygen by ROL, RA-AsA and AsA-Pal. **A, C, E** - Time dependent changes of singlet oxygen phosphorescence upon excitation with 422 nm light depending on the quencher concentrations: ROL (A), AsA-Pal (C) and RA-AsA (E). **B, D, F** - Linear regression of rate constant of decay values, based on measurements in triplicates over a range of increasing concentration of quenchers (ROL (B), AsA-Pal (D) and RA-AsA (F). 95% confidence intervals of the linear regression are indicated by dashed lines. **G** – absorption spectra of RA-AsA solutions at indicated concentrations in acetone. **H** – concentration-dependent increase of maximum absorbance at 355 nm for RA-AsA in acetone.

	k_Q [$M^{-1}s^{-1}$]	Slope: 95% CI
ROL	**(3.1** ±0.2)×10^6	**(2.7 - 3.5)**×10^6
AsA-Pal	**(6.8** ±2.6)×10^6	**(1.4 - 12.2)**×10^6
RA-AsA	**(18.9** ±7.5)×10^6	**(1.2 - 36.6)**×10^6

Tabel 8.2 Summary of singlet oxygen quenching by ATR, ROL and RA-AsA, showing the slope of the linear regression ±SD that is equal to the bimolecular constant rate of singlet oxygen quenching (k_Q) (from data in Figure 8.3 B, D and F).

8.4 Discussion

ATR appeared to be the strongest sensitiser amongst all components tested. The slope of the linear regression showed that the yield of singlet oxygen was 1.8 times greater for retinal when compared with ROL.

The lifetime of the observed signal after excitation of RA-AsA was significantly lower than the value for samples with ATR or ROL. Since the lifetime was different than expected for $^1O_2$ in acetone, either the emission was due to phosphorescence of RA-AsA and not singlet oxygen, or RA-AsA exhibits strong singlet oxygen quenching properties.

The rate constant of singlet oxygen quenching by ROL in acetone of 3.1 × 10^6 $M^{-1}s^{-1}$ was smaller than rate constants of singlet oxygen quenching previously reported using different solvents – 3.5 × 10^6 $M^{-1}s^{-1}$ in benzene and 6.0 × 10^6 $M^{-1}s^{-1}$ in methanol (Bhattacharyya and Das, 1985).

Both RA-AsA and AsA-Pal appeared to be stronger quenchers of singlet oxygen than ROL. There was a substantial error in the determination of the singlet oxygen quenching rate for RA-AsA and AsA-Pal. RA-AsA exhibited the greatest dose-dependent increase of quenching rate, but overlapping 95% confidence intervals for RA-AsA and other components tested suggest insignificant differences.

In summary, it can be stated that the ability of ATR in acetone to generate singlet oxygen was significantly greater than the ability of ROL. There were no significant differences in the rates of singlet oxygen quenching for RA-AsA, AsA-Pal and ROL.

Chapter 9

Effect of exposure of RPE to POS +/- ATR and +/- light

9.1 Introduction

As already discussed in the general Introduction section, daily exposure of the RPE to POS results in formation of lipofuscin-like granules. It was reported by Boulton and colleagues (1989) that autofluorescent granules were observed as early as two weeks following the challenge with POS with increasing number of granules as the number of POS dose.

As mentioned in the general Introduction section, ATR and its accumulation have a great influence on lipofuscin formation. There have been studies on ATR accumulation in the retina based on monitoring the activity of ROL dehydrogenases, rhodopsin regeneration and activity of ABCR protein (Różanowska and Różanowski, 2008). ATR and its role is of a great interest since, as discussed in previous chapters, ATR and products of its degradation are able to act as photosensitisers and have a direct contribution to toxicity towards cells. It has been shown that ATR can also mediate secondary damage as availability of ATR in the retina, together with exposure to light, have been shown to be the main factors contributing to formation of the age pigment, lipofuscin (Różanowska and Różanowski, 2008). ATR is involved in formation of various identified fluorophores of retinal lipofuscin - A2E, ATR dimer-PE, a phosphatidyldihydropyridine bisretinoid (A2-DHP-PE) and A2-dihydropyridine-ethanolamine (A2-DHP-E) (Różanowska and Różanowski, 2008). Other known constituents of retinal lipofuscin are formed by photooxidation of the bisretinoids A2E and all-*trans*-retinal dimer as reported by Kim and colleagues (2010). As discussed in the Introduction section, excessive levels of lipofuscin have been proposed to compromise essential RPE functions and even contribute to development of AMD. Lipofuscin and one of its components, A2E have been shown to be able to reduce the normal degradative capacity of liposomes responsible for degradation of material phagocytosed by the RPE, leading to formation of undegradable material (Wihlmark et al., 1996; Holz et al., 1999; Shamsi and Boulton, 2001; Bergmann et al., 2004; Kaemmerer et al., 2007).

The aim of this chapter was to elucidate the effect of simultaneous exposure of RPE to light and POS at different states with respect to bleached or unbleached rhodopsin and ATR or photoexcited ATR.

9.2 Experimental design

9.2.1 Fluorescence of lipofuscin and its precursors

RPE lipofuscin was isolated from human eyes divided into different age groups (Methods section 2.8.4.1) in order to provide a comparison. The layer between 1.2 and 1.4 M sucrose was collected as lipofuscin granules. Also layers between lower concentrations of sucrose were collected and presumed to be lipofuscin precursors - middle layer: 1.0/1.2 M sucrose, and upper layer: 0.25/0.1 M sucrose.

Quantification of fluorescence was performed for all samples normalised to the same number of granules. Two excitation wavelengths were used: 360 and 488 nm (Method section 2.8.4.2).

9.2.2 Cell viability

Assessment of cell viability was necessary to reveal the direct influence of POS, ATR and light. The initial step was to assess mitochondrial activity of cells fed with POS under the same conditions as cells dedicated to fluorescence measurements. Additionally, mitochondrial activity of cells exposed to POS at different concentrations (1×10^7 and 1.5×10^7 POS/ml based on the number of outer segments per cell of RPE) when unexposed or exposed to green or white light, was assessed in order to determine the effect of ATR.

The assessment was based on MTT assay described in the Methods section 2.7.2.2.

9.2.3 Feeding ARPE-19 cells with POS

To reveal changes in fluorescence of cells depending on ATR availability, POS with and without exogenous ATR were used to feed a confluent monolayer of ARPE-19 cells (Methods section 2.5.1). Since POS were not dark-adapted there was only a small proportion of remaining rhodopsin when compared with opsin. To be able to reveal ATR-dependent influence on cell fluorescence, the retinoid was added at three chosen concentrations: the same as opsin, twice higher and 3.5 times higher (equalling the maximum concentration of ATR in the retina) for POS exposed to green light. POS exposed to white light with or without exogenous ATR at the highest concentrations were also included to compare activated and non-activated action of ATR (Methods section 2.8.1). Pre-treatment of POS and treatment of cells is presented in the diagram below (Fig. 9.1).

Cells were fed every day (Methods section 2.8.1) to mimic *in vivo* conditions under which POS are phagocytosed every 24 hours. Concentration of POS was 1×10^7 POS/ml, the maximum number of POS phagocytosed by RPE (Kennedy et al., 1994).

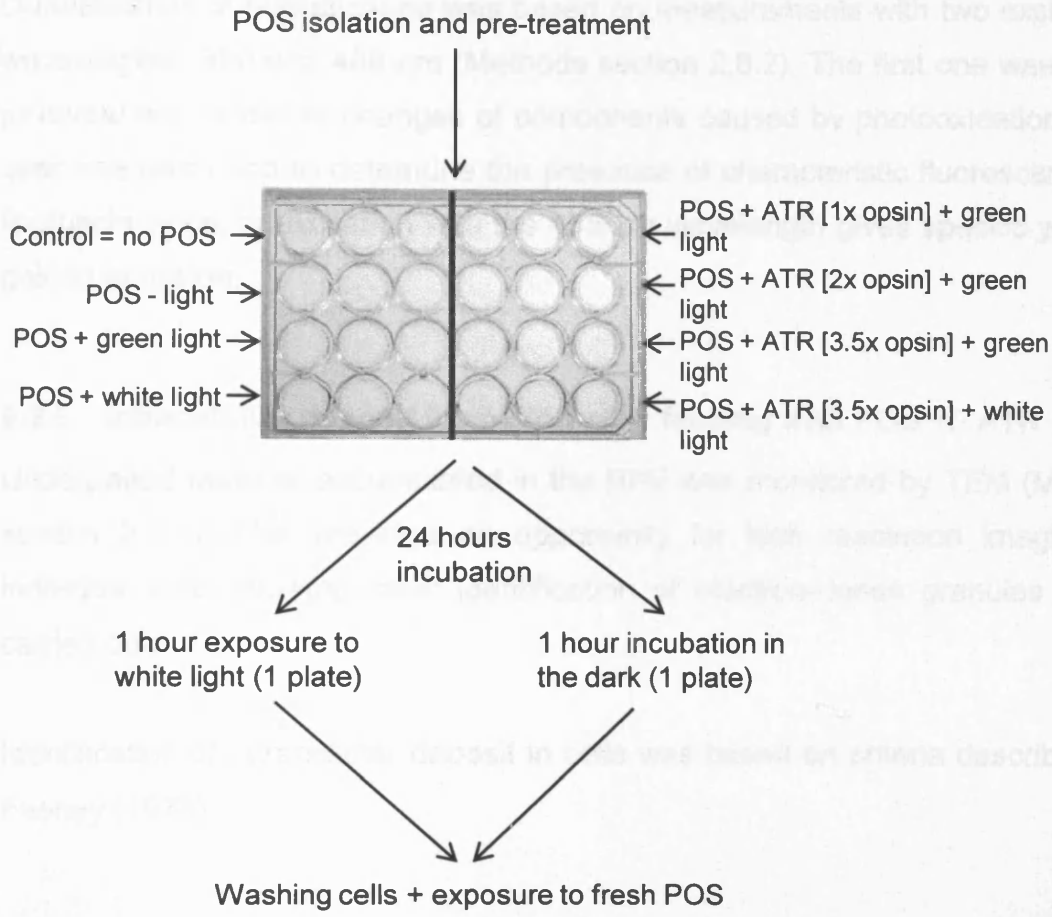

Figure 9.1 A diagram showing the sequence of treatments of ARPE-19 cells with POS +/-ATR and +/- light.

9.2.4 Quantification of fluorescence by fluorescence microscopy and fluorescence spectrofluorymetry

Wassell and colleagues (1998) reported formation of lipofuscin-like granules in the RPE *in vitro* with some spectral similarities to isolated RPE lipofuscin. Emission spectral profiles revealed a shift in maximum of fluorescence after excitation with 364 nm towards shorter wavelengths for granules generated by RPE fed with POS when compared with human RPE lipofuscin.

In this experiment, autofluorescence of cells was initially assessed by measurements with fluorescence microscopy with broad-band excitation and emission filters as described in the Methods section 2.8.2.

Quantification of fluorescence was based on measurements with two excitation wavelengths: 360 and 488 nm (Methods section 2.8.2). The first one was used to reveal any oxidative changes of components caused by photooxidation. The later one was used to determine the presence of characteristic fluorescence of lipofuscin since its excitation with the 488 nm wavelength gives specific yellow-golden emission.

9.2.5 Intracellular deposit formation after feeding with POS +/- ATR

Undegraded material accumulated in the RPE was monitored by TEM (Method section 2.8.5). This provided an opportunity for high resolution imaging of individual cells allowing clear identification of electron-dense granules to be carried out.

Identification of intracellular deposit in cells was based on criteria described by Feeney (1978).

9.3 Results

9.3.1 Fluorescence of lipofuscin and precursors of lipofuscin

Figure 9.2 shows fluorescence emission spectra of lipofuscin granules (lower phase) and layers believed to be its precursors, using excitation with 360 and 488 nm. Samples were divided based on selected age groups (15-25 pairs of eyes per age group). Their comparison revealed layer- and age-dependent changes of emission spectra.

All samples excited with 360 nm were characterised by the presence of peak fluorescence at ~530 nm with the highest fluorescence intensity for the age group above 80 years old for the upper and middle phases for the lipofuscin layer (Fig. 9.2 G-I). Additional peaks were present in the upper and lower phases with maximum at ~440 nm, for the youngest age group (<47 years). The

greatest contribution of emission at shorter wavelengths (<500 nm) was observed for the youngest age group in samples with upper phase.

In all samples excited with 488 nm a peak with maximum at ~600 nm was present (Fig. 9.2 J-L). In all layers, there was an increase in signal observed with increasing age of eyes used for isolation. The emission spectral profiles were comparable between all lipofuscin granules and its precursors.

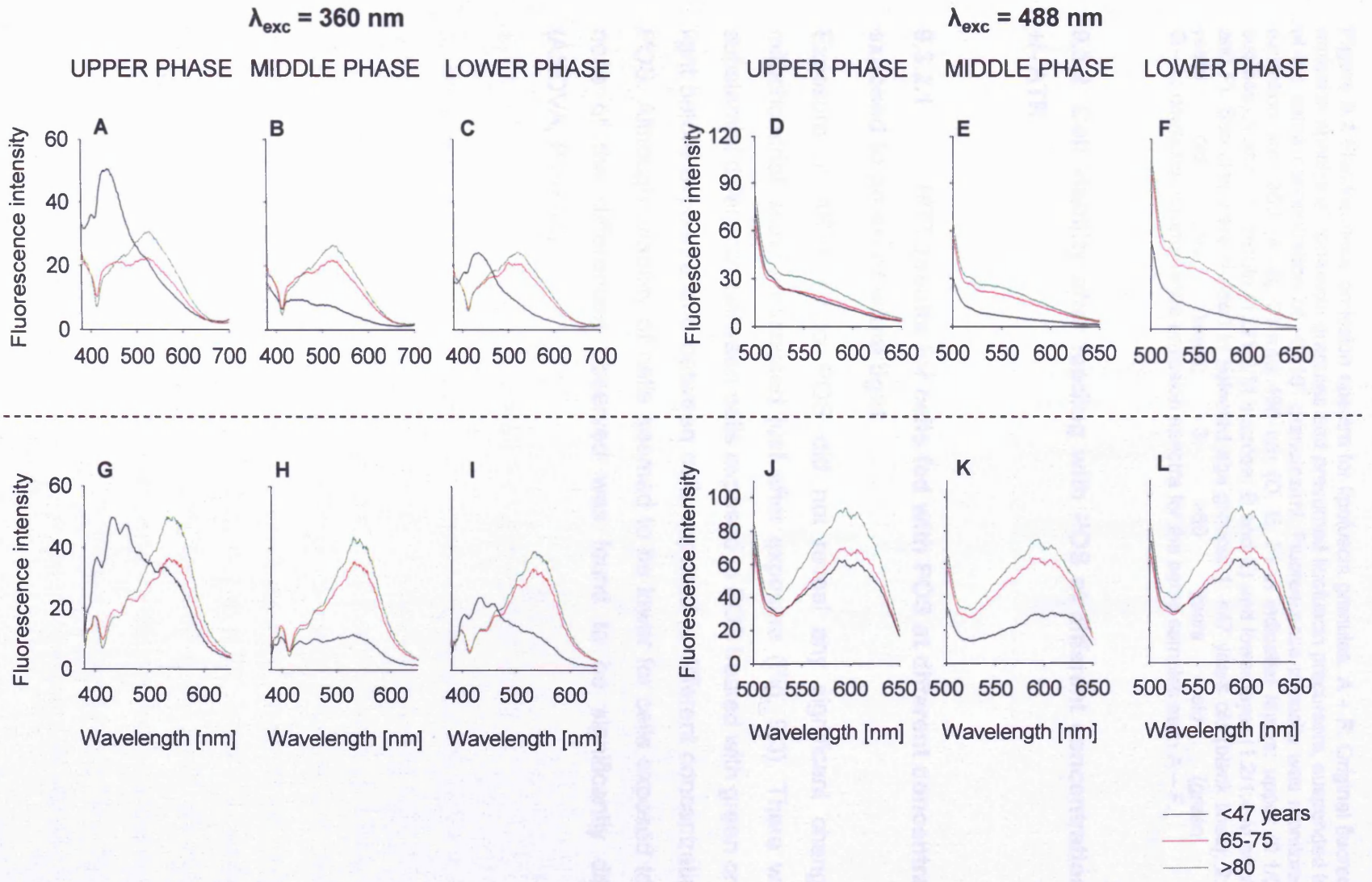
λexc = 360 nm
λexc = 488 nm
UPPER PHASE
MIDDLE PHASE
LOWER PHASE
UPPER PHASE
MIDDLE PHASE
LOWER PHASE
A
B
C
D
E
F
G
H
I
J
K
L
Fluorescence intensity
Fluorescence intensity
Fluorescence intensity
Wavelength [nm]
Wavelength [nm]
Wavelength [nm]
Wavelength [nm]
Wavelength [nm]
Wavelength [nm]
<47 years
65-75
>80

Figure 9.2 Fluorescence emission spectra for lipofuscin granules. **A – F**: Original fluorescence emission spectra of lipofuscin granules and presumed lipofuscin precursors, suspended in PBS, at the same concentration of ~5×10^7 granules/ml. Fluorescence intensity was monitored after excitation with 360 (A, B, C) and 488 nm (D, E, F) in indicated layers: upper (0.1/0.25 M sucrose; A and D), middle (1.0/1.2 M sucrose; B and E) and lower layer (1.2/1.4 M sucrose; C and F). Samples were divided in selected age groups: 1: <47 years old (black lines); 2: 65-75 years old (red lines); 3: >80 years old (green lines). **G – L**: corrected fluorescence emission spectra for the same samples as in A – F.

9.3.2 Cell viability after feeding with POS at different concentration and +/- ATR

9.3.2.1 MTT results for cells fed with POS at different concentrations exposed to green or white light

Exposure of ARPE-19 to POS did not reveal any significant changes in mitochondrial activity assessed just after exposure (Fig. 9.3). There was no substantial difference between cells exposed to POS treated with green or white light before exposure and between cells exposed to different concentrations of POS. Although, viability of cells seemed to be lower for cells exposed to light, none of the differences observed was found to be significantly different (ANOVA, $P > 0.05$).

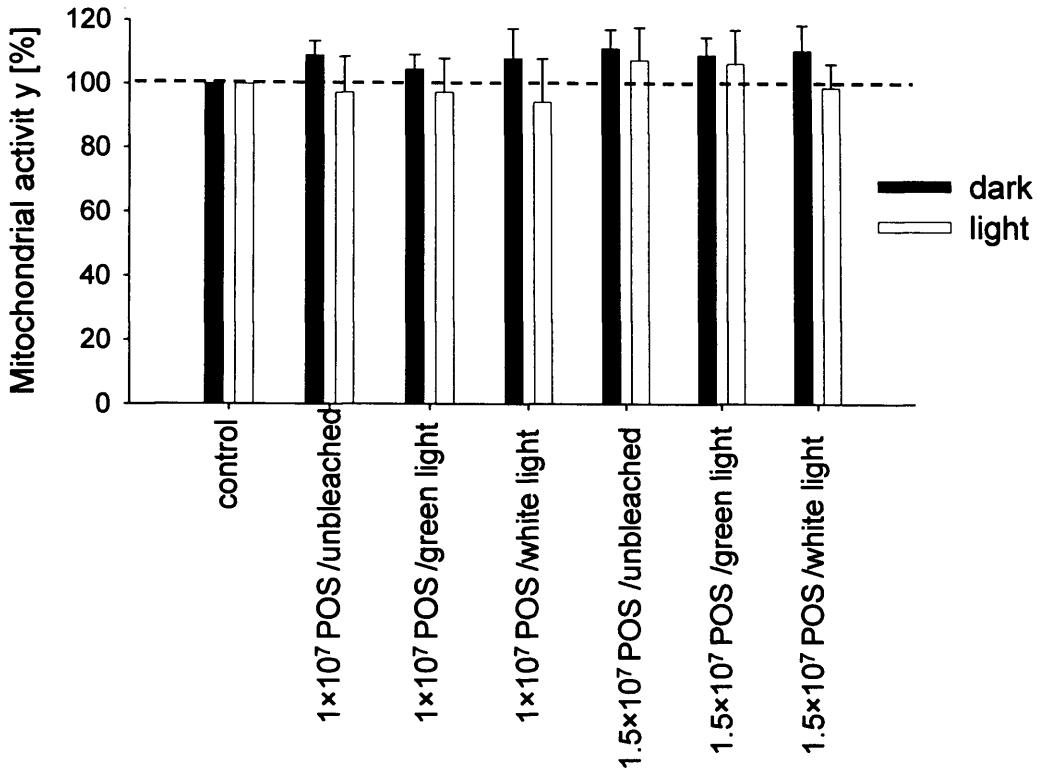

Figure 9.3 Effect on ARPE-19 cells of 1 hour exposures to POS at indicated concentrations, unbleached or exposed to green or white light. Cells were kept in the dark for 24 hours (black columns) or exposed to white light for 1 hour ~24 hours after exposure (white blocks). MTT test was performed 24 hour after the last exposure to light . n=3. Bars = SEM.

9.3.2.2 MTT results for cells fed with POS +/- ATR

Mitochondrial activity of cells fed with POS was significantly higher than for control cells not exposed to POS both in the dark and in the light (Fig. 9.4; $P<0.05$). Exposure of the RPE to light resulted in a decrease of mitochondrial activity of cells fed with POS with or without exogenous ATR when compared with cells kept in the dark, and the differences were found to be significant ($P <0.05$). Cells kept in the dark and exposed to POS and ATR + white light were characterised by the lowest percentage of viable cells among cells exposed to POS. Unbleached POS seemed to have a less damaging effect both in the dark and in light, but the difference between unbleached POS and POS + ATR + light in the dark was not found to be significant ($P >0.05$).

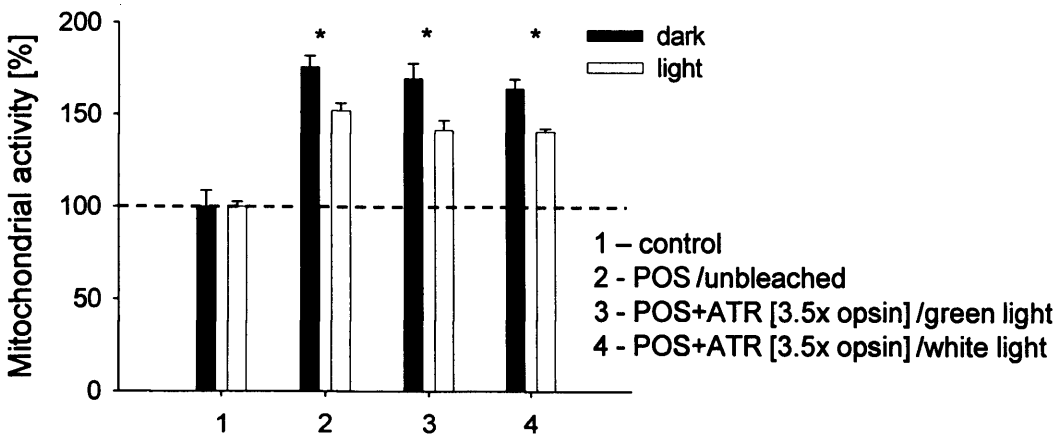

Figure 9.4 Effect on ARPE-19 cells of exposures to POS +/- ATR, unbleached or exposed to green or white light with addition of exogenous ATR at a concentration 3.5 times greater than opsin concentration. Daily exposures to fresh POS were preceded by exposures to white light for 1 hour (white blocks). Cells kept in the dark were covered with black foil and kept under the same conditions (black columns). 1 experiment; 3 wells/treatment. Error bars = SD.

9.3.3 Fluorescence in the RPE after feeding with POS +/- ATR

Representative images show fluorescence intensity observed in live cells after a 2-week treatment (Fig. 9.5). Cells when excited with blue light exhibited golden-yellow fluorescence, which is characteristic for RPE lipofuscin.

Monitoring of fluorescence intensity after excitation with 360 and 488 nm of cells after a 1 hour daily exposure to POS revealed differences between cells kept in the dark and those exposed to light (Fig. 9.6 and 9.7). When solutions solubilised with Triton-X-100 cells were excited with 360 nm light, a signal with the maximum at ~460 nm was observed for all samples. All samples fed with POS with or without added ATR exhibited significantly higher signals at the maximum when compared with control cells ($P < 0.05$). The highest intensity at the maximum was observed in samples with the highest concentration of exogenous ATR added to POS used for feeding and pre-exposed to green or white light (Fig. 9.8). Cells fed with unbleached and POS bleached with green or white light without exogenous ATR exhibited similar fluorescence intensity both in the dark and in light. There was a ~30% and 15% increase of signal observed in samples with ATR present at the highest concentration in the dark and in light, respectively, when compared with cells treated with unbleached or bleached POS. Exposure of POS to white light did not seem to have a

substantial influence on fluorescence intensity. Fluorescence at 460 nm for cells exposed to unbleached POS, POS bleached with green or white light and POS bleached with green light with ATR added at the lowest concentration in the dark significantly differed from fluorescence intensity of cells exposed to light and POS treated with green or white light and with ATR added at the highest concentration ($P < 0.05$). Cells kept in the dark and exposed to POS bleached with green or white light exhibited significantly lower fluorescence than cells exposed to light and POS + green light + ATR at a concentration equal or twice greater than opsin concentration.

Long-wavelength fluorescence observed after excitation of samples with 488 nm was significantly greater in samples with cells kept in the dark and exposed to unbleached POS, POS bleached with green or white light and POS pre-treated with green light and with added ATR at concentrations twice greater than opsin concentrations (Fig. 9.7 C, D and 9.8 B). Fluorescence at 560 nm for control cells significantly differed from all cells exposed to POS ($P < 0.05$).

Comparison of fluorescence spectra with 360 nm as the excitation wavelength, obtained for lipofuscin granules and their precursors, with spectra recorded for cells fed with POS +/- ATR and +/- light revealed different maxima of fluorescence intensity. Cells exhibited a maximum at ~460 nm, whereas the main peak of fluorescence in lipofuscin granules and its precursor was detected at ~530 nm. However, samples with lipofuscin and upper phase obtained from the youngest age group were characterised by a presence of increased fluorescence intensity for shorter wavelengths <500 nm with a peak reaching ~450 nm.

Emission spectra obtained after excitation of samples with 488 nm revealed a shift in maximum of fluorescence towards shorter wavelengths for cells exposed to POS +/- ATR and +/- light (~560 nm) when compared with the maximum observed for lipofuscin granules and its precursors (~600 nm).

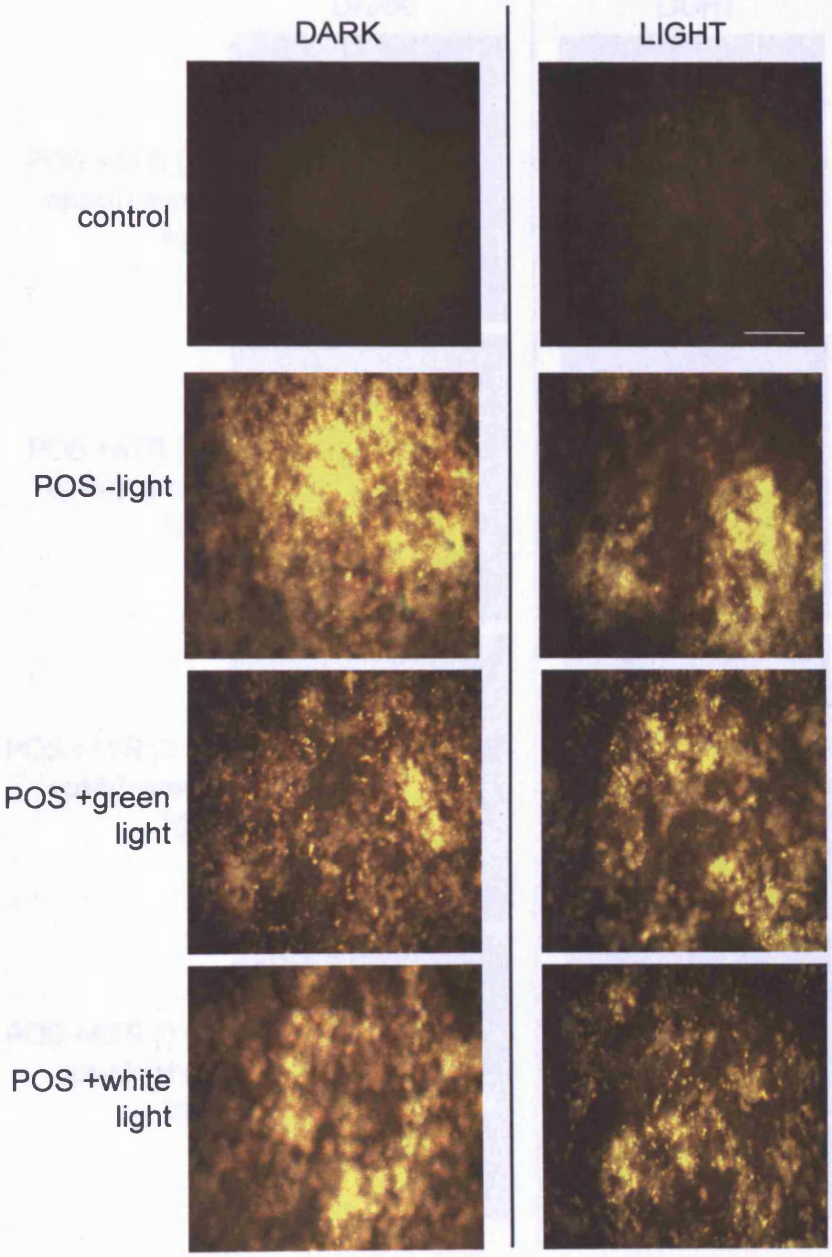
DARK
LIGHT
control
POS -light
POS +green light
POS +white light

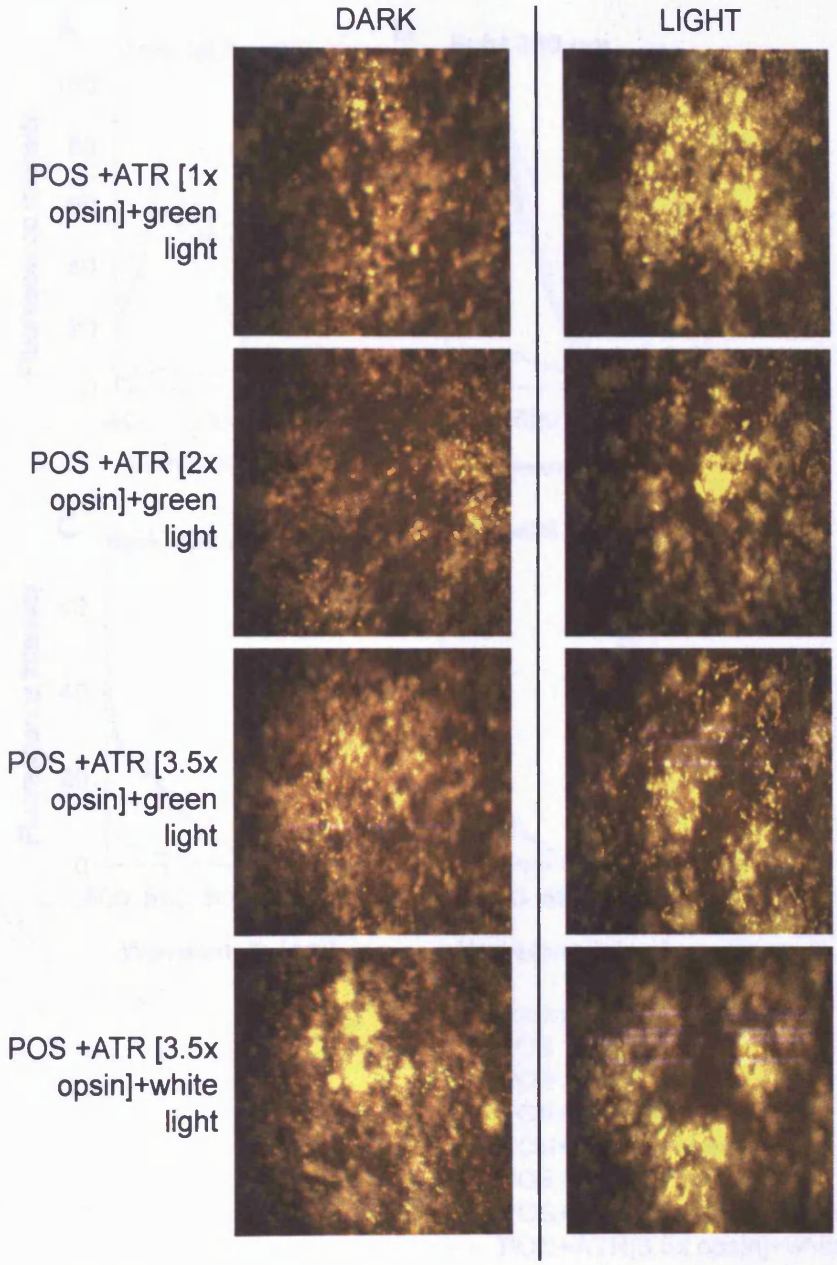

Figure 9.5 Representative images of cells after a 2-week exposure to POS +/- ATR in the dark (left column) or in light (right column). Cells were exposed to unbleached POS, bleached with green or white light, with or without ATR added in indicated concentrations. Bar = 50 μm

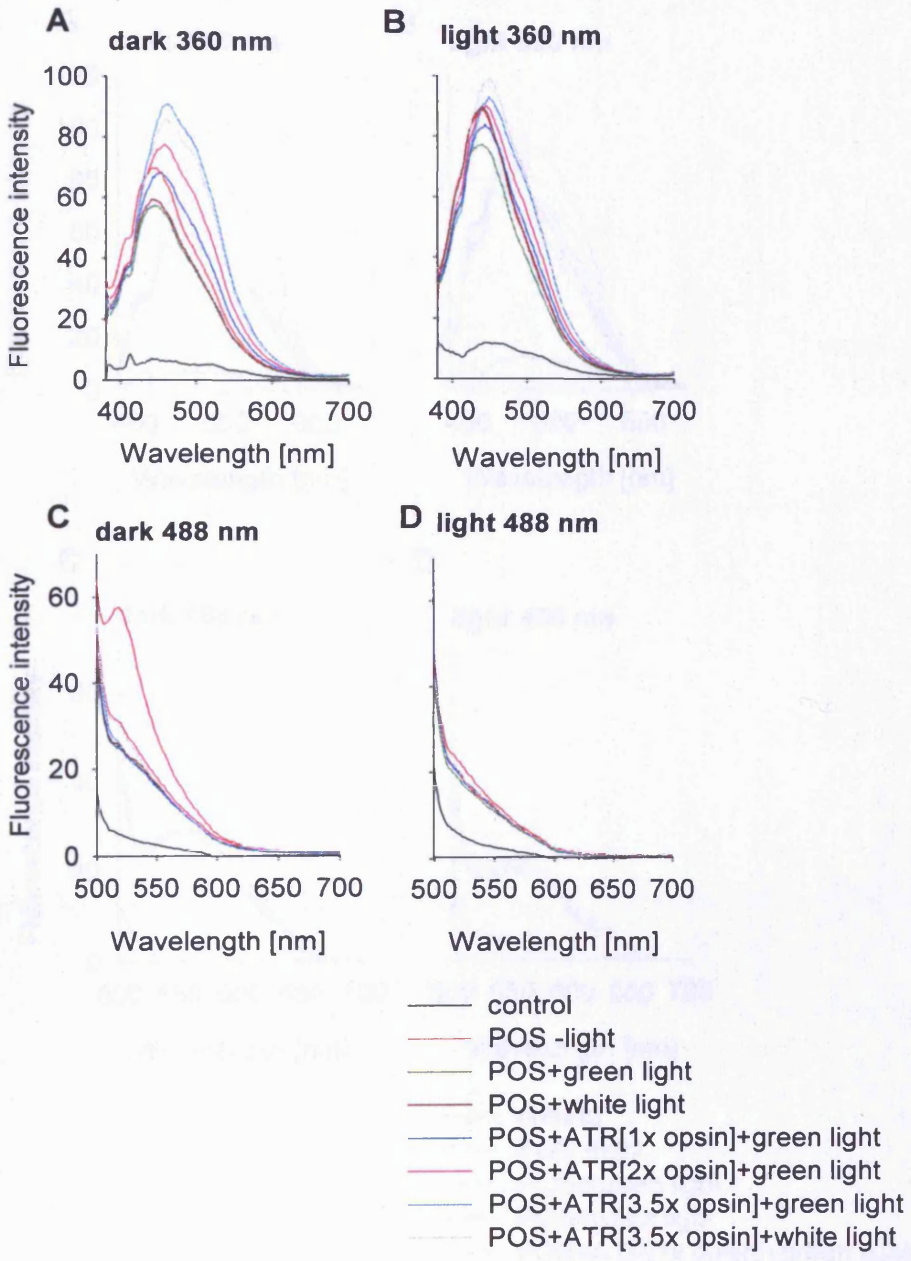

Figure 9.6 Representative fluorescence emission spectra of the RPE fed with POS pre-treated as indicated in the legend in the presence and absence of ATR, suspended in 2% Triton X-100. Cells were fed daily with POS +/- ATR for 2 weeks. Cells were kept in the dark (A, C) or exposed to light (B, D; every day for 1 hour, ~12 mW/cm^2 about 24 hours after feeding). POS were unbleached or exposed to green or light with or without addition of ATR at indicated concentrations expressed as molar equivalents of opsin. For fluorescence measurements cells were solubilised in 2% Triton X-100 and fluorescence spectra were assessed with excitation wavelengths of 360 nm (A, B) and 488 nm (C, D).

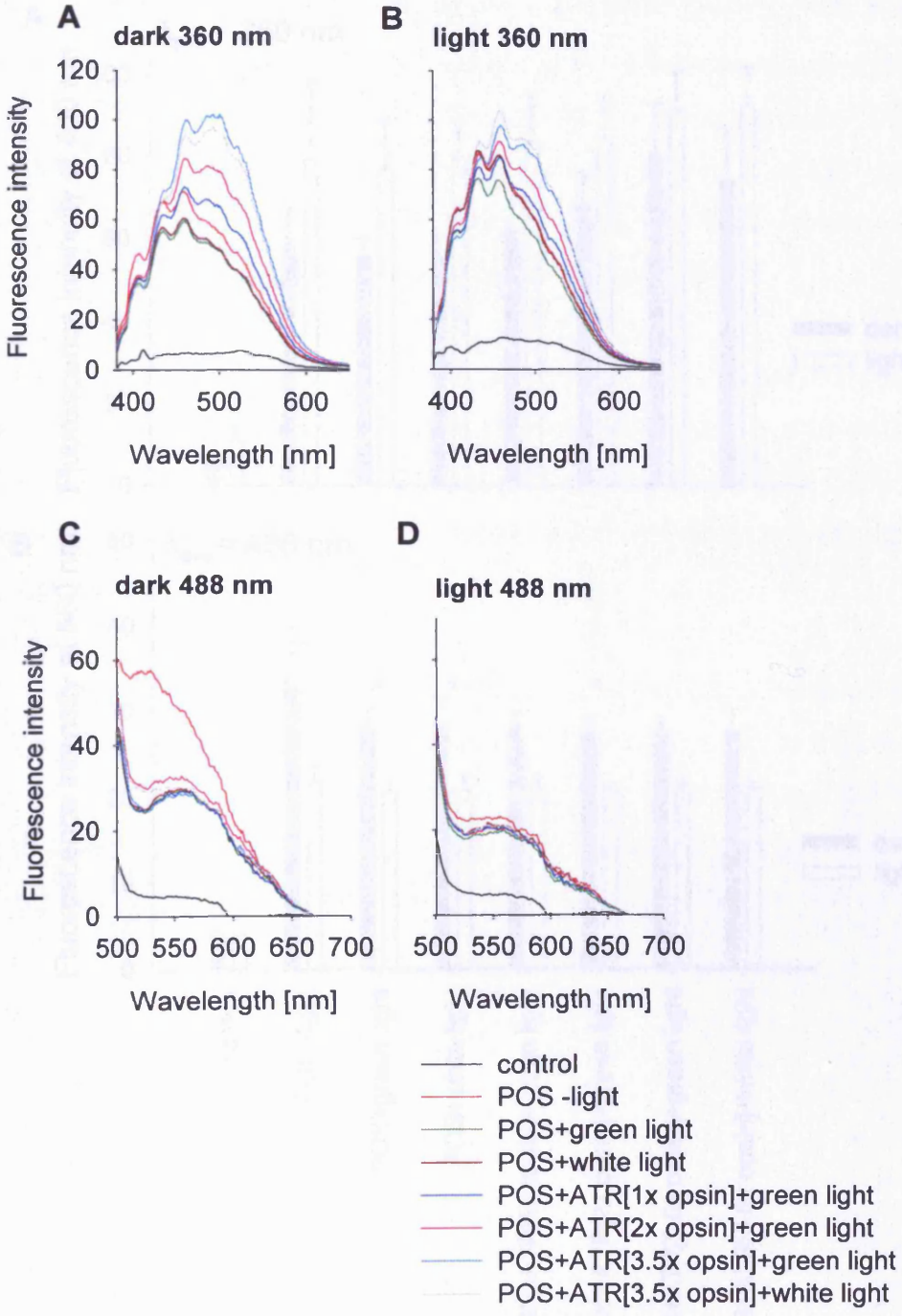

Figure 9.7 Representative corrected fluorescence emission spectra for the same samples as in Fig. 9.6.

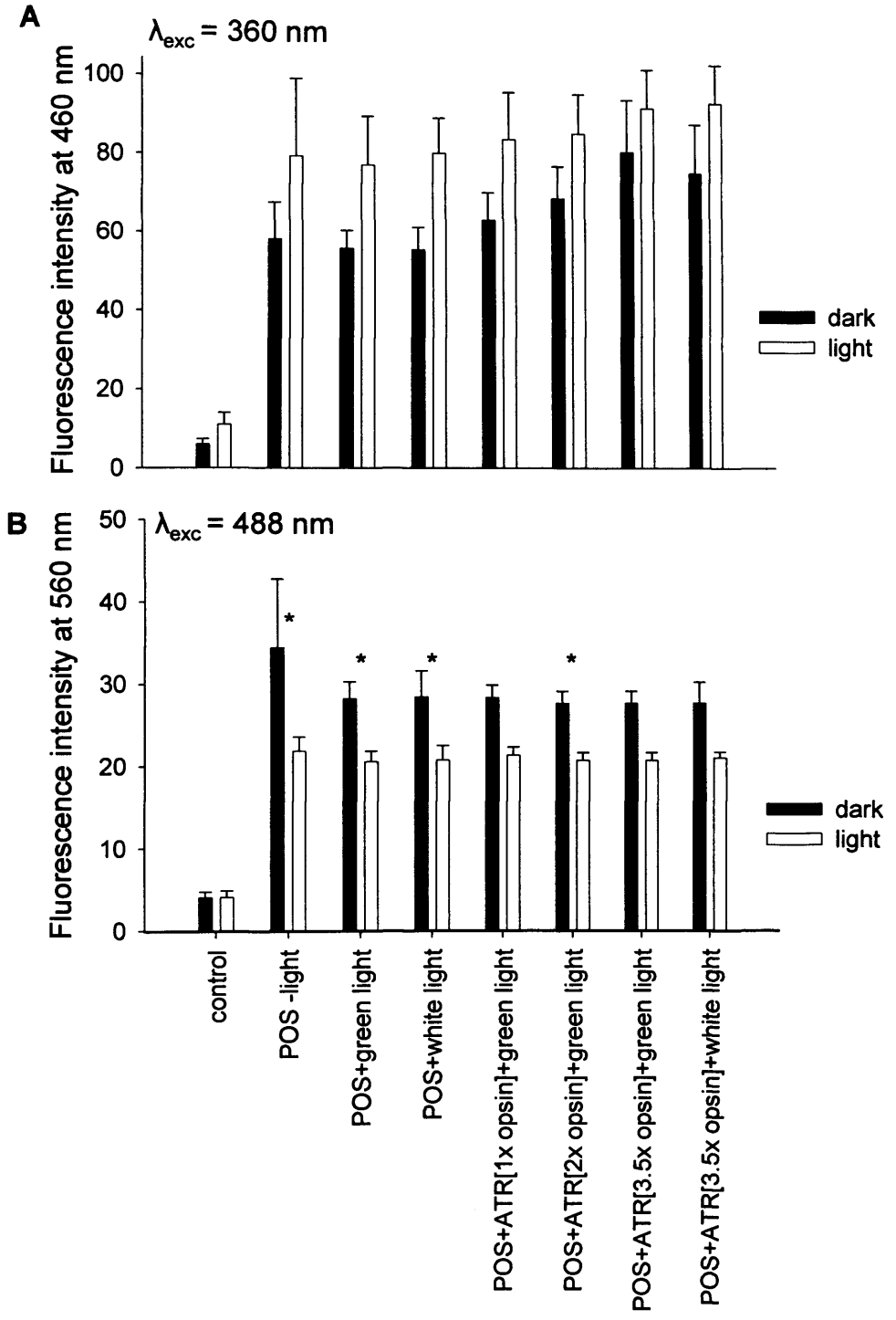

Figure 9.8 Fluorescence intensity at maxima of emission spectra: 460 (A) and 560 nm (B) for 360 and 488 nm excitation wavelengths, respectively. Asterisks indicate statistical significance of results compared between cells kept in the dark or exposed to light. Experimental conditions as in Fig. 9.7.

9.3.4 Formation of intracellular deposits after feeding with POS +/- ATR

TEM images of cells fed for two weeks with medium alone (control), unbleached bovine POS and bleached POS with green or white light with addition of exogenous ATR at concentrations 3.5 times greater than the concentration of POS opsin are shown in Figure 9.9. Figure 9.10 shows the averaged percentage of cytoplasmic area occupied by granules.

The percentage of cytoplasmic area occupied by granules for control cells was four times greater in light when compared with cells kept in the dark. All cells exposed to POS with or without addition of exogenous ATR were characterised by higher values determined for cells kept in the dark than values for cells exposed to light ($P < 0.05$).

The percentage of cytoplasmic area occupied by granules reached the highest value for cells fed with POS exposed to green light with addition of exogenous ATR and kept in darkness (4% ±2). Cells fed with unbleached POS exhibited the lowest percentage of cytoplasm area occupied by lipofuscin-like granules both in the dark and in the light (3.0% ±1.9 and 0.5% ±0.4, respectively).

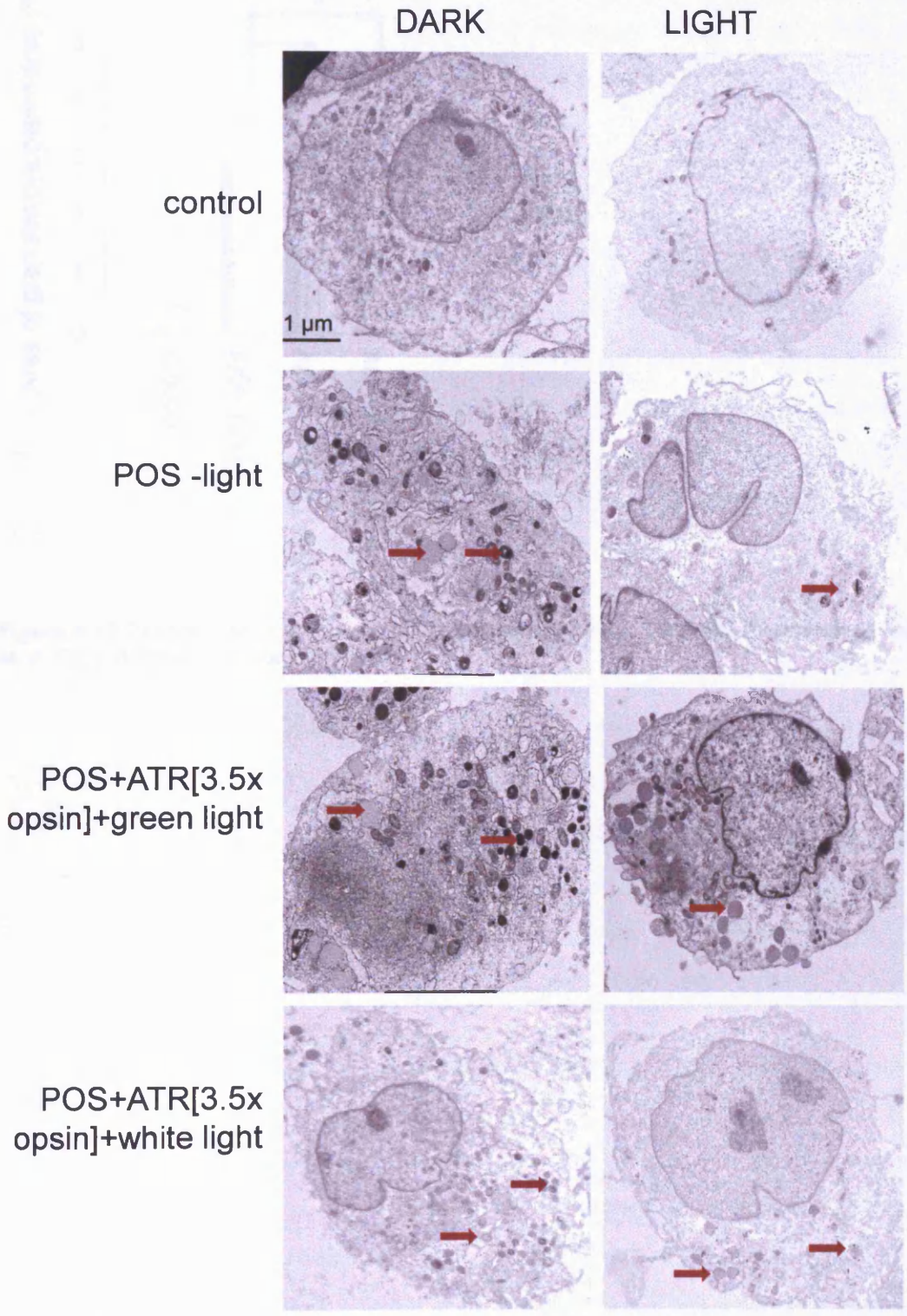

Figure 9.9 Representative TEM images of ARPE-19 cells after 2 week daily exposures to unbleached POS or POS bleached with green or white light with addition of exogenous ATR. Cells were kept in darkness (DARK) or exposed daily to white light (LIGHT). Control cells were fed in the same manner with the culture medium only. Red arrows indicate granules of lipofuscin included in the analysis.

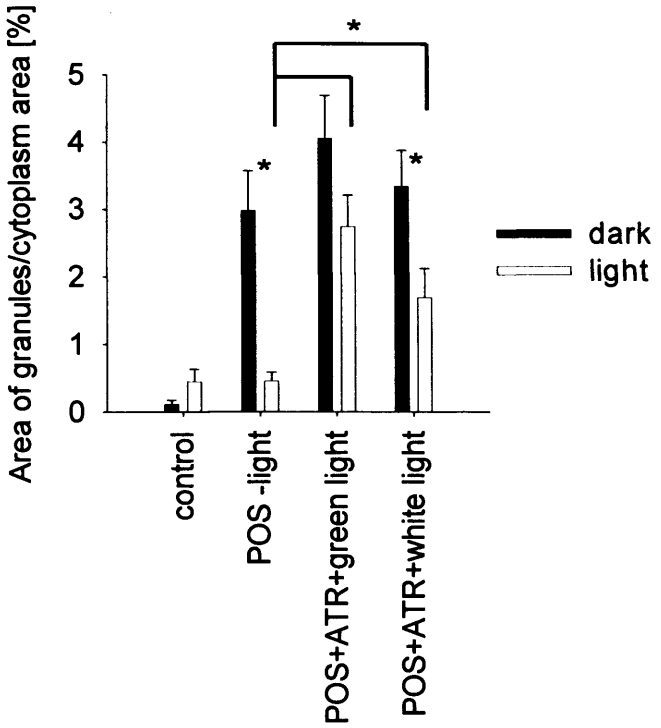

Figure 9.10 Percentage of cytoplasmic area occupied by the granules. Experimental conditions as in Fig. 9.8. n=9-10. Error bars=SEM.

9.4 Discussion

This chapter has attempted to reveal the influence of exposure of the RPE to POS *+/- ATR* and light, and similarities to characteristics of lipofuscin.

The effect of short-term exposure of the RPE to POS on cell viability

Comparison of cell viability determined just after treatment between control cells and cells fed with POS with unbleached rhodopsin and POS with bleached rhodopsin and hydrolysed ATR, with or without activation by white light, did not show any significant differences. It needs to be noticed that the potential ATR-driven damaging effect can be observed after 24 hours as discussed in Chapter 6. Therefore, if ATR was to exert a damaging effect on cell viability, it would be detectable by the time the MTT assay was performed.

The effect of 2-week exposure of the RPE to POS on cell viability

There was a significant difference in cell viability between control cells and cells after two weeks of daily exposures to POS kept in darkness or exposed to light. It can be suggested that exposure to POS increases mitochondrial activity of the cell reflecting an increase in their metabolic/catabolic activity and/or increases activity of NADPH oxidases which can also lead to reduction of MTT to formazan (Bernas and Dobrucki, 1999).

There were no significant differences between cells kept in dark after 2-weeks of daily exposures to unbleached POS and POS bleached with green or white light with an addition of exogenous ATR. It provides a good starting point for further experiments testing accumulation of lipofuscin-like inclusion bodies, excluding a possibility of toxicity of POS and eliminating a need to count cells or to measure their protein content in order to normalise results to the same number of cells.

The exposure of cells to light seemed to significantly influence cell viability, leading to a 14-17% decrease of cell vitality after treatment in comparison to cells exposed to corresponding POS but kept in darkness. As Wihlmark and colleagues (1997) reported, exposure of lipofuscin-loaded RPE to blue light leads to a considerably enhanced loss of both viability and lysosomal stability when compared to control cells.

The influence of POS +/- ATR and light on the RPE and comparison with isolated lipofuscin and its precursors

Exposure of cells to POS resulted in accumulation of intracellular inclusion bodies emitting broad-band fluorescence when excited with UVA (360 nm) or blue light (488 nm).

Analysis of short-wavelength fluorescence induced by 360 nm light revealed an increase of signal in cells exposed to ATR and regularly exposed to light in comparison to cells kept in darkness without exogeneous ATR. It would suggest an increase in the level of oxidative changes caused by these treatments. Fluorescence spectra of cell suspensions exhibited similarities with fluorescence spectra obtained for lipofuscin granules and upper phase for the youngest age group. It can suggest that biochemical changes of the material formed in cells after 2-week exposures is comparable with lipofuscin and/or its precursor formed early in life.

In the case of long-wavelength fluorescence induced by 488 nm light, for all types of pre-treated POS there was a trend of exhibiting greater intensity of the long-wavelength fluorescence for cells kept in darkness than for cells exposed to light, but those differences were statistically significant for POS subjected to less oxidising conditions before feeding, and were insignificant for POS with addition of ATR corresponding to 3.5 mol equivalent of opsin.

RPE lipofuscin exhibits a characteristic fluorescence emission spectrum with maximum at ~600 nm as presented in the Results section. As reported by Kim

and colleagues (2010), excitation of A2E and *iso*A2E results in emission spectra with maxima at ~600 nm. It has been demonstrated that A2E can act as an acceptor of energy from different light-absorbing molecules within lipofuscin granules, and can emit the photoexcitation energy as fluorescence. Thus, A2E is the major emitter in the lipofuscin granule (Haralampus-Grynaviski et al., 2003). Similar maxima are observed after excitation of all-*trans*-retinal dimer-PE and all-*trans*-retinal dimer-E with 500 nm, but the fluorescence emission is considerably weaker. It is worth mentioning that excitation of unconjugated all-*trans*-retinal dimer with 430 nm gives greater, blue-shifted emission intensity with peak emission occurring at approximately 510 nm. This could suggest that all-*trans*-retinal dimer and possibly oxidised all-*trans*-retinal dimer may substantially contribute to the observed emission spectra.

Additionally, the time of feeding of the RPE with POS was too short to mimic changes undergoing *in vivo* over years or even decades, leading to the formation of final product – lipofuscin. This could also provide an explanation for a lack of substantial differences between RPE fed with POS + ATR at increasing concentrations.

Formation of lipofuscin-like granules in the RPE

Results have shown that a greater area of cytoplasm is occupied by lipofuscin-like granules for cells kept in the dark with bleached POS in the presence of exogenous ATR in comparison with cells fed with unbleached POS and exposed to light. As discussed in the Introduction section, availability of ATR play an important role in the process of lipofuscin formation and the results are in agreement with the expectations.

Wihlmark and colleagues (1996) reported that exposure of RPE to pre-oxidised POS (by irradiation with UV light) leads to an increased formation of lipofuscin-like inclusions in the RPE when compared with native POS. It was expected that products of ATR photo-oxidation obtained by irradiation of POS with white light in the presence of exogenous ATR would provide additional substrates for

formation of lipofuscin-like granules, leading to an increase in their numbers. Indeed, the results demonstrate that exposure of cells to light and POS bleached with green or white light with exogenous ATR lead to the formation of a greater number of cytoplasmic lipofuscin-like inclusion bodies than in cells exposed to light and unbleached POS without exogenous ATR. In contrast to expectations, the results have shown that the total area of cytoplasm occupied by lipofuscin-like granules is not statistically different for cells exposed to POS irradiated with white light than for POS exposed to green light. It may suggest that the 2-week treatment was too short to reveal expected changes and longer exposure would need to be applied.

In summary, 2-week exposures of RPE to POS with or without exogenous ATR resulted in an increase of cellular fluorescence and accumulation of lipofuscin-like bodies. The results were greater for dark-adapted cells when compared with those exposed to light. Cells exposed to POS and light were characterised by accumulation of lipofuscin-like bodies and an increase of cellular fluorescence induced by UVA light.

Chapter 10

Discussion and conclusions

10.1 General discussion

The overall aim of this thesis was to determine the role of the visual pigment in oxidative stress in the retina, which may contribute to the pathogenesis of age-related macular degeneration. The results show that the product of isomerisation of rhodopsin chromophore after bleaching - ATR, can act as a photosensitiser in photoreceptor membranes, leading to formation of singlet oxygen and can be directly toxic to the RPE. In addition, products of ATR degradation may contribute to the toxic effect. Accumulation of products of rhodopsin bleaching may result in the formation of lipofuscin within the RPE, leading to dysfunction of epithelial cells, and finally, contributing to the development of age-related macular degeneration. The physiological relevance of these *in vitro* studies is discussed below.

The studies on the kinetics of ATR hydrolysis and ROL formation have been presented for both room temperature and a physiologically relevant temperature of 37°C. The changes were strictly temperature-dependent with significantly higher rates at 37°C when compared with 21°C. Although it is impossible to extrapolate directly the results to the human eye, exposure of the dark adapted eye to a high intensity light such as a flash lamp may result in rapid accumulation of ATR within POS occurring on a timescale of several minutes.

The concentrations of ATR tested in the experiments covered ranges up to 0.2 and 1 mM in DMSO and liposomes, respectively. The concentration of ATR in the retina depends on the level of rhodopsin and the level of storage form of rhodopsin chromophore – 11-*cis*-retinyl esters. Taking into account a rhodopsin concentration of 3.8 mM in normal subjects and a 2.5-fold excess of retinoids stored as retinyl esters, the total concentration of ATR could be 13.3 mM in the case of total dysfunction in ATR removal from the OS. Thus, the concentrations of ATR studied here *in vitro* represent only a minor fraction (1.5 and 7.5 % in DMSO and liposomes, respectively) of free ATR possibly released *in vivo*.

As demonstrated in Chapter 5, photoreceptor outer segments are very susceptible to oxidative modifications. As the retina functions in an environment

that favours oxidative changes, it is of great importance for proper functioning of enzymes involved in the retinoid cycle and the membrane structure. Any disruptions in the chain of reaction after rhodopsin bleaching caused by an impaired enzymatic system may result in accumulation of a toxic compound of the retinoid cycle – ATR, which is efficiently cleared from the retina under normal conditions. Experiments *in vitro* have already shown that ATR under illumination can induce photooxidation of both lipid and protein membrane components (Loginova et al., 2008; Sokolov et al., 2008).

As mentioned in section 5.1, metal ions have been shown to play a major role in oxidative stress by initiating a free radical chain of lipid peroxidation by decomposition of lipid hydroperoxides. The retina is of special interest in terms of oxidative stress due to its oxygen-rich environment being highly susceptible to oxidative modification. Homeostasis of metal ions, iron in particular, is crucial for protection against oxidative stress. Elevated levels of iron in the retina have been correlated with retinal degeneration (reviewed by He et al., 2007). Mice given iron ions exogenously demonstrated increased levels of superoxide radicals formation in photoreceptor inner segments, lipid peroxidation ultimately leading to retinal degeneration (Rogers et al., 2007). It has been shown that disrupted homeostasis of iron between the neural retina and the RPE may lead to iron overload (He et al., 2007). This has been shown to be a feature present in patients suffering from AMD. Although the role of iron in the AMD pathogenesis is not fully understood, there have been some studies suggesting that it might be directly involved (reviewed by He et al., 2007).

Retinoids have been shown to play a dual role in lipid peroxidation as prooxidants and may be potential inhibitors of lipid peroxidation. ROL, for instance, due to its unsaturated nature, is very reactive toward peroxyl radicals (Boulton et al., 2001; Różanowska et al., 2005). The inhibition of peroxidation by retinoids has been attributed to their ability to act as a trap for peroxyl radicals or electron donation.

ATR-induced oxidative modification of cellular components may involve singlet oxygen formation, as shown in Chapter 4. As previously mentioned, the ability of ATR to generate singlet oxygen depends on its position in opsin with the highest yield of $^1O_2$ generated upon ATR releasing to the inner leaflet of the disc membrane after rhodopsin regeneration. Interestingly, it has been demonstrated that reduction of ATR to ROL at the exit site of opsin is not correlated with a decrease of singlet oxygen yield despite a decrease in efficiency of photon absorption. Comparison of quantum yields of singlet oxygen generation by ATR and ROL indicates that ROL has smaller or at most equal quantum yield of singlet oxygen than ATR. However, the quantum yields are strongly solvent dependent, particularly for ATR, with the highest values for ATR observed in non-polar solvents, such as benzene (Różanowska and Sarna, 2005), decreasing 6-fold in polar methanol (Dillon et al., 1996). ROL, on the other hand, exhibits smaller quantum yields in photosensitised generation of singlet oxygen in non-polar solvents, but this difference becomes negligible in polar methanol. Thus, the equal efficiency in the generation of singlet oxygen by ATR and ROL at the opsin exit site may be explained if the environment of ATR at the opsin exit site is polar, but upon enzymatic reduction to ROL, ROL becomes exposed mostly to the non-polar environment.

As the retina is continuously exposed to light, it is highly likely that accumulated ATR undergoes rapid (photo)degeneration since its structure is not stable under exposure to light (as confirmed in Chapter 6). The toxic effect of degraded ATR has been shown to be even more deleterious when compared with ATR on its own.

In *in vitro* experiments ATR and dATR were toxic not only upon light exposure, but also to a lesser extent in the dark. Toxicity in dark conditions suggests that mechanisms other than formation of singlet oxygen are involved, such as the formation of a superoxide. *In vivo*, the RPE can be protected against superoxide formation by an extracellular antioxidant enzyme – SOD (Halliwell and Gutteridge, 2007), which calalyses dismutation of rather non-reactive superoxide to potentially more dangerous hydrogen peroxide. Hydrogen

peroxide, upon decomposition by metal ions, can lead to generation of the most reactive free radical – hydroxyl radical. To prevent from that interaction, hydrogen peroxide is decomposed to molecular oxygen and water by catalase and glutathione peroxidase.

Antioxidants play a very important role against oxidative stress that the retina may be exposed to. In this thesis ROL, VitE and PE have been shown *in vitro* to have a potential to protect cells against tested (photo)toxicity of ATR and/or dATR. Several studies showed a positive effect of carotenoids and antioxidants supplementation on risk of AMD (reviewed by Neelam et al., 2008). Antioxidants may increase their protective effects if provided in a combined therapy, such as a combination of a singlet oxygen quencher (carotenoid) and a free radical scavenger (VitC or VitE), which can offer better protection against photo-oxidative damage than increasing concentrations of individual antioxidants (Palozza and Krinsky, 1992; Bohm et al., 1998; Wrona et al., 2003). There is a thin barrier between antioxidants being protectors and exhibiting pro-oxidative properties. Protective mechanisms of antioxidants may be based on their reaction with radicals, but as a result, they react with free radicals and become free radicals themselves, which in turn may lead to their accumulation and ultimately pro-oxidant effects. It was demonstrated in the experiments showing pro-oxdiatve properties of ROL in the presence of ATR (Chapter 6).

The levels of ATR and products of its condensation and degradation may increase with age of photoreceptor discs, with the oldest and the most peroxidised lipids/discs present at the distal end of rod outer segment. This agrees with studies showing that lipid peroxidation may provide signals for increased rate of phagocytosis (Finnemann and Silverstein, 2001; Sun et al., 2006), indicating that phagocytosis is a necessary process to physically remove peroxidised POS tips (Winkler, 2008). The results confirm the need to remove or detoxify the ATR and products of its oxidation, and/or condensation as extracellular ATR and dATR are highly (photo)toxic to the RPE. The protective effect of antioxidants is very important here as they would be capable of preventing or reducing ATR degradation, and also subsequently reducing their

toxicity. The role of PE in POS membranes is important in particular as its complex with ATR and dATR significantly reduces ATR toxicity as observed in experiments described in this thesis. It has been suggested that both A2E and its oxidised derivatives can be considered as causative candidates for retinal damage. However, formation of A2E takes days since it involves POS phagocytosis by epithelial cells. Secondly, products of A2E oxidation, which can be produced quickly as a result of light exposure, were not detected in $Rdh8^{-/-}$ $Abca4^{-/-}$ mice (Maeda et al., 2009). This would support the view that ATR and products of its oxidation are involved in the pathogenesis of the light-induced rapid retinal degeneration. Maeda and colleagues (2009) showed that impairment of ATR clearance may result in an acute retinal degeneration in mice after exposure to bright light, and suggested that the mechanism of retinal damage by ATR may include plasma membrane permeability and damage to mitochondria, leading to mitochondria-associated death. Although, A2E has been shown to be toxic to the RPE, ATR and products of its degradation have been shown to be more toxic than A2E. It would suggest that formation of A2E may play a protective role, leading to a decrease in the toxic effect of the retinoid and its derivatives. Regular exposure of the retina to light and possible ATR accumulation suggest that the role of products of ATR degradation require even more investigation and may play an important role in oxidative damage to the retina.

There is a significant potential in controlling of ATR transport and accumulation in the retina to constitute potential therapies for eye diseases such as AMD and Stargardt's disease. It can involve facilitating transport of ATR from inner to outer disc membranes, inhibition of ATR formation and removal of its excess from the retina.

One of the pharmacological approaches of slowing down ATR accumulation in POS by slowing down of rhodopsin regeneration is by delivery of inhibiting agents of RPE65 as well as other enzymes involved in synthesis or transport of 11-*cis*-retinal (Gollapalli and Rando, 2004; Golczak et al., 2005a, Golczak et al., 2005b; Maeda et al., 2006; Maiti et al., 2006; Golczak et al., 2008).

13-*cis*-retinoic acid is a well known inhibitor of the retinoid cycle. Experiments on rats showed that 13-*cis*-retinoic acid inhibits RPE65 and 11-*cis*-retinal dehydrogenase (11cRDH), effectively protecting the retina from light-induced damage (Gollapalli and Rando, 2004; Sieving et al., 2001; Radu et al., 2003).

Other inhibitors of the visual cycle include 11-*cis*-retinyl bromoacetate, 11-fluoro-all-*trans*-retinol, retinylamine and its derivatives, as well as non-retinoid agents such as certain isoprenoids and farnesylamine (Golczak et al., 2005a; Maiti et al., 2006; Golczak et al., 2008). Testing of all-*trans*-retinylamine on rodents revealed that it is much more effective in terms of retinoid cycle inhibition, and its potential toxicity is smaller than other inhibitors (Golczak et al., 2008; Golczak et al., 2005b).

In summary, the results of this project support the hypothesis that accumulation of ATR in POS as a result of rhodopsin bleaching imposes a risk of oxidative stress. The risk is high during exposure to light in particular, when both superoxide and singlet oxygen are generated. The toxic effect may be exacerbated by products of ATR photodegradation. Unless counteracted by repair mechanisms and efficient antioxidants, reactive oxygen species lead to damage to lipids and proteins. As a consequence, enzyme dysfunction occurs and formation of products not susceptible to lysosomal degradation are produced. It results in accumulation of incompletely digested outer segment discs and formation of residual bodies similar to lipofuscin. Lipofuscin can potentially impose further toxic effects to the RPE, including lipofuscin-mediated oxidative damage leading to dysfunction of the RPE, cytotoxicity and triggering angiogenic and proinflammatory signalling potentially resulting in retina degenerations.

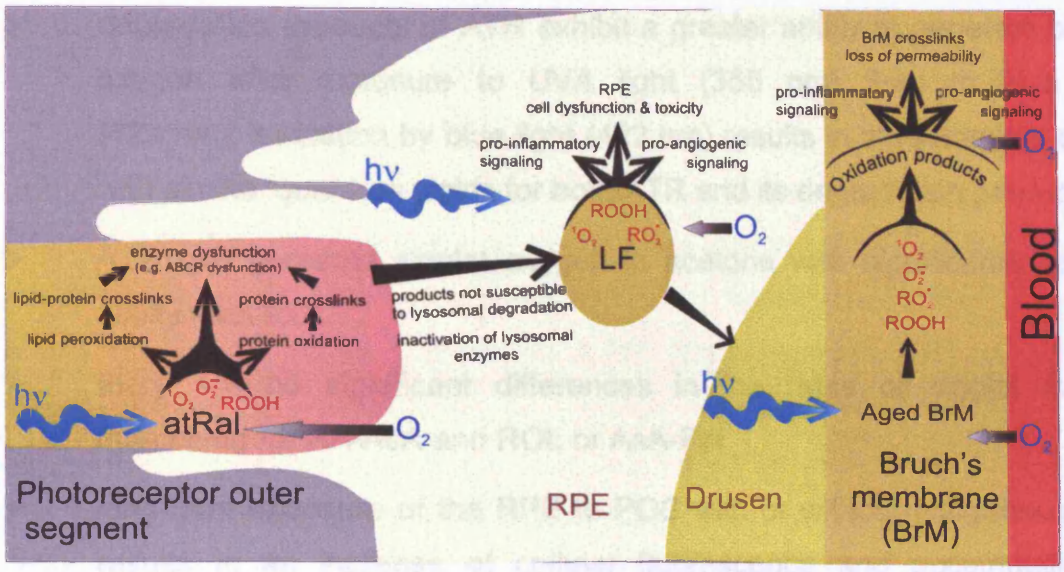

Figure 10.1 Hypothetical pathways leading to retinal dysfunction, ageing and AMD (adapted from Różanowska and Różanowski, 2008).

10.2 Conclusions:

- the time needed to hydrolyse 50% of ATR after rhodopsin bleaching is 4.3 and 2.2 min at 21°C and 37°C, respectively and it takes 17 and 12 minutes to reduce ATR to ROL in 50% at 21°C and 37°C, respectively
- the yield of singlet oxygen generated by ATR increases upon hydrolysis of ATR from opsin and further upon its release to the disc membrane
- POS lipids are extremely susceptible to oxidation and initially formed lipid hydroperoxides undergo decomposition on the timescale of minutes; thus monitoring of lipid hydroperoxides is not an optimal tool to assess the progress of lipid peroxidation in POS
- exposure of ARPE-19 cells to ATR and even more to dATR induces reduction in mitochondrial activity and subsequent cell death, and exposure to light aggravates both ATR and dATR-induced cytotoxicity
- the toxic effect of ATR was substantially prevented by PE, whereas dATR (photo)toxicity was at least partly prevented by PE, α-tocopherol, and ROL, whereas RA-AsA, AsA-Pal, N-acetyl-cysteine, GSH and vitamin B_6 did not exhibit a protective effect

- degradation products of ATR exhibit a greater ability to generate singlet oxygen after exposure to UVA light (355 nm) than to blue light (422 nm); excitation by blue light (422 nm) results in the formation of $^1O_2$ with similar quantum yields for both ATR and its degradation products
- ATR can generate singlet oxygen in acetone with significantly greater ability than ROL
- there are no significant differences in the rates of singlet oxygen quenching for RA-AsA and ROL or AsA-Pal
- long-term exposure of the RPE to POS with or without exogenous ATR results in an increase of cellular fluorescence and accumulation of lipofuscin-like bodies with results greater in the dark compared with light
- exposure of cells fed with POS to light leads to accumulation of lipofuscin-like inclusion bodies and an increase of cellular fluorescence induced by UVA light

Overall, this thesis supports the theory that products of rhodopsin bleaching can be accumulated in the retina and can cause retinal damage. In summary, ATR and dATR have a significant potential to cause direct damage to photoreceptors and RPE dysfunction. Toxicity of ATR and dATR can lead to a loss of the support role provided by the RPE and further dysfunction or death of photoreceptors and disruptions in the visual cycle. ATR- and dATR-induced accumulation of undegraded material can lead to formation of potentially toxic products. This suggests that ATR and products of its degradation play a prominent role in age-related changes in the retina and the pathogenesis of AMD.

10.3 Future work

Further investigation into the effect of ATR, depending on its position in opsin, on cellular components such as proteins could provide further evidence of its potential toxicity and mechanism of action in POS. Clearance of ATR from POS and susceptibility of POS to photo-oxidation can be studied as a function of pH within a range of pH 4.0 to pH 7.4 to provide data on whether the risk of

photooxidative damage to OS is increased or decreased due to lysosomal acidification of phagosomes.

Components of Chapter 9 would benefit from further investigation. Longer feeding durations could render the results more relevant to *in vivo* conditions of the accumulation of undegraded material. *In vivo* models would provide a tool of great interest for both studies on ATR (photo)toxicity and on possible therapeutic or preventing agents.

The effect of photobleaching of visual pigment on lysosomal degradation of POS can be investigated. The effect of visual pigment photobleaching on the pH of intracellular organelles can be studied in RPE cell culture by fluorimetric methods involving acridine orange dye. Many lysosomal enzymes can be studied for inhibition by ATR and dATR.

Studies have implicated inflammation and complement activation amongst the processes involved in the pathogenesis of AMD. Following studies of Zhou and colleagues (2006), showing that the products of A2E oxidation may serve as a trigger for the complement system, ATR and dATR can be investigated as potential triggers of complement activation that would predispose the retina to disease and that, over time, might contribute to chronic inflammation.

The involvement of ATR in acute light-induced retinopathy of mice has been reported by Maeda and colleagues (2009). Although they suggested that one of the possible mechanisms of ATR toxicity involved plasma membrane permeability and poisoning of mitochondria, leading to activation of caspase and cell death, further studies including products of ATR degradation are needed in order to understand the mechanisms underlying retinal damage.

Appendices

Appendix 1 – statistical results for Chapter 3.

All P-values marked with grey are considered to be "not significant" (i.e. ≥0.05).

	Comparison 21°C and 37°C
F_0	0.849
A	0.206
k	<0.001
τ	0.007
$t_{1/2}$	0.007

Table A1.1 P-values for t-test to investigate differences between F_0, A, k, τ and $t_{1/2}$ for Trp fluorescence kinetics at 21 and 37 °C (corresponding to data in Tab. 3.1).

	Comparison 21°C and 37°C
F_0	0.013
A	0.003
k	0.013
τ	0.023
$t_{1/2}$	0.023

Table A1.2 P-values for t-test to investigate differences between F_0, A, k, τ and $t_{1/2}$ for RoI fluorescence kinetics at 21 and 37 °C (corresponding to data in Tab. 3.2).

F_0	NADPH + 9-*cis*RAL	NADPH + ATP + 9-*cis*RAL
NADPH	<0.001	<0.001
NADPH + 9-*cis*RAL		<0.001
A		
NADPH	<0.001	<0.001
NADPH + 9-*cis*RAL		<0.001

F_1	NADPH + 9-*cis*RAL	NADPH + ATP + 9-*cis*RAL
NADPH	<0.001	<0.001
NADPH + 9-*cis*RAL		<0.001
k		
NADPH	0.101	0.650
NADPH + 9-*cis*RAL		0.387

F_0	NADPH + ATP	NADPH + ATP + 9-cisRAL	NADPH + ATP + 13-cisRAL
NADPH	<0.001	0.036	<0.001
NADPH + ATP		0.123	0.271
NADPH + ATP + 9-cisRAL			0.112
F_1			
NADPH	<0.001	<0.001	<0.001
NADPH + ATP		0.106	<0.001
NADPH + ATP + 9-cisRAL			0.031
A			
NADPH	<0.001	<0.001	<0.001
NADPH + ATP		0.002	<0.001
NADPH + ATP + 9-cisRAL			0.011
k			
NADPH	0.047	0.067	0.057
NADPH + ATP		0.643	0.725
NADPH + ATP + 9-cisRAL			0.482

Table A1.3 P-values for t-test to compare F_0, F1, A and k for the kinetics of ROL after rhodopsin bleaching depending on NADPH and ATP (corresponding to data in Fig. 3.3 and 3.4).

Appendix 2 – statistical results for Chapter 4

All P-values marked in grey are considered to be "not significant" (i.e. ≥0.05).

	1.5 min	2.5 min	4.33 min	8 min	10 min	15 min	20 min
unbleached	<0.001	<0.001	<0.001	<0.001	<0.001	<0.001	<0.001
1.5 min		0.486	0.174	0.017	0.002	0.030	<0.001
2.5 min			0.599	0.092	0.009	0.011	0.001
4.33 min				0.160	0.012	0.013	0.001
8 min					0.059	0.033	0.002
10 min						0.197	0.016
15 min							0.664

Table A2.1 P-values for t-test to compare singlet oxygen yields in POS discs after indicated time points after rhodopsin bleaching (corresponding to data in Fig. 4.6).

	$A_{1\ unbl}$ pH 7.8	$A_{2\ unbl}$ pH 7.8	$A_{2\ unbl}$ pH 7.8
$A_{1\ unbl}$ pH 4.5	>0.05		
$A_{2\ unbl}$ pH 4.5		>0.05	
$A_{3\ unbl}$ pH 4.5			>0.05
	$A_{1\ bl}$ pH 7.8	$A_{2\ bl}$ pH 7.8	$A_{3\ bl}$ pH 7.8
$A_{1\ bl}$ pH 4.5	>0.05		
$A_{2\ bl}$ pH 4.5		>0.05	
$A_{3\ bl}$ pH 4.5			>0.05
	$A_{1\ 20min\ bl}$ pH 7.8	$A_{2\ 20min\ bl}$ pH 7.8	$A_{3\ 20min\ bl}$ pH 7.8
$A_{1\ 20min\ bl}$ pH 4.5	<0.05		
$A_{2\ 20min\ bl}$ pH 4.5		>0.05	
$A_{3\ 20min\ bl}$ pH 4.5			>0.05

	$k_{1\ unbl}$ pH 7.8	$k_{2\ unbl}$ pH 7.8	$k_{3\ unbl}$ pH 7.8
$k_{1\ unbl}$ pH 4.5	>0.05		
$k_{2\ unbl}$ pH 4.5		>0.05	
$k_{3\ unbl}$ pH 4.5			>0.05
	$k_{1\ bl}$ pH 7.8	$k_{2\ bl}$ pH 7.8	$k_{3\ bl}$ pH 7.8
$k_{1\ bl}$ pH 4.5	>0.05		
$k_{2\ bl}$ pH 4.5		>0.05	
$k_{3\ bl}$ pH 4.5			>0.05
	$k_{1\ 20min\ bl}$ pH 7.8	$k_{2\ 20min\ bl}$ pH 7.8	$k_{3\ 20min\ bl}$ pH 7.8
$k_{1\ 20min\ bl}$ pH 4.5	>0.05		
$k_{2\ 20min\ bl}$ pH 4.5		>0.05	
$k_{3\ 20min\ bl}$ pH 4.5			>0.05

	$A_{1\ bl}$ pH 4.5	$A_{1\ 20min\ bl}$ pH 4.5
$A_{1\ unbl}$ pH 4.5	<0.05	<0.05
$A_{1\ bl}$ pH 4.5		<0.05
	$A_{2\ bl}$ pH 4.5	$A_{2\ 20min\ bl}$ pH 4.5
$A_{2\ unbl}$ pH 4.5	>0.05	>0.05
$A_{2\ bl}$ pH 4.5		>0.05
	$A_{3\ bl}$ pH 4.5	$A_{3\ 20min\ bl}$ pH 4.5
$A_{3\ unbl}$ pH 4.5	>0.05	>0.05
$A_{3\ bl}$ pH 4.5		>0.05

	$A_{1\ bl}$ pH 7.8	$A_{1\ 20min\ bl}$ pH 7.8
$A_{1\ unbl}$ pH 7.8	<0.05	<0.05
$A_{1\ bl}$ pH 7.8		>0.05
	$A_{2\ bl}$ pH 7.8	$A_{2\ 20min\ bl}$ pH 7.8
$A_{2\ unbl}$ pH 7.8	>0.05	>0.05
$A_{2\ bl}$ pH 7.8		>0.05
	$A_{3\ bl}$ pH 7.8	$A_{3\ 20min\ bl}$ pH 7.8
$A_{3\ unbl}$ pH 7.8	>0.05	>0.05
$A_{3\ bl}$ pH 7.8		>0.05

	$k_{1\ bl}$ pH 4.5	$k_{1\ 20min\ bl}$ pH 4.5
$k_{1\ unbl}$ pH 4.5	>0.05	>0.05
$k_{1\ bl}$ pH 4.5		>0.05
	$k_{2\ bl}$ pH 4.5	$k_{2\ 20min\ bl}$ pH 4.5
$k_{2\ unbl}$ pH 4.5	>0.05	>0.05
$k_{2\ bl}$ pH 4.5		>0.05
	$k_{3\ bl}$ pH 4.5	$k_{3\ 20min\ bl}$ pH 4.5
$k_{3\ unbl}$ pH 4.5	>0.05	>0.05
$k_{3\ bl}$ pH 4.5		>0.05

	$k_{1\ bl}$ pH 7.8	$k_{1\ 20min\ bl}$ pH 7.8
$k_{1\ unbl}$ pH 7.8	>0.05	>0.05
$k_{1\ bl}$ pH 7.8		>0.05
	$k_{2\ bl}$ pH 7.8	$k_{2\ 20min\ bl}$ pH 7.8
$k_{2\ unbl}$ pH 7.8	>0.05	>0.05
$k_{2\ bl}$ pH 7.8		>0.05
	$k_{3\ bl}$ pH 7.8	$k_{3\ 20min\ bl}$ pH 7.8
$k_{3\ unbl}$ pH 7.8	>0.05	>0.05
$k_{3\ bl}$ pH 7.8		>0.05

Table A2.2 P-values for t-test to compare the singlet oxygen yields in POS discs before and after rhodopsin bleaching depending on pH (corresponding to data in Fig. 4.7).

Appendix 3 – statistical results for Chapter 5

All P-values marked in grey are considered to be "not significant" (i.e. ≥0.05).

A

	1.5 min	8 min	10 min	20 min
unbleached	0.169	0.230	0.908	0.186

B

	20 min bl +10 min D	20 min bl +10 min L	20 min bl +20 min D	20 min bl +20 min L
20 min bl	0.228	0.398	0.289	0.971
20 min bl +10 min D		0.460		
20 min bl +20 min D				0.575

C

	20 min bl + NADPH	20 min bl + NADPH + ATP+ 9-*cis*RAL	20 min bl + ATP+ 9-*cis*RAL
20 min bl	0.656	0.353	0.161
20 min bl + NADPH		0.399	0.120
20 min bl + NADPH + ATP+ 9-*cis*RAL			0.372

Table A2.1 P-values for t-test to investigate the differences between the levels of lipid hydroperoxides in POS (corresponding to data in Fig. 5.2 (A), 5.3 (B) and 5.4 (C)).

Appendix 4 – statistical results for Chapter 6

All P-values marked in grey are considered to be "not significant" (i.e. ≥0.05).

	control D	0% dATR D	5% dATR D	40% dATR D	65% dATR D	75% dATR D	80% dATR D	Control L	0% dATR L	5% dATR L	40% dATR L	65% dATR L	75% dATR L
0% dATR D	>0.05												
5% dATR D	<0.05	>0.05											
40% dATR D	<0.05	>0.05	>0.05										
65% dATR D	<0.05	<0.05	>0.05	>0.05									
75% dATR D	<0.05	<0.05	>0.05	>0.05	>0.05								
80% dATR D	<0.05	<0.05	>0.05	>0.05	>0.05	>0.05							
0% dATR L		>0.05	>0.05	>0.05	>0.05	>0.05	>0.05	<0.05					
5% dATR L		<0.05	>0.05	>0.05	>0.05	>0.05	>0.05	<0.05	>0.05				
40% dATR L		<0.05	>0.05	>0.05	>0.05	>0.05	>0.05	<0.05	>0.05	>0.05			
65% dATR L		<0.05	>0.05	>0.05	>0.05	>0.05	>0.05	<0.05	>0.05	>0.05	>0.05		
75% dATR L		<0.05	>0.05	>0.05	>0.05	>0.05	>0.05	<0.05	>0.05	>0.05	>0.05	>0.05	
80% dATR L		<0.05	>0.05	>0.05	>0.05	>0.05	>0.05	<0.05	>0.05	>0.05	>0.05	>0.05	>0.05

Table A4.1 P-values for one-way ANOVA test and Hochberg post-tests to compare toxicity of ATR depending on the level of its degradation (corresponding to data in Fig. 6.3). ANOVA: P <0.001.

	control D	0.1 mM ATR D	0.05 mM ATR D	0.025 mM ATR D	0.1 mM dATR D	0.05 mM dATR D	0.025 mM dATR D	Control L	0.1 mM ATR L	0.05 mM ATR L	0.1 mM dATR L
0.1 mM ATR D	<0.05										
0.05 mM ATR D	>0.05	>0.05									
0.025 mM ATR D	>0.05	<0.05	>0.05								
0.1 mM dATR D	<0.05	>0.05	<0.05	<0.05							
0.05 mM dATR D	>0.05	>0.05	>0.05	>0.05	>0.05						
0.025 mM dATR D	>0.05	>0.05	>0.05	>0.05	<0.05	>0.05					
0.1 mM ATR L		>0.05	<0.05	<0.05	>0.05	>0.05	<0.05	<0.05			
0.05 mM ATR L		>0.05	<0.05	<0.05	>0.05	>0.05	<0.05	<0.05	>0.05		
0.1 mM dATR L		>0.05	<0.05	<0.05	>0.05	>0.05	<0.05	<0.05	>0.05	>0.05	
0.05 mM dATR L		>0.05	<0.05	<0.05	>0.05	>0.05	<0.05	<0.05	>0.05	>0.05	>0.05

Table A4.2 P-values for one-way ANOVA test and Hochberg post-tests for dose-dependent (photo)toxicity of ATR and dATR (corresponding to data in Fig. 6.5). ANOVA: P <0.001.

DARK 10mM PC + dATR	Control	0.25mM dATR	0.5mM dATR	1mM dATR
0.25mM dATR	>0.05			
0.5mM dATR	>0.05	>0.05		
1mM dATR	<0.05	<0.05	<0.05	
1mM ATR	>0.05	>0.05	>0.05	<0.05

LIGHT 10mM PC + dATR	Control	0.1mM dATR	0.25mM dATR	0.5mM dATR
0.1mM dATR	>0.05			
0.25mM dATR	<0.05	<0.05		
0.5mM dATR	<0.05	<0.05	>0.05	
0.5mM ATR	<0.05	<0.05	>0.05	>0.05

Table A4.3 P-values for one-way ANOVA test and Hochberg post-tests to test ATR and dATR toxicity in liposomes (corresponding to data in Fig. 6.7). ANOVA: DARK - P = 0.002,

LIGHT - P <0.001.

	control D	0.1 mM ATR D	ATR 50 µM ROL D	ATR 150 µM ROL D	0.05 mM dATR D	dATR 50 µM ROLE D	dATR 100 µM ROL D	dATR 150 µM ROL D	Control L	0.1 mM ATR L	ATR 50 µM ROL L	ATR 150 µM ROL L	0.05 mM dATR L	dATR 50 µM ROL L	dATR 100 µM ROL L
0.1 mM ATR D	>0.05														
ATR 50 µM ROL D	<0.05	>0.05													
ATR 150 µM ROL D	<0.05	<0.05	>0.05												
0.05 mM dATR D	<0.05	<0.05	<0.05	<0.05											
dATR 50 µM ROL D	<0.05	<0.05	<0.05	>0.05	>0.05										
dATR 100 µM ROL D	<0.05	<0.05	>0.05	>0.05	>0.05	>0.05									
dATR 150 µM ROL D	<0.05	>0.05	>0.05	>0.05	<0.05	<0.05	>0.05								
0.1 mM ATR L		>0.05	>0.05	<0.05	<0.05	<0.05	<0.05	>0.05	>0.05						
ATR 50 µM ROL L		>0.05	>0.05	>0.05	<0.05	<0.05	>0.05	>0.05	<0.05	>0.05					
ATR 150 µM ROL L		<0.05	>0.05	>0.05	<0.05	<0.05	>0.05	>0.05	<0.05	>0.05	>0.05				
0.05 mM dATR L		<0.05	<0.05	>0.05	>0.05	>0.05	>0.05	<0.05	<0.05	<0.05	<0.05	<0.05			
dATR 50 µM ROL L		<0.05	>0.05	>0.05	>0.05	>0.05	>0.05	<0.05	<0.05	<0.05	<0.05	>0.05	>0.05		
dATR 100 µM ROL L		<0.05	>0.05	>0.05	>0.05	>0.05	>0.05	>0.05	<0.05	<0.05	>0.05	>0.05	>0.05	>0.05	
dATR 150 µM ROL L		<0.05	>0.05	>0.05	<0.05	<0.05	>0.05	>0.05	<0.05	<0.05	>0.05	>0.05	>0.05	>0.05	>0.05

Table A4.4 P-values for one-way ANOVA test and Hochberg post-tests to investigate the effect of ROL against ATR and dATR (photo)toxicity (corresponding to data in Fig. 6.12). ANOVA: $P < 0.001$.

	ATR D	ATR L	dATR D	dATR L
0.05 mM NAC	>0.05	>0.05	>0.05	>0.05
0.125 mM NAC	>0.05	>0.05	>0.05	>0.05
0.25 mM NAC	>0.05	>0.05	>0.05	>0.05
0.5 mM NAC	>0.05	>0.05	>0.05	>0.05
0.5 mM GSH	>0.05	>0.05	>0.05	>0.05

Table A4.5 P-values for one-way ANOVA test and Hochberg post-tests to test the effect of NAC and GSH against ATR and dATR (photo)toxicity (corresponding to data in Fig. 6.14). ANOVA: P <0.001.

	0.2 mM ATR D	0.2 mM ATR L	0.05 mM dATR D	0.05 mM dATR L
0.15 mM PXAL	>0.05	>0.05	>0.05	>0.05
0.25 mM PXAL	>0.05	>0.05	>0.05	>0.05
0.35 mM PXAL	>0.05	>0.05	>0.05	>0.05
0.15 mM PXAM	>0.05	>0.05	>0.05	>0.05
0.25 mM PXAM	>0.05	>0.05	>0.05	>0.05
0.35 mM PXAM	>0.05	>0.05	>0.05	>0.05

Table A4.4 P-values for one-way ANOVA test and Hochberg post-tests to test the effect of pyridoxal and pyridoxamine against ATR and dATR (photo)toxicity (corresponding to data in Fig. 6.16). ANOVA: P <0.001.

	control D	0.1 mM ATR D	ATR 15 µM VitE D	ATR 50 µM VitE D	0.05 mM dATR D	dATR 15 µM VitE D	dATR 25 µM VitE D	dATR 50 µM VitE D	Control L	0.1 mM ATR L	ATR 15 µM VitE L	ATR 50 µM VitE L	0.05 mM dATR L	dATR 15 µM VitE L	dATR 25 µM VitE L
0.1 mM ATR D	>0.05														
ATR 15 µM VitE D	>0.05	>0.05													
ATR 50 µM VitE D	>0.05	>0.05	>0.05												
0.05 mM dATR D	<0.05	<0.05	<0.05	<0.05											
dATR 15 µM VitE D	>0.05	>0.05	>0.05	>0.05	>0.05										
dATR 25 µM VitE D	>0.05	>0.05	>0.05	>0.05	>0.05	>0.05									
dATR 50 µM VitE D	>0.05	>0.05	>0.05	>0.05	<0.05	>0.05	>0.05								
0.1 mM ATR L		>0.05	>0.05	>0.05	<0.05	>0.05	>0.05	>0.05	>0.05						
ATR 15 µM VitE L		>0.05	>0.05	>0.05	<0.05	>0.05	>0.05	>0.05	>0.05	>0.05					
ATR 50 µM VitE L		>0.05	>0.05	>0.05	<0.05	>0.05	>0.05	>0.05	>0.05	>0.05	>0.05				
0.05 mM dATR L		<0.05	<0.05	<0.05	>0.05	>0.05	>0.05	<0.05	<0.05	<0.05	<0.05	<0.05			
dATR 15 µM VitE L		<0.05	<0.05	<0.05	>0.05	>0.05	>0.05	<0.05	<0.05	<0.05	<0.05	<0.05	>0.05		
dATR 25 µM VitE L		<0.05	<0.05	<0.05	>0.05	>0.05	>0.05	<0.05	<0.05	<0.05	<0.05	<0.05	>0.05	>0.05	
dATR 50 µM VitE L		>0.05	>0.05	>0.05	>0.05	>0.05	>0.05	>0.05	>0.05	>0.05	>0.05	>0.05	>0.05	>0.05	>0.05

Table A4.7 P-values for one-way ANOVA test and Hochberg post-tests to test the effect of vitamin E against ATR and dATR (photo)toxicity (corresponding to data in Fig. 6.18). ANOVA: $P < 0.001$.

DARK	Control	0% PE 1mM dATR	20% PE 1mM dATR	35% PE 1mM dATR
0% PE 1mM dATR	<0.05			
20% PE 1mM dATR	>0.05	<0.05		
35% PE 1mM dATR	>0.05	<0.05	>0.05	
55% PE 1mM dATR	>0.05	<0.05	>0.05	>0.05

LIGHT	Control	0% PE 0.05mM dATR	20% PE 1mM dATR0.05	35% PE 0.05mM dATR
0% PE 0.05mM dATR	<0.05			
20% PE 0.05mM dATR	>0.05	<0.05		
35% PE 0.05mM dATR	>0.05	<0.05	>0.05	
55% PE 0.05mM dATR	>0.05	<0.05	>0.05	>0.05

Table A4.8 P-values for one-way ANOVA test and Hochberg post-tests to test the effect of PE against dATR (photo)toxicity (corresponding to data in Fig. 6.18). ANOVA: DARK - $P < 0.001$, LIGHT - $P = 0.001$.

Appendix 5 – statistical results for Chapter 9

All P-values marked in grey are considered to be "not significant" (i.e. ≥0.05).

	D Unbl POS	D Gr light ATR 3.5x[opsin]	D Wh light ATR 3.5x[opsin]	L Unbl POS	L Gr light ATR 3.5x[opsin]	L Wh light ATR 3.5x[opsin]
D control	0.002	0.004	0.003			
D Gr light ATR 3.5x[opsin]	0.594					
D Wh light ATR 3.5x[opsin]	0.229	0.597				
L control				0.001	0.002	<0.001
L Unbl POS	0.034					
L Gr light ATR 3.5x[opsin]		0.044		0.194		
L Wh light ATR 3.5x[opsin]			0.013	0.069	0.901	

Table A5.1 P-values for t-test to compare mitochondrial activity of ARPE-19 cells of exposures to POS +/- ATR, unbleached or exposed to green or white light with addition of exogenous ATR at a concentration 3.5 times greater than opsin concentration (corresponding to data in Fig. 9.4).

	D control	D Unbl POS	D Green light POS	D White light POS	D Gr light ATR 1x[opsin]	D Gr light ATR 2x[opsin]	D Gr light ATR 3.5x[opsin]	D Wh light ATR 3.5x[opsin]	L control	L Unbl POS	L Green light POS	L White light POS	L Gr light ATR 1x[opsin]	L Gr light ATR 2x[opsin]	L Gr light ATR 3.5x[opsin]
D Unbl POS	<0.05														
D Green light POS	<0.05	>0.05													
D White light POS	<0.05	>0.05	>0.05												
D Gr light ATR 1x[opsin]	<0.05	>0.05	>0.05	>0.05											
D Gr light ATR 2x[opsin]	<0.05	>0.05	>0.05	>0.05	>0.05										
D Gr light ATR 3.5x[opsin]	<0.05	>0.05	>0.05	>0.05	>0.05	>0.05									
D Wh light ATR 3.5x[opsin]	<0.05	>0.05	>0.05	>0.05	>0.05	>0.05	>0.05								
L Unbl POS		>0.05	>0.05	>0.05	>0.05	>0.05	>0.05	>0.05	<0.05						
L Green light POS		>0.05	>0.05	>0.05	>0.05	>0.05	>0.05	>0.05	<0.05	>0.05					
L White light POS		>0.05	>0.05	>0.05	>0.05	>0.05	>0.05	>0.05	<0.05	>0.05	>0.05				
L Gr light ATR 1x[opsin]		>0.05	<0.05	<0.05	>0.05	>0.05	>0.05	>0.05	<0.05	>0.05	>0.05	>0.05			
L Gr light ATR 2x[opsin]		>0.05	<0.05	<0.05	>0.05	>0.05	>0.05	>0.05	<0.05	>0.05	>0.05	>0.05	>0.05		
L Gr light ATR 3.5x[opsin]		<0.05	<0.05	<0.05	<0.05	>0.05	>0.05	>0.05	<0.05	>0.05	>0.05	>0.05	>0.05	>0.05	
L Wh light ATR 3.5x[opsin]		<0.05	<0.05	<0.05	<0.05	>0.05	>0.05	>0.05	<0.05	>0.05	>0.05	>0.05	>0.05	>0.05	>0.05

Table A5.2 P-values for one-way ANOVA test and Hochberg post-tests to compare maximum fluorescence intensity in cell suspensions after excitation with 360 nm light (corresponding to data in Fig. 9.8 A). ANOVA: P <0.001.

	D control	D Unbl POS	D Green light POS	D White light POS	D Gr light ATR 1x[opsin]	D Gr light ATR 2x[opsin]	D Gr light ATR 3.5x[opsin]	D Wh light ATR 3.5x[opsin]	L control	L Unbl POS	L Green light POS	L White light POS	L Gr light ATR 1x[opsin]	L Gr light ATR 2x[opsin]	L Gr light ATR 3.5x[opsin]
D Unbl POS	<0.05														
D Green light POS	<0.05	>0.05													
D White light POS	<0.05	>0.05	>0.05												
D Gr light ATR 1x[opsin]	<0.05	>0.05	>0.05	>0.05											
D Gr light ATR 2x[opsin]	<0.05	>0.05	>0.05	>0.05	>0.05										
D Gr light ATR 3.5x[opsin]	<0.05	>0.05	>0.05	>0.05	>0.05	>0.05									
D Wh light ATR 3.5x[opsin]	<0.05	>0.05	>0.05	>0.05	>0.05	>0.05	>0.05								
L Unbl POS		<0.05	>0.05	>0.05	>0.05	>0.05	>0.05	>0.05	<0.05						
L Green light POS		<0.05	<0.05	<0.05	<0.05	<0.05	<0.05	<0.05	<0.05	>0.05					
L White light POS		<0.05	<0.05	<0.05	<0.05	<0.05	>0.05	>0.05	<0.05	>0.05	>0.05				
L Gr light ATR 1x[opsin]		<0.05	>0.05	<0.05	>0.05	>0.05	>0.05	>0.05	<0.05	>0.05	>0.05	>0.05			
L Gr light ATR 2x[opsin]		<0.05	<0.05	<0.05	<0.05	<0.05	<0.05	<0.05	<0.05	>0.05	>0.05	>0.05	>0.05		
L Gr light ATR 3.5x[opsin]		<0.05	<0.05	<0.05	<0.05	<0.05	>0.05	>0.05	<0.05	>0.05	>0.05	>0.05	>0.05	>0.05	
L Wh light ATR 3.5x[opsin]		<0.05	<0.05	<0.05	<0.05	<0.05	>0.05	>0.05	<0.05	>0.05	>0.05	>0.05	>0.05	>0.05	>0.05

Table A5.3 P-values for one-way ANOVA test and Hochberg post-tests to compare maximum fluorescence intensity in cell suspensions after excitation with 488 nm light (corresponding to data in Fig. 9.8 B). ANOVA: P <0.001.

	D control	D Unbl POS	D Gr light ATR 3.5x[opsin]	D Wh light ATR 3.5x[opsin]	L Unbl POS	L Gr light ATR 3.5x[opsin]	L Wh light ATR 3.5x[opsin]
D control							
D Unbl POS	<0.001		0.233	0.657			
D Gr light ATR 3.5x[opsin]	<0.001			0.404			
D Wh light ATR 3.5x[opsin]	<0.001						
L control	0.225				0.816	0.001	0.019
L Unbl POS		0.002				0.001	0.021
L Gr light ATR 3.5x[opsin]			0.115				0.114
L Wh light ATR 3.5x[opsin]				0.028			

Table A5.3 P-values for t-test to compare percentage of cytoplasmic area of the RPE occupied by the lipofuscin-like granules (corresponding to data in Fig. 9.10).

Appendix 6 – Conference presentations of this work

K Handzel, M Różanowska: *Photoreactivity and phototoxicity of Vitamin A derivatives.* Skin Focus Meeting, January 2008, Cardiff, UK (talk).

K Handzel, M Boulton, A Pawlak, M Różanowska, B Różanowski: *(Photo)toxicity of all-trans-retinal (ATR) and products of its degradation to the retinal pigment epithelium (RPE) and protection of antioxidants.* 2nd Meeting of the International Society for Ocular Cell Biology (ISOCB), September 2008, San Diego, USA (poster).

K Handzel, M Boulton, M Różanowska: *(Photo)toxicity of all-trans-retinal (ATR) and products of its degradation.* 8th Annual meeting of the Cardiff Institute of Tissue Engineering and Repair (CITER), September 2009, Cardiff, UK (poster).

K Handzel, M Boulton, M Różanowska: *Mechanistic insight into phototoxic effects of visual pigment photobleaching.* 13th Congress of the European Society for Photobiology, September 2009, Wroclaw, Poland (poster).

References

Abdulmajed K, Heard CM (2004) Topical delivery of retinyl ascorbate co-drug 1. Synthesis, penetration into and permeation across human skin. *International Journal of Pharmaceutics,* 280:113–24.

Abdulmajed K, McGuigan C, Heard CM (2005) Topical delivery of retinyl ascorbate: 4. Comparative anti-oxidant activity towards DPPH. *Free Radical Research*, 39:491-8.

Age-Related Eye Disease Study Research Group (2000) Risk factors associated with age-related macular degeneration. A case-control study in the age-related eye disease study: age-related eye disease study report number 3. *Ophthalmology*, 107:2224–32.

Ahuja S, Crocker E, Eilers M, Hornak V, Hirshfeld A, Ziliox M, Syrett N, Reeves PJ, Khorana HG, Sheves M, Smith SO (2009) Location of the retinal chromophore in the activated state of rhodopsin. *Journal of Biological Chemistry,* 284:1019–20.

Allikmets R (2000) Further evidence for an association of ABCR alleles with age-related macular degeneration. The International ABCR Screening Consortium. *American Journal of Human Genetics*, 67:487-91.

Allikmets R, Shroyer NF, Singh N, Seddon JM, Lewis RA, Bernstein PS, Peiffer A, Zabriskie NA, Li Y, Hutchinson A, Dean M, Lupski JR, Leppert M (1997) Mutation of the Stargardt disease gene (ABCR) in age-related macular degeneration. *Science*, 277:1805-7.

Altenbach C, Kusnetzow AK, Ernst OP, Hofmann KP, Hubbell WL (2008) High-resolution distance mapping in rhodopsin reveals the pattern of helix movement due to activation. *Proceedings of the National Academy of Sciences of the United States of America,* 105:7439-44.

Anderson DH, Fisher SK, Steinberg RH (1978) Mammalian cones: disc shedding, phagocytosis, and renewal. *Investigative Ophthalmology and Visual Science,* 17:117-33.

Arakawa M, Ito Y (2007) N-acetylcysteine and neurodegenerative diseases: Basic and clinical pharmacology. *Cerebellum (London, England),* pp. 1-7.

Aruoma O I, Halliwell B, Hoey B M, Butler J (1989) The antioxidant action of N-acetylcysteine: Its reaction with hydrogen peroxide, hydroxyl radical, superoxide, and hypochlorous acid. *Free Radical Biology & Medicine*, 6:593–7.

Baron MH, Coulange MJ, Coupry C, Baron D, Favrot J, Aly MMA (1989) All-trans retinal photoisomerization and photooxidation from UV laser radiation. Vibrational assignments of all-trans 5,8-peroxyretinal. *Photochemistry and Photobiology*, 49:739-51.

Barouch FC, Miller JW (2007) The role of inflammation and infection in age-related macular degeneration. *International Ophthalmology Clinics,* 47:185-97.

Bartl FJ, Vogel R (2007) Structural and functional properties of metarhodopsin III: recent spectroscopic studies on deactivation pathways of rhodopsin. *Physical Chemistry Chemical Physics: PCCP*, 9:1648-58.

Bazan HEP, Bazan N G, Feeney-Burns L, Berman ER (1990) Lipids in human lipofuscin-enriched subcellular fractions of two age populations: comparison with rod outer segments and neural retina. *Investigative Ophthalmology & Visual Science,* 31:1433-43.

Beatty S, Koh H, Phil M, Henson D, Boulton M (2000) The role of oxidative stress in the pathogenesis of age-related macular degeneration. *Survey of Ophthalmology,* 45:115-34.

Ben-Shabat S, Parish CA, Vollmer HR, Itagaki Y, Fishkin N, Nakanishi K, Sparrow JR (2002) Biosynthetic studies of A2E, a major fluorophore of retinal pigment epithelial lipofuscin. *The Journal of Biological Chemistry,* 277:7183-90.

Berendschot TT, Willemse-Assink JJ, Bastiaanse M, de Jong PT, van Norren D (2002) Macular pigment and melanin in age-related maculopathy in a general population. *Investigative Ophthalmology & Visual Science,* 43:1928–32.

Berg JM, Tymoczko JL, Stryer L (2002) The biosynthesis of Amino Acids. *Biochemistry*. 5th edition; W. H. Freeman and Company.

Berger JW, Fine SL, Maguire MG (1999) Age-related macular degeneration. Mosby, Inc.

Bergmann M, Schütt F, Holz FG, Kopitz J (2004) Inhibition of the ATP-driven proton pump in RPE lysosomes by the major lipofuscin fluorophore A2-E may contribute to the pathogenesis of age-related macular degeneration. *The FASEB journal: official publication of the Federation of American Societies for Experimental Biology,* 18:562-4.

Berman ER (1971) Acid hydrolases of the retinal pigment epithelium. *Investigative Ophthalmology,* 10:64-8.

Bernas T, Dobrucki J (1999) Reduction of a tetrazolium salt, CTC, by intact HepG2 human hepatoma cells: subcellular localisation of reducing systems. *Biochimica et Biophysica Acta*, 51:73-81.

Bernstein PS (1999) Macular biology. In: Berger, JW, Fine, SL, and Maguire, MG [eds.] *Age-related Macular Degeneration.* Mosby, pp. 1-16.

Besharse JC, Hollyfield JG, and Rayborn ME (1977) Turnover of rod photoreceptor outer segments. II. Membrane addition and loss in relationship to light. *The Journal of Cell Biology*, 75:507-27.

Bhattacharyya K, Das PK (1985) Quantitative aspects of all-trans-retinol singlet and triplet quenching by oxygen. *Chemical Physics Letters,* 116:326-32.

Bhutto IA, McLeod DS, Hasegawa T, Kim SY, Merges C, Tong P, Lutty GA (2006) Pigment epithelium-derived factor (PEDF) and vascular endothelial growth factor (VEGF) in aged human choroid and eyes with age-related macular degeneration. *Experimental Eye Research,* 82:99-110.

Bisby RH, Morgan CG, Hamblett I, Gorman AA (1999) Quenching of singlet oxygen by trolox C, ascorbate, and amino acids: effects of ph and temperature, *The Journal of Physical Chemistry A,* 103:7454–59.

Boettner E A, Wolter J R (1962) *Transmission of the Ocular Media. Investigative Ophthalmology & Visual Science,* 1:776-83.

Bohm F, Edge R, Lange L, Truscott TG (1998) Enhanced protection of human cells against ultraviolet light by antioxidant combinations involving dietary carotenoids. *The Journal of Photochemistry and Photobiology B: Biology,* 44:211–5.

Bok D (1985) Retinal photoreceptor-pigment epithelium interactions. Friedenwald lecture. *Ophthalmology & Visual Science,* 26:1659-94.

Borhan B, Souto ML, Imai H, Shichida Y, Nakanishi K. (2000) Movement of retinal along the visual transduction path. *Science*, 288:2209-12.

Boulton M (1998) Melanin and the RPE. *The Retinal Pigment Epithelium.* New York: Oxford University Press, pp. 68-85.

Boulton M, Docchio F, Dayhaw-Barker P, Ramponi R, Cubeddu R (1990) Age-related changes in the morphology, absorption and fluorescence of melanosomes and lipofuscin granules of the retinal pigment epithelium. *Vision Research*, 30:1291-303.

Boulton M, Dontsov A, Jarvis-Evans J, Ostrovsky M, Svistunenko D (1993) Lipofuscin is a photoinducible free radical generator. *Journal of Photochemistry and Photobiology B: Biology,* 19:201-4.

Boulton M, Marshall J (1985) Repigmentation of human retinal pigment epithelial cells in vitro. *Experimental Eye Research,* 41:209-18.

Boulton M, McKechnie N M, Breda J, Bayly M, Marshall J (1989) The formation of autofluorescent granules in cultured human RPE. *Investigative Ophthalmology & Visual Science,* 30:82-9.

Boulton M, Różanowska M, Różanowski B (2001) Retinal photodamage. *Journal of Photochemistry and Photobiology. B: Biology,* 64:144-61.

Boulton M, Różanowska M, Różanowski B, Wess T (2004) The photoreactivity of ocular lipofuscin. *Photochemistry and Photobiology*, 3:759-64.

Bressler SB, Munoz B, Solomon SD, West SK (2008) Racial differences in the prevalence of age-related macular degeneration: The Salisbury eye evaluation (SEE) project. *Archives* of *Ophthalmology,* 126:241–5.

Brigelius-Flohe R, Banning A, Schnurr K (2003) Selenium-dependent enzymes in endothelial cell function. *Antioxidants & Redox Signalling*, 5:205–15.

Burke JM, Skumatz CM (1998) Autofluorescent inclusions in long-term postconfluent cultures of retinal pigment epithelium. *Investigative Ophthalmology & Visual Science*, 39:1478-86.

Catalá A (2006) An overview of lipid peroxidation with emphasis in outer segments of photoreceptors and the chemiluminescence assay. *The International Journal of Biochemistry & Cell Biology*, 38:1482-95.

Chader GJ, Pepperberg DR, Crouch R, and Wiggert B (1998) Retinoids and the retinal pigment epithelium. In: Marmor, MF, and Wolfensberger, TJ [eds.] *The Retinal Pigment Epithelium.* New York: Oxford University Press, pp. 135-51.

Chattopadhyay SK, Kumar CV, Das PK (1984) Laser flash photolytic determination of triplet yields via singlet oxygen generation. *Journal of Photochemistry,* 24:1-9.

Chen C, Blakeley LR, Koutalos Y (2009) Formation of all-*trans* retinol after visual pigment bleaching in mouse photoreceptors. *Investigative Ophthalmology and Visual Science,* 50:3589-95.

Chen C, Tsina E, Cornwall MC, Crouch RK, Vijayaraghavan S, Koutalos Y (2005) Reduction of all-trans retinal to all-trans retinol in the outer segments of frog and mouse rod photoreceptors. *Biophysical Journal,* 88:2278-87.

Choe E (2008) Effects and mechanisms of minor compounds in oil on lipid oxidation. In: Akoh CC, Min DB [eds.] Food lipids. Chemistry, Nutrition, and Biotechnology. 3rd ed. Boca Raton: Taylor & Francis Group, pp. 449-74.

Christen WG, Glynn RJ, Chew EY, Albert CM, Manson JE (2009) Folic acid, pyridoxine, and cyanocobalamin combination treatment and age-related macular Ddegeneration in women. *Archives of Internal Medicine*, 169:335-41.

Clemons TE, Milton RC, Klein R, Seddon JM, Ferris FL III, Age-related eye disease study research group (2005) Risk factors for the incidence of advanced age-related macular degeneration in the age-related eye disease study (AREDS) AREDS report no. 19. *Ophthalmology,* 112:533–9.

Clennan EL, Noe LJ, Wen T, Szneler E (1989) Solvent effects on the ability of amines to physically quench singlet oxygen as determined by time-resolved infrared emission studies. *The Journal of Organic Chemistry*, 54:3581-4.

Cohen AI (1992) The retina. In: Hart, W [ed.] *Adler's Physiology of the Eye.* (9 edn.) Mosby, pp. 579-616.

Constable IJ (2004) Age-related macular degeneration and its possible prevention. *The Medical Journal of Australia,* 181:471-2.

Cook HL, Patel PJ,Tufail A (2008) Age-related macular degeneration: diagnosis and management. *British Medical Bulletin*, 85:127-49.

Cort WM (1974) Antioxidant activity of tocopherols, ascorbyl palmitate, and ascorbic acid and their mode of action. *Journal of the American Oil Chemists' Society*, 51:321-5.

Crocker E, Eilers M, Ahuja, Hornak V, Hirshfeld A, Sheves M, Smith SO (2006) Location of Trp265 in metarhodopsin II: Implications for the activation mechanism of the visual receptor rhodopsin. *Journal of Molecular Biology*, 357:163-72.

Cruickshanks KJ, Klein R, Klein BE (1993) Sunlight and age-related macular degeneration: The beaver dam eye study. *Archives of Ophthalmology,* 111:514–8.

Curcio CA, Medeiros NE, Millican CL (1996) Photoreceptor loss in age-related macular degeneration. *Investigative Ophthalmology & Visual science*, 37:1236-49.

Curcio CA, Millican CL, Allen KA, Kalina RE (1993) Aging of the human photoreceptor mosaic: evidence for selective vulnerability of rods in central retina. *Investigative Ophthalmology & Visual Science,* 34:3278–96.

Darmanyan AP (1993) Mechanism of singlet oxygen interaction with solvent removing prohibition of the radiative $^1\Delta_g \rightarrow {}^3\Sigma^-_g$ transition in oxygen. *Chemical Physics Letters*, 215:477-82.

Darzins P, Mitchell P, Heller RF (1997) Sun exposure and age-related macular degeneration. An Australian case-control study. *Ophthalmology*, 104:770–6.

D'Cruz PM, Yasumura D, Weir J, Matthes MT, Abderrahim H, LaVail MM, Vollrath D (2000) Mutation of the receptor tyrosine kinase gene Mertk in the retinal dystrophic RCS rat. *Human Molecular Genetics*, 9:645-51.

Deadwyler G, Sima PD, Fu Y, Kanofsky JR (1997) Singlet oxygen-mediated inactivation of acetylcholinesterase: a comparison of purified enzyme in solution and enzyme bound to K562 leukemia cells. *Photochemistry and Photobiology,* 65:884-94.

Dean RT, Fu S, Stocker R, Davies MJ (1997) Biochemistry and pathology of radical-mediated protein oxidation. *Biochemical Journal*, 324:1–18.

Delcourt C, Carrière I, Ponton-Sanchez A, Fourrey S, Lacroux A, Papoz L; POLA Study Group (2001) Light exposure and the risk of age-related macular degeneration: the Pathologies Oculaires Liées à l'Age (POLA) study. *Archives of Ophthalmology,* 119:1463-8.

Delcourt C, Diaz JL, Ponton-Sanchez A, Papoz L (1998) Smoking and age-related macular degeneration. The POLA Study. Pathologies Oculaires Liées à l'Age. *Archives of Ophthalmology*, 116:1031–5.

Delmelle M (1977) Retinal damage by light: possible implication of singlet oxygen. *Biophysics of structure and Mechanism,* 3:195-8.

Delmelle M (1978a) An investigation of retinal as a source of singlet oxygen. *Photochemistry and Photobiology,* 27:731–4.

Delmelle M (1978b) Retinal sensitized photodynamic damage to liposomes. *Photochemistry and Photobiology,* 28:357-60.

Dillon J, Gaillard ER, Bilski P, Chignell CF, Reszka KJ (1996) The photochemistry of the retinoids as studied by steady-state and pulsed methods. *Photochemistry and Photobiology,* 63:680-5.

Dillon J, Zheng L, Merriam JC, Gaillard ER (2004) Transmission of light to the aging human retina: possible implications for age related macular degeneration. *Experimental Eye Research*, 79:753-9.

Ding X, Patel M, Chan CC (2009) Molecular pathology of age-related macular degeneration. *Progress in Retinal and Eye Research*, 28:1-18.

Dontsov AE, Glickman RD, Ostrovsky MA (1999) Retinal pigment epithelium pigment granules stimulate the photo-oxidation of unsaturated fatty acids. *Free Radical Biology and Medicine,* 26:1436-46.

Dorey CK, Wu G, Ebenstein D, Garsd A, Weiter JJ (1989) Cell loss in the aging retina. Relationship to lipofuscin accumulation and macular degeneration. *Investigative Ophthalmology & Visual Science*, 30:1691-9.

Dowling JE, Sidman RL (1962) Inherited retinal dystrophy in the rat. *The Journal of Cell Biology*, 14:73–109.

Dunn KC, Aotaki-Keen AE, Putkey FR, and Hjelmeland LM (1996) ARPE-19, a human retinal pigment epithelial cell line with differentiated properties. *Experimental Eye Research,* 62:155-69.

Eldred GE (1998) Lipofuscin and other lysosomal storage deposits in the retinal pigment epithelium. In: Marmor, MF, and Wolfensberger, TJ [eds.] *The retinal pigment epithelium.* New York: Oxford University Press, pp. 651-68.

Engin KN (2009) Alpha-tocopherol: looking beyond an antioxidant. *Molecular Vision*, 15:855-60.

Fan J, Rohrer B, Frederick JM, Baehr W, Crouch RK (2008) *Rpe65*$^{-/-}$ and *Lrat*$^{-/-}$ mice: Comparable models of leber congenital amaurosis. *Investigative Ophthalmology and Visual Science*, 49:2384-9.

Fan J, Rohrer B, Moiseyev G, Ma J, Crouch RK (2003) Isorhodopsin rather than rhodopsin mediates rod function in RPE65 knock-out mice. *Proceedings of the National Academy of Sciences of the United States of America,* 100:13662–7.

Feeney L (1978) Lipofuscin and melanin of human retinal pigment epithelium. Fluorescence, enzyme cytochemical, and ultrastructural studies. *Investigative Ophthalmology & Visual Science*, 17:583-600.

Finnemann SC, Leung LW, Rodriguez-Boulan E (2002) The lipofuscin component A2E selectively inhibits phagolysosomal degradation of photoreceptor phospholipid by the retinal pigment epithelium. *The Proceedings of the National Academy of Sciences of the United States of America*, 99:3842-7.

Finnemann SC, Silverstein RL (2001) Differential roles of CD36 and αvβ5 integrin in photoreceptor phagocytosis by the retinal pigment epithelium. *Journal of Experimental Medicine,* 194:1289-98.

Fisher D, Lichti FU, Lucy JA (1972) Environmental effects on the autoxidation of retinol. *The Biochemical Journal*, 130:259-70.

Fishkin N, Jang YP, Itagaki Y, Sparrow JR, Nakanishi K (2003) A2-rhodopsin: a new fluorophore isolated from photoreceptor outer segments. *Organic & Biomolecular Chemistry,* 1:1101-5.

Fishkin NE, Sparrow JR, Allikmets R, Nakanishi K (2005) Isolation and characterization of a retinal pigment epithelial cell fluorophore: an all-trans-

retinal dimer conjugate. *Proceedings of the National Academy of Sciences of the United States of America,* 102:7091-6.

Fliesler SJ, Anderson RE (1983) Chemistry and metabolism of lipids in the vertebrate retina. *Progress in Lipid Research*, 22:79-131.

Forrester JV, Dick AD, McMenamin PG, Lee WR (2002) Anatomy of the eye and orbit. In: Forrester JV, Dick AD, McMenamin PG, Lee WR *[eds]. The Eye: Basic Sciences in Practice. Philadelphia: WB Saunders*, pp. 1-98.

Fox JA, Pfeffer BA, Fain GL (1988) Single-channel recordings from cultured human retinal pigment epithelial cells. *The Journal of General Physiology*, 91:193-222.

Friedman DS, Katz J, Bressler NM, Rahmani B, Tielsch JM (1999) Racial differences in the prevalence of age-related macular degeneration: The Baltimore eye survey. *Ophthalmology,* 106:1049–55.

Friedman E, Kuwabara T (1968) The retinal pigment epithelium. IV. The damaging effects of radiant energy. *Archives of Ophthalmology*, 80:265-79.

Fu PP, Cheng SH, Coop L, Xia Q, Culp SJ, Tolleson WH, Wamer W G, Howard PC (2003) Photoreaction, phototoxicity, and photocarcinogenicity of retinoids. *Journal of Environmental Science and Health. Part C, Environmental Carcinogenesis & Ecotoxicology Reviews,* 21:165-97.

Gal A, Li Y, Thompson DA, Weir J, Orth U, Jacobson SG, Apfelstedt-Sylla E, Vollrath D (2000) Mutations in MERTK, the human orthologue of the RCS rat retinal dystrophy gene, cause retinitis pigmentosa. *Nature Genetics*, 26:270-1.

Gao H, Hollyfield JG (1992) Aging of the human retina: differential loss of neurons and retinal pigment epithelial cells. *Investigative Ophthalmology & Visual Science*, 33:1-17.

Glenn JV, Stitt AW (2009) The role of advanced glycation end products in retinal ageing and disease. *Biochimica et Biophysica Acta*, 1790:1109-16.

Golczak M, Imanishi Y, Kuksa V, Maeda T, Kubota R, Palczewski K (2005a) Lecithin: Retinol acyltransferase is responsible for amidation of retinylamine, a potent inhibitor of the retinoid cycle. *The Journal of Biological Chemistry*, 280:42263-73.

Golczak M, Kuksa V, Maeda T, Moise AR, Palczewski K (2005b) Positively charged retinoids are potent and selective inhibitors of the trans-cis isomerization in the retinoid (visual) cycle. *Proceedings of the National Academy of Sciences of the United States of America*, 102:8162-7.

Golczak M, Maeda A, Bereta G, Maeda T, Kiser PD, Hunzelmann S, von Lintig J, Blaner WS, Palczewski K (2008) Metabolic basis of visual cycle inhibition by retinoid and nonretinoid compounds in the vertebrate retina. *The Journal of Biological Chemistry,* 283:9543-54.

Gollapalli DR, Rando RR (2004) The specific binding of retinoic acid to RPE65 and approaches to the treatment of macular degeneration. *Proceedings of the National Academy of Sciences of the United States of America*, 101:10030-5.

Gonzalez-Fernandez F, Bevilacqua T, Lee KI, Chandrashekar R, Hsu L, Garlipp MA, Griswold JB, Crouch RK, Ghosh D (2009) Retinol-binding site in interphotoreceptor retinoid-binding protein (IRBP): A novel hydrophobic cavity. *Investigative Ophthalmology & Visual Science*, 50:5577-86.

Gorgels T, van Norren D (1995) Ultraviolet and green light cause different types of damage in rat retina. *Investigative Ophthalmology & Visual Science,* 36:851-63.

Grau S, Richards PJ, Kerr B, Hughes C, Caterson B, Williams AS, Junker U, Jones SA, Clausen T, Ehrmann M (2006) The role of human HtrA1 in arthritic disease, *The Journal of Biological Chemistry*, 28:6124–9.

Grimm C, Wenzel A, Hafezi F, Yu S, Redmond TM, Reme CM (2000) Protection of RPE65-deficient mice identifies rhodopsin as a mediator of light-induced retinal degeneration. *Nature Genetics*, 25:63–6.

Grimm C, Wenzel A, Williams TP, Rol PO, Hafezi F, Reme CE (2001) Rhodopsin-mediated blue-light damage to the rat retina: Effect of photoreversal of bleaching. *Investigative Ophthalmology & Visual Science,* 42:497–505.

Gu X R, Meer SG, Miyagi M, Rayborn ME, Hollyfield JG, Crabb JW, Salomon RG (2003) Carboxyethylpyrrole protein adducts and autoantibodies, biomarkers for age-related macular degeneration. *Journal of Biological Chemistry,* 278:42027-35.

Guajardo M, Terrasa A, Catalá A (1998) The effect of α-tocopherol, all-trans retinol and retinyl palmitate on the non enzymatic lipid peroxidation of rod outer segments. *Molecular and Cellular Biochemistry,* 197:173–8.

Guymer RH, Héon E, Lotery AJ, Munier FL, Schorderet DF, Baird PN, McNeil RJ, Haines H, Sheffield VC, Stone EM (2001) Variation of codons 1961 and 2177 of the Stargardt disease gene is not associated with age-related macular degeneration. *Archives of Ophthalmology*, 119:745-51.

Haeseleer F, Jang GF, Imanishi Y, Driessen CA, Matsumura M, Nelson PS, Palczewski K (2002) Dual-substrate specificity short chain retinol dehydrogenases from the vertebrate retina. *The Journal of Biological Chemistry,* 277:45537-46.

Halliwell B, Gutteridge JMC (2007) Cellular responses to oxidative stress. In: *Free Radicals in Biology and Medicine.* New York: Oxford University Press Inc.

Ham W Jr, Ruffolo J, Mueller H, Clarke A, Moon M (1978) Histologic analysis of photochemical lesions produced in rhesus retina by short-wavelength light. *Investigative Ophthalmology & Visual Science,* 17:1029–35.

Ham WT, Mueller HA, Ruffolo JJ, Guerry D, Guerry RK (1982) Action spectrum for retinal injury from near-ultraviolet radiation in the aphakic monkey. *American Journal of Ophthalmology,* 93:299–306.

Haralampus-Grynaviski NM, Lamb LE, Clancy CM, Skumatz C, Burke JM, Sarna T, Simon JD (2003) Spectroscopic and morphological studies of human retinal lipofuscin granules. *Proceedings of the National Academy of Sciences of the United States of America*, 100:3179-84.

Harper WS, Gaillard ER (2001) Studies of all-trans-retinal as a photooxidizing agent. Studies of all-trans-retinal as a photooxidizing agent. *Photochemistry and Photobiology,* 73:71-6.

Harwerth RS, Sperling HG (1975) Effects of intense visible radiation on the increment-threshold spectral sensitivity of the rhesus monkey eye. *Vision Research,* 15:1193–204.

Hayes JD, Flanagan JU, Jowsey IR (2005) Glutathione transferases. *Annual Review of Pharmacology and Toxicology*, 45:51-88.

He X, Hahn P, Iacovelli J, Wong R, King C, Bhisitkul R, Massaro-Giordano M, Dunaief JL (2007) Iron homeostasis and toxicity in retinal degeneration. *Progress in Retinal and Eye Research*, 26:649-73.

Heck M, Schadel SA, Maretzki D, Bartl FJ, Ritter E, Palczewski K, Hofmann KP (2003) Signaling states of rhodopsin. Formation of the storage form, metarhodopsin III, from active metarhodopsin II. *The Journal of Biological Chemistry*, 278:3162-9.

Heckenlively JR, Rodriguez JA, Daiger SP (1991) Autosomal dominant sectoral retinitis-pigmentosa—2 families with transversion mutation in codon 23 of rhodopsin. *Archives of Ophthalmology*, 109:84–91.

Herrera E, Barbas C (2001) Vitamin E: action, metabolism and perspectives. *Journal of Physiology and Biochemistry*, 57:43-56.

Higgins GT, Wang JH, Dockery P, Cleary PE, Redmond HP (2003) Induction of angiogenic cytokine expression in cultured RPE by ingestion of oxidized photoreceptor outer segments. *Investigative Ophthalmology & Visual Science*, 44:1775-82.

Higuchi O, Nakagawa K, Tsuzuki T, Suzuki T, Oikawa S, Miyazawa T (2006) Aminophospholipid glycation and its inhibitor screening system: A new role of pyridoxal 59-phosphate as the inhibitor. *Journal of Lipid Research*, 47:964-74.

Hildebrand PW, Scheerer P, Park JH, Choe HW, Piechnick R, Ernst OP, Hofmann KP, Heck M (2009) A ligand channel through the G protein coupled receptor opsin. *PloS one*, 4:e4382.

Hirakawa M, Tanaka M, Tanaka Y, Okubo A, Koriyama C, Tsuji M, Akiba S, Miyamoto K, Hillebrand G, Yamashita T, Sakamoto T (2008) Age-related maculopathy and sunlight exposure evaluated by objective measurement. *The British Journal of Ophthalmology,* 92:630-4.

Holz FG, Schütt F, Kopitz J, Eldred GE, Kruse FE, Völcker HE, Cantz M (1999) Inhibition of lysosomal degradative functions in the RPE by a retinoid component of lipofuscin. *Investigative Ophthalmology & Visual Science,* 40:737-43.

Hoppe G, O'Neil J, Hoff HF, Sears J (2004a) Products of lipid peroxidation induce missorting of the principal lysosomal protease in retinal pigment epithelium. *Biochimica et Biophysica Acta (BBA) - Molecular Basis of Disease,* 1689:33-41.

Hoppe G, O'Neil J, Hoff HF, Sears J (2004b) Accumulation of oxidized lipid-protein complexes alters phagosome maturation in retinal pigment epithelium. *Cellular and Molecular Life Sciences*, 61:1664-74.

Hubbard R, Wald (1952) Cis-trans isomers of vitamin A and retinene in the rhodopsin system. *The Journal of General Physiology*, 36:269-315.

Hyman L, Scahchat AP, He Q, Leske MC (2000) Hypertension, cardiovascular disease, and age-related macular degeneration. Age-related macular degeneration risk factors study group. *Archives of Ophthalmology*, 118:351–8.

Ishizawa Y, Pidikiti R, Liebman PA, and Eckenhoff RG (2002) G protein-coupled receptors as direct targets of inhaled anesthetics. *Molecular Pharmacology,* 61:945-52.

Jablonski MM, Tombran-Tink J, Mrazek DA, Iannaccone A (2000) Pigment epithelium-derived factor supports normal development of photoreceptor neurons and opsin expression after retinal pigment epithelium removal. *The Journal* of *Neuroscience,* 20:7149-57.

Janeway CA, Travers P, Walport M, Shlomchik M (2001) An introduction to immunology and innate immunity. *Immunobiology: The Immune System in Health and Disease*, 5th ed. New York: Garland Science.

Jessup W, Dean RT, Gerbicki JM (1994) Iodometric determination of hydroperoxides in lipids and proteins. *Methods in Enzymology*, Vol. 233: 292–303. New York: Academic Press.

Johnson EJ (2005) Obesity, lutein metabolism, and age-related macular degeneration: a web of connections. *Nutrition Reviews*, 63:9–15.

Kaemmerer E, Schutt F, Krohne TU, Holz FG, Kopitz J (2007) Effects of lipid peroxidation-related protein modifications on RPE lysosomal functions and POS phagocytosis. *Investigative Ophthalmology & Visual Science*, 48:1342-7.

Kaplan MW (1985) Distribution and axial diffusion of retinol in bleached rod outer segments of frogs (Rana pipiens). *Experimental Eye Research*, 40:721-9.

Katta S, Kaur I, Chakrabarti S (2009) The molecular genetic basis of age-related macular degeneration: an overview. *Journal of Genetics*, 88:425-49.

Katz ML (1989) Incomplete proteolysis may contribute to lipofuscin accumulation in the retinal pigment epithelium. *Advances in Experimental Medicine and Biology*, 266:109-16; discussion 116-8.

Katz ML (2002) Potential role of retinal pigment epithelial lipofuscin accumulation in age-related macular degeneration. *Archives of Gerontology and Geriatrics*, 34:359-70.

Katz ML and Robison WG (1986) Evidence of cell loss from the rat retina during senescence. *Experimental Eye Research,* 42:293–304.

Katz ML, Christianson JS, Gao CL, Handelman GJ (1994) Iron-induced fluorescence in the retina: Dependence on vitamin A. *Investigative Ophthalmology & Visual Science*, 35:3613-24.

Katz ML, Gao CL, Rice LM (1999) Long-term variations in cyclic light intensity and dietary vitamin A intake modulate lipofuscin content of the retinal pigment epithelium. *Journal* of *Neuroscience Research*, 57:106–16.

Katz ML, Redmond TM (2001) Effect of RPE65 knockout on accumulation of lipofuscin fluorophores in the retinal pigment epithelium. *Investigative Ophthalmology & Visual Science*, 42:3023–30.

Keller C, Grimm C, Wenzel A, Hafezi F, Remé CE (2001) Protective effect of halothane anesthesia on retinal light damage: Inhibition of metabolic rhodopsin regeneration. *Investigative Ophthalmology & Visual Science,* 42:476-80.

Kennedy CJ, Rakoczy PE, Constable IJ (1995) Lipofuscin of the retinal pigment epithelium: A review. *Eye,* 9:763-71.

Kennedy CJ, Rakoczy PE, Robertson TA, Papadimitriou JM, Constable IJ (1994) Kinetic studies on phagocytosis and lysosomal digestion of rod outer segments by human retinal pigment epithelial cells in vitro. *Experimental Cell Research,* 210:209-14.

Kessler M, Ubeaud G, Walter T, Sturm F, Jung L (2002) Free radical scavenging and skin penetration of troxerutin and vitamin derivatives. *The Journal of Dermatological Treatment*, 13:133-41.

Khan JC, Shahid H, Thurlby DA, Bradley M, Clayton DG, Moore AT, Bird AC, Yates JRW, (2006) Age related macular degeneration and sun exposure, iris color, and skin sensitivity to sunlight. *British Journal* of *Ophthalmology,* 90:29–32.

Kim SR, Fishkin N, Kong J, Nakanishi K, Allikmets R, Sparrow JR (2004) Rpe65 Leu450Met variant is associated with reduced levels of the retinal pigment epithelium lipofuscin fluorophores A2E and iso-A2E. *Proceedings of the National Academy of Sciences, USA,* 101:11668–72.

Kim SR, Jang YP, Sparrow JR (2010) Photooxidation of RPE lipofuscin bisretinoids enhances fluorescence intensity. *Vision Research,* 50:729-36.

Kindzelskii AL, Elner VM, Elner SG, Yang D, Hughes BA, Petty HR (2004) Toll-like receptor 4 (TLR4) of retinal pigment epithelial cells participates in transmembrane signaling in response to photoreceptor outer segments. *The Journal of General Physiology*, 124:139-49.

Kinlay S, Fang JC, Hikita H, Ho I, Delagrange DM, Frei B, Suh JH, Gerhard M, Creager MA, Selwyn AP, Ganz P (1999) Plasma α-tocopherol and coronary endothelium-dependent vasodilator function. *Circulation,* Brief Rapid Communications, 100:219-21.

Kirkness CM (1986) Do ophthalmic instruments pose a hazard of light-induced damage to the eye? In Hazards of Light; Myths & Realities; Eye and Skin, 1st edition (Edited by J. Cronly-Dillon, E. S. Rosen and J. Marshall), pp. 179–86. Pergamon Press, Oxford.

Klaver CC, Kliffen M, van Duijn CM, Hofman A, Cruts M, Grobbee DE, van Broeckhoven C, de Jong PT (1998) Genetic association of apolipoprotein E with age-related macular degeneration. *The American Journal of Human Genetics*, 63:200–6.

Klein ML, Mauldin WM, Stoumbos VD (1994) Heredity and age-related macular degeneration. Observations in monozygotic twins. *Archives of Ophthalmology*, 112:932–7.

Krasnovsky AA Jr, Kagan VE (1979) Photosensitization and quenching of singlet oxygen by pigments and lipids of photoreceptor cells of the retina. *FEBS letters*, 108:152-4.

Kuksa V, Imanishi Y, Batten M, Palczewski K, Moise AR (2003) Retinoid cycle in the vertebrate retina: Experimental approaches and mechanisms of isomerisation. *Vision Research,* 43:2959–81.

Kuroiwa S, Kojima H, Kikuchi T, Yoshimura N (1999) ATP binding cassette transporter retina genotypes and age related macular degeneration: An analysis on exudative non-familial Japanese patients. *The British Journal of Ophthalmology*, 83:613-5.

Lamb LE, Simon JD (2004) A2E: A component of ocular lipofuscin. *Photochemistry and Photobiology*, 79:127-36.

Lamb TD, Pugh EN (2004) Dark adaptation and the retinoid cycle of vision. *Progress in Retinal and Eye Research*, 23:307–80.

Launay S, Maubert E, Lebeurrier N, Tennstaedt A, Campioni M, Docagne F, Gabriel C, Dauphinot L, Potier MC, Ehrmann M, Baldi A, Vivien D (2008) HtrA1-dependent proteolysis of TGF-beta controls both neuronal maturation and developmental survival. *Cell Death & Differentiation*, 15:1408–16.

LaVail MM, Gorrin GM, Yasumura D, Matthes MT (1999) Increased susceptibility to constant light in nr and pcd mice with inherited retinal degenerations. *Investigative Ophthalmology & Visual Science*, 40:1020-4.

Law WC, Rando RR (1989) The molecular basis of retinoic acid induced night blindness. *Biochemical and Biophysical Research Communications,* 161:825–9.

Lea CH (1931) The effect of light on the oxidation of fats. *Proceedings of the Royal Society of London (London) B,* 108:175–89.

Lee KH, Jung MY, Kim SY (1999) Quenching mechanism and kinetics of ascorbyl palmitate for the reduction of the gamma irradiation-induced oxidation of oils. *Journal of the American Oil Chemists' Society*, 76:921- 5.

Lentrichia BB, Bruner WE, and Kean EL (1978) Glycosidases of the retinal pigment epithelium. *Investigative Ophthalmology & Visual Science,* 17:884-95.

Lin SW and Sakmar TP (1996) Specific tryptophan UV-absorbance changes are probes of the transition of rhodopsin to its active state. *Biochemistry,* 35:11149-59.

Liu J, Itagaki Y, Ben-Shabat S, Nakanishi K, Sparrow JR (2000) The biosynthesis of A2E, a fluorophore of aging retina, involves the formation of the precursor, A2-PE, in the photoreceptor outer segment membrane. *The Journal of Biological Chemistry*, 275:29354-60.

Loew A, Baer C, Gonzalez-Fernandez F (2001) The functional unit of interphotoreceptor retinoid-binding protein (IRBP)--purification, characterization and preliminary crystallographic analysis. *Experimental Eye Research*, 73:257-64.

Loginova MY, Rostovtseva YV, Feldman TB, Ostrovsky MA (2008) Light damaging action of all-trans-retinal and its derivatives on rhodopsin molecules in the photoreceptor membrane. *Biochemistry (Moscow)*, 73:130-8.

Lopez PF, Sippy BD, Lambert HM, Thach AB, Hinton DR (1996) Transdifferentiated retinal pigment epithelial cells are immunoreactive for vascular endothelial growth factor in surgically excised age- related macular degeneration-related choroidal neovascular membranes. *Investigative Ophthalmology & Visual Science*, 37:855-68.

Lukiw WJ, Mukherjee PK, Cui JG, Bazan NG (2006) A2E selectively induces cox-2 in ARPE-19 and human neural cells. *Current Eye Research*, 31:259-63.

MacDonald PN, Ong DE (1987) Binding specificities of cellular retinol-binding protein and cellular retinol-binding protein, type II. *The Journal of Biological Chemistry*, 262:10550-6.

Maeda A, Golczak M, Maeda T, Palczewski K (2009) Limited roles of Rdh8, Rdh12, and Abca4 in all-trans-retinal clearance in mouse retina. *Investigative Ophthalmology & Visual Science*, 50:5435-43.

Maeda A, Maeda T, Golczak M, Chou S, Desai A, Hoppel CL, Matsuyama S, Palczewski K (2009) Involvement of all-trans-retinal in acute light-induced retinopathy of mice. *The Journal of Biological Chemistry*, 284:15173-83.

Maeda A, Maeda T, Golczak M, Imanishi Y, Leahy P, Kubota R, Palczewski K (2006) Effects of potent inhibitors of the retinoid cycle on visual function and photoreceptor protection from light damage in mice. *Molecular Pharmacology*, 70:1220-9.

Maeda A, Maeda T, Golczak M, Palczewski K (2008) Retinopathy in mice induced by disrupted all-trans-retinal clearance. *The Journal of Biological Chemistry*, 283:26684-93.

Maeda A, Maeda T, Imanishi Y, Sun W, Jastrzebska B, Hatala DA, Winkens HJ, Hofmann KP, Janssen JJ, Baehr W, Driessen CA, Palczewski K (2006) Retinol dehydrogenase (RDH12) protects photoreceptors from light-induced degeneration in mice. *The Journal of Biological Chemistry*, 8:37697-704.

Maeda A, Maeda T, Imanishi Y, Kuksa V, Alekseev A, Bronson JD, Zhang H, Zhu L, Sun W, Saperstein DA, Rieke F, Baehr W, Palczewski K (2005) Role of photoreceptor-specific retinol dehydrogenase in the retinoid cycle in vivo. *The Journal of Biological Chemistry*, 280:18822-32.

Maeda A, Maeda T, Sun W, Zhang H, Baehr W, Palczewski K (2007) Redundant and unique roles of retinol dehydrogenases in the mouse retina. *Proceedings of the National Academy of Sciences of the United States of America*, 104:19565-70.

Mahley RW (1988) Apolipoprotein E: Cholesterol transport protein with expanding role in cell biology. *Science*, 240:622-30.

Maiti P, Kong J, Kim SR, Sparrow JR, Allikmets R, Rando RR (2006) Small molecule RPE65 antagonists limit the visual cycle and prevent lipofuscin formation. *Biochemistry,* 45:852-60.

Marlor RL, Blais BR, Preston FR, Boyden DG (1973) Foveomacular retinitis, an important problem in military medicine: epidemiology. *Investigative Ophthalmology*, 12:5-16.

Marmor MF (1998) Structure, function, and disease of the retinal pigment epithelium. In: Marmor, MF, and Wolfensberger, TJ [eds.] *The Retinal Pigment Epithelium.* New York: Oxford University Press, pp. 3-9.

Martínez-Martos JM, Ramírez-Expósito MJ, Mayas-Torres MD, García-López MJ, Ramírez-Sánchez M (2000) Utility of the 3-(4,5-dimethylthiazol-2-yl)-2,5-diphenyl tetrazolium bromide (MTT) assay to measure mitochondrial activity in K+- and ATP-stimulated rodent cortex synaptosomes. *Neuroscience Research Communication*, 27:103-7.

Mata NL, Weng J, Travis GH (2000) Biosynthesis of a major lipofuscin fluorophore in mice and humans with ABCR-mediated retinal and macular degeneration. *Proceedings of the National Academy of Sciences of the United States of America,* 97:7154-9.

Matsumoto B, Defoe DM, and Besharse JC (1987) Membrane turnover in rod photoreceptors: Ensheathment and phagocytosis of outer segment distal tips by pseudopodia of the retinal pigment epithelium. *Proceedings of the Royal Society of London. Series B, Containing papers of a Biological character. Royal Society (Great Britain),* 230:339-54.

Matthews RG, Hubbard R, Brown PK, and Wald G (1963) Tautomeric forms of metarhodopsin. The *Journal* of General *Physiology,* 47:215-40.

McDonald HR, Harris MJ (1988) Operating microscope-induced retinal phototoxicity during pars plana vitrectomy. *Archives of Ophthalmology*, 106:521–3.

McDonald HR, Irvine AR (1983) Light-induced maculopathy from the operating microscope in extracapsular cataract-extraction and intraocular-lens implantation. *Ophthalmology,* 90:945–51.

Meister A (1989) in *Glutathione: Chemical, Biochemical and Medical Aspects,* [eds.] Dolphin, D., Poulson, R. & Avramovic, O. New York: Wiley, pp. 22-3.

Murata M, Kawanishi S (2000) Oxidative DNA damage by vitamin A and its derivative via superoxide generation. *The Journal of Biological Chemistry*, 275:2003-8.

Neelam K, Hogg RE, Stevenson MR, Johnston E, Anderson R, Beatty S, Chakravarthy U (2008) Carotenoids and co-antioxidants in age-related

maculopathy: Design and methods. *Ophthalmic Epidemiology*, 15:389-401.

Ng K-P, Davies MW, Kim SR, Gu X, Gugiu B, Renganathan K, Bonilha VL, Crabb JS, Różanowska MB (2008) Retinal pigment epithelium lipofuscin proteomics. *Molecular and Cellular Proteomics,* 7:1397-405.

Nirmalan PK, Katz J, Robin AL, Tielsch JM, Namperumalsamy P, Kim R, Narendran V, Ramakrishnan R, Krishnadas R, Thulasiraj RD, Suan E (2004) Prevalence of vitreoretinal disorders in a rural population of southern India: The Aravind comprehensive eye study. *Archives of Ophthalmology*, 122:581–6.

Noell WK, Walker VS, Kang BS, Berman S (1966) Retinal damage by light in rats. *Investigative Ophthalmology and Visual Science,* 5:450-73.

O'Day WT, Young RW (1978) Rhythmic daily shedding of outer-segment membranes by visual cells in the goldfish. *The Journal of Cell Biology*, 76:593-604.

Oka C, Tsujimoto R, Kajikawa M, Koshiba-Takeuchi K, Ina J, Yano M, Tsuchiya A, Ueta Y, Soma A, Kanda H, Matsumoto M, Kawaichi M (2004) HtrA1 serine protease inhibits signaling mediated by Tgfß family proteins. *Development,* 131:1041-53.

Onorato JM, Jenkins AJ, Thorpe SR, Baynes JW (2000) Pyridoxamine, an inhibitor of advanced glycation reactions, also inhibits advanced lipoxidation reactions. *The Journal of Biological Chemistry*, 275:21177-84.

Organisciak DT, Darrow RA, Barsalou L, Kutty RK, Wiggert B (2003) Susceptibility to retinal light damage in transgenic rats with rhodopsin mutations. *Investigative Ophthalmology & Visual Science*, 44:486–492.

Organisciak DT, Vaughan DK (2010) Retinal light damage: mechanisms and protection. *Progress in Retinal and Eye Research*, 29:113-34.

Organisciak DT, Winkler BS (1994) Retinal light damage: Practical and theoretical considerations. *Progress in Retinal and Eye Research,* 13:1–29.

Organisciak DT, Xie A, Wang HM, Jiang YL, Darrow RM, Donoso LA (1991) Adaptive-changes in visual cell transduction protein-levels — effect of light. *Experimental Eye Research*, 53:773–9.

Ostrovskiĭ MA, Fedorovich IB (1994) Retinal as a photo-damage sensitizer of retinal-containing retina proteins. *Biofizika*, 39:13-25.

Ostwald TJ, Steinberg RH (1981) Transmembrane components of taurine flux across frog retinal pigment epithelium. *Current Eye Research,* 1:437-43.

Oyster CW (1999) *The Human Eye: Structure and Function.* Sunderland: Sinauer Associates, Inc.

Palace VP, Khaper N, Qin Q, Singal PK (1999) Antioxidant potentials of vitamin A and carotenoids and their relevance to heart disease. *Free Radical Biology and Medicine,* 26:746-61.

Palczewski K (2006) G protein-coupled receptor rhodopsin. *Annual Review of Biochemistry,* 75:743-67.

Palozza, P, Krinsky NI (1992) ß-Carotene and α-tocopherol are synergistic antioxidants. *Archives of Biochemistry and Biophysics*, 297:184–7.

Papermaster DS (1982) Preparation of retinal rod outer segments. *Methods in Enzymology,* 81:48-52.

Pawlak A, Wrona M, Różanowska M, Zareba M, Lamb LE, Roberts J, Simon JD, Sarna T (2003) Comparison of the aerobic photoreactivity of A2E with its precursor retinal. *Photochemistry and Photobiology*, 77:253-8.

Peters S, Lamah T, Kokkinou D, Bartz-Schmidt KU, and Schraermeyer U (2006) Melanin protects choroidal blood vessels against light toxicity. *Z Naturforsch [C],* 61:427-33.

Plack PA, Pritchard DJ (1969) Schiff bases formed from retinal and phosphatidylethanolamine, phosphatidylserine, ethanolamine or serine. *The Biochemical Journal*, 115:927-34.

Poliner LS, Tornambe PE (1992) Retinal pigment epitheliopathy after macular hole surgery. *Ophthalmology,* 99:1671–7.

Porter NA (1990) Autoxidation of polyunsaturated fatty acids: Introduction, propagation, and product distribution (Basic Chemistry). In C. Vigo-Pelfrey [Ed.]. *Membrane Lipid Oxidation*: Vol. I (pp. 33-62). Boca Raton: CRC Press.

Pulido JS (2002) Functional anatomy of the retina, choroid, and vitreous. In: Krachmer, JH [ed.] *Retina, choroid, and vitreous. The Requisites in Ophthalmology.* St. Louis: Mosby, pp. 10-7.

Qtaishat NM, Wiggert B, Pepperberg DR (2005) Interphotoreceptor retinoid-binding protein (IRBP) promotes the release of all-trans retinol from the isolated retina following rhodopsin bleaching illumination. *Experimental Eye Research,* 81:455-63.

Quillen DA, Barber AJ (2002) Anatomy and physiology of the retina. In: Quillen, DA, and Blodi, BA [eds.] *Clinical retina.* (1st ed.) Chicago: American Medical Association, pp. 1-14.

Radu RA, Mata NL, Nusinowitz S, Liu XR, Sieving PA, Travis GH (2003) Treatment with isotretinoin inhibits lipofuscin accumulation in a mouse model of recessive Stargardt's macular degeneration. *Proceedings of the National Academy of Sciences of the United States of America*, 100:4742-7.

Rakoczy PE, Zhang D, Robertson T, Barnett NL, Papadimitriou J, Constable IJ, Lai CM (2002) Progressive age-related changes similar to age-related macular degeneration in a transgenic mouse model. *The American Journal of Pathology*, 161:1515-24.

Rattner A, Smallwood PM, Nathans J. (2000) Identification and characterization of all-trans-retinol dehydrogenase from photoreceptor outer segments, the visual cycle enzyme that reduces all-trans-retinal to all-trans-retinol. *The Journal of Biological Chemistry*, 275:11034-43.

Renganathan K, Sun M, Darrow R, Shan L, Gu X, Salomon RG, Hazen S, Organisciak D, Crabb JW (2003) Light induced protein modifications and

lipid oxidation products in rat retina. *Investigative Ophthalmology and Visual Science,* 44: E-Abstract 5129.

Ridge KD, Palczewski K (2007) Visual rhodopsin sees the light: Structure and mechanism of G protein signaling. *The Journal of Biological Chemistry,* 282:9297-301.

Ritter E, Elgeti M, Bartl FJ (2008) Activity switches of rhodopsin. *Photochemistry and Photobiology*, 84:911-20.

Ritter E, Elgeti M, Hofmann KP, Bartl FJ (2007) Deactivation and proton transfer in light-induced metarhodopsin II/metarhodopsin III conversion: A time-resolved Fourier transform infrared spectroscopic study. *The Journal of Biological Chemistry,* 282:10720-30.

Rivera A, Fisher SA, Fritsche LG, Keilhauer CN, Lichtner P, Meitinger T, Weber BH (2005). Hypothetical LOC387715 is a second major susceptibility gene for age-related macular degeneration, contributing independently of complement factor H to disease risk. *Human Molecular Genetics*, 14:3227–36.

Rodieck RW (1988) The primate retina. In: Streklis HD, Erwin J, [eds.] *Comparative Primate Biology*, Vol. 4, Neurosciences, New York: Liss, pp. 203-78.

Rogers BS, Symons RC, Komeima K, Shen J, Xiao W, Swaim ME, Gong YY, Kachi S, Campochiaro PA (2007) Differential sensitivity of cones to iron-mediated oxidative damage. *Investigative Ophthalmology & Visual Science,* 48:438–45.

Rotmans JP, Kropf A (1975) The analysis of retinal isomers by high speed liquid chromatography. *Vision Research*, 15:1301-2.

Różanowska M, Jarvis-Evans J, Korytowski W, Boulton ME, Burke JM, Sarna T (1995) Blue light-induced reactivity of retinal age pigment - in vitro generation of oxygen-reactive species. *Journal of Biological Chemistry,* 270:18825-30.

Różanowska M, Różanowski B (2008) *Visual transduction and non-visual light perception*; Chapter 20. J. Tombran-Tink and C. J. Barnstable [eds.], Totowa: Humana Press, pp. 421-62.

Różanowska M, Sarna T (2005) Light-induced damage to the retina : Role of rhodopsin chromophore revisited. *Photochemistry and Photobiology*, 81:1305-30.

Różanowska M, Wessels J, Boulton M, Burke JM, Rodgers MA, Truscott TG, Sarna T (1998) Blue light-induced singlet oxygen generation by retinal lipofuscin in non-polar media. *Free Radical Biology & Medicine,* 24:1107-12.

Różanowska MB, Pawlak A, Różanowski B, Skumatz C, Zarba M, Boulton ME, Burke JM, Sarna T, Simon JD (2004) Age-related changes in the photoreactivity of retinal lipofuscin granules: Role of chloroform-insoluble components. *Investigative Ophthalmology and Visual Science,* 45:1052-60.

Różanowska MB, Cantrell A, Edge R, Land EJ, Sarna T, Truscott TG (2005) Pulse radiolysis study of the interaction of retinoids with peroxyl radicals. *Free Radical Biology & Medicine*, 39:1399-405.

Różanowska MB, Korytowski W, Różanowski B, Skumatz C, Boulton ME, Burke JM, Sarna T (2002) Photoreactivity of aged human RPE melanosomes: A comparison with lipofuscin. *Investigative Ophthalmology & Visual Science,* 43:2088-96.

Różanowska MB, Różanowski B, Pawlak A, Zareba M, Boulton ME, Sarna T (2003) Phosphatidylethanolamine prevents retinal photodamage. In Honingsmann, H [ed.], *10th Congress of the European Society for Photobiology,* Programme and Book of Abstracts, Vienna, Austria, p. 48.

Różanowski B, Boulton ME, Różanowska MB (2004) Action spectra of photo-oxidation for bleached and dark-adapted photoreceptor outer segments. *Investigative Ophthalmology and Visual Science,* 44, E-Abstract 717.

Różanowski B, Burke JM, Boulton ME, Sarna T, Różanowska M (2008) Human RPE melanosomes protect from photosensitized and iron-mediated oxidation but become pro-oxidant in the presence of iron upon photodegradation. *Investigative Ophthalmology & Visual Science*, 49:2838-47.

Różanowski B, Różanowska MB, Boulton ME (2003) Toxicity of all-trans retinal to the retinal pigment epithelium. *Investigative Ophthalmology & Visual Science,* 44:1643.

Saari JC (2000) Biochemistry of visual pigment regeneration: The Friedenwald lecture. *Investigative Ophthalmology & Visual Science*, 41:337-48.

Salom D, Lodowski DT, Stenkamp RE, Le Trong I, Golczak M, Jastrzebska B, Harris T, Ballesteros JA, Palczewski K (2006) Crystal structure of a photoactivated deprotonated intermediate of rhodopsin. *Proceedings of the National Academy of Sciences of the United States of America,* 103:16123-8.

Schadel SA, Heck M, Maretzki D, Filipek S, Teller DC, Palczewski K, and Hofmann KP (2003) Ligand channeling within a G-protein-coupled receptor: The entry and exit of retinals in native opsin. *The Journal of Biological Chemistry,* 278:24896-903.

Schatz P, Eriksson U, Ponjavic V, Andreasson S (2004) Multifocal electroretinography and optical coherence tomography in two patients with solar retinopathy. *Acta Ophthalmologica Scandinavica,* 82:476–80.

Schmidt S, Postel EA, Agarwal A, Allen IC Jr, Walters SN, De la Paz MA, Scott WK, Haines JL, Pericak-Vance MA, Gilbert JR (2003) Detailed analysis of allelic variation in the ABCA4 gene in age-related maculopathy. *Investigative Ophthalmology & Visual Science*, 44:2868-75.

Schmidt SY, Peisch RD (1986) Melanin concentration in normal human retinal pigment epithelium. Regional variation and age-related reduction. *Investigative Ophthalmology & Visual Science,* 27:1063-7.

Schmitz-Valckenberg S, Bindewald-Wittich A, Dolar-Szczasny J, Dreyhaupt J, Wolf S, Scholl HPN, Holz FG (2006) Correlation between the area of

increased autofluorescence surrounding geographic atrophy and disease progression in patients with AMD. *Investigative Ophthalmology & Visual Science*, 47:2648-54.

Scholl HP, Fleckenstein M, Issa PC, Keilhauer C, Holz FG, Weber BH (2007) An update on the genetics of age-related macular degeneration. *Molecular Vision,* 13:196–205.

Schutt F, Bergmann M, Holz FG, Kopitz J (2002) Isolation of intact lysosomes from human The RPE and effects of A2-E on the integrity of the lysosomal and other cellular membranes. *Graefe's Archive for Clinical and Experimental Ophthalmology,* 240:983-8.

Schutt F, Holz FG (2001) Age-related macular degeneration: Current concepts of pathogenesis and risk factors. In: Brady, LW, Heilmann, HP, and Molls, M [eds.] *Age-related Macular Degeneration. Current Treatment Concepts.* Berlin: Springer-Verlag Heidelberg, pp. 3-10.

Scurlock RD, Ogilby PR (1993) Production of singlet oxygen ($^1\Delta_g$ O_2) by 9,10-dicyanoanthracene and acridine: quantum yields in acetonitrile. *Journal of Photochemistry and Photobiology A:* Chemistry, 72:1-7.

Seagle B-LL, Gasyna EM, Mieler WF, Norris JR, Jr. (2006) Photoprotection of human retinal pigment epithelium cells against blue light-induced apoptosis by melanin free radicals from Sepia officinalis. *Proceedings of the National Academy of Sciences of the United States of America,* 103:16644-8.

Shamsi FA, Boulton M (2001) Inhibition of RPE lysosomal and antioxidant activity by the age pigment lipofuscin. *Investigative Ophthalmology & Visual Science,* 42:3041-6.

Shichi H (1999) Molecular Biology of Vision. In: Siegel GJ, Agranoff BW, Albers RW, Fisher SK, Uhler MD [eds.] *Basic Neurochemistry. Molecular, Cellular and Medical Aspects* (6 Edn.) Philadelphia: Lippincott-Raven.

Shiono T, Hayasaka S, and Mizuno K (1983) Effect of temperature and pH on release of enzymes from lysosomes of the bovine retinal pigment epithelium in vitro. *Experimental Eye Research*, 36:871-6.

Sieving PA, Chaudhry P, Kondo M, Provenzano M, Wu D, Carlson TJ, Bush RA, Thompson DA (2001) Inhibition of the visual cycle in vivo by 13-*cis* retinoic acid protects from light damage and provides a mechanism for night blindness in isotretinoin therapy. *Proceedings of the National Academy of Sciences of the United States of America*, 98:1835-40.

Sliney D H (1983) Eye protective techniques for bright light. *Ophthalmology*, 90:937-44.

Sliney DH (2002) How light reaches the eye and its components. *International Journal of Toxicology*, 21:501-9.

Smith HG Jr, Litman BJ (1982) Preparation of osmotically intact rod outer segment disks by Ficoll flotation. *Methods in Enzymology*, 81:57-61.

Sokolov AV, Sokolov VS, Feldman TB, Ostrovsky MA (2008) Interaction of all-*trans*-retinal with bilayer lipid membranes. *Biochemistry (Moscow) Supplemental Series A: Membrane and Cell Biology*, 2(4).

Sousa C, Botelho do Rego AM, Melo T (2008) Singlet oxygen reactivity in water-rich solvent mixtures. *Química Nova*, 31:1392-9.

Spaide R (2006) Etiology of late-age-related macular degeneration. In: Alfaro, D V, Liggett, P E, Mieler, W F, Quiroz-Merdaco, H, Jager, R D, and Tano, Y [eds.] *Age-related macular degeneration. A comprehensive Textbook.* Phipadelphia: Lippincott Williams & Wilkins, pp. 23-39.

Sparrow JR, Boulton M (2005) RPE lipofuscin and its role in retinal pathobiology (2005) *Experimental Eye Research*, 80:595-606.

Sparrow JR, Fishkin N, Zhou JL, Cai BL, Jang YP, Krane S, Itagaki Y, Nakanishi K (2003) A2E, a by-product of the visual cycle. *Vision Research,* 43:2983-90.

Sperling HG, Johnson C, Harwerth RS (1980) Differential spectral photic damage to primate cones. *Vision Research,* 20:1117–25.

Spooner PJ, Sharples JM, Goodall SC, Bovee-Geurts PH, Verhoeven MA, Lugtenburg J, Pistorius AM, Degrip WJ, Watts A (2004) The ring of the rhodopsin chromophore in a hydrophobic activation switch within the binding pocket. *Journal of Molecular Biology,* 22; 343:719-30.

Starita C, Hussain AA, Pagliarini S, Marshall J (1996) Hydrodynamics of ageing Bruch's membrane: Implications for macular disease. *Experimental Eye Research*, 62:565–72.

Stitt A, Gardiner TA, Alderson NL, Canning P, Frizzell N, Duffy N, Boyle C, Januszewski AS, Chachich M, Baynes JW, Thorpe SR (2002) The AGE inhibitor pyridoxamine inhibits development of retinopathy in experimental diabetes. *Diabetes*, 51:2826-32.

Strauss O (2005) The retinal pigment epithelium in visual function. *Physiological Reviews,* 85:845-81.

Sun H, Nathans J (2001) ABCR, the ATP-binding cassette transporter responsible for Stargardt macular dystrophy, is an efficient target of all-trans-retinal-mediated photooxidative damage in vitro. Implications for retinal disease. *The Journal of Biological Chemistry*, 276:11766-74.

Sun MJ, Finnemann SC, Febbraio M, Shan L, Annangudi SP, Podrez EA, Hoppe G, Darrow R, Organisciak DT, Salomon RG, Silverstein RL, Hazen SL (2006) Light-induced oxidation of photoreceptor outer segment phospholipids generates ligands for CD36-mediated phagocytosis by retinal pigment epithelium - A potential mechanism for modulating outer segment phagocytosis under oxidant stress conditons. *Journal of Biological Chemistry,* 281:4222-30.

Surya A, Foster KW, Knox BE (1995) Transducin activation by the bovine opsin apoprotein. *The Journal of Biological Chemistry,* 270:5024-31.

Swaroop A, Chew EY, Rickman CB, Abecasis GR (2009) Unraveling a multifactorial late-onset disease: From genetic susceptibility to disease mechanisms for age-related macular degeneration. *Annual Review of Genomics and Human Genetics,* 10:19–43.

Takagi H, Tanihara H, Seino Y, Yoshimura N (1994) Characterization of glucose transporter in cultured human retinal pigment epithelial cells: gene

expression and effect of growth factors. *Investigative Ophthalmology and Visual Science,* 35:170-7.

Taylor HR, Munoz B, West S, Bressler NM, Bressler SB, Rosenthal FS (1990) Visible light and risk of age-related macular degeneration. *Transactions of the American Ophthalmological Society,* 88:163–73.

Taylor HR, West S, Munoz B, Rosenthal FS, Bressler SB, Bressler NM (1992) The long-term effects of visible light on the eye. *Archives of Ophthalmology*, 110:99–104.

Thompson W (2006) Classification of age-related macular degeneration. In: Alfaro, DV, Liggett, PE, Mieler, WF, Quiroz-Merdaco, H, Jager RD, Tano, Y [eds.] *Age-related macular degeneration. A comprehensive Textbook,* Phipadelphia: Lippincott Williams & Wilkins, pp. 44-52.

Ting AY, Lee TK, MacDonald IM (2009) Genetics of age-related macular degeneration. *Current Opinion in Ophthalmology*, 20:369-76.

Tomany SC, Klein R, Klein BE (2003) The relationship between iris color, hair color, and skin sun sensitivity and the 10-year incidence of age-related maculopathy: The Beaver dam eye study. *Ophthalmology*, 110:1526–33.

Travis GH, Golczak M, Moise AR, and Palczewski K (2007) Diseases caused by defects in the visual cycle: Retinoids as potential therapeutic agents. *Annual Review of Pharmacology and Toxicology,* 47:469-512.

Tsina E, Chen C, Koutalos Y, Ala-Laurila P, Tsacopoulos M, Wiggert B, Crouch RK, Cornwall MC (2004) Physiological and microfluorometric studies of reduction and clearance of retinal in bleached rod photoreceptors. *The Journal of General Physiology*, 124:429-43.

Turrens JF (1997) Superoxide production by the mitochondrial respiratory chain. *Bioscience Reports,* 17:3-8.

Van Leeuwen R, Ikram MK, Vingerling JR, Witteman JC, Hofman A, de Jong PT (2003) Blood pressure, atherosclerosis, and the incidence of age-related maculopathy. The Rotterdam study. *Investigative Ophthalmology & Visual Science,* 44:3771–7.

Vaughan DK, Coulibaly SF, Darrow RM, Organisciak DT (2003) A morphometric study of light-induced damage in transgenic rat models of retinitis pigmentosa. *Investigative Ophthalmology & Visual Science*, 44:848–55.

Vever-Bizet C, Dellinger M, Brault D, Rougee M, Bensasson RV (1989) Singlet molecular oxygen quenching by saturated and unsaturated fatty-acids and by cholesterol. *Photochemistry and Photobiology*, 50:321-5.

Wald G (1935) Carotenoids and the visual cycle. *The Journal of General Physiology,* 19:351-71.

Wang JJ, Klein R, Smith W, Klein BE, Tomany S, Mitchell P (2003) Cataract surgery and the 5-year incidence of late-stage age-related maculopathy: pooled findings from the beaver dam and blue mountains eye studies. *Ophthalmology*, 110:1960–7.

Wang M, Lam TT, Tso MOM, Naash MI (1997) Expression of a mutant opsin gene increases the susceptibility of the retina to light damage. *Visual Neuroscience,* 14:55–62.

Wassell J, Ellis S, Burke J, Boulton M (1998) Fluorescence properties of autofluorescent granules generated by cultured human the RPE. *Investigative Ophthalmology & Visual Science*, 39:1487-92.

Webster AR, Héon E, Lotery AJ, Vandenburgh K, Casavant TL, Oh KT, Beck G, Fishman GA, Lam BL, Levin A, Heckenlively JR, Jacobson SG, Weleber RG, Sheffield VC, Stone EM (2001) An analysis of allelic variation in the ABCA4 gene. *Investigative Ophthalmology & Visual Science*, 42:1179-89.

Weiter JJ, Delori FC, Wing GL, Fitch KA (1986) Retinal pigment epithelial lipofuscin and melanin and choroidal melanin in human eyes. *Investigative Ophthalmology & Visual Science*, 27:145-52.

Weng J, Mata NL, Azarian SM, Tzekov RT, Birch DG, Travis GH (1999) Insights into the function of rim protein in photoreceptors and etiology of Stargardt's disease from the phenotype in *abcr* knockout mice. *Cell*, 98:13-23.

West SK, Rosenthal FS, Bressler NM, Bressler SB, Munoz B, Fine SL, Taylor HR (1989) Exposure to sunlight and other risk factors for age-related macular degeneration. *Archives of Ophthalmology,* 107:875-9.

Whikehart DR (2003) Proteins: Essential components of the eye. In: Whikehart, DR [ed.] *Biochemistry of the Eye.* (2nd Edn.) Philadelphia: Butterworth-Heinemann, pp. 15-54.

Wihlmark U, Wrigstad A, Roberg K, Brunk UT, Nilsson SE (1996) Formation of lipofuscin in cultured retinal pigment epithelial cells exposed to pre-oxidized photoreceptor outer segments. *APMIS : Acta Pathologica, Microbiologica, et Immunologica Scandinavica*, 104:272-9.

Wihlmark U, Wrigstad A, Roberg K, Nilsson SE, Brunk UT (1997) Lipofuscin accumulation in cultured retinal pigment epithelial cells causes enhanced sensitivity to blue light irradiation. *Free Radical Biology & Medicine*, 22:1229-34.

Williams TP, Howell WL (1983) Action spectrum of retinal light-damage in albino rats. *Investigative Ophthalmology & Visual Science,* 24:285-7.

Winkler BS (2008) An hypothesis to account for the renewal of outer segments in rod and cone photoreceptor cells: renewal as a surrogate antioxidant. *Investigative Ophthalmology & Visual Science,* 49:3259-61.

Wolf G (2005) Function of the protein RPE65 in the visual cycle. *Nutrition Reviews,* 63:97-100.

Wrona M, Korytowski W, Różanowska M, Sarna T, Truscott TG (2003) Cooperation of antioxidants in protection against photosensitized oxidation. *Free Radical Biology & Medicine*, 35:1319-29.

Wu Y, Fishkin NE, Pande A, Pande J, Sparrow JR (2009) A novel lipofuscin bisretinoid prominent in human retina and in a model of recessive Stargardt disease. *The Journal of Biological Chemistry,* 284:20155-66.

Young RW (1967) The renewal of photoreceptor cell outer segments. *The Journal of Cell Biology*, 33:61-72.

Young RW (1988) Solar radiation and age-related macular degeneration. *Survey of Ophthalmology,* 32:252–69.

Young RW, Droz B (1968) The renewal of protein in retinal rods and cones. *The Journal of Cell Biology*, 39:169-84.

Yuzawa T, Hamaguchi H (1995) Investigation of the photoisomerization of all-*trans*-retinal by singular-value-decomposition analysis of nanosecond time-resolved infrared spectra. *Journal of Molecular Structure*, 352-3:489-95.

Zareba M, Raciti MW, Henry MM, Sarna T, Burke JM (2006) Oxidative stress in ARPE-19 cultures: Do melanosomes confer cytoprotection? *Free Radical Biology and Medicine,* 40:87-100.

Zebger I, Snyder JW, Andersen LK, Poulsen L, Gao Z, Lambert JDC, Kristiansen U, Ogilby PR (2004) Direct optical detection of singlet oxygen from a single cell. *Photochemistry and Photobiology*, 79:319-22.

Zhou J, Jang YP, Kim SR, Sparrow JR (2006) Complement activation by photooxidation products of A2E, a lipofuscin constituent of the retinal pigment epithelium. *Proceedings of the National Academy of Sciences of the United States of America*, 103:16182-7.

Zurdel J, Richard G (2001) Clinical manifestations and natural history of age-realated macular degeneration. In: Brady, LW, Heilmann, HP, Molls, M [eds.] *Age-related Macular Degeneration. Current Treatment Concepts.* Berlin: Springer-Verlag Heidelberg, pp. 11-8.